UNIVERSIDADE
BEIRA INTERIOR

Mitochondrial Gene Therapy: Development of a mitochondrial targeted peptide/plasmid DNA vector

Rúben Miguel Ribeiro Faria

Tese para obtenção do Grau de Doutor em
Biomedicina
(3º ciclo de estudos)

Orientadora: Prof.ª Doutora Diana Rita Barata Costa
Co-orientadora: Prof.ª Doutora Ângela Maria Almeida de Sousa
Co-orientadora: Prof.ª Doutora Prisca Boisguérin

Júri:
Prof. Doutor Miguel Castelo Branco Craveiro Sousa
Prof.ª Doutora Fani Peireira de Sousa
Prof. Doutor Carlos Adriano Albuquerque Andrade de Matos
Prof. Doutor José Alberto Gonçalves das Neves
Prof. Doutor João Manuel Marques Rodrigues
Prof.ª Doutora Carina Isabel Crucho

14 de abril de 2025

Declaração de Integridade

Eu, Rúben Miguel Ribeiro Faria, que abaixo assino, estudante com o número de inscrição D2696 do 3º Ciclo de Estudos em Biomedicina da Faculdade de Ciências da Saúde, declaro ter desenvolvido o presente trabalho e elaborado o presente texto em total consonância com o **Código de Integridades da Universidade da Beira Interior**.

Mais concretamente afirmo não ter incorrido em qualquer das variedades de Fraude Académica, e que aqui declaro conhecer, que em particular atendi à exigida referenciação de frases, extratos, imagens e outras formas de trabalho intelectual, e assumindo assim na íntegra as responsabilidades da autoria.

Universidade da Beira Interior, Covilhã 09/05/2025

Assinado por: Rúben Miguel Ribeiro Faria
Num. de Identificação: BI14839102
Data: 09-05-2025 15:20:42 +01:00

CHAVE MÓVEL

Acknowledgments

Às minhas orientadoras, Professora Doutora Diana Costa e Professora Doutora Ângela Sousa, por terem partilhado comigo este percurso que teve início na dissertação de Mestrado. Quero agradecer a confiança e força que me deram para realizar o meu doutoramento nos vossos grupos de investigação e poder continuar a trabalhar na área da terapia génica que tanto me fascina. Agradeço imenso pelo apoio e aconselhamento nos momentos mais difíceis e por partilharem comigo o vosso conhecimento e experiência que foi fundamental para os resultados que alcançámos nesta tese. Obrigado por terem contribuído para o meu desenvolvimento pessoal e profissional, por fomentarem o meu espírito critico e pela orientação ao longo desta tese de doutoramento que possibilitou irmos além dos objetivos inicialmente traçados. Foi um prazer ter realizado a minha tese de doutoramento com vocês e só tenho a agradecer por tudo.

To my supervisor, Dr. Prisca Boisguérin, for welcoming me so warmly into your research group and for assisting with all the logistics of my stay in Montpellier. I am very grateful to you for sharing your scientific knowledge with me and for your help and guidance in the work we carried out at the Centre de Recherche en Biologie Cellulaire de Montpellier (CRBM) and at the PhyMedExp research unit, as well as throughout my doctoral thesis. It was a pleasure to work with you and be part of your research group for six months, and to have the opportunity to learn about peptide synthesis and conduct tests with *in vivo* models for the first time. Thank you for your availability and for opening the doors to the world of peptides for me.

To Dr. Eric Vivès, for your help and kindness in sharing your scientific knowledge with me and teaching me the process of peptide synthesis and purification. Thank you for welcoming me so warmly.

To Dr. Swati Biswas, for your help in the synthesis and purification of the polymers used in this doctoral thesis. Thank you for providing your own resources to help us synthesize the polymers.

À Universidade da Beira Interior, mais especificamente ao Centro de Investigação em Ciências da Saúde da Universidade da Beira Interior (CICS-UBI), por disponibilizar as suas instalações, recursos humanos e técnicos necessários à realização das tarefas inerentes a esta tese. I would also like to thank the CRBM and PhyMedExp research

centers for providing their facilities and resources to carry out some tasks during my PhD.

À Fundação para a Ciência e Tecnologia (FCT), por financiar o meu doutoramento com uma bolsa mista (SFRH/BD/148393/2019).

Aos meus colegas e amigos de laboratório, pela companhia e partilha ao longo destes anos. Agradecer o espírito de entreajuda que sempre houve entre todos, a partilha de conhecimento que nos enriqueceu a todos e principalmente pela boa disposição que cria um ambiente de trabalho agradável. As histórias e conquistas que alcançámos juntos ficam para sempre na minha memória e espero que possamos acrescentar outras tantas no futuro.

Por fim, agradecer à minha família, que são as pessoas mais importantes da minha vida. Quero agradecer aos meus pais por todo o amor, carinho e suporte que me deram ao longo do meu percurso académico. Bem sei o esforço que fizeram ao longo destes anos para que pudesse estudar tão longe de casa e para que nunca me faltasse nada. Estarei eternamente grato por tudo o que fizeram e fazem por mim. Aos meus irmãos agradecer toda a força e carinho que me transmitiram ao longo deste percurso. Apesar de separados há tantos anos por 200km de distância, o mano mais velho está sempre com vocês e estará sempre para o que precisarem. À minha esposa, obrigado pela paciência e compreensão ao longo destes últimos anos. Não tenho como agradecer o apoio e incentivo que me deste para terminar esta etapa da minha vida. Obrigado por estares sempre do meu lado e pelo amor incondicional. A todos vocês, só quero que saibam que vos amo mais que tudo e que sem partilhar com vocês as minhas conquistas elas não tinham o mesmo significado. E sim avó, já podes dizer que sou o teu doutor.

Resumo

As mitocôndrias são organelos celulares com tamanhos de 1 micrómetro, aproximadamente, que podem ser encontradas em grande número nas células eucarióticas. Estes pequenos organelos têm um papel crucial na atividade celular, sendo essenciais em processos de sinalização intracelular, mecanismos de apoptose e produção de energia, entre outros. As mitocôndrias geram 90% de toda a energia consumida nas células, através do sistema de fosforilação oxidativa que produz energia sob a forma de moléculas de adenosina trifosfato (ATP). As mitocôndrias, à semelhança do núcleo, possuem o seu próprio genoma, designado ácido desoxirribonucleico mitocondrial (ADNmt). O ADNmt humano é composto por moléculas de ADN circular de dupla cadeia, sendo que cada cadeia tem a sua própria composição e codificam diferentes ácidos ribonucleicos (ARN). A cadeia rica em guanina codifica 14 ARNt, 2 ARNr e 12 polipeptídeos, enquanto que a cadeia mais leve tem informação para transcrever apenas 8 ARNt e um polipeptídeo. No total, o ADNmt é constituído apenas por 37 genes que codificam 13 ARNm, dando origem a 13 proteínas que fazem parte do sistema de transporte de eletrões e do complexo ATPase. O sistema de fosforilação oxidativa é composto por 5 complexos (Complexo NADH-ubiquinona redutase (complexo I); complexo succinato desidrogenase (complexo II); ubiquinol-citocromo c oxidoredutase (complexo III); complexo citocromo-c oxidase (complexo IV) e complexo ATP sintase (complexo V)), que formam a cadeia respiratória.

O ADNmt é muito mais suscetível a mutações quando comparado com o genoma nuclear. As alterações no ADNmt comprometem o normal funcionamento das células, afetando principalmente tecidos neuronais e musculares. A maior frequência de mutações no ADNmt pode ser explicada pelo facto de este não possuir telómeros nem intrões na sua constituição. As disfunções mitocondriais levam ao aparecimento de doenças multissistémicas, podendo afetar o normal funcionamento da resposta imunológica, função motora e cerebral, regulação metabólica e levar ao envelhecimento. A grande maioria das patologias com origem nas mitocôndrias são herdadas do ADNmt materno. No entanto, fatores ambientais como o stress e a consequente presença de espécies reativas de oxigénio contribuem também para o aparecimento de mutações no ADNmt. As doenças mitocondriais mais comuns são a neuropatia ótica hereditária de Leber (NOHL), encefalomiopatia mitocondrial, Síndrome de Pearson, Parkinson, doença de Huntington, Alzheimer e alguns tipos de cancro (mamário, renal e colorretal).

O complexo I da cadeia respiratória mitocondrial é o principal ponto de entrada de eletrões na cadeia de transporte de eletrões. Devido a este facto, este complexo é muito importante no normal funcionamento da mitocôndria. É no complexo I que ocorre a transferência de eletrões do Dinucleótido de nicotinamida e adenina + Hidrogénio (DNAH) para a ubiquinona, o transporte de protões através da membrana mitocondrial interna e é a principal fonte de espécies reativas de oxigénio (ERO). Mutações nos genes mitocondriais responsáveis por proteínas estruturais e de montagem deste complexo levam ao aumento da produção de ERO e à perda de funções. Um desses genes é o gene mitocondrial ND1 (DNAH desidrogenase 1). A proteína mt-ND1 desempenha um papel crucial na estrutura do complexo I. Mutações no mt-ND1 estão associadas ao aparecimento de NOHL; miopatia mitocondrial, encefalopatia, acidose lática e episódios semelhantes a acidente vascular cerebral ("MELAS"); cardiomiopatia progressiva e alguns tipos de cancro.

Dados de 2020 revelaram que 1 em cada 250 pessoas apresentam mutações no ADNmt e que 1 em cada 5000 apresentam patologias graves associadas a disfunções mitocondriais. Atualmente os fármacos disponíveis no mercado servem apenas para mitigar os sintomas. Nenhum medicamento aprovado, pela Administração Federal de Alimentos e Medicamentos dos Estados Unidos da América, ou em desenvolvimento conseguiu curar ou retardar a progressão das doenças mitocondriais. Embora existam agentes antioxidantes e outras drogas para aliviar os sintomas, a ineficácia dos medicamentos atuais ressalta a necessidade urgente de tratamentos mais eficientes. A terapia génica mitocondrial é uma abordagem promissora que pode focar a sua ação diretamente na causa das doenças mitocondriais e desenvolver terapias ajustadas ao tipo de mutação.

A terapia génica consiste na aplicação de técnicas de ADN recombinante em que são utilizados genes funcionais para substituir genes defeituosos e repor o seu funcionamento normal. Uma vez que a maioria das doenças mitocondriais têm origem em mutações no ADNmt, a terapia génica mitocondrial aparece como uma estratégia muito promissora para o tratamento deste tipo de doenças. A terapia génica mitocondrial foca-se na origem da patologia e permite repor o gene mitocondrial afetado, reestabelecendo a função mitocondrial normal. Este tipo de terapia necessita de sistemas de entrega que sejam eficazes na proteção e entrega do material genético às células/organelos alvo. A principal dificuldade na implementação da terapia génica tem sido precisamente desenvolver nanotransportadores eficientes. Para a terapia génica mitocondrial a dificuldade tem sido ainda maior, uma vez que os sistemas precisam de atravessar mais barreiras e terem a capacidade de entregar o gene terapêutico

especificamente naquele organelo. Assim, o principal objetivo desta tese é desenvolver sistemas de entrega que tenham afinidade pela mitocôndria e que consigam entregar eficazmente genes mitocondriais como abordagem terapêutica de patologias associadas à mitocôndria.

O trabalho realizado consistiu no desenvolvimento de sistemas de entrega à base de péptidos (péptidos de penetração celular (PPC)) e de polímeros (polietilenimina (PEI)), com o objetivo de entregar o gene mitocondrial ND1. Para isso, estes biomateriais foram funcionalizados com ligandos que permitem o direcionamento específico para as mitocôndrias. Os ligandos utilizados foram o trifenilfosfónio (TPP) e cloreto de dequalínio (DQA) para funcionalizar o PEI e para os PPC foi utilizada uma sequência de direcionamento para a mitocôndria (MTS). O primeiro passo para o desenvolvimento dos sistemas poliméricos PEI-TPP/pND1 foi determinar, através de um desenho experimental, as condições ótimas para a formulação das nanopartículas. De seguida, esses sistemas foram caracterizados em termos de tamanho, carga superficial e morfologia. Estes sistemas de entrega demonstraram capacidade de internalizar em fibroblastos e células HeLa, e através da microscopia de confocal foi demonstrada a sua acumulação preferencial nas mitocôndrias. Para além disso, estes sistemas demonstraram capacidade de entregar o gene ND1 nas mitocôndrias e levar à sua transcrição. Os sistemas poliméricos PEI-DQA/pND1 desenvolvidos demonstraram igualmente excelentes propriedades físico-químicas, evidenciando a capacidade de transfetar e internalizar em células HeLa e fibroblastos. Estes nanotransportadores entregaram o gene ND1 diretamente nas mitocôndrias, levando à transcrição do gene de interesse e produção da proteína ND1. No entanto, os sistemas à base de péptidos que foram desenvolvidos (MTS-PPC), exibiram um desempenho superior em termos de internalização celular e direcionamento para a mitocôndria. A sua maior capacidade de complexar o plasmídeo (pND1) levou à formulação de nanopartículas com menores tamanhos e consequentemente uma maior entrega do gene de interesse e da expressão proteica. Os sistemas MTS-PPC que apresentaram melhores resultados *in vitro*, foram testados em modelos *in vivo* (embriões de peixe-zebra (PZ)). Os sistemas peptídicos demonstraram capacidade de internalizar e distribuir-se por todo o organismo dos PZ, sem causar nenhuma toxicidade nestes modelos *in vivo*.

Em suma, o trabalho desenvolvido durante esta tese de doutoramento procurou encontrar sistemas de entrega eficazes para aplicação em terapia génica mitocondrial, com o intuito de poder tornar esta terapia viável para o tratamento de doenças mitocondriais. Os resultados obtidos durante a tese demonstram que os sistemas de entrega desenvolvidos são muito promissores para desenvolvimento de protocolos de

terapia génica mitocondrial. Este trabalho contribuiu para o progresso e inovação numa área de investigação ainda pouco explorada como é a terapia génica mitocondrial. Os sistemas à base de péptidos apresentam potencial para serem considerados em futuras investigações, com o intuito de poder ser avaliada a sua translação para a clínica. Os nanotransportadores desenvolvidos durante esta tese foram otimizados para a entrega do gene mitocondrial ND1, no entanto estes sistemas podem ser facilmente adaptados para a entrega de quaisquer genes mitocondriais que estejam envolvidos em patologias associadas a mutações no ADNmt.

Palavras-chave

Doenças mitocondriais; Gene mitocondrial ND1; Mutações no genoma mitocondrial; Nanotransportadores peptídicos; Nanotransportadores poliméricos; Péptidos de penetração celular; Polietilenimina; Sistemas de entrega de genes; Terapia génica mitocondrial.

Abstract

Mitochondria are cellular organelles measuring approximately 1 micron that can be found in large numbers in eukaryotic cells. These small organelles play a crucial role in cellular activity, being essential in intracellular signaling processes, apoptosis mechanisms, and energy production, among others. Mitochondria generate 90% of all energy consumed in cells, through the oxidative phosphorylation system that produces energy in the form of adenosine triphosphate (ATP) molecules. Mitochondria, similar to the nucleus, have their own genome, called mitochondrial DNA (mtDNA). Human mtDNA is composed of double-stranded circular DNA molecules, with each strand having its own composition and encoding different ribonucleic acids (RNA). The guanine-rich strand encodes 14 tRNAs, 2 rRNAs, and 12 polypeptides, while the lighter strand has information to transcribe only 8 tRNAs and one polypeptide. In total, mtDNA consists of just 37 genes that encode 13 mRNA, giving rise to 13 proteins that are part of the electron transport system and the ATPase complex. The oxidative phosphorylation system is composed of 5 complexes (NADH-ubiquinone reductase complex (complex I); succinate dehydrogenase complex (complex II); ubiquinol-cytochrome c oxidoreductase (complex III); cytochrome-C oxidase complex (complex IV) and ATP synthase (complex V)), which form the respiratory chain.

mtDNA is much more susceptible to mutations when compared to the nuclear genome. Changes in mtDNA compromise the normal functioning of cells, mainly affecting neuronal and muscle tissues. The higher frequency of mutations in mtDNA can be explained by the fact that it does not have telomeres or introns in its constitution. Mitochondrial dysfunctions lead to the emergence of multisystem diseases, which can affect the normal functioning of the immune response, motor and brain function, and metabolic regulation and lead to aging. The vast majority of pathologies originating from mitochondria are inherited from maternal mtDNA. However, environmental factors such as stress and the consequent presence of reactive oxygen species, also contribute to the emergence of mutations in mtDNA. The most common mitochondrial diseases are Leber's hereditary optic neuropathy (LHON), mitochondrial encephalomyopathy, Pearson's syndrome, Parkinson's, Huntington's disease, Alzheimer's, and some types of cancer (breast, kidney, and colorectal).

Complex I of the mitochondrial respiratory chain is the main entry point for electrons into the electron transport chain. Due to this fact, this complex is very important in the normal functioning of mitochondria. It is in complex I that the transfer of electrons from

Nicotinamide Adenine Dinucleotide + Hydrogen (NADH) to ubiquinone occurs, the transport of protons across the inner mitochondrial membrane and is the main source of reactive oxygen species (ROS). Mutations in mitochondrial genes responsible for structural and assembly proteins of this complex lead to increased ROS production and loss of functions. One of these genes is the mitochondrial gene ND1 (NADH dehydrogenase 1). The mt-ND1 protein plays a crucial role in the structure of complex I. Mutations in mt-ND1 are associated with the emergence of LHON; Mitochondrial myopathy, encephalopathy, lactic acidosis, and stroke-like episodes (MELAS); progressive cardiomyopathy, and some types of cancer.

Data from 2020 revealed that 1 in every 250 people have mutations in mtDNA and that 1 in every 5,000 have serious pathologies associated with mitochondrial dysfunction. However, currently, the medications available on the market only serve to mitigate the symptoms. No drug approved by the FDA or in development has been able to cure or slow the progression of mitochondrial diseases. Although there are approaches such as the use of antioxidant agents and other drugs to alleviate symptoms, the ineffectiveness of current medications highlights the urgent need for more effective treatments. Mitochondrial gene therapy is a promising approach that can focus its action directly on the cause of mitochondrial diseases and develop therapies tailored to the type of mutation.

Gene therapy consists of the application of recombinant DNA techniques in which functional genes are used to replace defective genes and restore their normal functioning. As most mitochondrial diseases originate from mutations in mtDNA, mitochondrial gene therapy appears as a very promising strategy for treating this type of disease. Mitochondrial gene therapy makes it possible to attack the problem at its source and restore normal function to the affected mitochondrial gene. However, this type of therapy needs delivery systems that are effective in protecting and delivering genetic material to target cells/organelles. The greatest difficulty in applying gene therapy has been the development of nanocarriers that can effectively deliver genetic material. For mitochondrial gene therapy, the difficulty has been even greater, as the systems need to cross more barriers and be able to deliver only to that organelle. Thus, the main objective of this thesis is to develop delivery systems that have an affinity for mitochondria and can effectively deliver mitochondrial genes for the treatment of mitochondria-associated pathologies.

The work carried out consisted of the development of delivery systems based on peptides (cell-penetrating peptides (CPP)) and polymers (polyethylenimine (PEI)), to deliver the

mitochondrially encoded NADH dehydrogenase 1 protein (ND1) gene. To achieve this, these delivery systems were functionalized with ligands that allow specific targeting of mitochondria. The ligands used were triphenylphosphonium (TPP) and dequalinium chloride (DQA) to functionalize PEI and for CPP a mitochondrial targeting sequence (MTS) was used. The first step for the PEI-TPP/pND1 polymeric systems was to evaluate, through an experimental design, the optimal conditions for the formulation of nanoparticles. These systems were then characterized in terms of size, surface charge, and morphology. These delivery systems demonstrated the ability to internalize into cells and, through confocal microscopy, their preferential accumulation in mitochondria was demonstrated. Furthermore, these systems have demonstrated the ability to deliver the ND1 gene to mitochondria and lead to its transcription. The PEI-DQA/pND1 polymeric systems developed also demonstrated excellent physicochemical properties, showing the ability to transfect and internalize into cells. These nanocarriers delivered the ND1 gene directly into the mitochondria, leading to transcription of the gene of interest and production of the ND1 protein. However, the peptide-based systems (MTS-CPP) exhibited superior performance in terms of cellular internalization and targeting to mitochondria. Its greater ability to complex pND1 led to the formulation of nanoparticles with smaller sizes and consequently greater delivery of the gene of interest and protein expression. Showing better *in vitro* results, the MTS-CPP systems were tested in *in vivo* models (zebrafish embryos (ZF)). The peptide systems demonstrate the ability to internalize and distribute throughout the ZF organism, without causing any toxicity in these *in vivo* models.

In short, the work carried out during this doctoral thesis sought to find solutions to the lack of effective delivery systems in mitochondrial gene therapy, to make this therapy viable for the treatment of mitochondrial diseases. The results obtained during the thesis demonstrate that the delivery systems developed are very promising for the development of mitochondrial gene therapy protocols. This work contributed to progress and innovation in an area of research that is still little explored, such as mitochondrial gene therapy. In the case of peptide-based systems, these systems have the potential to be considered in future investigations, to evaluate their translation to the clinic. The nanocarriers developed during this thesis were optimized for the delivery of the mitochondrial ND1 gene, however, these systems can be easily adapted for the delivery of any mitochondrial genes that are involved in pathologies associated with mtDNA mutations.

Keywords

Cell-penetrating peptides; Gene delivery systems; Mitochondrial diseases; Mitochondrial gene therapy; Mutations in the mitochondrial genome; ND1 mitochondrial gene; Peptide nanocarriers; Polyethylenimine; Polymeric nanocarriers.

Funding

The experimental research developed in this doctoral thesis was supported by the funding attributed to author Rúben Faria (SFRH/BD/148393/2019), to collaborator Tânia Albuquerque (SFRH/BD/148406/2019) and to collaborator Ana Neves (2020.08310.BD) through individual PhD fellowships funded by FCT (Fundação para a Ciência e a Tecnologia); to supervisor Diana Costa through a FCT program contract (IF/01459/2015) and Researcher Contract (2021.03946.CEECIND); to supervisor Ângela Sousa through a Research Contract CEEC-INST/00016/2021/CP2828/CT0003 under the scope of the CEEC Institutional 2021, and the Project 2023.00136.RESTART funded by FCT; and to supervisor Prisca Boisguérin through "Agence Nationale de la Recherche, ANR-21-CE18-0022-01" and "Centre National de la Recherche Scientifique" (CNRS).

This thesis was also supported by:

- FCT (project FCOMP-01-0124-FEDER-041068 and FEDER funds through the POCI - COMPETE 2020 - Operational Program Competitiveness and Internationalisation in Axis I - Strengthening research, technological development and innovation (Project POCI-01-0145-FEDER-007491) and FCT (Project UID/Multi/00709/2019);
- CICS-UBI projects UIDB/00709/2020 and UIDP/00709/2020, financed by national funds through the Portuguese FCT/MCTES.
- Research grant (grant no. CRG/2018/001065) by Department of Science & Technology - Science and Engineering Research Board (DST-SERB);
- Synbio3 platform, which is supported by the GIS IBISA/ITMO Cancer (Plan Cancer 2014–2019) and Chimie Balard Cirimat Carnot Institute;

Index

List of Figures

List of Tables

List of Abbreviations

ADNmt	ADN mitocondrial
ADP	Adenosine diphosphate
ALS	Amyotrophic Lateral Sclerosis
ANOVA	Analysis of variance
ARN	Ácido ribonucleico
ATP	Adenosine triphosphate
CC	Complexation capacity
CLSM	Confocal laser scanning microscopy
CMC	Critical micelle concentration
CoQ10	Coenzyme Q10
CPP	Cell-penetrating peptides
CS	Chitosan
DCM	Dichloromethane
DLS	Dynamic Light Scattering
DMEM	Dulbecco´s Modified Eagle´s Medium
DMF	Dimethylformamide
DMSO	Dimethylsulphoxide
DNA	Deoxyribonucleic acid
DNAH	Dinucleótido de nicotinamida e adenina + Hidrogénio
DoE	Design of experiments
Dox	Doxorubicin
DQA	Dequalinium chloride
DQAsomes	Dequalinium-based liposome-like vesicles
ELS	Electrophoretic Light Scattering
ERO	Espécies reativas de oxigénio
ETS	Electron transport system
FBS	Fetal bovine serum
FITC	Fluorescein isothiocyanate
FTIR	Fourier-transform infrared
GFP	Green fluorescence protein
GPC	Gel permeation chromatography
HA	Human astrocyte
HEK	Human embryonic kidney
ITH	Heavy-strand transcription initiation site
ITL	Light-strand transcription initiation site
LHON	Leber's hereditary optic neuropathy
LNPs	Lipid nanoparticles

MELAS	Mitochondrial myopathy, encephalopathy, lactic acidosis, and stroke-like episodes
MEND	Multifunctional envelope-type nanodevices
MERRF	Myoclonus epilepsy and ragged red fibers
MPP	Mitochondrial Penetrating Peptide
mRNA	Messenger ribonucleic acid
mtDNA	Mitochondrial DNA
MTS	Mitochondrial targeting sequence
MTT	3-(4,5-Dimethylthiazol-2-yl)-2,5-diphenyltetrazolium bromide
NADH	Nicotinamide Adenine Dinucleotide + Hydrogen
ND1	Mitochondrially encoded NADH dehydrogenase 1 protein
NIBS	Non-invasive backscatter optics
NMR	Nuclear magnetic resonance
NOHL	Neuropatia ótica hereditária de Leber
OXPHOS	Mitochondrial oxidative phosphorylation system
PCR	Polymerase chain reaction
PDI	Polydispersity index
pDNA	Plasmid DNA
PEG	Polyethylene glycol
PEI	Polyethylenimine
PFA	Paraformaldehyde
pGFP	Plasmid DNA encoding green fluorescent protein
PLGA	Poly (lactic-co-glycolic acid)
PMDs	Primary mitochondrial diseases
PNAs	Peptide nucleic acids
pND1	Plasmid pCAG-GFP-ND1
PPC	Péptidos de penetração celular
PTU	1-phenyl 2-thiourea
PZ	Peixe-zebra
RBCs	Red blood cells
RNA	Ribonucleic acids
ROS	Reactive oxygen species
rRNA	Ribosomal ribonucleic acid
RT-PCR	Reverse transcription polymerase chain reaction
SEM	Scanning electron microscopy
SPPS	Solid-phase peptide synthesis
TFA	Trifluoroacetic acid
TIM	Mitochondrial inner membrane
TOM	Mitochondrial outer membrane
TPP	Triphenylphosphonium
tRNA	Transfer ribonucleic acid

UV	Ultraviolet
W1	WRAP1
W5	WRAP5
ZF	Zebrafish
$\Delta\Psi m$	Mitochondrial membrane potential

List of Scientific Publications

Scientific articles & book chapters included in the Thesis

•Faria R, Vivès E, Boisguérin P, Descamps S, Sousa Â, Costa D. Upgrading Mitochondria-Targeting Peptide-Based Nanocomplexes for Zebrafish *In Vivo* Compatibility Assays. Pharmaceutics. 2024; 16(7):961.
https://doi.org/10.3390/pharmaceutics16070961

• Faria R, Boisguérin P, Sousa Â, Costa D. Delivery Systems for Mitochondrial Gene Therapy: A Review. Pharmaceutics. 2023; 15(2):572.
https://doi.org/10.3390/pharmaceutics15020572

• Faria R, Albuquerque T, Neves AR, Sousa Â, Costa D. Nanotechnology to Correct Mitochondrial Disorders in Cancer Diseases. Cancer Nanotechnology. Springer, Cham. 2023; 179-203.
https://doi.org/10.1007/978-3-031-17831-3_6

• Faria R, Paul M, Biswas S, Vivès E, Boisguérin P, Sousa Â, Costa D. Peptides vs. Polymers: Searching for the Most Efficient Delivery System for Mitochondrial Gene Therapy. Pharmaceutics. 2022; 14(4):757.
https://doi.org/10.3390/pharmaceutics14040757

• Faria R, Vivés E, Boisguérin P, Sousa Â, Costa D. Development of Peptide-Based Nanoparticles for Mitochondrial Plasmid DNA Delivery. Polymers. 2021; 13(11):1836.
https://doi.org/10.3390/polym13111836

• Faria R, Albuquerque T, Neves AR, Bhatt H, Biswas S, Cardoso AM, Lima MP, Jurado AS, Costa D. Physicochemical characterization and targeting performance of triphenylphosphonium nano-polyplexes. Journal of Molecular Liquids. 2020; 316.
https://doi.org/10.1016/j.molliq.2020.113873

• Sousa Â, Faria R, Albuquerque T, Bhatt H, Biswas S, Queiroz JA, Costa D. Design of experiments to select triphenylphosphonium-polyplexes with suitable physicochemical properties for mitochondrial gene therapy. Journal of Molecular Liquids. 2020; 302.
https://doi.org/10.1016/j.molliq.2020.112488

Scientific articles & book chapters not included in the Thesis

• Neves AR, Albuquerque T, Faria R, Santos C, Vivès E, Boisguérin P, Carneiro D, Bruno DF, Pavlaki MD, Loureiro S, Sousa Â, Costa D. Evidence That a Peptide-Drug/p53 Gene Complex Promotes Cognate Gene Expression and Inhibits the Viability of Glioblastoma Cells. Pharmaceutics. 2024; 781.
https://doi.org/10.3390/pharmaceutics16060781

• Faria R, Neves AR, Costa D. Bioinspired drug delivery therapeutics. Novel Formulations and Future Trends: Recent and Future Trends in Pharmaceutics, Volume 3. Academic Press. 2024; 565-592.
https://doi.org/10.1016/B978-0-323-91816-9.00008-4

• Eusébio D, Albuquerque T, Neves AR, Faria R, Ventura C, Ferreira M, Sousa Â, Costa D. Drug delivery for bone tissue engineering. Advanced and Modern Approaches for Drug Delivery. 2023; 783-815.
https://doi.org/10.1016/B978-0-323-91668-4.00008-3

• Neves AR, Faria R, Biswas S, Costa D. Plant polysaccharides in formulation coating. Plant Polysaccharides as Pharmaceutical Excipients. 2023; 391-413.
https://doi.org/10.1016/B978-0-323-90780-4.00010-3

• Albuquerque T, Neves AR, Faria R, Quintela T, Costa D. Chronobiology and Nanotechnology for Personalized Cancer Therapy. Cancer Nanotechnology. Springer, Cham. 2023; 205-227.
https://doi.org/10.1007/978-3-031-17831-3_7

• Neves AR, Albuquerque T, Faria R, Gonçalves AM, Santos C, Vivès E, Boisguérin P, Passarinha LA, Sousa Â, Costa D. Development of WRAP5 Peptide Complexes for Targeted Drug/Gene Co-Delivery toward Glioblastoma Therapy. Pharmaceutics. 2022; 14(10):2213.
https://doi.org/10.3390/pharmaceutics14102213

• Neves AR, Faria R, Albuquerque T, Quintela T, Sousa Â, Costa D. Future perspectives of biological macromolecules in biomedicine. Biological Macromolecules. 2022; 607-632.
https://doi.org/10.1016/B978-0-323-85759-8.00026-9

• Neves AR, Albuquerque T, Faria R, Paul M, Biswas S, Sousa Â, Costa D. Development of Tailor-Made Dendrimer Ternary Complexes for Drug/Gene Co-Delivery in Cancer. Pharmaceutics. 2021; 13(8):1256.
https://doi.org/10.3390/pharmaceutics13081256

• Costa D, Sousa Â, Faria R, Neves AR, Queiroz JA. Conception of Plasmid DNA and Polyethylenimine Delivery Systems with Potential Application in DNA Vaccines Field. DNA Vaccines. Methods in Molecular Biology. 2021; 271-284.
https://doi.org/10.1007/978-1-0716-0872-2_15

• Albuquerque T, Faria R, Sousa Â, Neves AR, Queiroz JA, Costa D. Polymer-peptide ternary systems as a tool to improve the properties of plasmid DNA vectors in gene delivery. Journal of Molecular Liquids. 2020; 309.
https://doi.org/10.1016/j.molliq.2020.113157

• Neves AR, Sousa Â, Faria R, Albuquerque T, Queiroz JA, Costa D. Cancer gene therapy mediated by RALA/plasmid DNA vectors: Nitrogen to phosphate groups ratio (N/P) as a tool for tunable transfection efficiency and apoptosis. Colloids Surf B Biointerfaces. 2020; 185.
https://doi.org/10.1016/j.colsurfb.2019.110610

• Sousa A, Almeida AM, Faria R, Konate K, Boisguérin P, Queiroz JA, Costa D. Optimization of peptide-plasmid DNA vectors formulation for gene delivery in cancer therapy exploring design of experiments. Colloids Surf B Biointerfaces. 2019; 183.
https://doi.org/10.1016/j.colsurfb.2019.110417

Chapter 1

This chapter was partly published in:
Rúben Faria, Prisca Boisguérin, Ângela Sousa, and Diana Costa. 2023. 'Delivery Systems for Mitochondrial Gene Therapy: A Review', Pharmaceutics, 15
https://doi.org/10.3390/pharmaceutics15020572

Introduction

1.1 Mitochondria

Mitochondria are small organelles present in eukaryotic cells that play a key role in maintaining cellular activity through intracellular signaling and energy production processes. These multifunctional organelles adapt their role depending on the cells in which they are present, having specific functions in different cell types[1]. Mitochondria are the engines of cells, as they are responsible for about 90% of the energy that is produced in each cell. Through the mitochondrial oxidative phosphorylation system (OXPHOS), the oxidative phosphorylation of glucose occurs in the mitochondria, which gives rise to energy in the form of adenosine triphosphate (ATP) molecules[2]. In addition to its energetic function, mitochondria are involved in a wide range of biological processes within the cell, namely in amino acid metabolism, protein synthesis, gluconeogenesis, fatty acid oxidation, generation of reactive oxygen species (ROS), ions and calcium homeostasis and initiation of apoptotic cascade[3-5]. In addition, mitochondria play a fundamental role in oxidative stress situations, endoplasmic reticulum stress, and stress due to the lack of nutrients that are involved in the origin of DNA and RNA molecules and the processes of transcription correction[6]. These organelles, with a size of around 1 micron, can be found in large numbers (1,000 to 2,000) in the cytoplasm of eukaryotic cells[7].

Mitochondria have their own DNA allowing their reproduction without the need for outside stimuli. These unique characteristics tend to prove the bacterial origin of this cell organelle. Despite having their own genome, many of the mitochondrial genes were passed to the nucleus, still maintaining a small number of genes that encode essential and exclusive proteins. Among these proteins expressed, only in the mitochondrial matrix, are the four enzymes of the OXPHOS complex: NADH-ubiquinone reductase complex (complex I); succinate dehydrogenase complex (complex II); ubiquinol–cytochrome c oxidoreductase (complex III) and cytochrome-C oxidase complex (complex IV)[8].

Mitochondria are formed by an outer and an inner membrane in which the two membranes are composed of phospholipids where several proteins and enzymes are found[9]. The outer membrane is formed by a lipid bilayer that allows the passage of small molecules and ions, due to the presence of porins[10]. This membrane has the function of maintaining the structural integrity of mitochondria and providing protection. Furthermore, it is involved in the import of

proteins encoded in the nucleus through its protein translocator complexes and has an important role in the regulation of apoptosis, becoming permeable to apoptotic factors such as cytochrome c, which is released into the cytosol of cells and initiates the apoptotic cascade[11, 12]. The inner mitochondrial membrane is made up of numerous folds, called cristae, where the electron transport chain is located and where oxidative phosphorylation occurs. The inner membrane is impermeable to ions and small molecules, being essential to maintain the electrochemical proton gradient[13].

The mitochondrial membrane potential (ΔΨm) generated in the inner of the mitochondrial membrane results from the action of proton pumps in complexes I, III, and IV of the electron transport chain, which transport protons (H+) from the interior of the mitochondria (mitochondrial matrix) to the intermembrane space[14]. The electrical potential that is established in the mitochondrial membrane has implications in the process of oxidative phosphorylation and the respective production of energy in the form of ATP molecules. The electrical potential is also important in the maintenance of mitochondrial and cellular homeostasis and in the transport of ions and proteins essential to the normal functioning of this organelle[15]. The constant and/or permanent changes in ΔΨm can lead to the appearance of neurodegenerative and metabolic diseases and cancer, being one of the essential parameters for identifying dysfunctional mitochondria that are eliminated through a process called mitophagy[16, 17].

1.2 Mitochondrial genome

The mitochondrial genome consists of circular double-stranded deoxyribonucleic acid (mitochondrial DNA, mtDNA), a structural feature shared with bacterial plasmids, providing evidence of the bacterial origin of mitochondria [18]. Mitochondria evolved from proteobacteria, and throughout this evolution, these organelles had significant changes in their genome, where there was a significant gain of new genes and the loss and transfer of others to the nuclear genome. This transition led to changes in the mitochondrial proteome and the development of additional roles in both the metabolism and biosynthetic pathways, forming a specialized organelle for ATP production[19, 20].

The human mitochondrial genome is made up of only 37 genes that encode 13 messenger ribonucleic acids (mRNAs), which in turn are translated into 13 proteins. It also presents 22 transfer ribonucleic acid (tRNA) and 2 ribosomal ribonucleic acid (rRNA) molecules (12S and 16S) in its constitution[21]. However, to control the expression of mitochondrial genes, the intervention of proteins originating in the nucleus is also necessary, which causes this regulation to have two origins, namely mitochondrial RNAs and nucleus proteins. Most of the proteins necessary for the role of the mitochondria are encoded by the nucleus, being later synthesized in the cytoplasm, and imported into the mitochondria. To control their energy metabolism, mitochondria regulate the synthesis of their RNAs, which in turn determine the steady state of mitochondrial proteins[22, 23].

Each strand of double-stranded mtDNA has a different composition. The lighter chain only contains the information to transcribe 8 tRNAs and a polypeptide, while the guanine-rich chain

contains information to encode 14 tRNAs, 2 rRNAs, and 12 polypeptides[24]. The 13 polypeptides encoded by mtDNA give rise to 11 polypeptide constituents of the electron transport system (ETS) and 2 polypeptides of the ATPase complex. [22, 25]. In the NADH-ubiquinone reductase complex (complex I), there are 7 polypeptides encoded by the mitochondrial genome (subunits ND1, ND2, ND3, ND4, ND4L, ND5, and ND6). In the succinate dehydrogenase complex (complex II) there are 4 subunits encoded by nuclear genes (SDHA, SDHB, SDHC, and SDHD). In the ubiquinol–cytochrome c oxidoreductase (complex III), only cytochrome b is encoded by mtDNA[25]. The cytochrome-C oxidase complex (complex IV) consists of three mtDNA encoded subunits (MT-CO1, MT-CO2, and MT-CO3)[26]. The ATP synthase complex (complex V) has two subunits (ATP6, ATP8) issued from mitochondrial genes[27]. The OXPHOS system has ATP and water as final products, where the oxidation of NADH and FADH2 will generate electrons that are transferred through the respiratory chain (complexes I-IV) to oxygen. This transfer creates an electrochemical gradient that is used by ATP synthase to generate ATP molecules[28]. The OXPHOS system is represented in **Figure 1.1**.

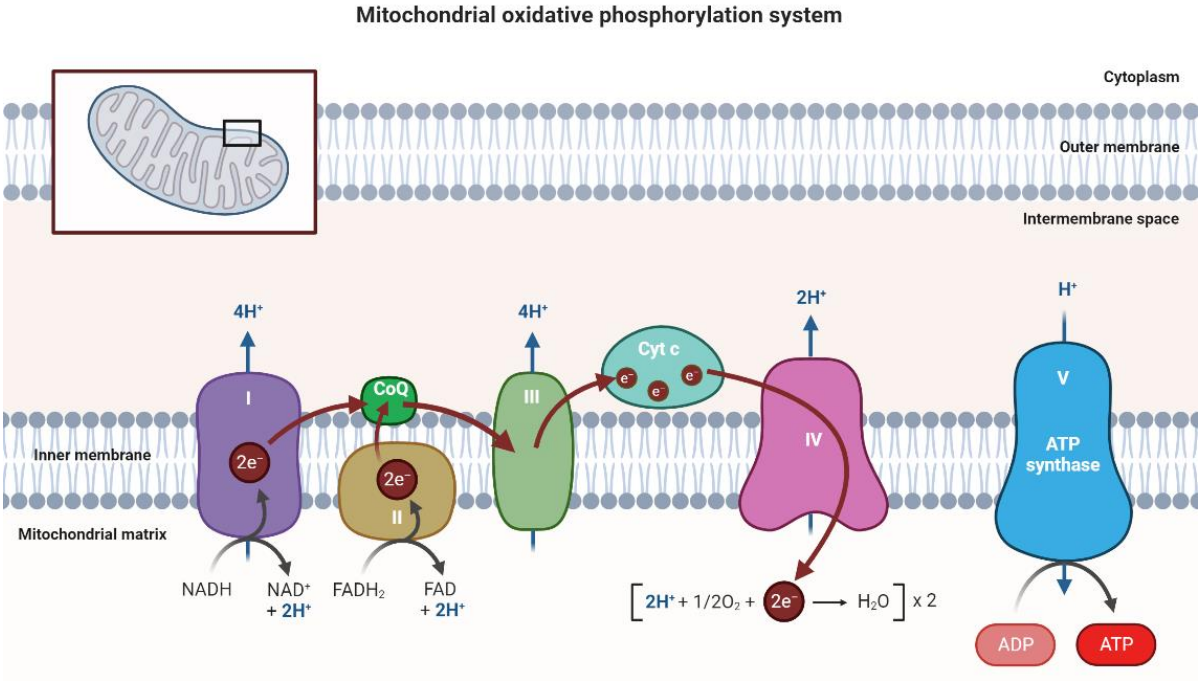

Figure 1.1 - Schematic representation of the OXPHOS system composed of five large complexes and functional proteins such as CoQ and Cyt c located in the inner mitochondrial membrane, where the flow of electrons and protons through the respiratory chain is observed and where ATP synthesis occurs. ADP: adenosine diphosphate; Cyt: cytochrome c oxidase; CoQ: Coenzyme Q; NADH: nicotinamide adenine dinucleotide (NAD) + hydrogen (H); FADH2: Flavin adenine dinucleotide. Image created at BioRender.com.

The mtDNA also has a region called the regulatory region, a non-coding region that is essential for the transcription of the genome and its replication. In this non-coding part, L-and-H strand promoters (light-strand transcription initiation site (ITL) and heavy-strand transcription initiation site (ITH), respectively) and 2 putative origins of replication (origins of leading (O_H) and lagging (O_L) strand replication) are present, from which mitochondrial transcription is initiated. This transcription process is carried out by the DNA-dependent RNA polymerase where the respective cofactors must be present[29].

The fact that mtDNA lacks both telomeres and introns makes it more susceptible to mutations when compared to the nuclear genome[18]. Alterations that compromise the normal expression of mtDNA can result in a multisystemic disease phenotype derived from the disturbance of the respiratory chain, mainly affecting neuronal and muscular tissues[22]. In recent years, several studies have shown that biochemical and genetic changes in mitochondria lead to the emergence of multisystemic diseases[30]. Research in animals has revealed that mitochondrial mutations have a direct influence on the immune response[31], metabolic regulation[32], brain function[33], and the aging rate and lifespan[34, 35].

1.3 Mitochondrial mutations and associated diseases

The full understanding of the origin of many mitochondrial diseases remains a mystery today. However, it is known that deregulated mechanisms and interactions will unbalance normal mitochondrial functioning. The maintenance of mitochondrial function depends on several processes, namely the correct assembly of the OXPHOS system as well as the regulation and control of protein importation and degradation in general. The coordinated interaction between the mitochondrial and the nuclear genome, the mechanisms for controlling replication, transcription, translation, and the correct functioning of DNA repair systems are other essential processes. Thus, these mechanisms are potential targets for understanding the origin of unknown mitochondrial dysfunctions[36].

Metabolic disorders resulting from changes that occur in genes regulating mitochondrial function are called primary mitochondrial diseases (PMDs)[37]. These types of diseases are characterized by having different origins and depending on the affected gene can result in multiple metabolic disorders. These disturbances in mitochondrial function and structure will compromise its normal activity, namely the processes of oxidative phosphorylation, mitochondrial fission and fusion, and the process of ion transport across the mitochondrial membrane. Both mtDNA and nuclear DNA mutations can give rise to PMDs and cause mitochondria-associated metabolic changes[38]. Due to the presence of mitochondria in almost every type of organ in the human body, PMDs rarely involve just a single tissue. PMDs can affect many organs and the age factor does not seem to have an influence [39].

Mutations in mtDNA occur at a much higher frequency than mutations in nuclear DNA. These mutations result from errors during the replication, and these errors often remain uncorrected. Mutations in mtDNA can also be transmitted by maternal mtDNA, arise from antecedent mutations in nuclear DNA, or result from environmental factors[40]. One of the cases of

environmental factors is stress, which causes overexpression of reactive oxygen species (ROS). ROS are produced during the process of oxidative phosphorylation by the OXPHOS system. However, their production is at low levels and their presence is fundamental in physiological functions. Increased ROS levels can cause numerous mutations in mtDNA since they are produced within the mitochondria with high proximity to the genetic material [41]. The fact that mtDNA lacks protective histones, also makes it more susceptible to mutations caused by ROS[42]. Elevated levels of ROS in situations where antioxidant enzymes are reduced can result in changes in both proteins and lipids and in the mtDNA itself, leading to the appearance of mitochondrial dysfunction. In extreme cases, mutations caused by ROS can alter the OXPHOS system and lead to the production of even more ROS, causing successive changes in mitochondrial metabolism and inducing a decrease in ATP production, loss of cell communication, rupture of the mitochondrial membrane, and consequent apoptosis[43].

Other recurrent factors for mitochondrial deregulation are the mutations that occur simultaneously in the mitochondrial genome, and in genes of nuclear origin that influence mitochondrial metabolism. These mutations, when they appear in genes encoding proteins essential for the synthesis of ATP molecules, lead to the degradation of cells due to lack of energy and, consequently, contribute to the appearance of diseases of mitochondrial origin in the various organs of the human body. These mutations can also interfere with the normal functioning of the OXPHOS system, alter tissue specificities of different organs and alter metabolite homeostasis[44].

The heteroplasmy occurs with high frequency in mitochondria and plays a crucial role in the heterogeneity of clinical manifestations that mtDNA mutations can cause. Mitochondrial heteroplasmy is the name given to the coexistence of mutated mtDNA with wild-type mtDNA in the same cell[45]. This coexistence arises due to the high rate of mutations that occur during mtDNA replication, which together with the fact that mtDNA replicates independently of the cell cycle, leads to the replication of thousands of mtDNA molecules with somatic changes. As mtDNA can be segregated during replication also contributes to mitochondrial heteroplasmy, causing levels of heteroplasmy that change from cell to cell and throughout the lifespan in mitotic and post-mitotic cells[46]. Heteroplasmy levels are critical for maintaining homeostasis in mitochondria. Increased heteroplasmy leads to the onset and worsening of mitochondrial dysfunction, contributing to the loss of regulatory mechanisms present in mitochondria that interfere with cell metabolism and signaling pathways. Furthermore, high levels of heteroplasmy lead to the accumulation of dysfunctional mitochondria with a loss of membrane potential, resulting in increased reactive oxygen species (ROS) production [47]. Thus, it can be stated that the onset and/or severity of mitochondrial diseases is dependent on the type and number of mutations and the rate of heteroplasmy present in the cells. For many mitochondrial diseases, clinical manifestations appear when a certain percentage of mutated mtDNA (typically between 60% and 90%) is reached. However, this threshold can vary depending on the cell type, tissue energy demand, and mutation type, and some mitochondrial disorders do not strictly follow this threshold rule. Mitotic and meiotic cell division can also alter the levels of heteroplasmy in cells,

which means that the speed with which phenotypic changes appear depends on the ability of the cell or tissue to replicate[46].

Pathologies originating in the mitochondria arise, in most cases, from mutations that are inherited from the mother, resulting in dysfunctions in oxidative energy metabolism. However, there are also somatic mutations in mtDNA, and these modifications in the mitochondrial genome are at the origin of aging, neurodegenerative diseases, and cancer[48]. One of the changes that most contributes to the appearance of disturbances in the normal functioning of mitochondria are point mutations. This type of mutation consists of alterations of nitrogenous bases in mtDNA genes (tRNALeu(UUR), tRNALys, and ATP6 are the most common) and gives rise to diseases such as mitochondrial encephalopathy, stroke-like episodes (MELAS), myoclonus epilepsy and ragged red fibers (MERRF) syndrome[48]. Beyond point mutations, mtDNA deletions can occur, which result in a loss of part of the mitochondrial genome. The elimination of essential genetic information leads to the appearance of Pearson's syndrome, Kearns Sayre syndrome, and chronic progressive external ophthalmoplegia. This type of mtDNA change has no maternal origin and appears randomly in mtDNA molecules, which means that the mutation occurs in early embryogenesis or the germ line of the mother. The incidence of point mutations in mtDNA occurs more frequently in mitotic cells, whereas deletion mutations appear to a greater extent in postmitotic cells[49].

Several mutations in mitochondrial genes trigger the appearance of pathologies (**Figure 1.2**). In the case of type II diabetes, mutations in the mitochondrial genes ND1, ND3, and ATP6 are reported to be associated with this disease[50-52]. Mutations in the ND1 gene are also associated with the onset of Leber's hereditary optic neuropathy (LHON) syndrome[53, 54]. In the work published by Smolina and coworkers, 6 mutations in the Desmin gene (DES) that are associated with skeletal and Desmin myopathies were identified[55]. Mitochondrial encephalomyopathies are also associated with a mutation in the ATP6 gene[56]. In neurodegenerative diseases, mitochondrial mutations are also found to contribute to the onset of diseases. For example, in amyotrophic lateral sclerosis and associated frontotemporal dementia, mutations in the C9orf72/TARDBP genes have been identified[57]. Huntington's, Alzheimer's, and Parkinson's diseases are other neurodegenerative pathologies associated with mitochondrial dysfunction[58]. In the case of Parkinson's, a mutation (A10398G) was identified in the ND3 gene, while in Alzheimer's disease, there is a mutation in the mitochondrial ATP6 gene[59, 60]. Mutations in mtDNA can also cause myoclonic epilepsy with irregular red fibers (MERRF)[61], strokes and encephalopathies (MELAS syndrome)[62], obesity[63], and are also involved in the onset of cancer[64].

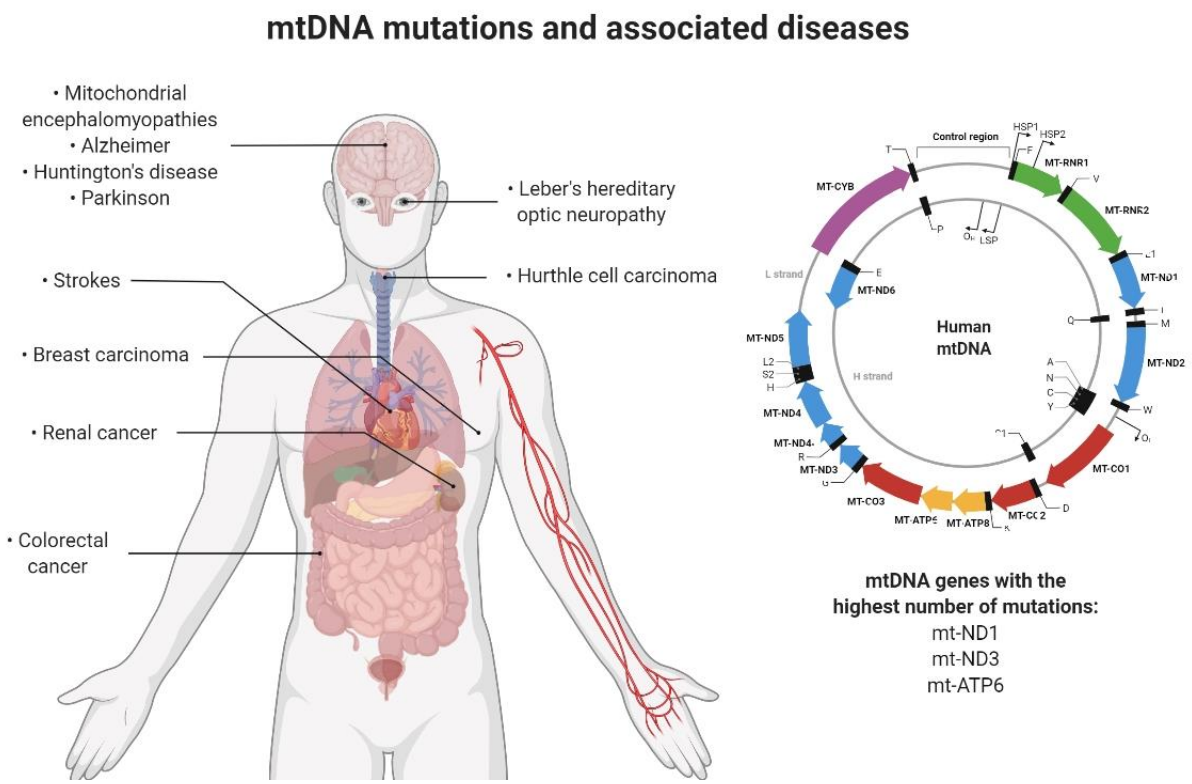

Figure 1.2 - Illustration of the mitochondrial genome with a focus on the mitochondrial genes that suffer the greatest number of mutations (ND1, ND3, and ATP6) and the organs/tissues affected by these mutations and their associated diseases. Image created at BioRender.com.

In recent years, a huge number of mutations in mtDNA have been discovered that are associated with the appearance of different types of cancer. For example, Ganly *et al.* reported mutations in virtually every mtDNA protein-coding gene, mutations identified in patients with Hurthle cell carcinoma[65]. Hurthle cell carcinoma is a type of tumor within the thyroid gland, and its appearance is associated with mutations in mtDNA, namely mutations in the ATP6 gene (Atp6-K90E) and deletions in several genes of complex I of the respiratory chain[66, 67]. In cancers of the digestive system, four mutations were identified in the mtDNA genome (11719A/12705T/15043A/15301A)[68], while in invasive lobular breast carcinoma, a mutation was identified in the mitochondrial gene COX3[69] and in breast cancer, the mutation "8584G>A" was identified in the gene ATP6[70]. The mitochondrial gene ND1 is involved in several types of cancer when it undergoes a mutation identified as "C3572ins", namely in renal cancer, thyroid carcinoma, oncocytic pituitary adenoma, and invasive ductal breast carcinoma[64, 69, 71, 72]. The mutated mitochondrial genes and their associated diseases are summarized in **Table 1.1**.

Table 1.1 - Summary of mitochondrial genes affected by mutations and the associated diseases.

Mutated mitochondrial gene	Associated disease	Reference
ND1	Type II diabetes	[51]
	Leber's hereditary optic neuropathy (LHON)	[53]
	Leigh's syndrome	[73]
	Progressive cardiomyopathy	[74]
	Neurodevelopmental delay	[75]
	Sensorineural hearing loss	
	Renal cancer	[64]
	Thyroid carcinoma	[69]
	Oncocytic pituitary adenoma	[71]
	Breast carcinoma	[72]
ND3	Type II diabetes	[52]
	Parkinson's disease	[59]
ND5	Invasive ductal breast carcinoma	[69]
ATP6	Type II diabetes	[50]
	Mitochondrial encephalomyopathies	[56]
	Alzheimer's disease	[60]
	Hurthle cell thyroid carcinoma	[65]
	Breast cancer	[70]
Desmin	Desmin myopathies	[55]
	Skeletal myopathy	
C9orf72/TARDBP	Frontotemporal dementia	[57]
	Amyotrophic lateral sclerosis	
COXIII	Invasive lobular breast carcinoma	[69]

1.4 Mutations of the mitochondrial ND1 gene and associated diseases

Complex I is the major entry point for electrons to the electron transport chain, being considered as a limiting step in overall respiration and energy production. In mitochondria, it catalyzes the transfer of electrons from NADH (ubiquinone oxidoreductase chain) to ubiquinone and translocates protons across the inner mitochondrial membrane. Along with complex III, it is also regarded as the main source of reactive oxygen species[76]. A deficiency in this complex can be attributed to a mutation affecting either a structural subunit or an assembly protein, to an increase in its ROS production, or both[77]. Mitochondrial DNA encodes 7 subunits of this enzyme complex, which are involved in proton translocation and ubiquinone binding. This represents roughly half of all mitochondrial genomes. Thus, it is expected that the activity of Complex I would be the most affected between other mitochondrial enzyme complexes.

Among these, the mt-ND1 (NADH-1) (**Figure 1.3**) has been shown to play a crucial role in the assembly of subunits in complex I[78]. Mitochondrial point mutations in ND1 have first been described in association with two distinct clinical phenotypes, LHON and MELAS[79-81]. Indeed, different point mutations occurring in mitochondrial genes might have variable phenotypes, which clinically can be difficult to diagnose. Moreover, mt-ND1 mutations have been associated with a few cases of adult-onset dystonia[82], hearing loss[83], fatal infantile mitochondrial encephalopathies such as Leigh's syndrome[73], progressive cardiomyopathy[74], among others. More recently, some studies have indicated a correlation between some mutations in the mtDNA and cancer states[64, 70].

Conventional clinical practices regarding mitochondrial respiratory chain dysfunction are sparse and very limited. Current treatment includes symptom-based management options, such as energy fuel supplements, oxidants, cofactors, and vitamins[84]. These focus on improving quality of life and mitigating the set of symptoms, being largely supportive rather than curative. Therefore, there is a clear requirement for innovative therapeutics.

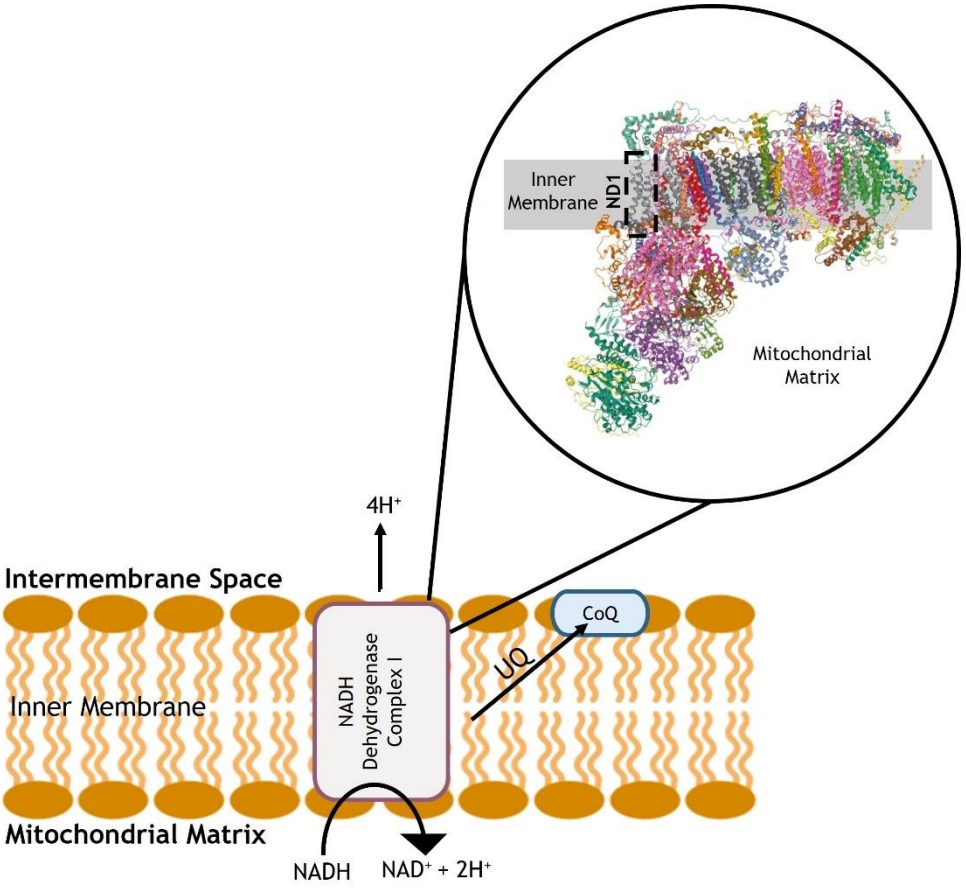

Figure 1.3 - NADH dehydrogenase complex I ND1 subunit.

1.5 Conventional treatments for mitochondrial dysfunctions

Recent research has shown that mtDNA mutations are present in one in 250 people with at least one in 5,000 suffering from severe disease. Currently, the drugs available on the market for mitochondrial diseases are very limited and only serve to mitigate the symptoms[85]. Of all the FDA-approved options and the multiple strategies that have been studied in recent years, no drug has managed to provide a cure or slow the progression of mitochondrial diseases. Clinical trials in recent years aimed at the development of new drugs for the treatment of mitochondrial diseases do not exceed 100 and very few reach Phase III. The ones reaching stage III demonstrate the potential to improve patient's quality of life by relieving symptoms caused by changes in mitochondria, but none can provide an effective cure[86].

The complexity of mitochondrial disorders and the heterogeneity of clinical manifestations lead to several approaches for the development of new mitochondrial therapies. One of the strategies studied is the use of antioxidants to reduce the toxicity caused by high levels of ROS formed in certain mitochondrial diseases. Among these, lipoic acid is particularly notable, as it acts as a cofactor in several dehydrogenases, including pyruvate dehydrogenase, branched-chain amino acid dehydrogenase, and α-ketoglutarate dehydrogenase[87]. Lipoic acid is administered together with other antioxidants, such as CoQ10 and creatine monohydrate, demonstrating the ability to decrease the levels of oxidative stress markers and muscle strength restoration in individuals diagnosed with mitochondrial diseases[88, 89]. Regulation of ROS levels can also be achieved indirectly, by administering cysteine to patients in whom glutathione levels are decreased due to mitochondrial disturbances. Glutathione is an antioxidant present inside cells whose synthesis depends on the presence of cysteine[90]. Another approach using vitamins C and E as antioxidants was tested in combination with other drugs but did not show promising results[90].

In patients with myopathy and mitochondrial encephalopathy, creatine monohydrate is administered to improve their quality of life. Creatine in the presence of phosphate creates phosphocreatine, which is essential in the process of releasing energy in tissues that need high amounts of energy such as the brain and muscles. In these patients, phosphocreatine levels are compromised, and the administration of creatine monohydrate improves motor skills and brain function[91, 92]. In patients diagnosed with dilated cardiomyopathy and skeletal myopathy, there is a change in the functioning of the mitochondrial respiratory chain and consequently in the production of ATP[93]. In these cases, the use of the synthetic peptide MTP-131 makes it possible to regulate the functioning of cardiolipin, a phospholipid essential for the structure of the inner membrane of the mitochondria and the correct functioning of the respiratory system[94, 95]. The binding of MTP-131 to cardiolipin improves the flow of electrons in the electron transport chain, which could lead to an increase in ATP production in these patients[96]. The benzoquinone idebenone compound (2,3-dimethoxy-5-methyl-6-(10-hydroxydecyl)-1,4-benzoquinone) was used in LHON patients and its administration was shown to be effective in protecting patient's

eyesight. The use of idebenone prevented the development of dyschromatopsia and the loss of the ability to see colors in patients with LHON[97].

The presented examples, among others available in the literature[98-100], demonstrate the inefficacy of the currently available drugs for the treatment of mitochondrial diseases. Therefore, there is an urgent need for more effective treatments/approaches that may solve the problem at the root, bringing hope to the millions of patients worldwide suffering from mitochondrial disorders. One of the approaches that can be explored is the use of mitochondrial gene therapy since it allows us to act directly on the origin of the problem and develop new personalized therapies for each case, using therapeutic genetic material.

1.6 Nanotechnology in mitochondrial gene therapy

1.6.1 Mitochondrial gene therapy

The development of nanotechnology has allowed the conception/emergence of new therapies, one of them being gene therapy. Gene therapy is based on the use of recombinant DNA techniques with functional genes to replace defective genes and consequently treat associated diseases[101]. This type of therapy can be used to especially treat diseases originating in monogenetic changes or when mutations are well identified[102]. Many dysfunctions that occur in mitochondria come from mutations in their genome, thus gene therapy emerges as a very promising approach to the treatment of mitochondrial diseases. Mitochondrial gene therapy arises from the need to find treatments for mitochondrial dysfunctions, as the solutions available on the market only serve to alleviate the symptoms and do not provide an effective cure[103]. The main advantage of this approach, to conventional treatments, is that it focuses the problem on its origin replacing the mutated mitochondrial gene and restoring mitochondria function. In addition, mitochondrial gene therapy is a technique with reduced costs that can provide continuous treatment in time on target cells[104].

Although most mitochondrial diseases in adults result from mtDNA mutations, alterations in nuclear genes that directly affect mitochondrial metabolism are the primary cause of mitochondrial dysfunction in children [37, 105]. Thus, nucleus targeting has been explored to correct mitochondrial disorders. The application of indirect mitochondrial gene therapy aims at the translation of a protein originating from the genes transferred to the nucleus that is later imported into the mitochondria, reestablishing its normal function. One example is mitochondrial dysfunction cardiomyopathy, where a mutation in the adenine nucleotide translocator 1 gene alters a protein in the inner membrane of the mitochondria and affects the exchange of adenosine diphosphate (ADP) and ATP[106]. Reyes *et al.* demonstrated that a mutation in the RNASEH1 gene compromises mtDNA replication, affecting several complexes of the respiratory chain, and consequently the metabolic activity of mitochondria. This mutation affects mtDNA integrity and can lead to chronic progressive external ophthalmoplegia[107].

Gene therapy requires exogenous DNA to reach target cells. Physical, chemical, and biological methods have been explored in recent years to assess which approach is more convenient for each

situation. Physical methods were the first approaches considered for the delivery of genetic material. These methods do not use carrier molecules for gene delivery. The advantages of these techniques are that transfection is not dependent on the ability of transporters to internalize cells and, therefore, there are no biocompatibility concerns related to the materials used in the conception of the delivery vectors. Despite this, physical methods can destroy the membrane of target cells as they are more invasive[108]. In this regard, the most used techniques are microinjections and bioballistics. Microinjections consist of introducing genetic material with the help of a micropipette. However, this procedure requires a lot of experience and technique to avoid the bursting of the cell membrane. The bioballistic technique uses air pressure to project complexes of nucleic acids that are normally coated with metals[109]. Other physical methods are emerging to overcome the disadvantages of these invasive techniques, which are the case of electroporation[110], optoporation[111], sonoporation[112], and magnetoporation techniques [113]. These techniques aim to internalize the exogenous genetic material in cells through physical forces, being much less invasive and for many of them, there is no contact with the cell membrane[108].

Physical methods have been used for mitochondrial gene therapy as described by Bonnefoy and Fox[114]. These researchers demonstrated the use of a helium shock wave to accelerate metal particles coated with DNA for the internalization in *Saccharomyces cerevisiae* cells. A low percentage of cells that survived this bioballistic technique was shown to have taken up exogenous DNA[114]. The use of injections as a technique for mitochondrial gene therapy was analyzed by Yasuzaki *et al.*[115]. By creating an artificial mitochondrial DNA vector with a mitochondrial promoter and a reporter gene, Yasuzaki demonstrated the possibility of delivering genes without the interference of any carrier molecule. The plasmid was injected directly into rat liver mitochondria *in vivo* by hydrodynamic injection and the exogenous mRNA was identified by polymerase chain reaction (PCR) technique. Afterward, the corresponding reporter protein was expressed in the liver and skeletal muscle[115].

Although physical methods have some ability to internalize DNA into mitochondria, the success rate is limited. This fact instigates the development of other approaches that could bypass mitochondrial membranes. The most promising and most explored method is the chemical one, since it meets the characteristics of mitochondrial and cell membranes. This method requires a cationic carrier that allows exogenous DNA to pass through the membranes, as both entities are negatively charged and would repel each other (**Figure 1.4**). Before reaching the outer membrane of the mitochondria, the developed systems must be able to bypass the cell membrane and/or the endosomes after an endocytosis-dependent internalization. Another aspect to consider is that mitochondrial membranes are hydrophobic, so the carrier molecules must have amphiphilic properties to penetrate membranes[116].

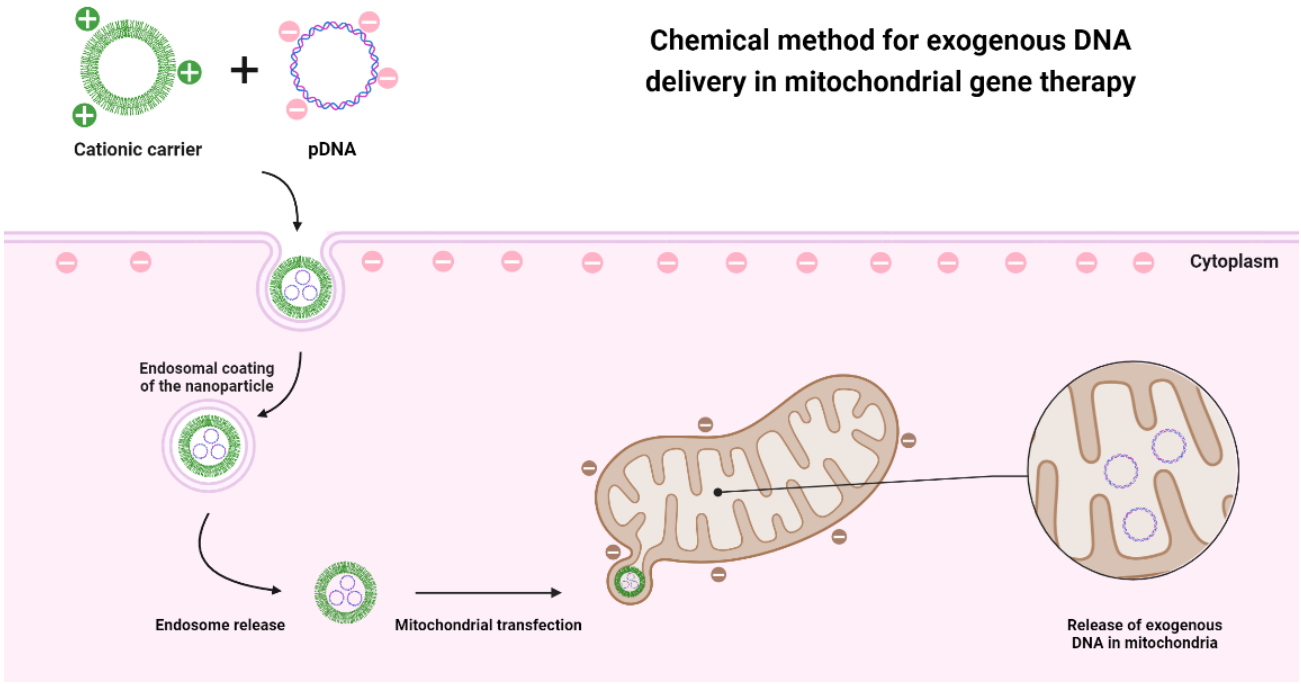

Figure 1.4 - Representative illustration of the application of chemical methods in the delivery of genetic material to the mitochondria, based on the use of a cationic nanotransporter that through electrostatic interactions manages to penetrate both the cell membrane and the mitochondrial membranes. pDNA – Plasmid DNA.

One of the fundamental steps for this therapy is the choice of the nanocarrier that enables the delivery of therapeutic DNA. The characteristics to consider when choosing the vector are, mainly, its production on a large scale, its biocompatibility, and the ability to carry DNA. Since mitochondria have specific receptors and have a double membrane that is impermeable to hydrophilic molecules, there is a need to create new approaches and specific therapeutic vectors for mitochondrial gene therapy[104, 116]. Due to the difficulty in targeting delivery systems to mitochondria, it is convenient to explore their receptors to facilitate their uptake by this organelle. It was found that mitochondrial proteins that are expressed in the cytosol enter the mitochondria through the translocase of the mitochondrial outer membrane (TOM) and mitochondrial inner membrane (TIM) allowing their recognition due to a sequence at the N-terminus of these proteins[117]. The mitochondrial targeting signal (MTS) peptide sequence allows preferential recognition of the TOM20-TOM22 receptor and thus facilitates protein translocation across mitochondrial membranes[118]. Therefore, the MTS sequence has been used as a ligand in mitochondrial gene therapy, mediated by delivery systems for a targeted delivery [119, 120]. Due to the unique characteristics of mitochondria, gene therapy targeting this organelle is even more challenging than nuclear gene therapy, as it involves crossing a double membrane and interacting with highly specific receptors. In this sense, it is necessary to find delivery systems that can internalize the cell and, at the same time, provide specificity and targeting to mitochondria after

they reach the cytoplasm. Nanotechnology has allowed the development of new transporters that can be used to deliver therapeutic genetic material to mitochondria.

1.6.2 Nanotechnology

Considered one of the most promising technologies of this century, nanotechnology enables the development of nanoscale materials for diverse applications across society, grounded in the principles of nanoscience. It allows the creation of technology at the nanometer scale which finds applications in areas such as engineering, electronics, physics, chemistry, biology, and medicine. Nanotechnology, by definition, deals with the design/development and application of materials with sizes between 1 and 100 nm. It also aims to tailor and optimize the physicochemical properties of these materials, as these characteristics directly influence their interactions with the surrounding environment and determine their performance in specific applications [121].

Nanotechnology has become a major object of study in the development of diagnostic methods and new therapies in the field of biomedicine. Its application in biology has enabled advanced therapeutic strategies, innovative drug delivery systems, and new diagnostic tools based on molecular imaging [122]. Over the past decades, nanotechnology has given rise to promising and innovative results, and it is not surprising that numerous nanomaterials have already been commercialized for medical purposes. The range of commercialized nanopharmaceuticals includes nanoparticles for the delivery of therapeutic drugs, such as anticancer drugs, nanostructures for application in bone restructuring and with antibacterial activity, and nanomaterials for the detection of biomarkers (nanosensors, nanoelectrodes, and nanochips)[123].

Consequently, nanotechnology has been extensively explored in the field of oncology, where its assets have been explored to develop new treatment methodologies and to improve the effectiveness of drugs in conventional chemotherapy. The application of nanoparticles allowed the development of more targeted therapies for tumors, using functionalized molecules. These nanoparticles can be used as direct therapeutic agents or to serve as carriers of therapeutic biomolecules with anticancer activity[124, 125]. Additionally, nanotechnology has been applied to enable simultaneous diagnosis and therapy. This approach, known as nanotheranostics, involves the development of a nanosystem designed to deliver a therapeutic effect while also allowing visualization of the targeted tissue or cells [126]. For example, this technology can be used to monitor drug release and biodistribution, and simultaneously assess the therapeutic effect of the delivered drug. These nanoscale systems also ensure targeted delivery to specific cells or tissues, using ligands that bind to receptors on the target cells, thereby increasing the precision and effectiveness of the therapy [127].

Nanotechnology can also help identify biomarkers associated with mitochondria and explore them in detecting mitochondrial disorders for early diagnosis. This technology can use mitochondrial biomarkers associated with specific mutations and thus combine with gene therapy to develop new therapeutic strategies[128]. Another approach is the application of mtDNA itself

as a biomarker to identify possible changes and pathologies and to assess the body's response to drug dosages, particularly in chemotherapy[129]. The identified mitochondrial biomarkers can then be used in gene therapy as therapeutic targets of diseases and enable the intervention in processes such as mitophagy, post-transcriptional regulation, modification of mitochondria, and interactions of this organelle with other cellular organelles[130].

The ability to use nanomaterials as carriers is also explored for gene delivery. One of the most explored applications is the combination of nucleic acids with nanotechnology, formulating nanostructures of reduced size. The use of nanomaterials allows the formulation of nanoparticles with sizes around 100 nanometers, which confers a fundamental physical property for the delivery of genetic material since the size of mitochondria varies between 0.5 and 1μm in diameter and 1μm in length. These nanocarriers are thus an excellent approach for mitochondrial gene therapy[1, 131]. These DNA or RNA nanostructures can be applied in diagnostic protocols, determination of the structure of biomolecules, formulation of nanoparticles, and in the areas of synthetic biology and biophysics. The materials most used in this DNA nanotechnology are polymers, lipids, and micelles[132]. This technology has led to emergent areas of study, namely gene therapy.

1.6.3 Delivery systems in mitochondrial gene therapy

1.6.3.1 Lipids

The use of lipids for the creation of gene delivery nanosystems has been extensively explored for many years due to their properties allowing the formation of a stable gene delivery system due to the electrostatic interactions between nucleic acids and lipids but also based on a controlled size of the formed nanoparticles and the protection of the therapeutics inside the core of these transporters[133]. In recent years, the use of multifunctional envelope-type nanodevices (MEND) has been widely explored. This type of lipid-based system allows the encapsulation of different types of molecules such as pDNA, RNA, oligonucleotides, and proteins. Due to the properties of lipids, they can be functionalized with multiple ligands (**Figure 1.5**). MEND allows, for example, to add peptides to its lipid envelope, improving the fusion and internalization of these systems in cells. Ligands can also be added to provide specific targeting to a certain organelle and PEG moieties to improve and prolong the circulation of lipid-based nanoparticles in the bloodstream[134].

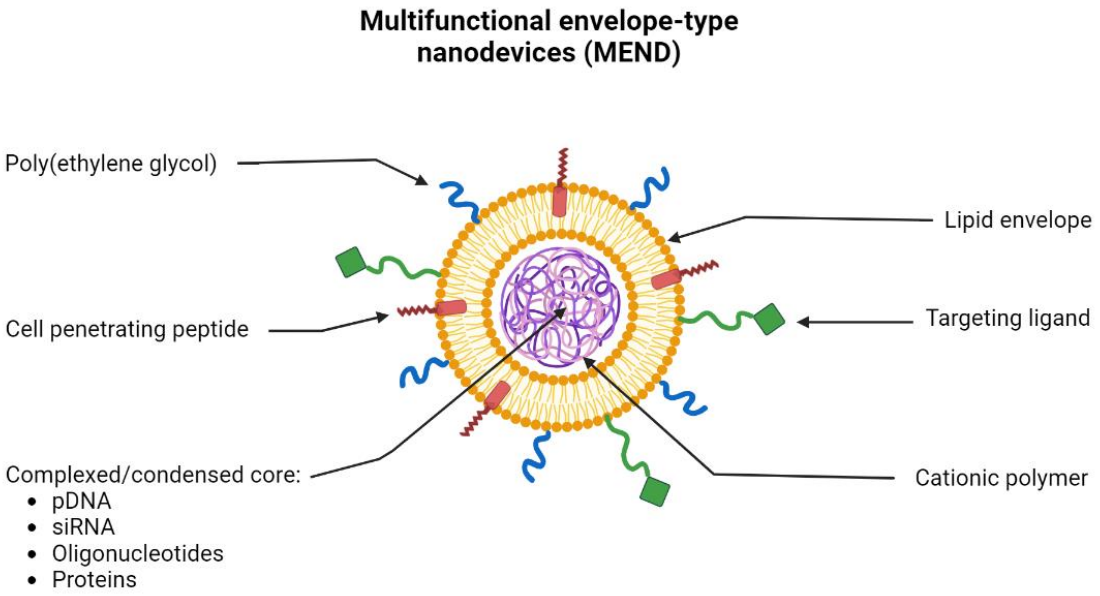

Figure 1.5 - Schematic representation of the morphology and constitution of the multifunctional envelope-type nanodevice (MEND). MEND consists of a lipid envelope that is modified with cell-penetrating peptides (CPP), poly(ethylene glycol) (PEG), and ligands that provide specific targeting. Inside, MEND can encapsulate/condense various therapeutic materials such as DNA, RNA, proteins, etc.

Khalil *et al.* managed to develop a MEND system composed of 1,2-dioleoyl-sn-glycero-3-phosphatidylethanolamine (DOPE) and cholesteryl hemisuccinate (CHEMS) with the CPP octa-arginine (R8) coupled at the surface. However, this delivery system did not demonstrate a great capacity to translocate through mitochondrial membranes despite having the ability to transfect dividing cells [135]. Thus, it became relevant to test new lipid compositions that could have greater fusion capacity with the mitochondrial membrane. This subject was explored by Yamada and his coworkers who developed two types of MEND-R8 systems, one with DOPE/SM/STR-R8 (9/2/1) and the other based on DOPE/PA/STR-R8 (9/2/1). Both compositions showed high fusogenic activity with the mitochondrial membrane. However, the lipid systems with sphingomyelin (SM) were considered more suitable for mitochondrial gene therapy because of their lower cytotoxicity[136]. Other researchers also demonstrated that the use of a tetra-lamellar MEND (T-MEND) composed of fusogenic lipids allowed the application of a gene therapy technique directed at mitochondria[137]. A study using two innovative MEND systems, β-MEND (DC-Chol/EPC/SM [3/4/3]) and RP/β-MEND (DC-Chol/EPC/SM/Chol-RP [3/4/3/0.25]), demonstrated that these nanocarriers can efficiently deliver genetic material directly into the mitochondria of H9c2 cells, a rat cardiomyocyte cell line. These two systems revealed the ability to target mitochondria and to be suitable for gene delivery, therefore, instigating further studies concerning mitochondrial gene therapy against cardiomyopathies[138].

Another type of lipid-based compound widely used for the delivery of nucleic acids to mitochondria is dequalinium-based liposome-like vesicles (DQAsomes). DQAsomes are positively charged lipid vesicles that allow the encapsulation of nucleic acids and display an affinity for binding to the membrane of mitochondria[116]. These complexes can escape from the endosomes without losing the encapsulated genetic material and carry out the therapeutic payload next to the mitochondria or even inside the mitochondrial matrix, depending on its composition[139, 140]. To overcome some difficulties that the DQAsome systems may present regarding cellular internalization, the incorporation of different lipids forming the DQA80s (a modified system composed of DOTAP and DOPE) was tested. The DQA80s system has a higher transfection efficiency when compared to the DQAsome, however, it delivers most of the genes around the mitochondria and not inside[139].

MITO-Porters are liposome-based delivery systems capable of transporting various types of encapsulated materials to mitochondria, regardless of their properties or size. Its membrane fusion mechanism responsible for the targeted delivery to mitochondria is divided into 3 phases. In the first phase, the systems must enter the cytosol, then they are targeted to the mitochondria and the pathway inside the cell has to be regulated, and finally the regulation of membrane fusion for delivery to the mitochondria[141]. In this sense, Yamada and Harashima created a high-density octa-arginine (R8)-modified MITO-Porter and demonstrated the ability of these systems to internalize into mitochondria. The presence of the cationic peptide R8 not only allowed binding to mitochondria, which are negatively charged in their membrane but also facilitated the internalization of these systems via macropinocytosis in the cytoplasm. These systems have demonstrated the capacity to deliver macromolecules such as nucleic acids and proteins directly to mitochondria[142]. In 2008, Yamada et al. coated the MITO-Porter surface with high-density octa-arginine (R8) to deliver green fluorescence protein (GFP) to rat-liver mitochondria[141]. Membrane fusion occurs by two extremely fusogenic lipid compositions: sphingomyelin (SM) and phosphatidic acid (PA) resulting in macropinocytosis instead of clathrin-mediated endocytosis, which allows particles to enter the cell without being damaged. The MITO-Porter was further optimized by the S2 peptide (Dmt-d-Arg-FK-Dmt-d-Arg-FK-NH2) instead of the R8 showing a high mitochondrial targeting activity with less cellular toxicity[143]. Another study demonstrated interesting results when using a MITO-Porter nanosystem that demonstrated the ability to encapsulate and deliver the antioxidant Coenzyme Q10 (CoQ10) in the liver tissues of mouse models. By confocal laser scanning microscopy, they confirmed the accumulation of this antioxidant in the mitochondria of liver cells from the transfected mice. They also verified that the presence of CoQ10 led to a decrease in ROS, which was confirmed by the decrease in Alanine Aminotransferase (ALT) levels in transfected hepatic tissues[144]. Kawamura *et al.* developed a MITO-Porter capable of delivering nucleic acids to mitochondria with its functioning altered by a heteroplasmic G625A mutation in mtDNA $tRNA^{Phe}$[145]. Once again, the MITO-Porter has been modified on its surface with R8, which makes it possible to escape from the macropinosomes to the cytosol. Once in the cytosol, MITO-Porter binds by electrostatic interactions to the mitochondrial membrane and fusion occurs between the delivery system and the mitochondria. The transfection capacity of this system was demonstrated by the PCR technique, where cells

transfected with MITO-Porter led to pre-WT-tRNA^{Phe}. Moreover, researchers observed that this effect lasted up to 8 days after the transfection. Furthermore, cells transfected with this liposome-based system demonstrated a replenishment of cellular respiration levels[145]. Another work also demonstrated the use of a MITO-Porter (ASO[COX2]/PEI) that managed to encapsulate and deliver an antisense RNA oligonucleotide (ASO) to the mitochondria, leading to the silencing of the target gene, and consequently, to the reduction of corresponding mRNA levels within the mitochondria[146]. An interesting study used a MITO-Porter in which the surface was modified with a mitochondrial RNA aptamer and the KALA peptide and inside it was encapsulated a DNA vector (pCMV-mtLuc (CGG)), specific to be transcribed in the mitochondria. Fibroblasts from a patient with mitochondrial dysfunction were transfected with the developed system and the transfected cells were found to have higher mitochondrial luciferase levels compared to untransfected cells[147].

1.6.3.2 Inorganic nanoparticles

Santos and his team developed calcium carbonate nanoparticles loaded with plasmid DNA and labeled with rhodamine, using CaCl2, Na2CO3, and cellulose in a co-precipitation method. The inorganic compounds were able to promote the encapsulation of three different plasmids and internalize them in several types of cell lines, also demonstrating the ability to target mitochondria, confirmed by confocal microscopy[148]. Rhodamine is a fluorescent compound with affinity to mitochondria, which facilitates the tracking of internalization into cells, and it has been applied as a probe for mitochondrial membrane potential[149]. This property of rhodamine has been explored for the targeting and gene delivery to mitochondria[148]. The team of D. Costa formulated $CaCO_3$-pDNA-Rho123 nanoparticles using the same co-precipitation method [150]. The vectors demonstrated the ability to encapsulate a plasmid containing the GFP gene, formulating stable nanoparticles of suitable size and surface charge for cell transfection. These delivery systems have demonstrated transfection capability into both normal and tumoral cells. Images obtained by two- and three-dimensional fluorescence confocal microscopy confirmed the targeting of these vectors to mitochondria in both fibroblasts and HeLa cells. This targeting was demonstrated by rhodamine fluorescence and by the expression of the GFP protein. To confirm the affinity of the systems for mitochondria, after cellular transfection, mitochondria were separated from the cytosolic fraction, verifying greater accumulation of nanoparticles in isolated mitochondria compared to the cytosol fraction, through quantification of rhodamine fluorescence[150]. Costa *et al.* also created calcium carbonate delivery systems capable of encapsulating p53 and ND1-GFP plasmids[151]. The nanoparticles formulated with the compound [16]phenN_2 showed an affinity for mitochondria. The fluorescence of [16]phenN_2 in isolated mitochondria was quite high when compared to the fluorescence of this compound in the cytosol or in lysosomes, where fluorescence was residual. Mitochondrial targeting of systems with [16]phenN_2 was further reinforced when plasmids were replaced by BSA, which resulted in an accumulation of BSA within the mitochondria of cells transfected with these nanoparticles, while this accumulation did not occur in the cytosol or the lysosome [151].

1.6.3.3 Polymers

Polymers are one of the most used materials to formulate nanocarriers. Their properties, such as easy manipulation of their structure and composition, ability to incorporate ligands, fast and economical production, and biocompatibility, make this type of material one of the most explored in gene therapy[152]. One of the polymers used in gene therapy is Poly (lactic-co-glycolic acid) (PLGA). PLGA is an FDA-approved biodegradable synthetic polymer that is used to formulate nanosystems and deliver nucleic acids and drugs to target cells[153]. Frede *et al.* used siRNA-loaded CaP/PLGA nanoparticles for the treatment of intestinal inflammation, obtaining good results in cell uptake and target gene silencing efficacy *in vitro*[154]. In another study using PLGA-based delivery systems, they demonstrated that the developed system (PLGA-PEG/PBAE) had better results in terms of transfection efficiency and target gene delivery compared to the commercial transfection reagent lipofectamine[155]. Chitosan is another polymer widely explored for gene therapy. This natural cationic polymer can bind to negatively charged molecules such as nucleic acids and drugs and form stable complexes that protect the therapeutic cargo from degradation by nucleases. Because it becomes protonated at acidic pH levels, this biomaterial has been used in gene therapy strategies against various types of cancer[156]. Raja and his group developed chitosan systems in which they tested 3 cross-linkers to improve the effectiveness and stability of the systems. The formulated nanoparticles chitosan-tripolyphosphate/dextran sulphate/poly-D-glutamic acid (CS-TPP/DS/PGA) demonstrated sizes between 100 and 400nm and zeta potentials of +25 to +40 mV. The formulated systems demonstrated reduced cytotoxicity and the ability to deliver siRNA into human colorectal cancer cells[157]. Robles-Planells *et al.* demonstrated that using chitosan-based nanoparticles, they were able to deliver and express the ARV-p10 gene *in vitro* in murine melanoma cells and consequently produce the protein. The use of these systems allowed to cause a slight cytotoxic effect on melanoma cells, associated with their cellular fusion and also delayed tumor growth[158]. In addition to the polymers mentioned above, others are used for gene therapy: dextran[159], gelatin[160], various types of polyesters[161-163], polycarbonates[164, 165], among others[166].

In addition to being used as carriers, polymers have also been explored as active agents in mitochondrial gene therapy. However, polymeric systems targeting mitochondria must overcome more barriers than those designed solely to cross the cell membrane. Therefore, these transporters must be supplemented with ligands that allow mitochondria targeting. To this goal, the most commonly applied ligands are lipophilic cations (e.g.: Triphenylphosphonium, TPP^+; Dequalinium, DQA; Rhodamine), Mitochondria-targeting sequence (MTS)/ Mitochondrial Penetrating Peptide (MPP) (**Figure 1.6**), and DNA and RNA aptamers. These ligands are intended to confer mitochondriotropic properties on polyplexes[152, 167].

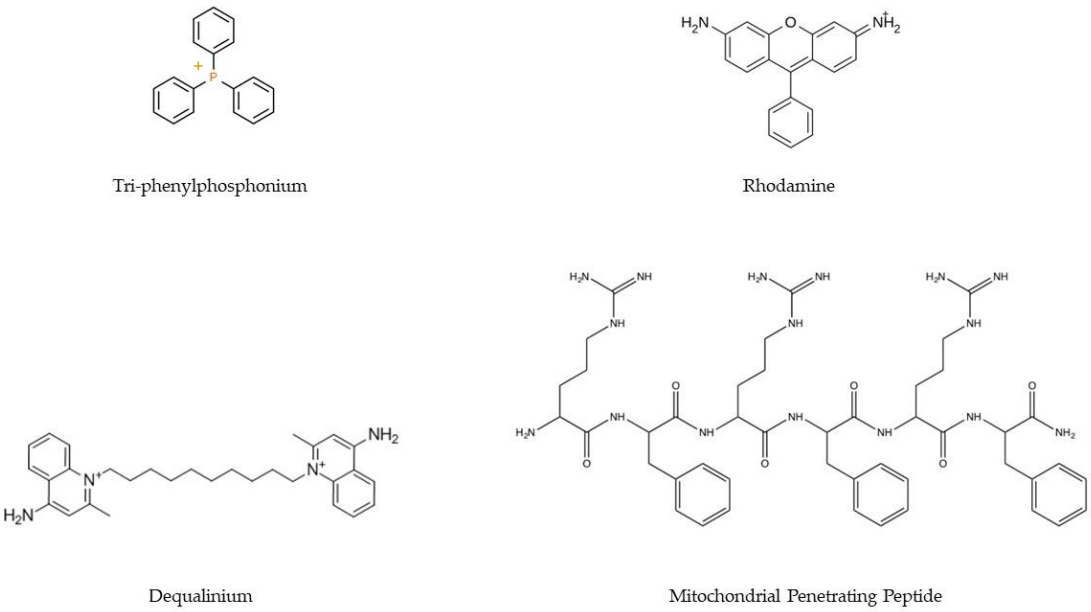

Figure 1.6 - Chemical structures of the main ligands (TPP+, rhodamine, DQA, and MPP) used in the development of delivery systems to confer targeting to the mitochondria.

The lipophilic cation ligands are frequently employed due to their positive charge that facilitates the penetration of polymeric systems through the mitochondrial double membrane. TPP^+ is one of the most used because of its easy incorporation into polymers[168, 169]. Marrache *et al.* demonstrated that systems with TPP^+ were effective in delivering genetic material to mitochondria[170-172]. These investigators created a PLGA-PEG-TPP^+ system, with PLGA-PEG-OH or PLGA-COOH and demonstrated the internalization of the systems in mitochondria. With this mitochondria-targeted polyplex, they demonstrated the ability to induce immunotherapy by increasing interferon-gamma (IFN-γ) in tumor cells[170-172]. Chitosan/sodium alginate nanoparticles to which a TPP^+-g-CS polymer was added were developed by Arafa *et al*[173]. These SAL/TPP^+-g-CS vectors demonstrated the ability to encapsulate therapeutic material through electrostatic interactions, forming stable nanoparticles with reduced and homogeneous size. Due to the presence of TPP^+ in the polymer used in the outer coating, these nanocarriers demonstrated targeting to the mitochondria. *In vitro* studies have shown that these mitotropic systems have low toxicity and induce a therapeutic response in tumor cells. These results were proven *in vivo*, where the profile of reduced toxicity and increased antitumor activity in tissues transfected with these systems was demonstrated[173].

DQA is another group of lipophilic cations explored for the development of polymer-based carriers toward mitochondria targeting/delivery. The use of DQA in delivery systems has already demonstrated the ability to accumulate in the mitochondrial matrix[174, 175]. Mallick and his group created a delivery system based on glycol chitosan in which DQA was added to provide targeting to the mitochondria. The formed polyplexes did not show toxicity in cancer cells or non-cancerous cells. The authors of this study also demonstrated that these systems can be

internalized in cells and mitochondria. Co-localization in mitochondria was confirmed by confocal microscopy and cellular uptake by flow cytometry[175].

1.6.3.3.1 Polyethylenimine

One of the most used polymers is polyethylenimine (PEI). PEI is a cationic polymer widely used in gene therapy, enabling the formulation of gene delivery systems. Its wide use is due to its versatility, solubility in various solvents, and ability to encapsulate large amounts of genetic material[176, 177]. Through electrostatic bonds between their positive charges and the negative charges of nucleic acids, PEI-based nanoparticles are stable and have adequate physicochemical properties to be excellent vehicles for delivering genetic material[178]. The PEI polymer consists of a repetition of amino group units and can have a linear or branched structure: primary amine end groups (NH2), secondary amine linear units (NH) and tertiary amine branched[179]. Linear PEIs have a lower capacity to encapsulate genetic material, forming larger delivery systems, while branched PEIs have greater chemical reactivity, forming smaller and more stable nanoparticles. However, branched PEI presents greater cytotoxicity when compared to linear PEI[180]. Furthermore, PEI can be synthesized with a molecular weight range from 700Da to 1000kDa[181].

The molecular weight of PEI and the type of structure they present have a great influence not only on toxicity but also on the efficiency of transfection and gene delivery. The PEI polymers that show greater performance in terms of gene transfer are those with a molecular weight between 5 and 25 kDa, with the branched structure being more effective than the linear one[176]. PEIs above this molecular weight range have greater associated toxicity, while those of 2 kDa prove to be safer but with lower transfection capacity[182]. A study revealed that the cytotoxicity of PEI polymers is associated with the damage they cause to the cell membrane, inducing a process of hydrolysis of cellular phospholipids. It was demonstrated that this toxicity is directly proportional to the dose administered and the molecular weight of the PEI used. Therefore, PEIs with higher molecular weight, branched, and more cationic induce greater toxicity[183].

Due to the toxicity associated with the use of high molecular weight PEI, several strategies have been tested to minimize this adverse effect. One of the solutions that demonstrated efficacy was the use of lower molecular weight PEI, resulting in less toxic systems but with the capacity to deliver genetic material[184-186]. Another strategy to circumvent toxicity was the conjugation of PEI with chitosan, which made the systems more stable and safer, with good capacity for gene delivery[187-189]. One of the most used approaches to reduce the cytotoxicity of PEI-based systems is the incorporation of PEG. The addition of PEG to the systems reduces the surface charge and increases the solubility of the nanoparticles, which reduces the toxic effects[190-193].

1.6.3.4 Dendrimers

Dendrimers are highly branched polymer-based nanostructures, consisting of a core, branches, and surface groups[194]. The structure and synthesis of dendrimers make this type of delivery

system very dynamic and capable of being molded to the intended use. The core–shell structure that characterizes dendrimers allows for the controlled creation of branch points during synthesis, radiating from a central core molecule. The outer shell can be functionalized with ligands to confer specificity, while the internal architecture - including the core - facilitates the encapsulation of therapeutic or diagnostic agents [195, 196].

Mitochondrial-targeted gene therapy using dendrimers as delivery systems was studied by Wang *et al.*[197]. An ethylenediamine-cored and amine-terminated generation 5 (G5) PAMAM dendrimer to which TPP was added, was synthesized, and tested in HeLa and COS-7 cells. The dendrimers under study showed reduced cytotoxicity in both cell lines and demonstrated transfection capacity similar to the commercial transfection reagent Lipofectamine 2000. Functionalization with TPP allowed the transfection of mitochondria, confirmed by the co-localization of the G5-TPP/DNA complexes (FITC-labeled G5-TPP) in the mitochondria, while this co-localization was not shown for the naked G5/DNA systems[197]. Biswas *et al.* studied a similar system, in which the ligand used was again TPP in combination with the generation 5 poly(amidoamine) (G(5)-D) PAMAM dendrimer. The TPP-modified dendrimers had less cytotoxicity than the TPP-free dendrimers in normal mouse fibroblasts (NIH-3T3). Furthermore, the TPP systems demonstrated specificity for mitochondria and a good ability to internalize into cells. In the work carried out, no molecule was encapsulated, however, the authors report that this system can be exploited for gene delivery into the mitochondria[198].

Biocompatible dendritic poly(L-lysine) (DGL) is a promising carrier for targeted drug/DNA delivery[199]. DGL is becoming one of the most versatile nanoscale drug/DNA carriers due to its highly branched 3D architecture containing an initiator core, several inner layers composed of repeating units, and many outer amino groups[200]. Compared with traditional nanocarriers, self-organized DGL nanoparticles are vastly superior in targeted therapy at the subcellular level due to their small size and their surface modifications (PEGylation and targeted ligands). In particular, DGL nanoparticles (DGL NPs) have a greater ability to facilitate intracellular internalization *via* endocytosis, and then in the endosomes, they act as proton-sponges to induce endo-lysosomal escape by osmotic swelling[201]. These properties of DGL NPs make them attractive nanocarriers for the construction of targeted drug delivery systems to mitochondria. Chen *et al.* synthesized a delivery system based on dendrigraft poly-L-lysines (DGL) with incorporated doxorubicin (Dox) that was intercalated into a DNA duplex containing an ATP aptamer. In addition, a Cytochrome C aptamer, and a nucleolin-specific binding aptamer, AS1411, were added to the nanoparticles (Dox/Mito-DGL). This study demonstrated that this dual system displayed targeting and accumulation in the mitochondria, the therapeutic agent was released and allowed to improve the therapeutic efficacy in multidrug-resistant cancer cells[202].

1.6.3.5 Cell-penetrating peptides

Cell-penetrating peptides are a set of peptides that range in size from 5 to 30 amino acids. CPP's main characteristics are their biocompatibility, ability to cross tissues and cell membranes, and serve as transporters of therapeutic agents such as proteins, nucleic acids, and drugs[203]. The

connection of CPPs with genetic material can be done through covalent and non-covalent bonds. Covalent bonds are used to deliver small drug and protein molecules, peptides, and peptide nucleic acids (PNAs)[204]. Covalent bonds are made through chemical bonds or the addition of the therapeutic agent to the CPP during its synthesis. However, this approach can affect the biological activity of the CPP and the therapeutic agents that are intended to be delivered. Non-covalent bonds are made through hydrophobic or electrostatic interactions between the opposite charges of the CPP and the therapeutic agent to be encapsulated. This approach protects the cargo from degradation by proteases and nucleases and ensures its delivery to the site of interest[204-206]. There are 3 types of CPP, cationic, hydrophobic, and amphipathic. Cationic CPPs are arginine-rich peptides. Amphipathic CPPs have both hydrophilic and hydrophobic domains, with the degree of amphipathicity defined by the lysine residues in their sequence. Hydrophobic CPPs are peptides that have only hydrophobic motifs/non-polar sequences in their structure[207].
Recently, amphipathic CPPs rich in tryptophan and arginine with a size between 15 and 16 amino acids, called WRAP, were developed[208]. The WRAP peptides revealed great stability, acquiring an amphipathic helical conformation. The WRAP1 and WRAP5 peptides (**Figure 1.7**) have only 3 amino acids in their sequence (tryptophan, arginine, and leucine), the difference being the position of the tryptophan amino acids in the peptide sequence. These two CPPs demonstrated the ability to encapsulate nucleic acids. Delivery systems based on these CPPs demonstrated a high capacity for cellular internalization without associated cytotoxicity[209-211].

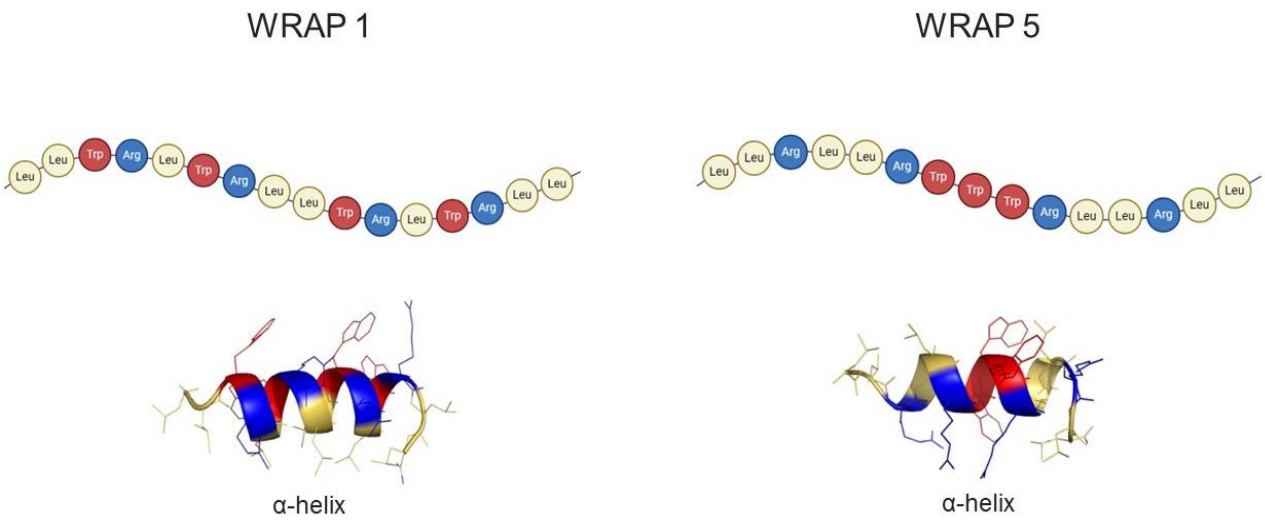

Figure 1.7 - Sequence of WRAP1 and WRAP5 peptides and respective 3D structure predicted by PEPstrMOD in a hydrophilic environment. Image adapted from[209].

1.7 *In vivo* studies to test the viability/efficacy of delivery systems

In vivo assays are essential for assessing the toxicity of biomaterials or medical devices intended for use in medicine. Although some *in vitro* assays are able to determine the cytotoxicity of materials, these results are very preliminary and require confirmation by *in vivo* assays. *In vivo* tests allow a more in-depth determination of the toxicity of a component, and acute, sub-acute, chronic and sub-chronic toxicity can be assessed[212-214]. These tests are essential in the investigation of new delivery systems for gene therapy, as they allow the assessment of systemic toxicity, possible adverse reactions and the determination of the affected tissues in animal models[215, 216]. Through animal models, the behavior of delivery systems can be evaluated in a much more complex environment, being able to determine pharmacokinetic parameters, circulation time in the blood and tissues where there is accumulation of delivery systems[217-219].

Another parameter that *in vivo* assays allow to assess is the transfection and biodistribution capacity of the delivery systems[220-223]. Compared to studies using cells alone, studies using animal models help determine the true transfection and cellular internalization capacity of the delivery systems, since they have to overcome numerous biological barriers and not just cell membranes. Furthermore, by considering animal tests, the effect of the interaction of nanosystems with the immune system, their distribution throughout the body and the metabolization of the therapeutic agent can be deeply investigated[224, 225].

Despite ethical issues, the advantages of using animal models in the development of new therapies and drugs are enormous and essential to ensure safety and efficacy[226]. Various types of mammalian animal models have been used over time, however, in recent decades new animal models have emerged. The use of zebrafish models in *in vivo* assays has grown exponentially in recent years, more specifically in toxicity assays. Due to its characteristics, this *in vivo* model can also be used for other types of studies[227-229].

1.7.1 Zebrafish (*Danio rerio*)

Zebrafish (*Danio rerio*) are small (2 to 5 cm) striped fish that can be found in the wild rivers in southern Asia[230]. Zebrafish (ZF) are vertebrate animal models increasingly used in scientific studies since their characteristics allow the evaluation of a series of parameters in a short period. One of the main advantages of using zebrafish (ZF) is that its life cycle is short, with high reproduction (females can produce between 200 and 300 eggs per week) and their embryonic development is fast (main organs formed within 48 hours after fertilization)[231]. Transparency in its embryonic phase makes it possible to monitor the development of various organs over time and evaluate possible therapeutic methods. The fact that it is a small animal model in adulthood facilitates its use and maintenance in the laboratory. ZF has a genome similarity of around 70% to human genes and since its genome has already been fully sequenced, it allows genetic studies and gene manipulation using advanced genetic tools such as CRISPR-Cas9[232, 233]. All these

properties of ZF have enhanced their application for scientific studies, particularly the ones focused on embryonic development, processes of cell division, migration, and differentiation, identification of genes involved in the appearance of a disease, toxicology studies, screening of chemical compounds and studies of effects and mechanisms of action of a drug. Following this, the ZF model has been widely considered in pre-clinical trials in the most varied toxicological studies[230, 234, 235].

1.8 References

[1] Aversa, R.; Petrescu, R. V. V.; Apicella, A.; Petrescu, F. I. T., Mitochondria are Naturally Micro Robots - A review. American Journal of Engineering and Applied Sciences. 2016, 9, 991-1002.

[2] Herrera, A. S.; Esparza, M. d. C. A.; Ashraf, G. M.; Jr., A. A. Z.; Aliev, G., Beyond Mitochondria, What Would be the Energy Source of the Cell? Central Nervous System Agents in Medicinal Chemistry. 2015, 15, 32-41.

[3] Obrador, E.; Salvador-Palmer, R.; Lopez-Blanch, R.; Jihad-Jebbar, A.; Valles, S. L.; Estrela, J. M., The Link between Oxidative Stress, Redox Status, Bioenergetics and Mitochondria in the Pathophysiology of ALS. Int J Mol Sci. 2021, 22, 6352-6370.

[4] Jerome, M. S.; Kuthethur, R.; Kabekkodu, S. P.; Chakrabarty, S., Regulation of mitochondrial function by forkhead transcription factors. Biochimie. 2022, 198, 96-108.

[5] Prasai, K., Regulation of mitochondrial structure and function by protein import: A current review. Pathophysiology. 2017, 24, 107-122.

[6] Spinelli, J. B.; Haigis, M. C., The multifaceted contributions of mitochondria to cellular metabolism. Nat Cell Biol. 2018, 20, 745-754.

[7] Fontanesi, F., Mitochondria: Structure and Role in Respiration. In eLS,. 2015; pp 1-13.

[8] Roger, A. J.; Munoz-Gomez, S. A.; Kamikawa, R., The Origin and Diversification of Mitochondria. Curr Biol. 2017, 27, R1177-R1192.

[9] Xian, H.; Liou, Y. C., Functions of outer mitochondrial membrane proteins: mediating the crosstalk between mitochondrial dynamics and mitophagy. Cell Death Differ. 2021, 28, 827-842.

[10] Grevel, A.; Becker, T., Porins as helpers in mitochondrial protein translocation. Biol Chem. 2020, 401, 699-708.

[11] Busch, J. D.; Fielden, L. F.; Pfanner, N.; Wiedemann, N., Mitochondrial protein transport: Versatility of translocases and mechanisms. Mol Cell. 2023, 83, 890-910.

[12] Dadsena, S.; Jenner, A.; Garcia-Saez, A. J., Mitochondrial outer membrane permeabilization at the single molecule level. Cell Mol Life Sci. 2021, 78, 3777-3790.

[13] Heine, K. B.; Parry, H. A.; Hood, W. R., How does density of the inner mitochondrial membrane influence mitochondrial performance? Am J Physiol Regul Integr Comp Physiol. 2023, 324, 242-248.

[14] Pereira, O., Jr.; Kowaltowski, A. J., Mitochondrial K(+) Transport: Modulation and Functional Consequences. Molecules. 2021, 26, 2935-2946.

[15] Zorova, L. D.; Popkov, V. A.; Plotnikov, E. Y.; Silachev, D. N.; Pevzner, I. B.; Jankauskas, S. S.; Babenko, V. A.; Zorov, S. D.; Balakireva, A. V.; Juhaszova, M.; Sollott, S. J.; Zorov, D. B., Mitochondrial membrane potential. Anal Biochem. 2018, 552, 50-59.
[16] Zimmermann, A.; Madeo, F.; Diwan, A.; Sadoshima, J.; Sedej, S.; Kroemer, G.; Abdellatif, M., Metabolic control of mitophagy. Eur J Clin Invest. 2024, 54, 14138-14157.
[17] Khan, T.; Waseem, R.; Zehra, Z.; Aiman, A.; Bhardwaj, P.; Ansari, J.; Hassan, M. I.; Islam, A., Mitochondrial Dysfunction: Pathophysiology and Mitochondria-Targeted Drug Delivery Approaches. Pharmaceutics. 2022, 14, 2657-2682.
[18] Picard, M.; McEwen, B. S., Psychological Stress and Mitochondria: A Systematic Review. Psychosom Med. 2018, 80, 141-153.
[19] Johnston, I. G.; Williams, B. P., Evolutionary Inference across Eukaryotes Identifies Specific Pressures Favoring Mitochondrial Gene Retention. Cell Syst. 2016, 2, 1-11.
[20] Reznik, E.; Miller, M. L.; Senbabaoglu, Y.; Riaz, N.; Sarungbam, J.; Tickoo, S. K.; Al-Ahmadie, H. A.; Lee, W.; Seshan, V. E.; Hakimi, A. A.; Sander, C., Mitochondrial DNA copy number variation across human cancers. Elife. 2016, 5, 10769-10789.
[21] Jedynak-Slyvka, M.; Jabczynska, A.; Szczesny, R. J., Human Mitochondrial RNA Processing and Modifications: Overview. Int J Mol Sci. 2021, 22, 7999-8022.
[22] D'Souza, A. R.; Minczuk, M., Mitochondrial transcription and translation: overview. Essays Biochem. 2018, 62, 309-320.
[23] Fox, T. D., Mitochondrial protein synthesis, import, and assembly. Genetics. 2012, 192, 1203-1234.
[24] Wang, F.; Zhang, D.; Zhang, D.; Li, P.; Gao, Y., Mitochondrial Protein Translation: Emerging Roles and Clinical Significance in Disease. Front Cell Dev Biol. 2021, 9, 1-24.
[25] Blier, P. U.; Dufresne, F.; Burton, R. S., Natural selection and the evolution of mtDNA-encoded peptides: evidence for intergenomic co-adaptation. TRENDS in Genetics. 2001, 17, 400-406.
[26] Brischigliaro, M.; Zeviani, M., Cytochrome c oxidase deficiency. Biochim Biophys Acta Bioenerg. 2021, 1862, 148335-148357.
[27] Buneeva, O.; Fedchenko, V.; Kopylov, A.; Medvedev, A., Mitochondrial Dysfunction in Parkinson's Disease: Focus on Mitochondrial DNA. Biomedicines. 2020, 8, 591-613.
[28] Nolfi-Donegan, D.; Braganza, A.; Shiva, S., Mitochondrial electron transport chain: Oxidative phosphorylation, oxidant production, and methods of measurement. Redox Biol. 2020, 37, 1-9.
[29] Kotrys, A. V.; Szczesny, R. J., Mitochondrial Gene Expression and Beyond-Novel Aspects of Cellular Physiology. Cells. 2019, 9, 1-23.
[30] Gorman, G. S.; Chinnery, P. F.; DiMauro, S.; Hirano, M.; Koga, Y.; McFarland, R.; Suomalainen, A.; Thorburn, D. R.; Zeviani, M.; Turnbull, D. M., Mitochondrial diseases. Nat Rev Dis Primers. 2016, 2, 1-22.
[31] Pearce, E. L.; Poffenberger, M. C.; Chang, C. H.; Jones, R. G., Fueling immunity: insights into metabolism and lymphocyte function. Science. 2013, 342, 1242454-1242465.

[32] Morrow, R. M.; Picard, M.; Derbeneva, O.; Leipzig, J.; McManus, M. J.; Gouspillou, G.; Barbat-Artigas, S.; Dos Santos, C.; Hepple, R. T.; Murdock, D. G.; Wallace, D. C., Mitochondrial energy deficiency leads to hyperproliferation of skeletal muscle mitochondria and enhanced insulin sensitivity. Proc Natl Acad Sci U S A. 2017, 114, 2705-2710.
[33] Hebert-Chatelain, E.; Desprez, T.; Serrat, R.; Bellocchio, L.; Soria-Gomez, E.; Busquets-Garcia, A.; Pagano Zottola, A. C.; Delamarre, A.; Cannich, A.; Vincent, P.; Varilh, M.; Robin, L. M.; Terral, G.; Garcia-Fernandez, M. D.; Colavita, M.; Mazier, W.; Drago, F.; Puente, N.; Reguero, L.; Elezgarai, I.; Dupuy, J. W.; Cota, D.; Lopez-Rodriguez, M. L.; Barreda-Gomez, G.; Massa, F.; Grandes, P.; Benard, G.; Marsicano, G., A cannabinoid link between mitochondria and memory. Nature. 2016, 539, 555-559.
[34] Azzouz, M.; Ralph, G. S.; Storkebaum, E.; Walmsley, L. E.; Mitrophanous, K. A.; Kingsman, S. M.; Carmeliet, P.; Mazarakis, N. D., VEGF delivery with retrogradely transported lentivector prolongs survival in a mouse ALS model. Nature. 2004, 429, 413-423.
[35] Latorre-Pellicer, A.; Moreno-Loshuertos, R.; Lechuga-Vieco, A. V.; Sanchez-Cabo, F.; Torroja, C.; Acin-Perez, R.; Calvo, E.; Aix, E.; Gonzalez-Guerra, A.; Logan, A.; Bernad-Miana, M. L.; Romanos, E.; Cruz, R.; Cogliati, S.; Sobrino, B.; Carracedo, A.; Perez-Martos, A.; Fernandez-Silva, P.; Ruiz-Cabello, J.; Murphy, M. P.; Flores, I.; Vazquez, J.; Enriquez, J. A., Mitochondrial and nuclear DNA matching shapes metabolism and healthy ageing. Nature. 2016, 535, 561-579.
[36] Saki, M.; Prakash, A., DNA damage related crosstalk between the nucleus and mitochondria. Free Radic Biol Med. 2017, 107, 216-227.
[37] Russell, O. M.; Gorman, G. S.; Lightowlers, R. N.; Turnbull, D. M., Mitochondrial Diseases: Hope for the Future. Cell. 2020, 181, 168-188.
[38] Tinker, R. J.; Lim, A. Z.; Stefanetti, R. J.; McFarland, R., Current and Emerging Clinical Treatment in Mitochondrial Disease. Mol Diagn Ther. 2021, 25, 181-206.
[39] Liang, C.; Ahmad, K.; Sue, C. M., The broadening spectrum of mitochondrial disease: shifts in the diagnostic paradigm. Biochim Biophys Acta. 2014, 1840, 1360-1367.
[40] Farrar, G. J.; Chadderton, N.; Kenna, P. F.; Millington-Ward, S., Mitochondrial disorders: aetiologies, models systems, and candidate therapies. Trends Genet. 2013, 29, 488-497.
[41] Hahn, A.; Zuryn, S., Mitochondrial Genome (mtDNA) Mutations that Generate Reactive Oxygen Species. Antioxidants (Basel). 2019, 8, 1-19.
[42] Bordoni, L.; Gabbianelli, R., Mitochondrial DNA and Neurodegeneration: Any Role for Dietary Antioxidants? Antioxidants (Basel). 2020, 9, 764-788.
[43] Nissanka, N.; Moraes, C. T., Mitochondrial DNA damage and reactive oxygen species in neurodegenerative disease. FEBS Lett. 2018, 592, 728-742.
[44] Bhatti, J. S.; Bhatti, G. K.; Reddy, P. H., Mitochondrial dysfunction and oxidative stress in metabolic disorders - A step towards mitochondria based therapeutic strategies. Biochim Biophys Acta Mol Basis Dis. 2017, 1863, 1066-1077.
[45] Stefano, G. B.; Kream, R. M., Mitochondrial DNA heteroplasmy in human health and disease. Biomed Rep. 2016, 4, 259-262.
[46] Nissanka, N.; Moraes, C. T., Mitochondrial DNA heteroplasmy in disease and targeted nuclease-based therapeutic approaches. EMBO Rep. 2020, 21, 49612-49624.

[47] Elorza, A. A.; Soffia, J. P., mtDNA Heteroplasmy at the Core of Aging-Associated Heart Failure. An Integrative View of OXPHOS and Mitochondrial Life Cycle in Cardiac Mitochondrial Physiology. Front Cell Dev Biol. 2021, 9, 1-17.
[48] Schon, E. A.; DiMauro, S.; Hirano, M., Human mitochondrial DNA: roles of inherited and somatic mutations. Nat Rev Genet. 2012, 13, 878-890.
[49] Lawless, C.; Greaves, L.; Reeve, A. K.; Turnbull, D. M.; Vincent, A. E., The rise and rise of mitochondrial DNA mutations. Open Biol. 2020, 10, 1-12.
[50] Permana Maksum, I.; Saputra, S. R.; Indrayati, N.; Yusuf, M.; Subroto, T., Bioinformatics Study of m.9053G>A Mutation at the ATP6 Gene in Relation to Type 2 Diabetes Mellitus and Cataract Diseases. Bioinform Biol Insights. 2017, 11, 1-5.
[51] Lalrohlui, F.; Thapa, S.; Ghatak, S.; Zohmingthanga, J.; Senthil Kumar, N., Mitochondrial complex I and V gene polymorphisms in type II diabetes mellitus among high-risk Mizo-Mongoloid population, Northeast India. Genes Environ. 2016, 38, 1-6.
[52] Lalrohlui, F.; Zohmingthanga, J.; Hruaii, V.; Kumar, N. S., Genomic profiling of mitochondrial DNA reveals novel complex gene mutations in familial type 2 diabetes mellitus individuals from Mizo ethnic population, Northeast India. Mitochondrion. 2020, 51, 7-14.
[53] Carreno-Gago, L.; Gamez, J.; Camara, Y.; Alvarez de la Campa, E.; Aller-Alvarez, J. S.; Moncho, D.; Salvado, M.; Galan, A.; de la Cruz, X.; Pinos, T.; Garcia-Arumi, E., Identification and characterization of the novel point mutation m.3634A>G in the mitochondrial MT-ND1 gene associated with LHON syndrome. Biochim Biophys Acta Mol Basis Dis. 2017, 1863, 182-187.
[54] Baertling, F.; Sanchez-Caballero, L.; van den Brand, M. A. M.; Distelmaier, F.; Janssen, M. C. H.; Rodenburg, R. J. T.; Smeitink, J. A. M.; Nijtmans, L. G. J., A Heterozygous NDUFV1 Variant Aggravates Mitochondrial Complex I Deficiency in a Family with a Homoplasmic ND1 Variant. J Pediatr. 2018, 196, 309-313.
[55] Smolina, N.; Khudiakov, A.; Knyazeva, A.; Zlotina, A.; Sukhareva, K.; Kondratov, K.; Gogvadze, V.; Zhivotovsky, B.; Sejersen, T.; Kostareva, A., Desmin mutations result in mitochondrial dysfunction regardless of their aggregation properties. Biochim Biophys Acta Mol Basis Dis. 2020, 1866, 1-10.
[56] Guo, Y.; Zhang, Y.; Li, F.; Liu, P.; Liu, Y.; Yang, C.; Song, J.; Zhang, N.; Chen, Z., The biochemical characterization of a missense mutation m.8914C>T in ATP6 gene associated with mitochondrial encephalomyopathy. Int J Dev Neurosci. 2018, 71, 172-174.
[57] Dafinca, R.; Barbagallo, P.; Farrimond, L.; Candalija, A.; Scaber, J.; Ababneh, N. A.; Sathyaprakash, C.; Vowles, J.; Cowley, S. A.; Talbot, K., Impairment of Mitochondrial Calcium Buffering Links Mutations in C9ORF72 and TARDBP in iPS-Derived Motor Neurons from Patients with ALS/FTD. Stem Cell Reports. 2020, 14, 892-908.
[58] van Horssen, J.; van Schaik, P.; Witte, M., Inflammation and mitochondrial dysfunction: A vicious circle in neurodegenerative disorders? Neurosci Lett. 2019, 710, 1-6.
[59] Chu, Q.; Luo, X.; Zhan, X.; Ren, Y.; Pang, H., Female genetic distribution bias in mitochondrial genome observed in Parkinson's Disease patients in northern China. Sci Rep. 2015, 5, 1-9.

[60] Bi, R.; Zhang, W.; Yu, D.; Li, X.; Wang, H. Z.; Hu, Q. X.; Zhang, C.; Lu, W.; Ni, J.; Fang, Y.; Li, T.; Yao, Y. G., Mitochondrial DNA haplogroup B5 confers genetic susceptibility to Alzheimer's disease in Han Chinese. Neurobiol Aging. 2015, 36, 1-10.
[61] Ban, R.; Guo, J. H.; Pu, C. Q.; Shi, Q.; Liu, H. X.; Zhang, Y. T., A Novel Mutation of Mitochondrial T14709C Causes Myoclonic Epilepsy with Ragged Red Fibers Syndrome in a Chinese Patient. Chin Med J (Engl). 2018, 131., 1569-1574.
[62] Henry, C.; Patel, N.; Shaffer, W.; Murphy, L.; Park, J.; Spieler, B., Mitochondrial Encephalomyopathy With Lactic Acidosis and Stroke-Like Episodes—MELAS Syndrome. Ochsner Journal. 2017, 17, 296–301.
[63] de Mello, A. H.; Costa, A. B.; Engel, J. D. G.; Rezin, G. T., Mitochondrial dysfunction in obesity. Life Sci. 2018, 192, 26-32.
[64] Kim, H.; Komiyama, T.; Inomoto, C.; Kamiguchi, H.; Kajiwara, H.; Kobayashi, H.; Nakamura, N.; Terachi, T., Mutations in the Mitochondrial ND1 Gene Are Associated with Postoperative Prognosis of Localized Renal Cell Carcinoma. Int J Mol Sci. 2016, 17, 1-13.
[65] Ganly, I.; Makarov, V.; Deraje, S.; Dong, Y.; Reznik, E.; Seshan, V.; Nanjangud, G.; Eng, S.; Bose, P.; Kuo, F.; Morris, L. G. T.; Landa, I.; Carrillo Albornoz, P. B.; Riaz, N.; Nikiforov, Y. E.; Patel, K.; Umbricht, C.; Zeiger, M.; Kebebew, E.; Sherman, E.; Ghossein, R.; Fagin, J. A.; Chan, T. A., Integrated Genomic Analysis of Hurthle Cell Cancer Reveals Oncogenic Drivers, Recurrent Mitochondrial Mutations, and Unique Chromosomal Landscapes. Cancer Cell. 2018, 34, 256-270.
[66] Ganly, I.; McFadden, D. G., Short Review: Genomic Alterations in Hurthle Cell Carcinoma. Thyroid. 2019, 29, 471-479.
[67] Smith, A. L. M.; Whitehall, J. C.; Greaves, L. C., Mitochondrial DNA mutations in ageing and cancer. Mol Oncol. 2022, 16, 3276-3294.
[68] Muramatsu, H.; Honda, K.; Akanuma, S.; Ishizawa, F.; Umino, K.; Iwabuchi, Y.; Mochizuki, N.; Sugano, Y., Trial to search for mitochondrial DNA mutation associated with cancer detected by massively parallel sequencing. Forensic Science International: Genetics Supplement Series. 2019, 7, 698-700.
[69] Gasparre, G.; Porcelli, A. M.; Bonora, E.; Pennisi, L. F.; Toller, M.; Iommarini, L.; Ghelli, A.; Moretti, M.; Betts, C. M.; Martinelli, G. N.; Ceroni, A. R.; Curcio, F.; Carelli, V.; Rugolo, M.; Tallini, G.; Romeo, G., Disruptive mitochondrial DNA mutations in complex I subunits are markers of oncocytic phenotype in thyroid tumors. PNAS. 2007, 104, 9001–9006.
[70] Thapa, S.; Lalrohlui, F.; Ghatak, S.; Zohmingthanga, J.; Lallawmzuali, D.; Pautu, J. L.; Senthil Kumar, N., Mitochondrial complex I and V gene polymorphisms associated with breast cancer in mizo-mongloid population. Breast Cancer. 2016, 23, 607-616.
[71] Porcelli, A. M.; Ghelli, A.; Ceccarelli, C.; Lang, M.; Cenacchi, G.; Capristo, M.; Pennisi, L. F.; Morra, I.; Ciccarelli, E.; Melcarne, A.; Bartoletti-Stella, A.; Salfi, N.; Tallini, G.; Martinuzzi, A.; Carelli, V.; Attimonelli, M.; Rugolo, M.; Romeo, G.; Gasparre, G., The genetic and metabolic signature of oncocytic transformation implicates HIF1alpha destabilization. Hum Mol Genet. 2010, 19, 1019-1032.

[72] Lang, M.; Vocke, C. D.; Merino, M. J.; Schmidt, L. S.; Linehan, W. M., Mitochondrial DNA mutations distinguish bilateral multifocal renal oncocytomas from familial Birt-Hogg-Dube tumors. Mod Pathol. 2015, 28, 1458-1469.
[73] Lenaz, G.; Baracca, A.; Carelli, V.; D'Aurelio, M.; Sgarbi, G.; Solaini, G., Bioenergetics of mitochondrial diseases associated with mtDNA mutations. Biochim Biophys Acta. 2004, 1658, 89-94.
[74] Moslemi, A. R.; Darin, N.; Tulinius, M.; Wiklund, L. M.; Holme, E.; Oldfors, A., Progressive encephalopathy and complex I deficiency associated with mutations in MTND1. Neuropediatrics. 2008, 39, 24-28.
[75] Ammar, M.; Tabebi, M.; Sfaihi, L.; Alila-Fersi, O.; Maalej, M.; Felhi, R.; Chabchoub, I.; Keskes, L.; Hachicha, M.; Fakhfakh, F.; Mkaouar-Rebai, E., Mutational screening in patients with profound sensorineural hearing loss and neurodevelopmental delay: Description of a novel m.3861A > C mitochondrial mutation in the MT-ND1 gene. Biochem Biophys Res Commun. 2016, 474, 702-708.
[76] Hirst, J.; King, M. S.; Pryde, K. R., The production of reactive oxygen species by complex I. Biochemical Society transactions. 2008, 36, 976-80.
[77] Tretter, L.; Sipos, I.; Adam-Vizi, V., Initiation of neuronal damage by complex I deficiency and oxidative stress in Parkinson's disease. Neurochemical research. 2004, 29, 569-77.
[78] Kirby, D. M.; McFarland, R.; Ohtake, A.; Dunning, C.; Ryan, M. T.; Wilson, C.; Ketteridge, D.; Turnbull, D. M.; Thorburn, D. R.; Taylor, R. W., Mutations of the mitochondrial ND1 gene as a cause of MELAS. Journal of medical genetics. 2004, 41, 784-9.
[79] Spruijt, L.; Smeets, H. J.; Hendrickx, A.; Bettink-Remeijer, M. W.; Maat-Kievit, A.; Schoonderwoerd, K. C.; Sluiter, W.; de Coo, I. F.; Hintzen, R. Q., A MELAS-associated ND1 mutation causing leber hereditary optic neuropathy and spastic dystonia. Archives of neurology. 2007, 64, 890-3.
[80] Blakely, E. L.; de Silva, R.; King, A.; Schwarzer, V.; Harrower, T.; Dawidek, G.; Turnbull, D. M.; Taylor, R. W., LHON/MELAS overlap syndrome associated with a mitochondrial MTND1 gene mutation. Eur J Hum Genet. 2005, 13, 623-627.
[81] Lin, J.; Zhao, C. B.; Lu, J. H.; Wang, H. J.; Zhu, W. H.; Xi, J. Y.; Lu, J.; Luo, S. S.; Ma, D.; Wang, Y.; Xiao, B. G.; Lu, C. Z., Novel mutations m.3959G>A and m.3995A>G in mitochondrial gene MT-ND1 associated with MELAS. Mitochondrial DNA. 2014, 25, 56-62.
[82] Spruijt, L.; Smeets, H. J.; Hendrickx, A.; Bettink-Remeijer, M. W.; Maat-Kievit, A.; Schoonderwoerd, K. C.; Sluiter, W.; de Coo, I. F.; Hintzen, R. Q., A MELAS-Associated ND1 Mutation Causing Leber Hereditary Optic Neuropathy and Spastic Dystonia. Archives of neurology. 2007, 64, 890-893.
[83] Mezghani, N.; Mnif, M.; Mkaouar-Rebai, E.; Kallel, N.; Charfi, N.; Abid, M.; Fakhfakh, F., A maternally inherited diabetes and deafness patient with the 12S rRNA m.1555A>G and the ND1 m.3308T>C mutations associated with multiple mitochondrial deletions. Biochemical and biophysical research communications. 2013, 431, 670-4.
[84] Murphy, M. P.; Hartley, R. C., Mitochondria as a therapeutic target for common pathologies. Nature reviews. Drug discovery. 2018, 17, 865-886.

[85] Zhang, L.; Zhang, Z.; Khan, A.; Zheng, H.; Yuan, C.; Jiang, H., Advances in drug therapy for mitochondrial diseases. Ann Transl Med. 2020, 8, 17-27.
[86] Weissig, V., Drug Development for the Therapy of Mitochondrial Diseases. Trends Mol Med. 2020, 26, 40-57.
[87] Solmonson, A.; DeBerardinis, R. J., Lipoic acid metabolism and mitochondrial redox regulation. J Biol Chem. 2018, 293, 7522-7530.
[88] Parikh, S.; Saneto, R.; Falk, M. J.; Anselm, I.; Cohen, B. H.; Haas, R., A Modern Approach to the Treatment of Mitochondrial Disease. Current Treatment Options in Neurology. 2009, 11, 414–430.
[89] Rodriguez, M. C.; MacDonald, J. R.; Mahoney, D. J.; Parise, G.; Beal, M. F.; Tarnopolsky, M. A., Beneficial effects of creatine, CoQ10, and lipoic acid in mitochondrial disorders. Muscle Nerve. 2007, 35, 235-342.
[90] Avula, S.; Parikh, S.; Demarest, S.; Kurz, J.; Gropman, A., Treatment of mitochondrial disorders. Curr Treat Options Neurol. 2014, 16, 291-311.
[91] Komura, K.; Hobbiebrunken, E.; Wilichowski, E. K. G.; Hanefeld, F. A., Effectiveness of creatine monohydrate in mitochondrial encephalomyopathies. Pediatric Neurology. 2003, 28, 53-58.
[92] Tarnopolsky, M. A., Creatine as a therapeutic strategy for myopathies. Amino Acids. 2011, 40, 1397-407.
[93] Schlame, M.; Ren, M., The role of cardiolipin in the structural organization of mitochondrial membranes. Biochim Biophys Acta. 2009, 1788, 2080-2083.
[94] Szeto, H. H., First-in-class cardiolipin-protective compound as a therapeutic agent to restore mitochondrial bioenergetics. Br J Pharmacol. 2014, 171, 2029-2050.
[95] Zhao, K.; Zhao, G. M.; Wu, D.; Soong, Y.; Birk, A. V.; Schiller, P. W.; Szeto, H. H., Cell-permeable peptide antioxidants targeted to inner mitochondrial membrane inhibit mitochondrial swelling, oxidative cell death, and reperfusion injury. J Biol Chem. 2004, 279, 34682–34690.
[96] Birk, A. V.; Chao, W. M.; Bracken, C.; Warren, J. D.; Szeto, H. H., Targeting mitochondrial cardiolipin and the cytochrome c/cardiolipin complex to promote electron transport and optimize mitochondrial ATP synthesis. Br J Pharmacol. 2014, 171, 2017-2028.
[97] Rudolph, G.; Dimitriadis, K.; Buchner, B.; Heck, S.; Al-Tamami, J.; Seidensticker, F.; Rummey, C.; Leinonen, M.; Meier, T.; Klopstock, T., Effects of idebenone on color vision in patients with leber hereditary optic neuropathy. J Neuroophthalmol. 2013, 33, 30-36.
[98] Sharma, S.; Trivedi, S.; Pandey, T.; Ranjan, S.; Trivedi, M.; Pandey, R., Wedelolactone Mitigates Parkinsonism Via Alleviating Oxidative Stress and Mitochondrial Dysfunction Through NRF2/SKN-1. Mol Neurobiol. 2021, 58, 65-77.
[99] Ma, J.; Kavelaars, A.; Dougherty, P. M.; Heijnen, C. J., Beyond symptomatic relief for chemotherapy-induced peripheral neuropathy: Targeting the source. Cancer. 2018, 124, 2289-2298.
[100] Chokchaiwong, S.; Kuo, Y. T.; Lin, S. H.; Hsu, Y. C.; Hsu, S. P.; Liu, Y. T.; Chou, A. J.; Kao, S. H., Coenzyme Q10 serves to couple mitochondrial oxidative phosphorylation and fatty acid

beta-oxidation, and attenuates NLRP3 inflammasome activation. Free Radic Res. 2018, 52, 1445-1455.
[101] Athanasopoulos, T.; Munye, M. M.; Yanez-Munoz, R. J., Nonintegrating Gene Therapy Vectors. Hematol Oncol Clin North Am. 2017, 31, 753-770.
[102] Gruntman, A. M.; Flotte, T. R., The rapidly evolving state of gene therapy. FASEB J. 2018, 32, 1733-1740.
[103] Faria, R.; Paul, M.; Biswas, S.; Vives, E.; Boisguerin, P.; Sousa, A.; Costa, D., Peptides vs. Polymers: Searching for the Most Efficient Delivery System for Mitochondrial Gene Therapy. Pharmaceutics. 2022, 14, 757-780.
[104] Coutinho, E.; Batista, C.; Sousa, F.; Queiroz, J.; Costa, D., Mitochondrial Gene Therapy: Advances in Mitochondrial Gene Cloning, Plasmid Production, and Nanosystems Targeted to Mitochondria. Mol Pharm. 2017, 14, 626-638.
[105] A, F. C. L., Mitochondrial metabolism and DNA methylation: a review of the interaction between two genomes. Clin Epigenetics. 2020, 12, 1-13.
[106] McManus, M. J.; Picard, M.; Chen, H. W.; De Haas, H. J.; Potluri, P.; Leipzig, J.; Towheed, A.; Angelin, A.; Sengupta, P.; Morrow, R. M.; Kauffman, B. A.; Vermulst, M.; Narula, J.; Wallace, D. C., Mitochondrial DNA Variation Dictates Expressivity and Progression of Nuclear DNA Mutations Causing Cardiomyopathy. Cell Metab. 2019, 29, 78-90.
[107] Reyes, A.; Melchionda, L.; Nasca, A.; Carrara, F.; Lamantea, E.; Zanolini, A.; Lamperti, C.; Fang, M.; Zhang, J.; Ronchi, D.; Bonato, S.; Fagiolari, G.; Moggio, M.; Ghezzi, D.; Zeviani, M., RNASEH1 Mutations Impair mtDNA Replication and Cause Adult-Onset Mitochondrial Encephalomyopathy. Am J Hum Genet. 2015, 97, 186-193.
[108] Du, X.; Wang, J.; Zhou, Q.; Zhang, L.; Wang, S.; Zhang, Z.; Yao, C., Advanced physical techniques for gene delivery based on membrane perforation. Drug Deliv. 2018, 25, 1516-1525.
[109] Herrero, M. J.; Sendra, L.; Miguel, A.; Aliño, S. F., Physical Methods of Gene Delivery. In Safety and Efficacy of Gene-Based Therapeutics for Inherited Disorders. 2017; 113-135.
[110] Schwarz, D.; Kollo, M.; Bosch, C.; Feinauer, C.; Whiteley, I.; Margrie, T. W.; Cutforth, T.; Schaefer, A. T., Architecture of a mammalian glomerular domain revealed by novel volume electroporation using nanoengineered microelectrodes. Nat Commun. 2018, 9, 1-14.
[111] Batabyal, S.; Kim, Y. T.; Mohanty, S., Ultrafast laser-assisted spatially targeted optoporation into cortical axons and retinal cells in the eye. J Biomed Opt. 2017, 22, 60504-60508.
[112] Nomikou, N.; Feichtinger, G. A.; Saha, S.; Nuernberger, S.; Heimel, P.; Redl, H.; McHale, A. P., Ultrasound-responsive gene-activated matrices for osteogenic gene therapy using matrix-assisted sonoporation. J Tissue Eng Regen Med. 2018, 12, 250-260.
[113] Polyakova, T.; Zablotskii, V.; Dejneka, A., Cell Membrane Pore Formation and Change in Ion Channel Activity in High-Gradient Magnetic Fields. IEEE Magnetics Letters. 2017, 8, 1-5.
[114] Bonnefoy, N.; Fox, T. D., Directed Alteration of Saccharomyces cerevisiae Mitochondrial DNA by Biolistic Transformation and Homologous Recombination. Methods in Molecular Biolog. 2007, 372, 153-166.

[115] Yasuzaki, Y.; Yamada, Y.; Ishikawa, T.; Harashima, H., Validation of Mitochondrial Gene Delivery in Liver and Skeletal Muscle via Hydrodynamic Injection Using an Artificial Mitochondrial Reporter DNA Vector. Mol Pharm. 2015, 12 (12), 4311-4320.
[116] Jang, Y. H.; Lim, K. I., Recent Advances in Mitochondria-Targeted Gene Delivery. Molecules. 2018, 23, 2316-2332.
[117] Horten, P.; Colina-Tenorio, L.; Rampelt, H., Biogenesis of Mitochondrial Metabolite Carriers. Biomolecules. 2020, 10, 1008-1021.
[118] Bykov, Y. S.; Rapaport, D.; Herrmann, J. M.; Schuldiner, M., Cytosolic Events in the Biogenesis of Mitochondrial Proteins. Trends Biochem Sci. 2020, 45, 650-667.
[119] Bae, Y.; Joo, C.; Kim, G.-Y.; Ko, K. S.; Huh, K. M.; Han, J.; Choi, J. S., Cationic Oligopeptide-Functionalized Mitochondria Targeting Sequence Show Mitochondria Targeting and Anticancer Activity. Macromolecular Research. 2019, 27, 1071-1080.
[120] Faria, R.; Vives, E.; Boisguerin, P.; Sousa, A.; Costa, D., Development of Peptide-Based Nanoparticles for Mitochondrial Plasmid DNA Delivery. Polymers (Basel). 2021, 13, 1836-1855.
[121] Bayda, S.; Adeel, M.; Tuccinardi, T.; Cordani, M.; Rizzolio, F., The History of Nanoscience and Nanotechnology: From Chemical-Physical Applications to Nanomedicine. Molecules. 2019, 25, 1-15.
[122] Kinnear, C.; Moore, T. L.; Rodriguez-Lorenzo, L.; Rothen-Rutishauser, B.; Petri-Fink, A., Form Follows Function: Nanoparticle Shape and Its Implications for Nanomedicine. Chem Rev. 2017, 117, 11476-11521.
[123] Weissig, V.; Pettinger, T. K.; Murdock, N., Nanopharmaceuticals: products on the market. Int J Nanomedicine. 2014, 9, 4357-4373.
[124] Yuan, Y.; Gu, Z.; Yao, C.; Luo, D.; Yang, D., Nucleic Acid-Based Functional Nanomaterials as Advanced Cancer Therapeutics. Small. 2019, 15, 1-16.
[125] Cordani, M.; Somoza, A., Targeting autophagy using metallic nanoparticles: a promising strategy for cancer treatment. Cell Mol Life Sci. 2019, 76, 1215-1242.
[126] Indoria, S.; Singh, V.; Hsieh, M. F., Recent advances in theranostic polymeric nanoparticles for cancer treatment: A review. Int J Pharm. 2020, 582, 1-15.
[127] Zheng, F.; Xiong, W.; Sun, S.; Zhang, P.; Zhu, J. J., Recent advances in drug release monitoring. Nanophotonics. 2019, 8, 391-413.
[128] Mohd Khair, S. Z. N.; Abd Radzak, S. M.; Mohamed Yusoff, A. A., The Uprising of Mitochondrial DNA Biomarker in Cancer. Dis Markers. 2021, 2021, 1-20.
[129] Trecarichi, A.; Duggett, N. A.; Granat, L.; Lo, S.; Malik, A. N.; Zuliani-Alvarez, L.; Flatters, S. J. L., Preclinical evidence for mitochondrial DNA as a potential blood biomarker for chemotherapy-induced peripheral neuropathy. PLoS One. 2022, 17, 1-15.
[130] Li, L.; Qi, R.; Zhang, L.; Yu, Y.; Hou, J.; Gu, Y.; Song, D.; Wang, X., Potential biomarkers and targets of mitochondrial dynamics. Clin Transl Med. 2021, 11, 529-544.
[131] Tian, H.; Chen, J.; Chen, X., Nanoparticles for gene delivery. Small 2013, 9, 2034-2044.
[132] Seeman, N. C.; Sleiman, H. F., DNA nanotechnology. Nature Reviews Materials. 2017, 3, 1-23.

[133] Ezzati Nazhad Dolatabadi, J.; Valizadeh, H.; Hamishehkar, H., Solid Lipid Nanoparticles as Efficient Drug and Gene Delivery Systems: Recent Breakthroughs. Adv Pharm Bull. 2015, 5, 151-159.
[134] Yamada, Y.; Akita, H.; Harashima, H., Multifunctional envelope-type nano device (MEND) for organelle targeting via a stepwise membrane fusion process. Methods Enzymol. 2012, 509, 301-326.
[135] Khalil, I. A.; Kogure, K.; Futaki, S.; Hama, S.; Akita, H.; Ueno, M.; Kishida, H.; Kudoh, M.; Mishina, Y.; Kataoka, K.; Yamada, M.; Harashima, H., Octaarginine-modified multifunctional envelope-type nanoparticles for gene delivery. Gene Ther. 2007, 14, 682-689.
[136] Yamada, Y.; Furukawa, R.; Yasuzaki, Y.; Harashima, H., Dual function MITO-Porter, a nano carrier integrating both efficient cytoplasmic delivery and mitochondrial macromolecule delivery. Mol Ther. 2011, 19, 1449-1456.
[137] Akita, H.; Kudo, A.; Minoura, A.; Yamaguti, M.; Khalil, I. A.; Moriguchi, R.; Masuda, T.; Danev, R.; Nagayama, K.; Kogure, K.; Harashima, H., Multi-layered nanoparticles for penetrating the endosome and nuclear membrane via a step-wise membrane fusion process. Biomaterials. 2009, 30, 2940-2949.
[138] Yamada, Y.; Fujishita, N.; Harashima, H., A nanocarrier for the mitochondrial delivery of nucleic acids to cardiomyocytes. Nucleosides Nucleotides Nucleic Acids. 2020, 39, 141-155.
[139] Bae, Y.; Jung, M. K.; Song, S. J.; Green, E. S.; Lee, S.; Park, H. S.; Jeong, S. H.; Han, J.; Mun, J. Y.; Ko, K. S.; Choi, J. S., Functional nanosome for enhanced mitochondria-targeted gene delivery and expression. Mitochondrion. 2017, 37, 27-40.
[140] D'Souza, G. G.; Boddapati, S. V.; Weissig, V., Mitochondrial leader sequence--plasmid DNA conjugates delivered into mammalian cells by DQAsomes co-localize with mitochondria. Mitochondrion. 2005, 5, 352-358.
[141] Yamada, Y.; Akita, H.; Kamiya, H.; Kogure, K.; Yamamoto, T.; Shinohara, Y.; Yamashita, K.; Kobayashi, H.; Kikuchi, H.; Harashima, H., MITO-Porter: A liposome-based carrier system for delivery of macromolecules into mitochondria via membrane fusion. Biochim Biophys Acta. 2008, 1778, 423-432.
[142] Yamada, Y.; Harashima, H., Mitochondrial drug delivery systems for macromolecule and their therapeutic application to mitochondrial diseases. Adv Drug Deliv Rev. 2008, 60, 1439-1462.
[143] Kawamura, E.; Yamada, Y.; Harashima, H., Mitochondrial targeting functional peptides as potential devices for the mitochondrial delivery of a DF-MITO-Porter. Mitochondrion. 2013, 13, 610-614.
[144] Yamada, Y.; Nakamura, K.; Abe, J.; Hyodo, M.; Haga, S.; Ozaki, M.; Harashima, H., Mitochondrial delivery of Coenzyme Q10 via systemic administration using a MITO-Porter prevents ischemia/reperfusion injury in the mouse liver. J Control Release. 2015, 213, 86-95.
[145] Kawamura, E.; Maruyama, M.; Abe, J.; Sudo, A.; Takeda, A.; Takada, S.; Yokota, T.; Kinugawa, S.; Harashima, H.; Yamada, Y., Validation of Gene Therapy for Mutant Mitochondria by Delivering Mitochondrial RNA Using a MITO-Porter. Mol Ther Nucleic Acids. 2020, 20, 687-698.

[146] Kawamura, E.; Hibino, M.; Harashima, H.; Yamada, Y., Targeted mitochondrial delivery of antisense RNA-containing nanoparticles by a MITO-Porter for safe and efficient mitochondrial gene silencing. Mitochondrion. 2019, 49, 178-188.
[147] Ishikawa, T.; Somiya, K.; Munechika, R.; Harashima, H.; Yamada, Y., Mitochondrial transgene expression via an artificial mitochondrial DNA vector in cells from a patient with a mitochondrial disease. J Control Release. 2018, 274, 109-117.
[148] Santos, J.; Sousa, F.; Queiroz, J.; Costa, D., Rhodamine based plasmid DNA nanoparticles for mitochondrial gene therapy. Colloids Surf B Biointerfaces. 2014, 121, 129-140.
[149] Wolfram, R. K.; Heller, L.; Csuk, R., Targeting mitochondria: Esters of rhodamine B with triterpenoids are mitocanic triggers of apoptosis. Eur J Med Chem. 2018, 152, 21-30.
[150] Salvado, R.; Sousa, F.; Queiroz, J.; Costa, D., Development of mitochondrial targeting plasmid DNA nanoparticles: Characterization and *in vitro* studies. Colloids and Surfaces A: Physicochemical and Engineering Aspects. 2015, 480, 287-295.
[151] Costa, D.; Costa, C.; Caldeira, M.; Cortes, L.; Queiroz, J. A.; Cruz, C., Targeting of Cellular Organelles by Fluorescent Plasmid DNA Nanoparticles. Biomacromolecules. 2017, 18, 2928-2936.
[152] Sun, Y.; Yang, Q.; Xia, X.; Li, X.; Ruan, W.; Zheng, M.; Zou, Y.; Shi, B., Polymeric Nanoparticles for Mitochondria Targeting Mediated Robust Cancer Therapy. Front Bioeng Biotechnol. 2021, 9, 1-11.
[153] Alvi, M.; Yaqoob, A.; Rehman, K.; Shoaib, S. M.; Akash, M. S. H., PLGA-based nanoparticles for the treatment of cancer: current strategies and perspectives. AAPS Open. 2022, 8, 1-17.
[154] Frede, A.; Neuhaus, B.; Klopfleisch, R.; Walker, C.; Buer, J.; Muller, W.; Epple, M.; Westendorf, A. M., Colonic gene silencing using siRNA-loaded calcium phosphate/PLGA nanoparticles ameliorates intestinal inflammation *in vivo*. J Control Release. 2016, 222, 86-96.
[155] Li, Z.; Ho, W.; Bai, X.; Li, F.; Chen, Y. J.; Zhang, X. Q.; Xu, X., Nanoparticle depots for controlled and sustained gene delivery. J Control Release. 2020, 322, 622-631.
[156] de Oliveira Pedro, R.; Hoffmann, S.; Pereira, S.; Goycoolea, F. M.; Schmitt, C. C.; Neumann, M. G., Self-assembled amphiphilic chitosan nanoparticles for quercetin delivery to breast cancer cells. Eur J Pharm Biopharm. 2018, 131, 203-210.
[157] Raja, M. A.; Katas, H.; Jing Wen, T., Stability, Intracellular Delivery, and Release of siRNA from Chitosan Nanoparticles Using Different Cross-Linkers. PLoS One. 2015, 10, 1-19.
[158] Robles-Planells, C.; Barrera-Avalos, C.; Rojo, L. E.; Spencer, E.; Cortez-San Martin, M.; Matiacevich, S.; Pavez, J.; Milla, L. A.; Navarro, F. D.; Martinez, B. A.; Bravo, F. J.; Mella, A.; Huidobro-Toro, J. P.; Fernandez, R.; Escobar, A.; Castillo, C. A., Chitosan-Based Delivery of Avian Reovirus Fusogenic Protein p10 Gene: *In Vitro* and *In Vivo* Studies towards a New Vaccine against Melanoma. Biomed Res Int. 2020, 1-11.
[159] Tang, Q.; Cao, B.; Lei, X.; Sun, B.; Zhang, Y.; Cheng, G., Dextran-peptide hybrid for efficient gene delivery. Langmuir. 2014, 30, 5202-5208.
[160] Madkhali, O.; Mekhail, G.; Wettig, S. D., Modified gelatin nanoparticles for gene delivery. Int J Pharm. 2019, 554, 224-234.

[161] Zhao, J.; Weng, G.; Li, J.; Zhu, J.; Zhao, J., Polyester-based nanoparticles for nucleic acid delivery. Mater Sci Eng C Mater Biol Appl. 2018, 92, 983-994.
[162] Nguyen, J.; Steele, T. W.; Merkel, O.; Reul, R.; Kissel, T., Fast degrading polyesters as siRNA nano-carriers for pulmonary gene therapy. J Control Release. 2008, 132, 243-251.
[163] Piperno, A.; Sciortino, M. T.; Giusto, E.; Montesi, M.; Panseri, S.; Scala, A., Recent Advances and Challenges in Gene Delivery Mediated by Polyester-Based Nanoparticles. Int J Nanomedicine. 2021, 16, 5981-6002.
[164] Chen, W.; Meng, F.; Cheng, R.; Deng, C.; Feijen, J.; Zhong, Z., Advanced drug and gene delivery systems based on functional biodegradable polycarbonates and copolymers. J Control Release. 2014, 190, 398-414.
[165] Ong, Z. Y.; Fukushima, K.; Coady, D. J.; Yang, Y. Y.; Ee, P. L.; Hedrick, J. L., Rational design of biodegradable cationic polycarbonates for gene delivery. J Control Release. 2011, 152, 120-126.
[166] Chen, C. K.; Huang, P. K.; Law, W. C.; Chu, C. H.; Chen, N. T.; Lo, L. W., Biodegradable Polymers for Gene-Delivery Applications. Int J Nanomedicine. 2020, 15, 2131-2150.
[167] K, S. A.; Almatroudi, A.; Alsahli, M. A.; Aljaghwani, A.; A, M. E.-K.; Rahmani, A. H.; Khan, A. A., Novel Strategies for Disrupting Cancer-Cell Functions with Mitochondria-Targeted Antitumor Drug-Loaded Nanoformulations. Int J Nanomedicine. 2021, 16, 3907-3936.
[168] Zielonka, J.; Joseph, J.; Sikora, A.; Hardy, M.; Ouari, O.; Vasquez-Vivar, J.; Cheng, G.; Lopez, M.; Kalyanaraman, B., Mitochondria-Targeted Triphenylphosphonium-Based Compounds: Syntheses, Mechanisms of Action, and Therapeutic and Diagnostic Applications. Chem Rev. 2017, 117, 10043-10120.
[169] Guzman-Villanueva, D.; Mendiola, M. R.; Nguyen, H. X.; Yambao, F.; Yu, N.; Weissig, V., Conjugation of Triphenylphosphonium Cation to Hydrophobic Moieties to Prepare Mitochondria-Targeting Nanocarriers. Methods Mol Biol. 2019, 2000, 183-189.
[170] Marrache, S.; Tundup, S.; Harn, D. A.; Dhar, S., Ex Vivo Programming of Dendritic Cells by Mitochondria-Targeted Nanoparticles to Produce InterferonGamma for Cancer Immunotherapy. American Chemical Society. 2013, 7, 7392–7402.
[171] Marrache, S.; Dhar, S., Engineering of blended nanoparticle platform for delivery of mitochondria-acting therapeutics. Proc Natl Acad Sci U S A. 2012, 109, 16288-16293.
[172] Marrache, S.; Tundup, S.; Harn, D. A.; Dhar, S., Ex vivo programming of dendritic cells by mitochondria-targeted nanoparticles to produce interferon-gamma for cancer immunotherapy. ACS Nano. 2013, 7, 7392-7402.
[173] Arafa, K. K.; Hamzawy, M. A.; Mousa, S. A.; El-Sherbiny, I. M., Mitochondria-targeted alginate/triphenylphosphonium-grafted-chitosan for treatment of hepatocellular carcinoma. RSC Adv. 2022, 12, 21690-21703.
[174] Bae, Y.; Jung, M. K.; Lee, S.; Song, S. J.; Mun, J. Y.; Green, E. S.; Han, J.; Ko, K. S.; Choi, J. S., Dequalinium-based functional nanosomes show increased mitochondria targeting and anticancer effect. Eur J Pharm Biopharm. 2018, 124, 104-115.
[175] Mallick, S.; Song, S. J.; Bae, Y.; Choi, J. S., Self-assembled nanoparticles composed of glycol chitosan-dequalinium for mitochondria-targeted drug delivery. Int J Biol Macromol. 2019, 132, 451-460.

[176] Casper, J.; Schenk, S. H.; Parhizkar, E.; Detampel, P.; Dehshahri, A.; Huwyler, J., Polyethylenimine (PEI) in gene therapy: Current status and clinical applications. J Control Release. 2023, 362, 667-691.
[177] Fattahi, N.; Gorgannezhad, L.; Masoule, S. F.; Babanejad, N.; Ramazani, A.; Raoufi, M.; Sharifikolouei, E.; Foroumadi, A.; Khoobi, M., PEI-based functional materials: Fabrication techniques, properties, and biomedical applications. Adv Colloid Interface Sci. 2024, 325, 1-44.
[178] Cheraghi, R.; Alipour, M.; Nazari, M.; Hosseinkhani, S., Optimization of conditions for gene delivery system based on PEI. Nanomed J. 2017, 4, 8-16.
[179] Ghriga, M. A.; Grassl, B.; Gareche, M.; Khodja, M.; Lebouachera, S. E. I.; Andreu, N.; Drouiche, N., Review of recent advances in polyethylenimine crosslinked polymer gels used for conformance control applications. Polymer Bulletin. 2019, 76, 6001-6029.
[180] Zakeri, A.; Kouhbanani, M. A. J.; Beheshtkhoo, N.; Beigi, V.; Mousavi, S. M.; Hashemi, S. A. R.; Karimi Zade, A.; Amani, A. M.; Savardashtaki, A.; Mirzaei, E.; Jahandideh, S.; Movahedpour, A., Polyethylenimine-based nanocarriers in co-delivery of drug and gene: a developing horizon. Nano Rev Exp. 2018, 9, 1-14.
[181] Ayalew, Z. M.; Guo, X.; Zhang, X., Synthesis and application of polyethyleneimine (PEI)-based composite/nanocomposite material for heavy metals removal from wastewater: A critical review. Journal of Hazardous Materials Advances. 2022, 8, 100158-100166.
[182] Zhang, H.; Chen, Z.; Du, M.; Li, Y.; Chen, Y., Enhanced gene transfection efficiency by low-dose 25 kDa polyethylenimine by the assistance of 1.8 kDa polyethylenimine. Drug Deliv. 2018, 25 (1), 1740-1745.
[183] Monnery, B. D.; Wright, M.; Cavill, R.; Hoogenboom, R.; Shaunak, S.; Steinke, J. H. G.; Thanou, M., Cytotoxicity of polycations: Relationship of molecular weight and the hydrolytic theory of the mechanism of toxicity. Int J Pharm. 2017, 521, 249-258.
[184] Yu, Q.; Zhang, M.; Chen, Y.; Chen, X.; Shi, S.; Sun, K.; Ye, R.; Zheng, Y.; Chen, Y.; Xu, Y.; Peng, J., Self-Assembled Nanoparticles Prepared from Low-Molecular-Weight PEI and Low-Generation PAMAM for EGFRvIII-Chimeric Antigen Receptor Gene Loading and T-Cell Transient Modification. Int J Nanomedicine. 2020, 15, 483-495.
[185] Karimov, M.; Appelhans, D.; Ewe, A.; Aigner, A., The combined disulfide cross-linking and tyrosine-modification of very low molecular weight linear PEI synergistically enhances transfection efficacies and improves biocompatibility. Eur J Pharm Biopharm. 2021, 161, 56-65.
[186] Kazemi, M.; Parhizkar, E.; Samani, S. M.; Firuzi, O.; Sadeghpour, H.; Ahmadi, F.; Dehshahri, A., Targeted co-delivery of paclitaxel and anti P-gp shRNA by low molecular weight PEI decorated with L-3,4-dihydroxyphenylalanine. Biotechnol Prog. 2023, 39, 1-13.
[187] Nicolle, L.; Casper, J.; Willimann, M.; Journot, C. M. A.; Detampel, P.; Einfalt, T.; Grisch-Chan, H. M.; Thony, B.; Gerber-Lemaire, S.; Huwyler, J., Development of Covalent Chitosan-Polyethylenimine Derivatives as Gene Delivery Vehicle: Synthesis, Characterization, and Evaluation. Int J Mol Sci. 2021, 22, 1-25.
[188] Casper, J.; Nicolle, L.; Willimann, M.; Kuzucu, E. U.; Tran, A.; Robin, P.; Detampel, P.; Grisch-Chan, H. M.; Thony, B.; Huwyler, J.; Gerber-Lemaire, S., Core-Shell Structured Chitosan-

Polyethylenimine Nanoparticles for Gene Delivery: Improved Stability, Cellular Uptake, and Transfection Efficiency. Macromol Biosci. 2023, 23, 1-14.
[189] Lee, Y. H.; Park, H. I.; Choi, J. S., Novel glycol chitosan-based polymeric gene carrier synthesized by a Michael addition reaction with low molecular weight polyethylenimine. Carbohydr Polym. 2016, 137, 669-677.
[190] Craciun, B. F.; Gavril, G.; Peptanariu, D.; Ursu, L. E.; Clima, L.; Pinteala, M., Synergistic Effect of Low Molecular Weight Polyethylenimine and Polyethylene Glycol Components in Dynamic Nonviral Vector Structure, Toxicity, and Transfection Efficiency. Molecules. 2019, 24, 1460-1473.
[191] Jwameer, M. R.; Salman, S. A.; Noori, F. T. M.; Sulaiman, G. M.; Jabir, M. S.; Khalil, K. A. A.; Ahmed, E. M.; Soliman, M. T. A.; Cherukula, K., Antiproliferative Activity of PEG-PEI-SWCNTs against AMJ13 Breast Cancer Cells. Journal of Nanomaterials. 2023, 2023, 1-8.
[192] Ke, X.; Shelton, L.; Hu, Y.; Zhu, Y.; Chow, E.; Tang, H.; Santos, J. L.; Mao, H. Q., Surface-Functionalized PEGylated Nanoparticles Deliver Messenger RNA to Pulmonary Immune Cells. ACS Appl Mater Interfaces. 2020, 12, 35835-35844.
[193] Li, A.; Qiu, J.; Zhou, B.; Xu, B.; Xiong, Z.; Hao, X.; Shi, X.; Cao, X., The gene transfection and endocytic uptake pathways mediated by PEGylated PEI-entrapped gold nanoparticles. Arabian Journal of Chemistry. 2020, 13, 2558-2567.
[194] Nikzamir, M.; Hanifehpour, Y.; Akbarzadeh, A.; Panahi, Y., Applications of Dendrimers in Nanomedicine and Drug Delivery: A Review. Journal of Inorganic and Organometallic Polymers and Materials. 2021, 31, 2246-2261.
[195] Surekha, B.; Kommana, N. S.; Dubey, S. K.; Kumar, A. V. P.; Shukla, R.; Kesharwani, P., PAMAM dendrimer as a talented multifunctional biomimetic nanocarrier for cancer diagnosis and therapy. Colloids Surf B Biointerfaces. 2021, 204, 111837-111862.
[196] Oddone, N.; Lecot, N.; Fernandez, M.; Rodriguez-Haralambides, A.; Cabral, P.; Cerecetto, H.; Benech, J. C., *In vitro* and *in vivo* uptake studies of PAMAM G4.5 dendrimers in breast cancer. J Nanobiotechnology. 2016, 14, 1-12.
[197] Wang, X.; Shao, N.; Zhang, Q.; Cheng, Y., Mitochondrial targeting dendrimer allows efficient and safe gene delivery. J Mater Chem B. 2014, 2, 2546-2553.
[198] Biswas, S.; Dodwadkar, N. S.; Piroyan, A.; Torchilin, V. P., Surface conjugation of triphenylphosphonium to target poly(amidoamine) dendrimers to mitochondria. Biomaterials. 2012, 33, 4773-4782.
[199] Huang, S.; Shao, K.; Liu, Y.; Kuang, Y.; Li, J.; An, S.; Guo, Y.; Ma, H.; Jiang, C., Tumor-Targeting and Microenvironment-Responsive Smart Nanoparticles for Combination Therapy of Antiangiogenesis and Apoptosis. Acsnano. 2013, 7, 2860–2871.
[200] Huang, R.; Ke, W.; Liu, Y.; Jiang, C.; Pei, Y., The use of lactoferrin as a ligand for targeting the polyamidoamine-based gene delivery system to the brain. Biomaterials. 2008, 29, 238-246.
[201] Han, L.; Guo, Y.; Ma, H.; He, X.; Kuang, Y.; Zhang, N.; Lim, E.; Zhou, W.; Jiang, C., Acid active receptor-specific peptide ligand for *in vivo* tumor-targeted delivery. Small. 2013, 9, 3647-3658.

[202] Chen, H.; Tian, J.; Liu, D.; He, W.; Guo, Z., Dual aptamer modified dendrigraft poly-l-lysine nanoparticles for overcoming multi-drug resistance through mitochondrial targeting. J Mater Chem B. 2017, 5, 972-979.
[203] Guidotti, G.; Brambilla, L.; Rossi, D., Cell-Penetrating Peptides: From Basic Research to Clinics. Trends Pharmacol Sc.i 2017, 38, 406-424.
[204] Li, C.; Callahan, A. J.; Phadke, K. S.; Bellaire, B.; Farquhar, C. E.; Zhang, G.; Schissel, C. K.; Mijalis, A. J.; Hartrampf, N.; Loas, A.; Verhoeven, D. E.; Pentelute, B. L., Automated Flow Synthesis of Peptide-PNA Conjugates. ACS Cent Sci. 2022, 8, 205-213.
[205] Copolovici, D. M.; Langel, K.; Eriste, E.; Langel, U., Cell-Penetrating Peptides: Design, Synthesis, and Applications. American Chemical Society. 2014, 8, 1972–1994
[206] Keller, A. A.; Mussbach, F.; Breitling, R.; Hemmerich, P.; Schaefer, B.; Lorkowski, S.; Reissmann, S., Relationships between Cargo, Cell Penetrating Peptides and Cell Type for Uptake of Non-Covalent Complexes into Live Cells. Pharmaceuticals (Basel). 2013, 6, 184-203.
[207] Derakhshankhah, H.; Jafari, S., Cell penetrating peptides: A concise review with emphasis on biomedical applications. Biomed Pharmacother. 2018, 108, 1090-1096.
[208] Konate, K.; Dussot, M.; Aldrian, G.; Vaissiere, A.; Viguier, V.; Neira, I. F.; Couillaud, F.; Vives, E.; Boisguerin, P.; Deshayes, S., Peptide-Based Nanoparticles to Rapidly and Efficiently "Wrap 'n Roll" siRNA into Cells. Bioconjug Chem. 2019, 30, 592-603.
[209] Konate, K.; Josse, E.; Tasic, M.; Redjatti, K.; Aldrian, G.; Deshayes, S.; Boisguerin, P.; Vives, E., WRAP-based nanoparticles for siRNA delivery: a SAR study and a comparison with lipid-based transfection reagents. J Nanobiotechnology. 2021, 19, 236-254.
[210] Boisguérin, P.; Konate, K.; Josse, E.; Vivès, E.; Deshayes, S., Peptide-Based Nanoparticles for Therapeutic Nucleic Acid Delivery. Biomedicines. 2021, 9, 1-27.
[211] Sousa, A.; Almeida, A. M.; Faria, R.; Konate, K.; Boisguerin, P.; Queiroz, J. A.; Costa, D., Optimization of peptide-plasmid DNA vectors formulation for gene delivery in cancer therapy exploring design of experiments. Colloids Surf B Biointerfaces. 2019, 183, 1-7.
[212] Kokova, V., Methods for determining sub-acute, sub-chronic, and chronic toxicity of chemical compounds. knowledge - International Journal 2023, 59, 257–261.
[213] De Jong, W. H.; Carraway, J. W.; Geertsma, R. E., In vivo and in vitro testing for the biological safety evaluation of biomaterials and medical devices. In Biocompatibility and Performance of Medical Devices, 2020; 123-166.
[214] Basu, B., Probing Toxicity of Biomaterials and Biocompatibility Assessment. In Biomaterials for Musculoskeletal Regeneration, 2017; 291-351.
[215] Morgan, S. J.; Elangbam, C. S.; Berens, S.; Janovitz, E.; Vitsky, A.; Zabka, T.; Conour, L., Use of animal models of human disease for nonclinical safety assessment of novel pharmaceuticals. Toxicol Pathol 2013, 41, 508-18.
[216] Fonseca-Gomes, J.; Loureiro, J. A.; Tanqueiro, S. R.; Mouro, F. M.; Ruivo, P.; Carvalho, T.; Sebastiao, A. M.; Diogenes, M. J.; Pereira, M. C., In vivo Bio-Distribution and Toxicity Evaluation of Polymeric and Lipid-Based Nanoparticles: A Potential Approach for Chronic Diseases Treatment. Int J Nanomedicine 2020, 15, 8609-8621.

[217] Wang, B.; HE, X.; Zhang, Z.; Zhao, Y.; Feng, W., Metabolism of Nanomaterials in Vivo: Blood Circulation and Organ Clearance. accounts of chemical research 2011, 46, 761–769.
[218] Zhang, A.; Meng, K.; Liu, Y.; Pan, Y.; Qu, W.; Chen, D.; Xie, S., Absorption, distribution, metabolism, and excretion of nanocarriers in vivo and their influences. Adv Colloid Interface Sci 2020, 284, 102261.
[219] Saeidnia, S.; Manayi, A.; Abdollahi, M., From in vitro Experiments to in vivo and Clinical Studies; Pros and Cons. Current drug discovery technologies 2015, 12, 218-24.
[220] Giselbrecht, J.; Pinnapireddy, S. R.; Alioglu, F.; Sami, H.; Sedding, D.; Erdmann, F.; Janich, C.; Schulz-Siegmund, M.; Ogris, M.; Bakowsky, U.; Langner, A.; Bussmann, J.; Wolk, C., Investigating 3R In Vivo Approaches for Bio-Distribution and Efficacy Evaluation of Nucleic Acid Nanocarriers: Studies on Peptide-Mimicking Ionizable Lipid. Small 2022, 18, 2107768.
[221] Wang, F.; Liu, L. S.; Li, P.; Lau, C. H.; Leung, H. M.; Chin, Y. R.; Tin, C.; Lo, P. K., Cellular uptake, tissue penetration, biodistribution, and biosafety of threose nucleic acids: Assessing in vitro and in vivo delivery. Mater Today Bio 2022, 15, 100299.
[222] Tariq, I.; Ali, M. Y.; Sohail, M. F.; Amin, M. U.; Ali, S.; Bukhari, N. I.; Raza, A.; Pinnapireddy, S. R.; Schafer, J.; Bakowsky, U., Lipodendriplexes mediated enhanced gene delivery: a cellular to pre-clinical investigation. Sci Rep 2020, 10, 21446.
[223] Gileva, A. M.; Koloskova, O. O.; Nosova, A. S.; Vishniakova, L. I.; Simonova, V. A.; Kurbanova, L. A.; Egorenkov, E. A.; Smirnov, V. V.; Budanova, U. A.; Sebyakin, Yu. L.; Suzina, N. E.; Khaitov, M. R.; Markvicheva, E., Transfection efficacy and drug release depends upon the PEG derivative in cationic lipoplexes: Evaluation in 3D in vitro model and in vivo. Journal of biomedical materials research. Part B, Applied biomaterials 2023, 111, 1614-1628.
[224] Engin, A. B.; Nikitovic, D.; Neagu, M.; Henrich-Noack, P.; Docea, A. O.; Shtilman, M. I.; Golokhvast, K.; Tsatsakis, A. M., Mechanistic understanding of nanoparticles' interactions with extracellular matrix: the cell and immune system. Part Fibre Toxicol 2017, 14, 22.
[225] Moros, M.; Mitchell, S. G.; Grazú, V.; de la Fuente, J. M., The fate of nanocarriers as nanomedicines in vivo: important considerations and biological barriers to overcome. Current medicinal chemistry 2013, 20, 2759-2778.
[226] Singh, V. K.; Seed, T. M., How necessary are animal models for modern drug discovery? Expert Opin Drug Discov 2021, 16, 1391-1397.
[227] Bailone, R. L.; Fukushima, H. C. S.; Ventura Fernandes, B. H.; De Aguiar, L. K.; Correa, T.; Janke, H.; Grejo Setti, P.; Roca, R. O.; Borra, R. C., Zebrafish as an alternative animal model in human and animal vaccination research. Lab Anim Res 2020, 36, 13.
[228] Dubey, A.; Ghosh, N. S.; Singh, R., Zebrafish as An Emerging Model: An Important Testing Platform for Biomedical Science. Journal of Pharmaceutical Negative Results 2022, 13 (3), 1-7.
[229] McGrath, P.; Li, C.-Q., Zebrafish: a predictive model for assessing drug-induced toxicity. Drug Discovery Today 2008, 13 (9-10), 394-401.
[230] Patton, E. E.; Zon, L. I.; Langenau, D. M., Zebrafish disease models in drug discovery: from preclinical modelling to clinical trials. Nature Reviews Drug Discovery. 2021, 20, 611-628.
[231] Li, J.; Ge, W., Zebrafish as a model for studying ovarian development: Recent advances from targeted gene knockout studies. Mol Cell Endocrinol. 2020, 507, 1-19.

[232] Haque, E.; Ward, A., Zebrafish as a Model to Evaluate Nanoparticle Toxicity. Nanomaterials. 2018, 8, 561-579.
[233] Teame, T.; Zhang, Z.; Ran, C.; Zhang, H.; Yang, Y.; Ding, Q.; Xie, M.; Gao, C.; Ye, Y.; Duan, M.; Zhou, Z., The use of zebrafish (*Danio rerio*) as biomedical models. Animal Frontiers. 2019, 9, 68-77.
[234] Bhattarai, P.; Turgutalp, B.; Kizil, C., Zebrafish as an Experimental and Preclinical Model for Alzheimer's Disease. ACS Chemical Neuroscience. 2022, 13, 2939-2941.
[235] Shen, C.; Zuo, Z., Zebrafish (*Danio rerio*) as an excellent vertebrate model for the development, reproductive, cardiovascular, and neural and ocular development toxicity study of hazardous chemicals. Environmental Science and Pollution Research. 2020, 27, 43599-43614.

Chapter 2

Aims of the Thesis

Mitochondrial DNA is very vulnerable to mutations and a quite frequent cause of mitochondrial cytopathy, resulting in a huge variety of clinical phenotypes. In terms of clinical relevance, mtDNA disorders are among the most prevalent of all genetic disorders, with approximately 1 in 8000 individuals affected. While there is no satisfactory treatment for these patients than the administration of a set of drugs, gene therapy emerges as an exciting approach and a valuable option for mitochondrial diseases due to mtDNA mutations. Despite the advances in the mitochondrial gene therapy field, researchers still seek the conception of an advanced and innovative vector for therapeutic applications. In this context, the main goal of this doctoral thesis is the design and development of delivery systems targeting mitochondria to contribute to the advancement of mitochondrial gene therapy. To achieve this, the present work was dedicated to create delivery systems based on polymers and peptides, in which ligands were added, that allow specific targeting to mitochondria and the delivery of mitochondrial ND1 gene.

To achieve the main objective, this doctoral thesis was divided into four big goals:

1. To design and synthesize delivery systems based on peptides and polymers, incorporating ligands in their constitution that allow targeting to the mitochondria;
2. The physicochemical and morphological characterization of the polymeric and peptide nanoparticles developed throughout this doctoral thesis;
3. *In vitro* studies on different types of cells to evaluate the efficiency of developed systems in terms of cytotoxicity, cellular uptake capacity, targeting to mitochondria, transcription of the mitochondrial ND1 gene, and translation of the respective protein;
4. Studies in ZF to determine the toxicity of formulated nanoparticles in animal models and verify their capacity for internalization and distribution throughout the body of this *in vivo* model.

In this way, this doctoral thesis was organized in 8 chapters:
Chapter 1 presents a general introduction to mitochondria, the mitochondrial genome, mtDNA mutations, mitochondrial diseases, and current treatments on the market. It also contains an introduction to mitochondrial gene therapy and the different systems used for this type therapy.

Chapter 2 presents the objectives of this doctoral thesis and a brief description of the content of each chapter.

Chapter 3 depicts the objective of the design and synthesis of PEI-based polymeric systems, in which TPP was added to confer affinity for mitochondria. Through the design of experiments, the

goal was to determine the best conditions for formulating nanoparticles with as few tests as possible. **Chapter 4** follows the previous chapter, intending to characterize the developed delivery systems and evaluate their *in vitro* efficiency, namely targeting mitochondria and production of the ND1 protein.

Chapter 5 describes the synthesis steps of several CPPs to which the MTS sequence was added to confer affinity for mitochondria. After the synthesis of the peptides and the formulation of the CPP-based systems, the nanoparticles were characterized in terms of size, surface charge, morphology, and encapsulation capacity of pND1. Having demonstrated that the vectors developed have suitable properties for the delivery of pND1, their specific targeting to the mitochondria was evaluated.

In **Chapter 6**, a comparison was made between the PEI/pND1 systems and the CPP/pND1 systems. To this end, PEI-based systems were developed in which DQA molecules were used as a ligand to confer affinity for mitochondria. After characterization of the PEI-DQA/pND1 systems, these systems were compared with the MTS-CPP/pND1 systems. The comparison was made in terms of cellular internalization, mitochondria targeting, delivery of the mitochondrial ND1 gene within mitochondria, and production of the ND1 protein. This chapter aimed to determine the most suitable delivery system developed during this doctoral thesis, to proceed to *in vivo* trials.

Chapter 7 demonstrates that the MTS-CPP/pND1 systems can be modified with the addition of PEG without altering their physicochemical properties. Furthermore, it has been demonstrated that these systems do not present toxicity in ZF embryos, which remain stable and do not induce changes in the growth of these living beings. Finally, it was also demonstrated that CPP-based systems can be internalized in ZF embryos and distributed evenly throughout the body of these organisms.

Chapter 8 presents the conclusions of the main results obtained in this doctoral thesis and future perspectives.

Fulfillment of these objectives allows for progress in mitochondrial gene therapy field, more specifically in the creation of efficient delivery systems that allow targeted gene delivery to mitochondria.

Chapter 3

Design of experiments to select triphenylphosphonium-polyplexes with suitable physicochemical properties for mitochondrial gene therapy

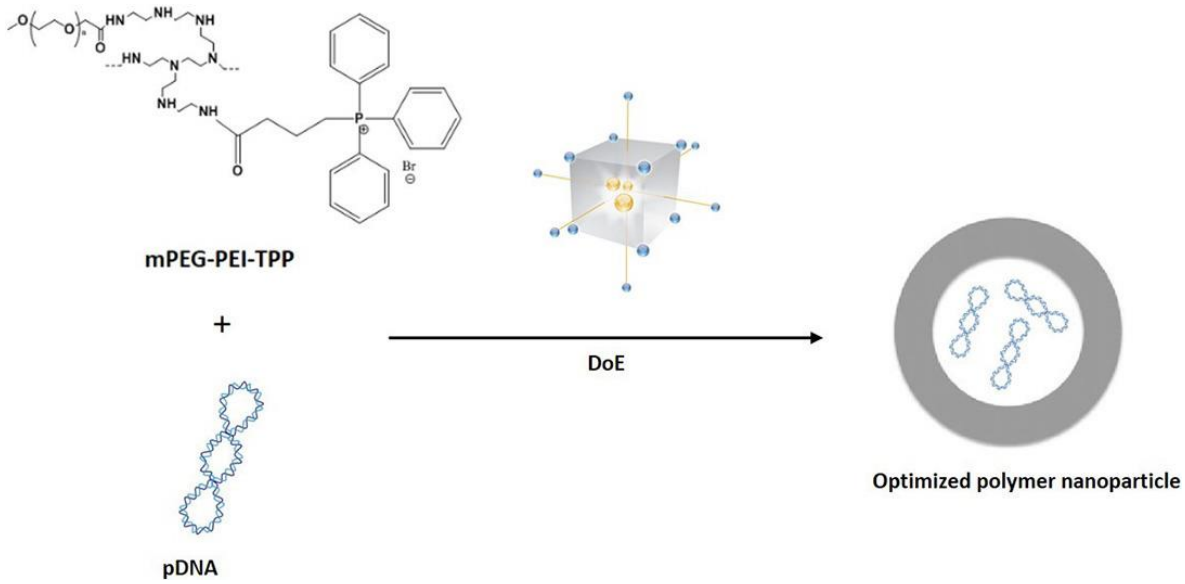

This chapter was published in:
Ângela Sousa, Rúben Faria, Tânia Albuquerque, Himanshu Bhatt, Swati Biswas, João A. Queiroz, and Diana Costa. 2020. 'Design of experiments to select triphenylphosphonium-polyplexes with suitable physicochemical properties for mitochondrial gene therapy', Journal of Molecular Liquids, 302.
https://doi.org/10.1016/j.molliq.2020.112488

3.1 Abstract

Mitochondrial gene therapy can be seen as a promising tool and a revolutionary approach toward mitochondrial diseases arising from mitochondrial DNA mutations. The conception of a viable and suitable mitochondrial targeted vector is imperative to turn this therapy clinically feasible. To accomplish this goal, different molecular weight polyethylenimine (PEI) have been conjugated with the mitochondriotropic agent triphenylphosphonium (TPP) and the interaction of this polycation with the ND1 (mitochondrially encoded NADH dehydrogenase 1 protein) plasmid DNA has been explored for the formation of nanometer complexes. To quickly, easily, and with reduced costs find out the most adequate gene delivery vector, a design of experiments (DoE) tool has been explored. For each different molecular weight PEI delivery system, the nitrogen to phosphate groups' ratio (N/P) and the pDNA volume were selected as DoE inputs and the pDNA complexation capacity (CC), surface charge, and polyplexes size were considered DoE outputs. The study revealed that the combination of high N/P ratios with lower pDNA volume of the inputs favors the formulation of optimal carriers after the output maximization of pDNA CC and positive surface charge and output minimization of the particle sizes. Moreover, it was demonstrated that the N/P ratio greatly influences its capacity to condense ND1-based pDNA along with PEI molecular weight. This work allows for the selection of the gene delivery vector possessing the most convenient physicochemical properties for further studies of mitochondrial gene therapy.

3.2 Introduction

The mitochondrion is a cellular organelle composed of four enzymatic complexes and responsible for the production of chemical energy (ATP). It also has important functions in several cellular processes, such as ion homeostasis and cellular signaling, and in the control of both cell cycle and cell growth [1–3]. Besides, mitochondria play a determining role in apoptosis [4,5]. Similar to the nucleus, the mitochondrion has its own genome, the mitochondrial DNA (mtDNA). This is a double-stranded and circular molecule (16 kbp) encoding 13 polypeptides exhibiting relevant roles in the oxidative phosphorylation chain, 2 rRNAs, and 22 tRNAs, all exclusive to the mitochondria. In the nucleus is encoded genetic information related to the control of mitochondria. Mutations in mtDNA originate a variety of severe metabolic and neuromuscular degenerative syndromes and/or pathologies, particularly affecting vital organs such as the heart and the brain, as well as the nervous and endocrine systems [6–8]. Specifically, mutations in complex I genes have been associated with Parkinson's and Alzheimer's diseases, diabetes, and a major tendency for cancer development [9–11]. Currently, the treatment of mtDNA-based disorders is focused on the administration of a set of pharmaceutics with the main aim of alleviating the various symptoms; a therapy largely supportive rather than curative, being ineffective. In this context and to properly address this gap, mitochondrial gene therapy emerges as an exciting and powerful technology to correct mtDNA mutations, by replacing the mutated genes, therefore restoring the normal mitochondrial function. To consider this therapy feasible and viable in a clinical setting, the conception of a suitable mitochondrial gene-based vector is

mandatory. Pursuing this challenge, several researchers have worked on the design and development of such delivery systems and relevant progress has been made [12–16]. Among them, Lyrawati *et al.* and Cardoso *et al.* greatly contributed to the mitochondrial gene therapy field through the creation of an artificial mini-mitochondrial genome and the application of gemini surfactants for gene delivery into mitochondria, respectively [17,18]. Recently, our team also added a crucial contribution to this area through the cloning, for the first time, of the mitochondrial gene ND1 in *E. coli*, which was maintained in a plasmid [19]. Following this, ND1 plasmid-based nanoparticles were produced and mitochondria targeting of these nano-systems, coupled with rhodamine 123, has been reported [19]. The strategy of using mitochondriotropic molecules, which exhibit a considerable degree of lipophilicity and have delocalized charges accumulating in the mitochondria in virtue of the mitochondrial membrane potential, appears as a great asset in the direct transfection of mitochondria [20,21]. In particular, triphenylphosphonium (TPP), a lipophilic cation, revealed a high affinity for mitochondria. Mitochondrial membrane potential is recognized to be approximately –180 mV, which ensures a TPP accumulation in this organelle in the range of 1000-fold [22]. The conjugation of TPP with therapeutic molecules or delivery systems promotes mitochondria targeting and enhancing therapeutic efficacy [23–28]. Unlike nuclear gene therapy, to date, few studies have demonstrated effective gene delivery and protein expression in mitochondria and this topic remains a great challenge [29]. Therefore, our research team has used their vast background in the development of synthetic carriers for biomedical applications in the conception of a promising mitochondrial gene delivery system. In this work, PEI was linked with polyethylene glycol (PEG) to reduce its toxicity, and the polycation PEG-PEI at different molecular weights was conjugated with TPP. PEG-PEI-TPP was used to condense the ND1-based plasmid. PEI can efficiently condense DNA into nanometer complexes due to its high cationic charge density, which favors its interaction with the negative phosphate groups of DNA [30,31]. Additionally, PEI possesses an impressive endosomolytic activity [32]. For gene therapy purposes, PEG-PEI-TPP/pDNA nano-systems should present a size below 200 nm for easy cellular uptake and internalization, a positive surface charge to facilitate the interaction with the negatively charged proteoglycans in the cellular membrane and pDNA must be efficiently complexed. In line with this, the formulation of the most suitable PEG-PEI-TPP/pDNA-based delivery system from different PEI molecular weights can be costly and a time-consuming task. Design of experiments (DoE) is an efficient tool to optimize the polyplexes formation in order to reveal the most appropriate carriers to be further explored in mitochondrial gene therapy. In this report, Central Composite Design (CCD) was applied to unravel the set of conditions, at the vector preparation step, that originate the most promising PEG-PEI-TPP/pDNA vehicles. DoE, with a reduced number of experiments relative to random strategy, allows for a wider understanding of complex formulation by systematically and simultaneously varying and combining different parameters [33–35].

3.3 Materials and Methods

3.3.1 Materials

Methoxy-polyethyleneglycol-Succinimidyl Carboxymethyl Ester (mPEG-SCM ester, MW2000 Da) was purchased from Jenkem Technology (Plano, TX). Branched polyethylenimine (PEI) (M.W.:1800 Da and 10,000 Da) was from Polysciences, Inc. (Warrington, PA, USA). Another Branched polyethylenimine (PEI) (M.W.:25,000 Da) was purchased from Sigma Aldrich (St. Louis, MO). 3-Carboxypropyltriphenylphosphonium bromide (TPP), N-ethyldiisopropylamine (DIPEA), N-(3-Dimethylaminopropyl)-N′-ethylcarbodiimide hydrochloride (EDC. HCl, 98%) and NHS (98%) were purchased from Sigma-Aldrich Chemicals (St. Louis, MO). Regenerated cellulose dialysis membrane (molecular weight-cutoff (MWCO) 1 kDa, 3.5 kDa, and 14 kDa, respectively) was obtained from Spectrum Laboratories, Inc. (Dominguez, CA). All chemicals were of analytical grade. All solutions were freshly prepared using ultra-pure grade water, purified with a Milli-Q system from Millipore (Billerica, MA, USA).

3.3.2 Plasmid

The pCAG-GFP-ND1 plasmid, developed by our research group, was used in this study [19]. In a previous work, for the first time, the mitochondrially NADH dehydrogenase 1 protein encoded gene (mtND1) was successfully cloned in *E. coli* and it remained stable in multi-copy pCAG-GFP plasmid. Full details from gene cloning and plasmid production are described elsewhere [19].

3.3.3 Synthesis of mPEG-PEI-TPP polymer

3.3.3.1 Synthesis of mPEG-SCM ester and PEI (mPEG-PEI)

To the solution of mPEG-SCM ester (50 mg) in chloroform ($CHCl_3$) (1 mL) in a round bottom flask, PEI (MW 1.8 kDa, 10 kDa, or 25 kDa) was added dropwise at a molar ratio of 1:1. DIPEA (20 μL) was added as a base to the reaction mixture. The reaction was continued overnight, the solvent was evaporated under vacuum, and the reaction mixture containing mPEG-PEI constituting of PEI (MW 1.8, 10, and 25 kDa) was dialyzed for 48 h using the dialysis membranes of 1, 3.5, and 12–14 kDa MWCO cellulose ester membranes, respectively. Solid mPEG-PEI was obtained after lyophilization of the dialysate. The attachment of mPEG to PEI was characterized and confirmed by ^{1}H, and ^{31}P nuclear magnetic resonance (NMR), Fourier-transform infrared spectroscopy (FTIR), and gel permeation chromatography.

3.3.3.2 Synthesis of mPEG-PEI and TPP (mPEG-PEI-TPP)

TPP was dissolved into 1 mL Dimethylsulphoxide (DMSO) in a round bottom flask. Carboxy terminal of TPP was activated using EDC/NHS and was reacted with a molar ratio of 3:1 in DMSO for 4 h. The previously synthesized mPEG-PEI was also dissolved in 2 mL DMSO and added dropwise into the activated TPP solution. DIPEA (20 mL) was added as a base to the reaction

mixture. The reaction was continued overnight and DMSO was evaporated under high vacuum. The final conjugate mPEG-PEI-TPP was collected as a solid after freeze-drying following dialysis of the product after the reaction. Solid mPEG-PEI-TPP was obtained after lyophilization. The final products were characterized by ^{1}H and ^{31}P nuclear magnetic resonance (NMR), Fourier-transform infrared spectroscopy (FTIR), and gel permeation chromatography.

3.3.4 Characterization of synthesized PEG-PEI-TPP conjugate

3.3.4.1 Fourier-transform infrared spectroscopy

FTIR analysis was carried out by the KBr method. PEG, PEI (1.8 kDa, 10 kDa, 25 kDa), TPP, and lyophilized PEG-PEI-TPP conjugates were mixed individually with KBr approximately at a ratio of 1:50. The FTIR spectrum was recorded from 4000 to 400 cm^{-1} using FTIR spectrometer (FT/IR-4200, Jasco Inc., MD, USA). The obtained spectrums of PEG-PEI-TPP conjugates were compared with PEG, PEI, and TPP to observe any formation of the bonds.

3.3.4.2 ^{1}H NMR and ^{31}P NMR of synthesized conjugates

The ^{1}H NMR and ^{31}P NMR for the synthesized PEG-PEI-TPP conjugates were performed using an NMR spectrometer (500 MHz, Bruker, USA) using Deuterated chloroform ($CDCl_3$) as the solvent.

3.3.4.3 Size exclusion chromatography (SEC)

The SEC was performed to estimate the molecular weight of the synthesized PEG-PEI-TPP conjugates. The samples were eluted through the SEC column, Ultrahydrogel™linear (7.8mm× 300mm) in the SEC system (Waters Corporation, MO, USA). Milli-Q water was used as a mobile phase with a flow rate of 0.7 mL/min. The SEC standards were run before analyzing the conjugates. The data of relative molecular weight obtained from the SEC was represented in **Table S3.1**, available in the Supplementary material.

3.3.4.4 Preparation of pDNA-based polyplexes

Different molecular weight PEG-PEI-TPP polymers (1.8 kDa, 10 kDa, and 25 kDa) and plasmid DNA stock solutions were prepared in sodium acetate buffer (0.1 mM sodium acetate/0.1 M acetic acid, pH 4.5). PEG-PEI-TPP/pDNA complexes were prepared at various nitrogen/phosphate (N/P) ratios, considering the mass per charge ratio of DNA (330 $gmol^{-1}$, relative to one phosphate group) and PEI (44 $gmol^{-1}$, correspondent to one amine group), and the pKa value of the polymer. Variable concentrations of PEI (100 µL) were added to a fixed volume of pDNA (50 µL, 275 µL or 500 µL), vortex mixed for 15 s, and left for equilibration for 30 min at 4 °C before use. The complexes were centrifuged at 10,000g for 20 min and the pellet contained the pDNA-based nanoparticles. The amount of non-bound pDNA was determined spectrophotometrically by measuring the absorbance of the supernatant at 260 nm using a NanoPhotometer™ (Implen, Inc.; CA, USA). The pDNA complexation capacity was obtained from the equation:

$$CC\ (\%) = [(pDNA_T - pDNA_F)/pDNA_T] \times 100 \quad (1)$$

where $pDNA_T$ stands for the total amount of pDNA and $pDNA_F$ is the non-bound fraction of pDNA found free in the supernatant.

3.3.4.5 Determination of size and zeta potential values

The average particle size and the zeta potential of pDNA-based vectors have been determined by Dynamic Light Scattering (DLS), at 25 °C, using a Zetasizer nano ZS. The pellet containing the particles was suspended in 5% glucose with 1 mM NaCl. Dynamic light scattering (DLS) using a He-Ne laser 633 nm with non-invasive backscatter optics (NIBS) and electrophoretic light scattering using M3-PALS laser technique (Phase Analysis Light Scattering) were applied for systems size and charge investigation, respectively. The Malvern zetasizer software v 6.34 was used.

3.3.4.6 Design of experiments

To optimize the formulation of PEG-PEI-TPP/pDNA polyplexes minimizing the size of the vectors and maximizing both positive surface charges and pDNA CC, a Response Surface Quadratic Model was explored with the CCD tool. Following this, the volume of added pDNA solution (maintaining the 20 μg of pDNA) and N/P ratio factors were considered as DoE inputs. These inputs were studied at three levels (–1; 0; +1). The pDNA volume range was set to 50–500 μL for both modified PEI polymers but the N/P ratio range was adapted to each polymer, being 5–35 for PEG-$PEI_{1.8KDa}$-TPP, 2–10 for PEG-PEI_{10KDa}-TPP and 1–5 for PEG-PEI_{25KDa}-TPP. The complexes size, zeta potential, and pDNA CC parameters were the evaluated responses (outputs); the vector size was minimized and both the positive surface charges and pDNA CC were maximized. Statistical analysis was performed through the use of Design-Expert version 7.0.0 trial software. The generalized second-order polynomial model equation used in the response surface analysis is shown below (Eq. (2)):

$$Y = \beta 0 + \beta 1X1 + \beta 2X2 + \beta 11X^2_1 + \beta 22X^2_2 + \beta 12X1X2 \quad (2)$$

3.3.4.7 Analysis of complexes biocompatibility

The biocompatibility of the developed PEG-PEI-TPP/pDNA complexes, at optimal points, was evaluated on fibroblast cells by 3-[4,5-dimethyl-thiazol-2-yl]-2,5-diphenyltetrazolium bromide (MTT) assay. Additionally, and for comparison purposes, the cytotoxic profile of correspondent pDNA/PEI nanoparticles was also studied. Primary Normal Human Dermal Fibroblasts (NHDF), Ref. C-12302, isolated from adult skin and cryopreserved, from Promocell, were used. Fibroblast cells, passage number of 20, were grown in Dulbecco's Modified Eagle's Medium with High Glucose (DMEM-HG) supplemented with 10% heat-inactivated fetal bovine serum, 0.5 g/L sodium bicarbonate, 1.10 g/L HEPES and 100 units/mL of penicillin. Before cell seeding, the 96-

well plates were ultraviolet irradiated for 30 min. Fibroblasts were plated at a density of 3×10^5 cells per well and grown at 37 °C in a 95% air/5% CO2 humidified atmosphere. The vectors were formulated, as described, resuspended in serum-free DMEM medium and without antibiotics, and applied to the well plates. After one and two days of incubation, the redox activity was assessed through the reduction of the MTT. The relative cell viability (%) related to control wells was calculated by $[A]_{test}/[A]_{control} \times 100$, where $[A]_{test}$ is the absorbance of the test sample and [A]control is the absorbance of the control sample. All the experiments were repeated in triplicate. The results were presented as mean ± standard deviation.

3.3.5 Confocal fluorescence microscopy

Cancer HeLa cells were grown in 75 cm^3 T-flasks with Dulbecco's Modified Eagle's Medium with High Glucose (DMEM-HG) (Sigma) supplemented with 10% heat-inactivated fetal calf serum, 0.5 g/ L sodium bicarbonate, 1.10 g HEPES L^{-1} and 100 μg mL^{-1} of streptomycin and 100 units/ mL of penicillin (Sigma), at 37 °C in a humidified atmosphere, until confluence was attained. For transfection studies, cells were seeded at a density of 2×10^5 cells/well onto the poly-L-lysine coverslip 12-well plate and grown in 1.5 mL complete medium. After 24 h and before transfection occurs, the complete medium was replaced by medium supplemented with 10% FBS and without antibiotic, to promote transfection. At confluency (50–60%), the medium was removed and washed with PBS. HeLa cells were transfected with different nanosystems (150 μL of vectors were added to each well). Cells were stained with 150 nM of MitoTracker Orange CMTMRos for a period of 60 min at 37 °C. These probes can only accumulate in active mitochondria. Once the mitochondria are labeled, the cells can be fixed. Cells were incubated with 4% paraformaldehyde (PFA) for a period of 10 min. To stain the nucleus, they were incubated with DAPI for 10 min. Cells were then mounted by placing the round-shaped lamellas in a lamina with the help of Entellan solution and visualized through confocal microscopy (Carl ZEISS LSM 710, Oberkochen, Germany). Between any incubation period, cells were always washed with PBS solution. All procedures were performed at room temperature and in the dark to ensure probe efficacy. All images were acquired under a 63× oil immersion objective, with the laser and the filters corresponding to the respective DAPI (445/450 nm), FITC (525/550 nm) and MitoTracker (555/580 nm) dyes. At the end, images was analyzed with the LSM software (Carl Zeiss SMT, Inc., Oberkochen, Germany).

3.4 Results and discussion

3.4.1 Synthesis of mPEG-PEI-TPP polymer

In general, PEI polymers exhibit some toxicity, and in particular as molecular weight increases or molecular architecture changes from linear to branched structure. PEI 25 kDa due to its high charge density exhibits a strong ability for the formation of PEI/pDNA complexes that can penetrate and accumulate into cellular membranes with, however, an associated toxic effect. In

some human cell lines, this polymer can lead to significant cell membrane damage and it, even, promotes apoptosis [36]. In the present work, a pegylation strategy has been employed to reduce the cytotoxicity of branched PEIs. The scheme for the synthesis of the polymer, mPEG-PEI-TPP is represented in **Figure 3.1**. The primary amine in PEI reacted freely with the active acid group of mPEG-SCM in the presence of a base to form mPEG-PEI. The purified conjugate was further reacted with the activated acid group of 3-Carboxypropyltriphenylphosphonium bromide to form the final polymer conjugate, mPEG-PEI-TPP. The ^{1}H NMR spectra from the produced polymer are represented in **Figure 3.2.** The chemical shift δ (ppm) at 3.5–3.9, 7.3, and 2.0–2.5 showed the protons of PEG chains, the aromatic protons of TPP and PEI protons, respectively. The aromatic protons are from the triphenylphosphonium group, and the –N-CH2-CH2-N- protons from PEI have been observed in 7.75 and 2.6 ppm, respectively. **Figure S3.1**, included in Supplementary material (SM), showed the phosphorous NMR of the PEG-PEI-TPP conjugates. The observed signal at δ (ppm) 23–24 is ascribed to the tri-phenyl phosphonium (P+-Ph3) ligand present in TPP. Moreover, the FTIR spectrum of PEG-$PEI_{1.8kDa}$-TPP conjugate showed the C=O stretching at 1646 cm^{-1}, N-H bending at 1566 cm^{-1} and N-H stretching at 3445 cm^{-1}, as presented in **Figure 3.3(A)**. The FTIR spectrum of PEG-PEI_{10kDa}-TPP conjugate showed the C=O stretching at 1653 cm^{-1}, N-H bending at 1567 cm–1 and N-H stretching at 3425 cm^{-1} as shown in **Figure 3.3(B)**. The FTIR spectrum of PEG-PEI_{25kDa}-TPP conjugate showed the C=O stretching at 1649 cm^{-1}, N-H bending at 1569 cm^{-1} and N-H stretching at 3449 cm^{-1}, as can be observed in **Figure 3.3(C)**. These wavenumbers of conjugates confirmed the successful formation of an amide bond between PEG, PEI, and TPP to form the PEG-PEI-TPP conjugates. Additionally, SEC chromatograms of PEG-$PEI_{1.8kDa}$-TPP, PEG-PEI_{10kDa}-TPP, and PEG-PEI_{25kDa}-TPP were depicted in Fig. S2, available in SM. SEC results proved the successful conjugation of PEG-PEI-TPP conjugates. The relative molecular weights of each PEG-PEI-TPP conjugate with varied PEI molecular weights are mentioned in **Table S3.1**.

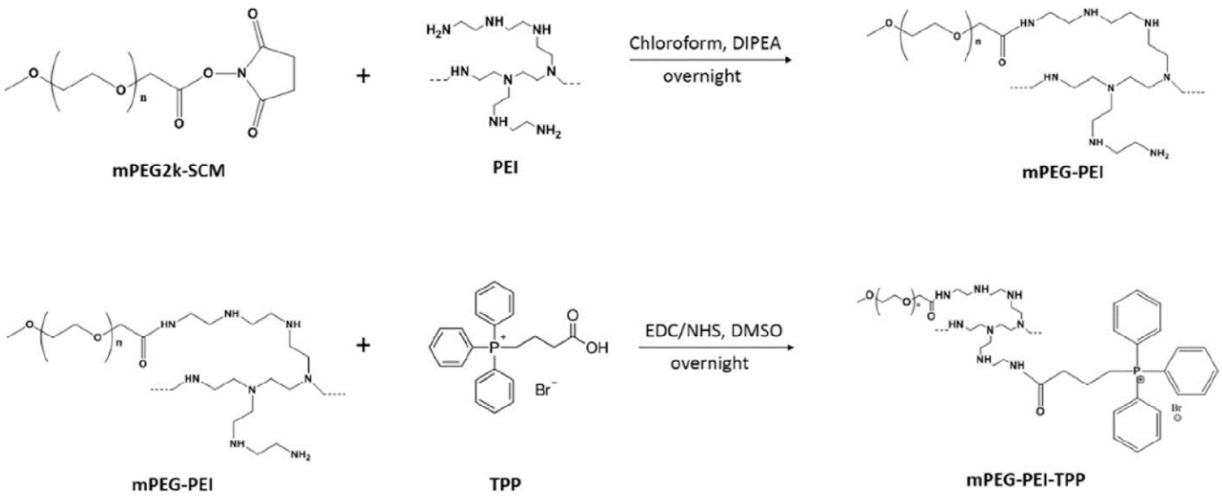

Figure 3.1 - Scheme illustrating the synthesis of mPEG-PEI-TPP polymer.

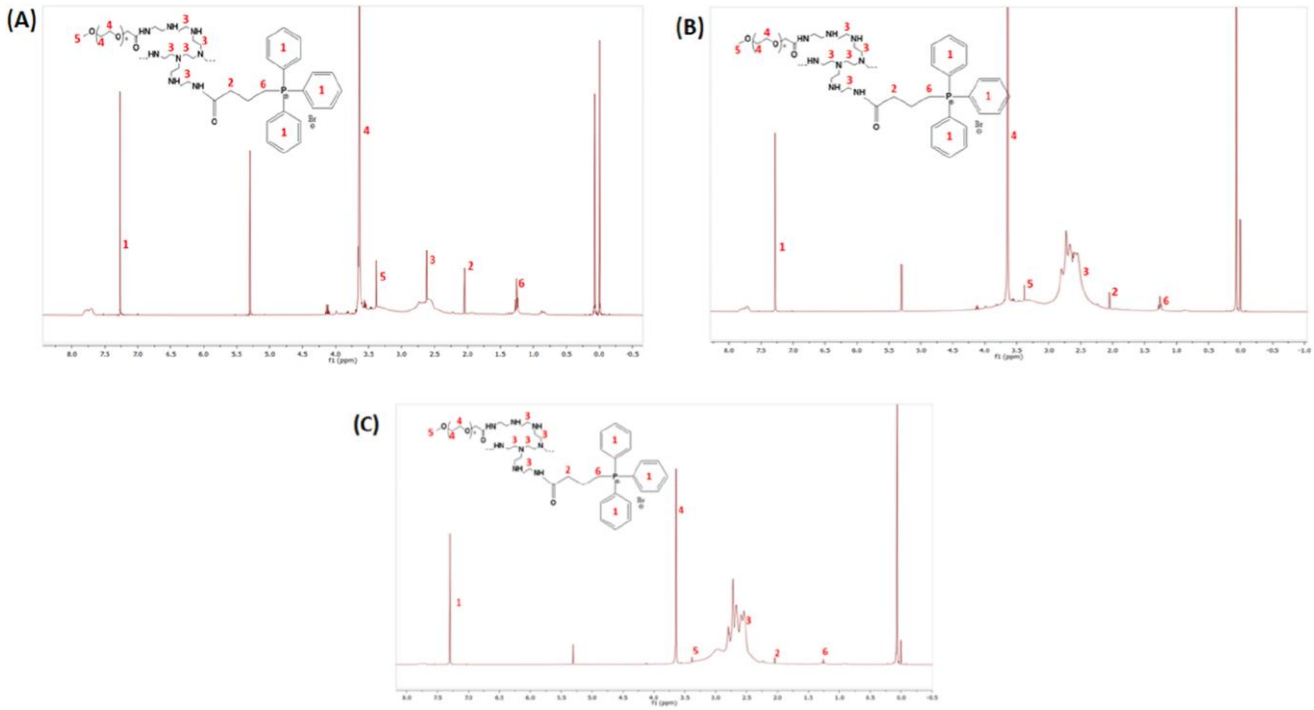

Figure 3.2 - 1H NMR spectra of the final polymers. (A) PEG-PEI$_{1.8kDa}$-TPP; (B) PEG-PEI$_{10kDa}$-TPP; (C) PEG-PEI$_{25kDa}$-TPP.

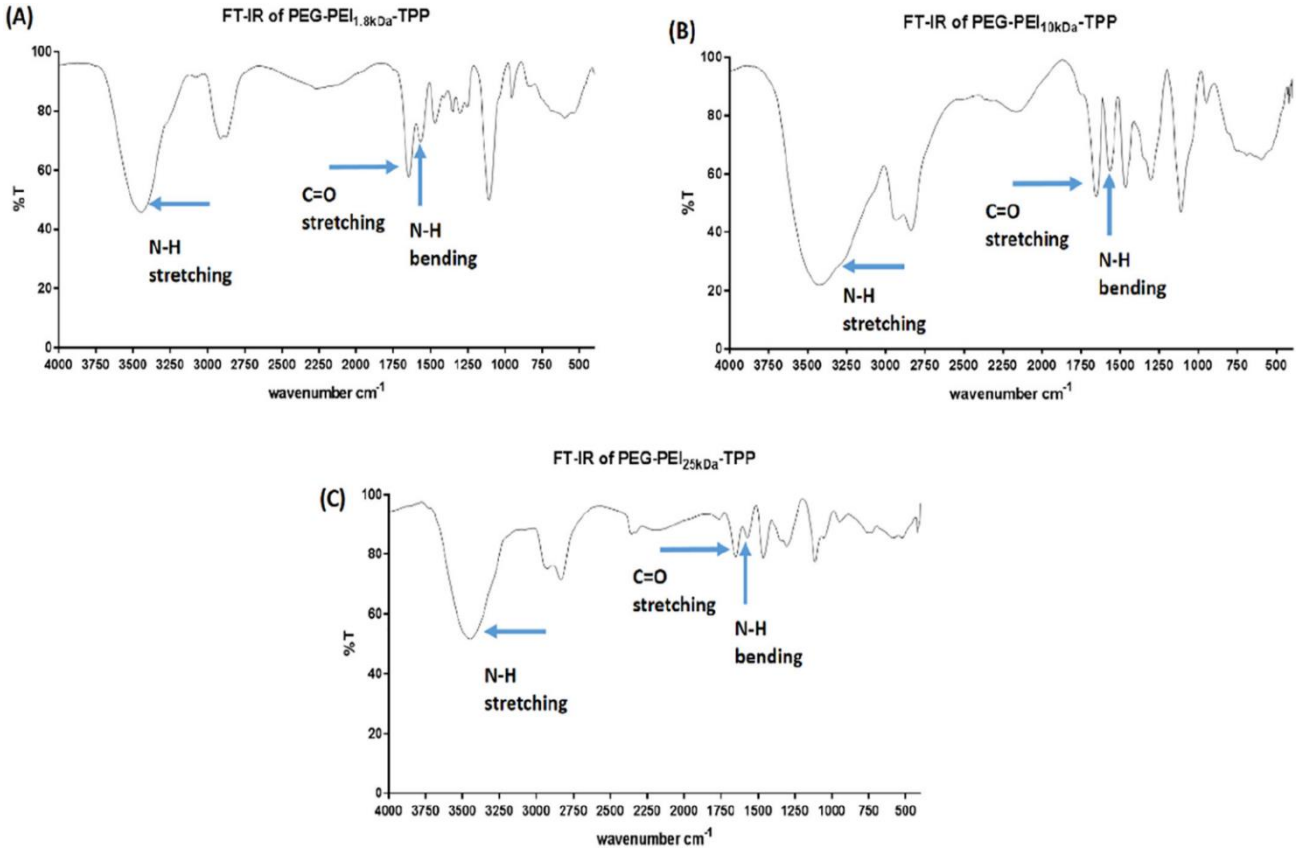

Figure 3.3 - FTIR spectra of final polymers. (A) PEG-PEI$_{1.8kDa}$-TPP; (B) PEG-PEI$_{10kDa}$-TPP; (C) PEG-PEI$_{25kDa}$-TPP.

3.4.1.1 The choice of DoE inputs

The DNA condensation by PEI has been well studied for some decades and it is based on a strong electrostatic interaction between the two molecules, originating nanometer polyplexes with potential application in the gene delivery field [30,31,37–42]. The extent of this phenomenon is dependent on the intrinsic characteristics of both DNA and polymer, as well as it is intimately related to the N/P ratio considered [36,39,40–42]. This parameter can be viewed as the main key factor in tailoring polyplexes properties, such as size, surface charges, gene loading, complexation capacity, gene release profile, and therefore therapy efficacy [39–42]. Following this, finding the appropriate N/P ratio range for each PEI/DNA delivery system is an important step when dealing with the conception of such vectors for biomedical applications. Not only N/P ratio influence the properties of formulated vectors, but also PEI molecular weight plays a relevant role in this issue [39,43]. High molecular weight PEIs interact strongly with DNA and complex it to a high extent, leading to smaller-sized complexes presenting higher positive charges. On the other hand, it is known that the cytotoxicity of branched PEI polymers increases when considering a higher molecular weight and by incrementing N/P ratio [39,42]. Based on the discussed considerations and in order to ensure an efficient pDNA complexation while avoiding cytotoxicity and unnecessary use of PEI, the N/P ratio interval for each PEG-PEI-TPP/pDNA system has been selected. The appropriate N/P ratios were, thus, considered for the inputs (starting points) when applying the DoE tool. Furthermore, the pDNA volume used when formulating PEG-PEI-TPP/pDNA vectors was also revealed, in a preliminary study, to influence pDNA CC (data not shown). Varying pDNA volume induces changes in the pDNA complexation profile. From this observation, pDNA volume was also chosen as DoE input and the respective range was selected based on the information from the screening study (data not shown).

3.4.2 Model application and analysis

In order to predict the smallest nanosystem size, maximizing the pDNA CC and positive charge, a DoE was implemented by combining the N/P ratio with the pDNA volume inputs. The Response Surface Quadratic Model of the CCD was considered a good tool to reach the best formulations of PEI-modified polymers with different molecular weights to efficiently encapsulate the pCAG-GFP-ND1 plasmid in fewer experiments than the random approach. Besides this statistical design extremely reduces the number of experiments needed to attain the intended formulation, it contains combinations where all the factors are at their higher or lower levels [44–46], revealing to be more adequate taking into consideration the defined input ranges. These conditions offer a significant advantage for the present work, as it was not necessary to explore conditions outside the defined ranges, which, according to the literature, are expected to yield unsatisfactory results. Thus, eleven experiments designed by the Design Expert software for each modified polymer were accomplished and the resultant formulations were characterized by DLS to assess the average particle size and the zeta potential of pDNA-based vectors and by spectrophotometrically for the pDNA CC quantification. In addition, to evaluate the model reproducibility, three central points, marked grey, were tested in the same conditions. The respective outputs are presented in **Table**

3.1. The data demonstrate that there is a variation on pDNA CC with the N/P ratio considered, for all delivery systems. An increase in the N/P ratio means a high content of nitrogen-positive charges available to neutralize the negatively charged pDNA, promoting its complexation. Therefore, by increasing the N/P ratio, higher pDNA CC can be achieved (**Table 3.1**). Moreover, as polymer molecular weight increases, pDNA can be condensed at lower N/P ratios. A significant difference can be observed between the lower and higher molecular weight PEI-based vectors. The increase in PEI molecular weight confers to the polymer a high charge density and, thus, strengthens its electrostatic interaction with pDNA, leading to a more efficient pDNA complexation [47]. Additionally, for each developed vector, we investigated the pDNA CC achieved considering N/P ratios higher than the maximum value in the selected range for the DoE study. The pDNA CC values obtained can be consulted in SM, **Table S3.2**. For all PEG-PEI-TPP/pDNA formulations a plateau phenomenon can be found at a certain N/P ratio, from which further increments on this parameter become irrelevant, with no clear effect on pDNA CC. Thus, for each studied delivery system, it is evident there is no significant advantage in increasing the N/P ratio beyond a certain value. Furthermore, these data strongly support the N/P ratio range that was chosen to perform the experimental design.

Considering the other parameters under study, it can be mentioned that the zeta potential and the particle size are both also affected by the N/P ratio and polymer molecular weight. Following the arguments of the discussion presented above, as a higher N/P ratio induces a strong interaction between polymer and pDNA, smaller-sized vectors are formed and display higher positive charges. Although minor compared with the N/P ratio, the effect of PEI molecular weight accompanies the tendency and cannot be neglected. For all PEG-PEI-TPP/pDNA carriers, as molecular weight increases, smaller nanoparticles are obtained, and more positive zeta potential values are achieved. The data presented in **Table 3.1** demonstrate the great differences in vector properties among the developed systems and support the evidence that both N/P ratio and PEI molecular weight strongly tailor the pDNA CC, size, and zeta potential.

Table 3.1 – Experiments designed by the Response Surface Quadratic Model of CCD and the respective reached outputs for the three synthesized polymers.

Polymer	Run	N/P ratio	pDNA volume (µL)	pDNA CC (%)	Zeta potential (mV)	Size (nm)
PEG-PEI$_{1.8KDa}$-TPP	1	20	500	59.6	13	300.6
	2	20	275	65.9	18.1	270.3
	3	5	50	55.7	16	338.4
	4	5	275	50.7	10.8	370.8
	5	35	50	88.3	32	145.3
	6	35	500	75.7	18.8	211.2
	7	5	500	45.9	3.9	401.3
	8	35	275	82.6	26.6	178.8
	9	20	275	65.6	19	270.9
	10	20	50	71.8	23.6	240.1
	11	20	275	65.8	18.1	271
PEG-PEI$_{10KDa}$-TPP	1	2	50	45.6	18.9	358.8
	2	10	50	84.2	39.2	132.2
	3	2	275	39.8	14.1	369
	4	2	500	34.3	9.7	378.3
	5	6	275	60.4	24.2	255.3
	6	6	50	65.2	28.1	245.1
	7	6	275	60.7	24	255.6
	8	6	275	60.4	23.9	255.9
	9	10	500	74.9	29	151.9
	10	6	500	54.3	19.2	264.9
	11	10	275	79.4	34.1	142.6
PEG-PEI$_{25KDa}$-TPP	1	5	275	83.8	30	109.3
	2	5	50	88.6	35.2	103.2
	3	3	275	59.2	14.1	276.8
	4	3	275	59	14.2	276.7
	5	5	500	79	24.7	115.2
	6	1	500	29.4	-6.6	449.9
	7	3	275	59.2	14.1	276.8
	8	3	500	54.6	9.8	282.4
	9	3	50	63.9	18.8	270.9
	10	1	50	39	2.2	438.2
	11	1	275	34.2	-2.2	444

The multiple regression equations, schematized in **Table 3.2**, are resultant of the Design Expert analysis and provide the level of the outputs as a function of different inputs, where the signal of

each factor designates a positive or negative effect in the outputs [46]. In general, the equation indicates that the factor A (N/P ratio) has a positive effect on the pDNA CC and zeta potential of formulations obtained with modified PEI polymers. This influence can be explained by the amine increment that the N/P ratio induces in the nanosystem structure. As discussed before, the increase of positive-charged groups contributes to higher complexation of negatively charged pDNA through electrostatic interactions with the phosphate groups, and consequently, to the positive surface charge of the formulations [39,42,43]. However, this input has a negative influence on the size of all nanosystems, probably due to the higher condensation of pDNA obtained with the increase of N/P ratio, thus resulting in smaller sizes. On the other hand, the pDNA volume has a positive effect mainly in the size output resultant from all modified polymers. This influence can be explained by the fact that a higher reaction volume allows the pDNA and polymers to be more dispersed, which may result in a less compact system with a higher size. In addition, this dispersion phenomenon consequently disfavors the pDNA CC and potential zeta outputs, such it is reflected by the negative signal in the multiple regression equations of **Table 3.2**. The reduction of pDNA volume implies an increment of the pDNA concentration, although the pDNA mass is kept constant, which can favor the molecule's organization and electrostatic interactions established between the pDNA and PEI polymers and consequently the nanosystems formulation. As already discussed in other works, high concentrations of cross-linking agents, for instance, result in more stable formulations with lower sizes [48,49].

Table 3.2 - Coded multiple regression equations for each output assessed in the nanosystems formulation of pDNA/PEG-$PEI_{1.8KDa}$-TPP, pDNA/PEG-PEI_{10KDa}-TPP and pDNA/PEG-PEI_{25KDa}-TPP. A – N/P ratio; B – pDNA volume.

Polymer	Output	Multiple regression equations
PEG-$PEI_{1.8KDa}$-TPP	pDNA CC	$+65.81+15.72\,A-5.77\,B-0.7\,AB+0.79\,A^2-0.16\,B^2$
	Zeta potential	$+18.59+7.78\,A-5.98\,B-0.28\,AB-0.19\,A^2-0.59\,B^2$
	Size	$+270.81-95.87\,A+31.55\,B+0.75\,AB+3.87\,A^2-0.58\,B^2$
PEG-PEI_{10KDa}-TPP	pDNA CC	$+60.31+19.80\,A-5.25\,B+0.5\,AB-0.43\,A^2-0.28\,B^2$
	Zeta potential	$+23.93+9.93\,A-4.72\,B-0.25\,AB+0.32\,A^2-0.13\,B^2$
	Size	$+255.58-113.23\,A+9.83\,B+0.05\,AB+0.25\,A^2-0.55\,B^2$
PEG-PEI_{25KDa}-TPP	pDNA CC	$+59.16+24.80\,A-4.75\,B+0\,AB-0.19\,A^2+0.055\,B^2$
	Zeta potential	$+14.17+16.08\,A-4.72\,B-0.43\,AB-0.33\,A^2+0.066\,B^2$
	Size	$+276.75-167.4\,A+5.87\,B+0.075\,AB-0.068\,A^2-0.068\,B^2$

Nonetheless, the effect of the input combination is revealed to be more marked in the size than the zeta potential outputs and less significant for pDNA CC, although both factors are fundamental for the formulation of these complexes.

The goodness of fit is given by statistical coefficients (**Table 3.3**) and through analysis of the variance (ANOVA) (**Table 3.4**). These parameters allow us to evaluate the significance and adequacy of the models used [50] and to understand if the statistical models generated from these experiments are valid and fit the data. To consider a model with high significance, the coefficient of determination (R^2) should vary between 0 and 1, being desirable close to 1 [33]. The results presented in **Table 3.3** indicate that the model fits the data, for all outputs. Furthermore, all outputs are well adjusted to the number of terms/inputs in the model, since the values of the Adjusted R^2 are near 1. The ability of the model to predict new data depends on the predicted value variation (Predicted R^2). The model has no predictive power if this parameter is negative. However, in the present work, the Predicted R2 results are all positive and higher than 0.96, which indicates the models can predict new data. Moreover, the Adequate Precision measures the signal due to the noise ratio and this parameter should be higher than 4 to consider that models provide an adequate signal [45]. As highlighted in **Table 3.3**, all models present an Adequate Precision higher than 52, confirming an adequate signal-to-noise ratio, thus suggesting this model can be used to navigate the design space. In line with this, the overall analysis of all these coefficients indicates that the chosen quadratic model was suitable for the output statistical analysis. By the Model F-value presented in **Table 3.4**, which was achieved by comparing the variability of the current model residuals with the variability between observations and replicate settings of the factors, it is perceivable that models are significant for the outputs. There is only a 0.01% chance that a "Model F-value" this large could occur due to noise. Finally, to prove the validity of the DoE, an ANOVA analysis should be performed and the results must present a significant value for the models and a non-significant value for the lack of fit [51]. According to the results shown in **Table 3.4**, the model data are statistically significant for the outputs, since the probability values (p-value) were lower than 0.05 for all outputs, and the lack of fit p-values was not significant (>0.05). Overall, regarding the presented results, the DoE models fitted the data and, among the independent test variables, a quadratic interaction was highly significant.

Table 3.3 - Summary of the statistical coefficients obtained by the DoE for all modified PEI polymers. R2 - coefficient of determination.

Polymer	Output	R^2	Adjusted R^2	Predicted R^2	Adequate precision
PEG-$PEI_{1.8KDa}$-TPP	pDNA CC	0.9997	0.9993	0.9967	173.134
	Zeta potential	0.9957	0.9913	0.9658	52.491
	Size	0.9999	0.9998	0.9991	329.141
PEG-PEI_{10KDa}-TPP	pDNA CC	0.9997	0.9995	0.9981	182.399
	Zeta potential	0.9994	0.9988	0.9952	136.740
	Size	1.0000	1.0000	1.0000	1654.043
PEG-PEI_{25KDa}-TPP	pDNA CC	1.0000	1.0000	0.9999	700.421
	Zeta potential	0.9999	0.9998	0.9990	304.104
	Size	1.0000	1.0000	1.0000	4272.350

Table 3.4 - ANOVA analysis for Response Surface Quadratic Model for the formulation of pDNA/PEG-PEI$_{1.8KDa}$-TPP, pDNA/PEG-PEI$_{10KDa}$-TPP and pDNA/PEG-PEI$_{25KDa}$-TPP nanosystems. P-value <0.05 is considered significant.

Output	Parameters	PEG-PEI$_{1.8KDa}$-TPP		PEG-PEI$_{10KDa}$-TPP		PEG-PEI$_{25KDa}$-TPP	
		Model	Lack of fit	Model	Lack of fit	Model	Lack of fit
EE	Sum of squares	1685.14	0.52	2519.49	0.63	3825.71	0.039
	df	5	3	5	3	5	3
	Mean square	337.03	0.17	503.9	0.21	765.14	0.013
	F value	2984.87	7.4	3643.1	7.02	58,619.77	0.96
	p-Value	<0.0001	0.1214	<0.0001	0.1273	<0.0001	0.5452
Zeta potential	Sum of squares	579.78	1.98	726.02	0.37	1686.53	0.16
	df	5	3	5	3	5	3
	Mean square	115.96	0.66	145.2	0.12	337.31	0.055
	F value	229.88	2.45	1725.03	5.35	9831.98	16.49
	p-Value	<0.0001	0.3033	<0.0001	0.1616	<0.0001	0.0577
Size	Sum of squares	61,155.75	5.21	77,511.69	0.023	1.68E+05	0.054
	df	5	3	5	3	5	3
	Mean square	12,231.15	1.74	15,502.34	0.0077	33,668.62	0.018
	F value	11,129.52	12.11	3.819E+05	0.085	2.79E+06	5.36
	p-Value	<0.0001	0.0772	<0.0001	0.9619	<0.0001	0.1611

After understanding the effect of each input on each output and validating the statistical models of the DoE, the optimal points to maximize the pDNA CC and the positive surface charge and to minimize the nanoformulations size were predicted by the Design Expert software (**Table 3.5**) for each modified PEI polymer. Thus, by using the predicted inputs of N/P ratio 35 for the PEG-PEI$_{1.8KDa}$-TPP polymer, 10 for the PEG-PEI$_{10KDa}$-TPP polymer, and 5 for the PEG-PEI$_{25KDa}$-TPP polymer, and a pDNA volume of 50 µL in all formulations, it should be obtained the best results of the predicted outputs indicated in **Table 3.5**. The mean of each obtained output, resultant from 3 experiments, was validated according to the data expected by Design-Expert software. For pDNA/PEG-PEI$_{1.8KDa}$-TPP nanosystems, the optimal point allowed a pDNA CC of 88.33%, a zeta potential of 31.33 mV, and a size of 145 nm. For pDNA/PEG-PEI$_{10KDa}$-TPP vectors, the optimal

point provided a pDNA CC of 84.75%, a zeta potential of +39.5 mV, and a size of 132.25 nm. For pDNA/PEG-PEI_{25KDa}-TPP carriers, the optimal point provided a pDNA CC of 88.67%, a zeta potential of +35.17 mV, and a size of 103.33 nm. All these results are within the confidence interval of 95% generated by the Design-Expert software where the outputs are considered valid. The obtained optimal points for each system revealed the significant impact of the N/P ratio and polymer molecular weight on the properties of PEG-PEI-TPP/pDNA complexes. It seems that a much higher N/P ratio has to be considered in order to a lower molecular weight PEI/pDNA system to present suitable properties for gene delivery. The reduction of the N/P ratio from 35 to 5 when considering the pDNA/PEG-$PEI_{1.8KDa}$-TPP and pDNA/PEG-PEI_{25KDa}-TPP nanoparticles, respectively, illustrates this phenomenon. By using a higher molecular weight PEI, much less PEG-PEI-TPP polymer is needed to efficiently condense pDNA and formulate vectors with adequate size and charge for mitochondrial gene therapy applications. Moreover, a cytotoxicity analysis for PEG-PEI-TPP/pDNA complexes at optimal points, presented in Table S3.3 (SM), confirmed that pegylation drastically reduces the toxicity of high molecular weight PEI polymers. For comparison purposes, the cytotoxic profile of PEI/pDNA vectors at the same N/P ratios was also evaluated (**Table S3.3**). The incorporation of PEG turned the complexes more biocompatible allowing for safe and promising *in vitro* applications of high molecular weight PEI-based nanoparticles. In this sense, and to further evolve on *in vitro* studies, PEG-PEI_{25KDa}-TPP/pDNA conquered special interest due to its size close to 100 nm and highest pDNA CC besides its positive surface charge and biocompatibility. Based on the information provided by the reported experimental design study, ongoing work is focused on the mitochondria targeting ability of pDNA/PEG-PEI_{25KDa}-TPP and its capacity to mediate efficient *in vitro* transfection with concomitant gene and ND1 protein expression into mitochondria. Some evidence of mitochondria targeting can already be anticipated. A fluorescence confocal microscopy study performed on HeLa cells to monitor the transfection capacity of PEG-PEI_{25KDa}-TPP-pND1-FITC carriers illustrates cellular uptake, internalization, and the mitochondria ability of the developed complexes. A summary of the study can be found in **Figure 3.4**. The figure presents confocal microscopy images at 24 h of transfection mediated by PEG-PEI_{25KDa}-TPP-pND1-FITC vectors at N/P ratios of 5 and 10. The merged images (C and D) show the co-localization of pND1 with mitochondria. This analysis seems to demonstrate that the complexes are efficiently targeted to the site of mitochondria.

Table 3.5 - Inputs predicted by the design of experiments to reach the optimal point for the formulation of pDNA nanosystems with each polymer, as well as the respective predicted and obtained outputs.

Polymer	Predicted input	Output	Predicted mean	95% CI low for mean	95% CI high for mean	Obtained mean
PEG-$PEI_{1.8KDa}$-TPP	A=35 B=50	EE (%)	88.61	87.84	89.38	88.33
		Zeta potential (mV)	31.86	30.24	33.49	31.33
		Size (nm)	145.94	143.54	148.34	145
PEG-PEI_{10KDa}-TPP	A=10 B=50	EE (%)	84.16	83.31	85.01	84.75
		Zeta potential (mV)	39.02	38.36	39.69	39.5
		Size (nm)	132.17	131.71	132.63	132.25
PEG-PEI_{25KDa}-TPP	A=5 B=50	EE (%)	88.57	88.31	88.83	88.67
		Zeta potential (mV)	35.13	34.71	35.55	35.17
		Size (nm)	103.27	103.02	103.52	103.33

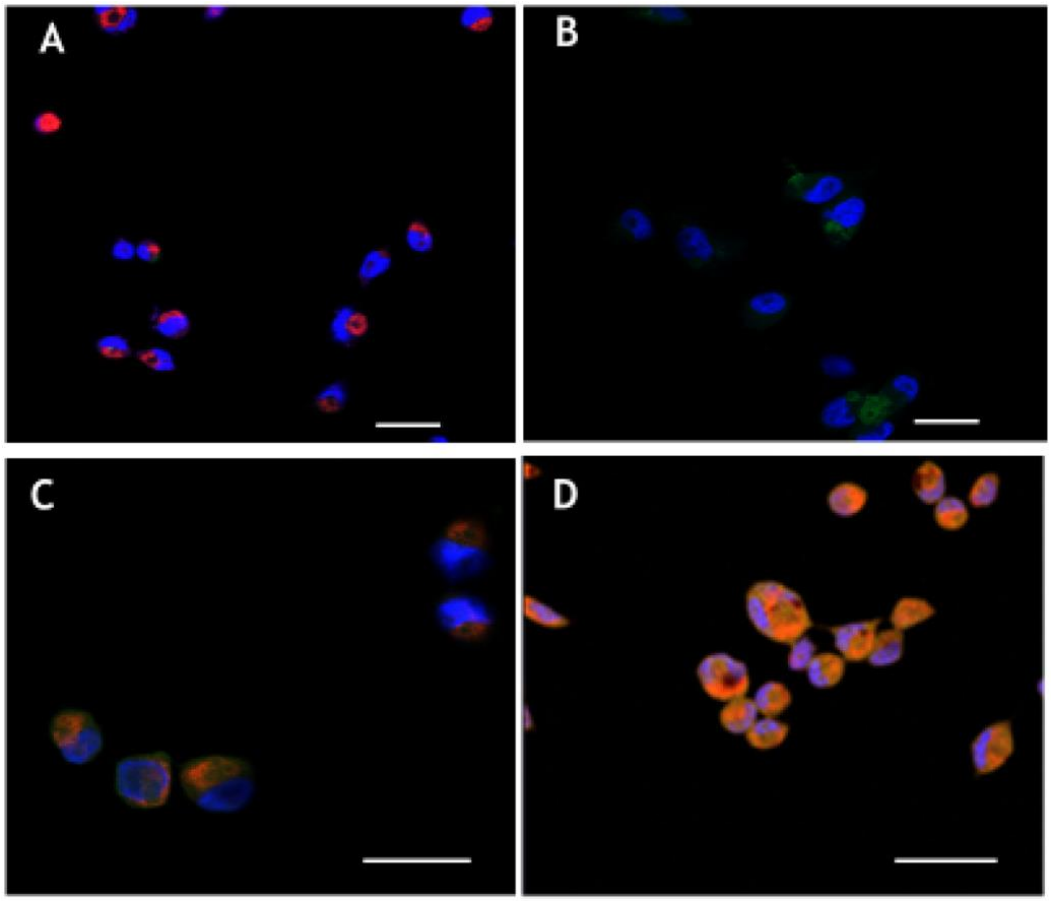

Figure 3.4 - Fluorescence confocal microscopy analysis of transfection ability and intracellular co-localization. In all cases, the nucleus is stained blue by DAPI and green represents the plasmid DNA labeled with FITC. (A) Mitochondria stained by MitoTracker Orange; (B) FITC labeled pND1; images of HeLa cells 24 h after transfection mediated by PEG-PEI_{25kDa}-TPP-pND1-FITC at N/P ratio of 5 (C) and 10(D). Scale bar = 10 μm.

3.5 Conclusions

Mitochondrial gene therapy can be a valuable and promising tool in the treatment of mitochondrial DNA disorders. Finding an ideal mitochondrial targeted vector to ensure gene and protein expression into mitochondria is a crucial step for the evolution of this therapy. In this work, different molecular weight PEIs were successfully conjugated with mitochondrial-targeted TPP, and the resultant polycations were used to condense ND1-based pDNA forming nanometer-sized particles. In the search for the most convenient PEG-PEI-TPP/pDNA vector, the design of experiments considering N/P ratio and pDNA volume as DoE inputs reveals to be powerful highlighting, for each system and in a reduced number of assays, the formulation conditions that gave rise to adequate pDNA complexation capacity, complexes size, and surface charges. For all systems under study, CCD models were statistically significant (p-value <0.05), fitted the data, and were validated. By using the predicted inputs of N/P ratio 35 for PEG-$PEI_{1.8KDa}$-TPP, 10 for

PEG-PEI$_{10KDa}$-TPP and 5 for PEG-PEI$_{25KDa}$-TPP polymer and a pDNA volume of 50 µL in all formulations, the optimal point provided a pDNA CC of 88.33%, a zeta potential of +31.33 mV and a size of 145 nm; a pDNA CC of 84.75%, a zeta potential of +39.5 mV and a size of 132.25 nm and a pDNA CC of 88.67%, a zeta potential of +35.17 mV and a size of 103.33 nm, for each PEG-PEI-TPP/pDNA system, respectively. These data demonstrate the strong tailor capacity of both the N/P ratio and PEI molecular weight in modulating the properties of developed complexes. Following this, by a fast and easy process, experimental design tools allow for the selection of PEG-PEI$_{25KDa}$-TPP/pDNA carriers, as the most suitable, for further studies towards effective mitochondrial gene delivery. This work represents a great asset for progress in the, yet poorly explored, field of mitochondrial gene therapy.

3.6 Supplementary Material

Supporting Information for Chapter 3

3.6.1 Synthesis and characterization of PEG-PEI-TPP conjugates

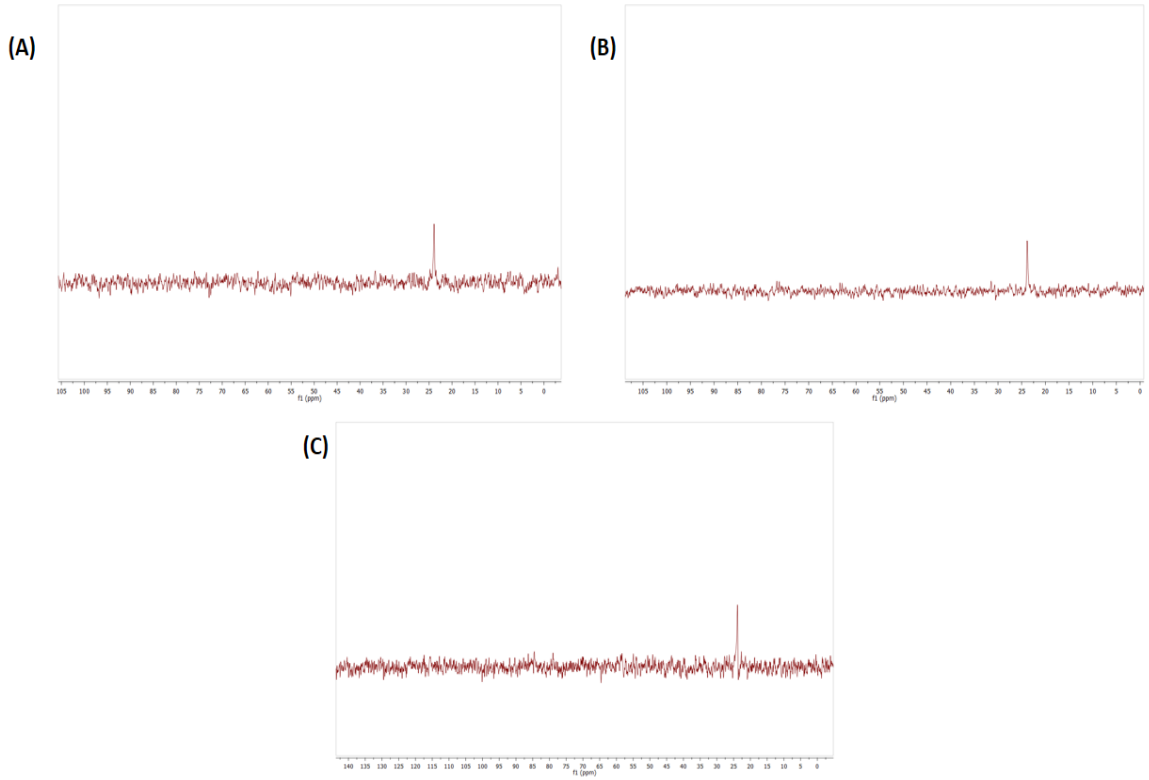

Figure S3.1 - 31P NMR spectra of final polymers. (A) PEG-PEI$_{1.8kDa}$-TPP; (B) PEG-PEI$_{10kDa}$-TPP; (C) PEG-PEI$_{25kDa}$-TPP.

3.6.2 Size exclusion chromatography (SEC)

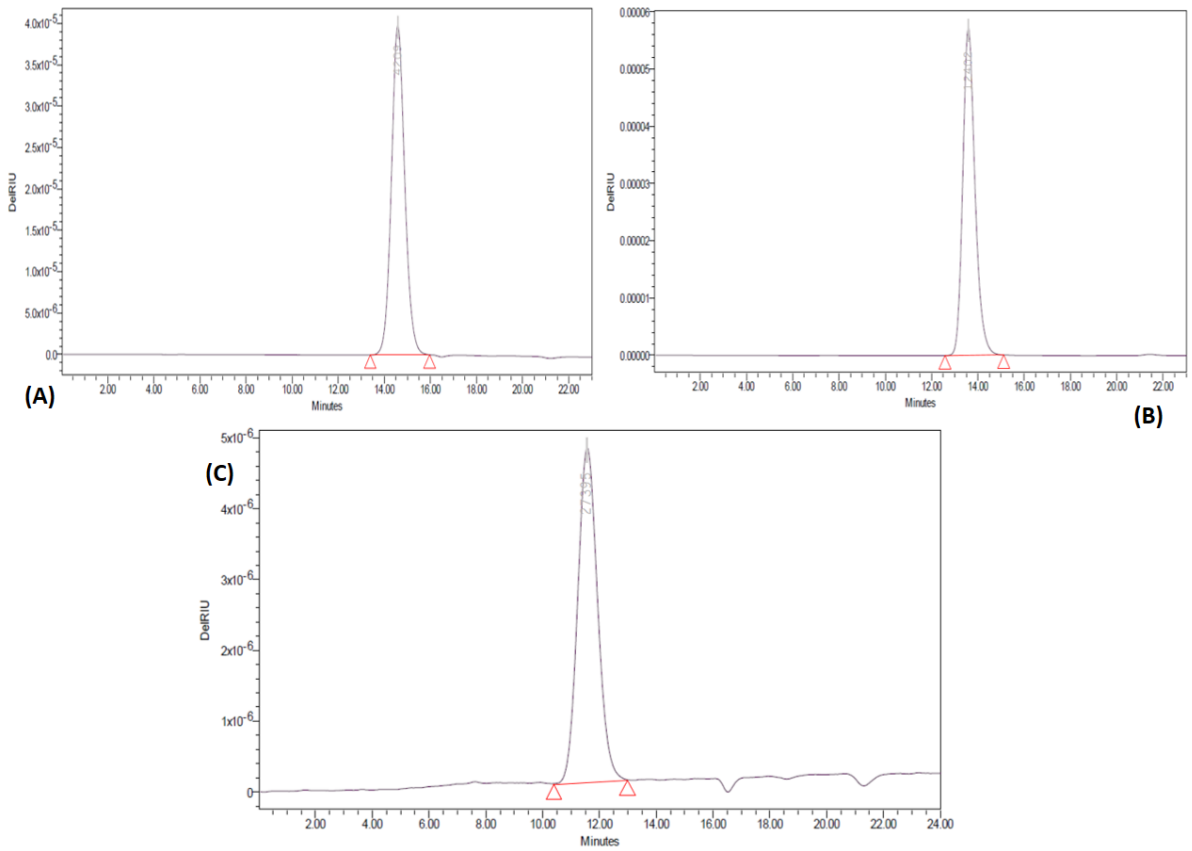

Figure S3.2 - Size exclusion chromatographic peaks of different polymer conjugates. (A) PEG-$PEI_{1.8kDa}$-TPP; (B) PEG-PEI_{10kDa}-TPP; (C) PEG-PEI_{25kDa}-TPP.

Table S3.1 - Molecular weight of each PEG-PEI-TPP conjugate obtained by SEC analysis using gel permeation chromatography.

Conjugates	Observed relative Molecular weight (Da)	Theoretical Molecular weight (Da)
PEG-$PEI_{1.8kDa}$-TPP	4209	4229
PEG-PEI_{10kDa}-TPP	12402	12429
PEG-PEI_{25kDa}-TPP	27395	27429

Table S3.2 - pDNA complexation capacity (CC) values for the various N/P ratio PEG-$PEI_{1.8kDa}$-TPP/pDNA (A), PEG-PEI_{10kDa}-TPP/pDNA (B) and PEG-PEI_{25kDa}-TPP/pDNA (C) based polyplexes, considering a pDNA volume of 500 μL. The values were calculated with the data obtained from three independent measurements (mean ± SD, n = 3).

A- PEG-$PEI_{1.8kDa}$-TPP	pDNA CC (%)
N/P 35	76
N/P 40	77
N/P 50	77

B- PEG-PEI_{10kDa}-TPP	pDNA CC (%)
N/P 10	75
N/P 12	76
N/P 15	77
N/P 20	78

C- PEG-PEI_{25kDa}-TPP	pDNA CC (%)
N/P 5	80
N/P 6	80
N/P 8	81
N/P 10	82
N/P 12	83
N/P 15	83

Table S3.3 - Cellular viability, 24 h at 48 h, in fibroblast cells after incubation with pDNA/PEI or pDNA/PEG-PEI-TPP based vectors. The values were calculated with the data obtained from three independent measurements (mean ± SD, n = 3) and analyzed by one-way ANOVA (GraphPad Software version 7.01, Inc., CA, USA). Statistical significance was accepted at a level of *p <0.05. For all systems, **p <0.01 relative to control.

System	Cellular Viability (%)	
	24 h	48 h
pDNA/$PEI_{1.8KDa}$ N/P 35	57 ± 4.8	56 ± 6.1
pDNA/PEI_{10KDa} N/P 10	45 ± 2.9	45 ± 3.6
pDNA/PEI_{25KDa} N/P 5	49 ± 4.1	47 ± 3.9
pDNA/PEG-$PEI_{1.8KDa}$-TPP N/P 35	91 ± 3.3	91 ± 3.8
pDNA/PEG-PEI_{10KDa}-TPP N/P 10	89 ± 2.8	88 ± 3.8
pDNA/PEG-PEI_{25KDa}-TPP N/P 5	86 ± 1.9	84 ± 2.7

3.7 References

[1] Saraste, M. Oxidative phosphorylation at the fin de siècle. Science. 1999, 283, 1488-1493.

[2] Ajioka, R. S.; Phillips, J. D.; Kushner, J. P. Biosynthesis of heme in mammals. Biochim. Biophys. Acta. 2006, 1763, 723-736.

[3] Hajnóczky, G.; Csordás, G.; Das, S.; Garcia-Perez, C.; Saotome, M.; Sinha Roy, S.; Yi, M. Mitochondrial calcim signalling and cell death: approaches for assessing the role of mitochondrial Ca2+ uptake in apoptosis. Cell Calcium. 2006, 40, 553-560.

[4] Tiwari, M.; Prasad, S.; Tripathi, A.; Pandey, A. N.; Ali, I.; Singh, A. K.; Shrivastav, T. G.; Chaube, S. K. Apoptosis in mammalian oocytes: a review. Apoptosis. 2015, 20, 1019-1025.

[5] Tavassoly, I.; Parmar, J.; Shajahan-Haq, A. N.; Clarke, R.; Baumann, W. T.; Tyson, J. J. Dynamic modelling of the interaction between autophagy and apoptosis in mammalian cells. CPT Pharmacometrics Syst. Pharmacol. 2015, 4, 263-272.

[6] Zhao, D.; Hong, D.; Zhang, W.; Yao, S.; Qi, X.; Lv, H.; Zheng, R.; Feng, L.; Huang, Y.; Yuan, Y.; Wang, Z. Mutations in mitochondrially encoded complex I enzyme as the second common cause in a cohort of Chinese patients with mitochondrial myopathy, encephalopathy, lactic acidosis and stroke-like episodes. J. Hum. Genet. 2011, 56, 759-764.

[7] Monlleo-Neila, L.; Del Toro, M.; Bornstein, B.; Garcia-Arumi, E.; Sarrias, A.; Roig-Quilis, M.; Munell, F. Leigh syndrome and the mitochondrial m.13513G > A mutation: expanding the clinical spectrum. J. Child Neurol. 2013, 28, 1531-1534.

[8] Zsurka, G.; Kunz, W. S. Mitochondrial dysfunction and seizures: the neuronal energy crisis. Lancet Neurol. 2015, 14, 956-966.

[9] Ciccone, S.; Maiani, E.; Bellusci, G.; Diederich, M.; Gonfloni, S. Parkinson´s disease: a complex interplay of mitochondrial DNA alterations and oxidative stress. Int. J. Mol. Sci. 2013, 14, 2388-2409.

[10] Spangenberg, L.; Graña, M.; Greif, G.; Suarez-Rivero, J. M.; Krysztal, K.; Tapié, A.; Boidi, M.; Fraga, V.; Lemes, A.; Gueçaimburú, R.; Cerisola, A; Sánchez-Alcázar, J. A.; Robello, C.; Raggio, V.; Naya, H. 3697G >A in MT-ND1 is a causative mutation in mitochondrial disease. Mitochondrion. 2016, 28, 54-59.

[11] Yu, M. Somatic mitochondrial DNA mutations in human cancers. Adv. Clin. Chem. 2012, 57, 99-138.

[12] Weissig, V.; Torchilin, V. P. Towards mitochondrial gene therapy: DQAsomes as a strategy. J. Drug Target. 2001, 9, 1-13.

[13] Yoon, Y. G.; Koob, M. D. Transformation of isolated mammalian mitochondria by bacterial conjugation. Nucleic Acids Res. 2005, 33, e139.

[14] Bonnefoy, N.; Fox, T. D. Directed alteration of Saccharomyces cerevisiae mitochondrial DNA by biolistic transformation and homologous recombination. Methods Mol. Biol. 2007, 372, 153-166.

[15] D´Souza, G. G. M.; Boddapati, S. V.; Weissig, V. Gene therapy of the other genome: the challenges of treating mitochondrial DNA defects. Pharmaceut. Res. 2007, 24, 228-238.

[16] Yasuzaki, Y.; Yamada, Y.; Ishikawa, T.; Harashima, H. Validation of mitochondrial gene delivery in live rand skeletal muscle via hydrodynamic injection using an artificial mitochondrial reporter DNA vector. Mol. Pharm. 2015, 12, 4311-4320.
[17] Lyrawati, D.; Trounson, A.; Cram, D. Expression of GFP in mitochondrial compartment using DQAsome-mediated delivery of an artificial mini-mitochondrial genome. Pharm. Res. 2011, 28, 2848-2862.
[18] Cardoso, A. M.; Morais, C. M.; Cruz, A. R.; Cardoso, A. L.; Silva, S. G.; Vale, M. L.; Marques, E. F.; Lima, C. P.; Jurado, A. Gemini Surfactants Mediate Efficient Mitochondrial Gene Delivery and Expression. Mol. Pharm. 2015, 12, 716-730.
[19] Coutinho, E.; Batista, C.; Sousa, F.; Queiroz, J. A.; Costa, D. Mitochondrial Gene Therapy: Advances in mitochondrial gene cloning, plasmid production and nanosystems targeted to mitochondria. Mol. Pharm. 2017, 14, 626-638.
[20] Santos, J.; Sousa, F.; Queiroz, J.; Costa, D. Rhodamine based plasmid DNA nanoparticles for mitochondrial gene therapy. Colloids Surf. B. 2014, 121, 129-140.
[21] Boddapati, S. V.; Tongcharoensirikul, P.; Hanson, R. N.; D´Souza, G. G.; Torchilin, V. P.; Weissig, V. Mitochondriotropic liposomes. J. Liposome Res. 2005, 15, 49-58.
[22] Yousif, L. F.; Stewart, K. M.; Kelley, S. O. Targeting mitochondria with organelle-specific compounds: strategies and applications. ChemBioChem. 2009, 10, 1939-1950.
[23] Biswas, S.; Dodwadkar, N. S.; Piroyan, A.; Torchilin, V. P. Surface conjugation of triphenylphosphonium to target poly(amidoamine) dendrimers to mitochondria. Biomaterials. 2012, 33, 4773-4782.
[24] Gruber, J.; Fong, S.; Chen, C. B.; Yoong, S.; Pastorin, G.; Schaffer, S.; Cheah, I.; Halliwell, B. Mitochondria-targeted antioxidants and metabolic modulators as pharmacological interventions to slow ageing. Biotechnol. Adv. 2013, 31, 563-592.
[25] Wang, B.; Wang, Y.; Wu, H.; Song, X.; Guo, X.; Zhang, D.; Ma, X.; Tan, M. A mitochondria-targeted fluorescent probe based on TPP-conjugated carbon dots for both one- and two-photon fluorescence cell imaging. RSC Advances. 2014, 4, 49960-49963.
[26] Bielski, E. R.; Zhong, Q.; Brown, M.; Rocha, S. R. P. Effect of the conjugation density of triphenylphosphonium cation on the mitochondrial targeting of poly(amidoamine) dendrimers. Mol. Pharmaceutics. 2015, 12, 3043-3053.
[27] Zhang, X-P.; Zhang, P-Y. Mitochondria targeting nano agents in cancer therapeutics. Oncol. Lett. 2016, 12, 4887-4890.
[28] Ozsvari, B.; Sotgia, F.; Lisanti, M. P. Exploiting mitochondrial targeting signal(s), TPP and bis-TPP, for eradicating cancer stem cells (CSCs). Aging. 2018, 10, No. 2.
[29] Jang, Y.; Lim, K. Recent advances in mitochondria-targeted gene delivery. Molecules. 2018, 23, E2316.
[30] Costa, D.; Briscoe, W. H.; Queiroz, J. Polyethylenimine coated plasmid DNA-surfactant complexes as potential gene delivery systems. Colloids Surf. B. 2015, 133, 156-163.
[31] Zhang, Y.; Liu, L.; Lin, L.; Chen, J.; Tian, H.; Chen, X.; Maruyama, A. In-situ dual-crosslinked nanoparticles for tumor targeting gene delivery. Acta Biomater. 2017, 65, 349-362.

[32] Benjaminsen, R. V.; Mattebjerg, M. A.; Henriksen, J. R.; Moghimi, S. M.; Andresen, T. L. The possible “proton sponge” effect of polyethylenimine (PEI) does not include change in lysosomal pH. Mol. Ther. 2013, 21, 149-157.
[33] Myers, J. L.; Well, A.; Lorch, R. F. Research design and statistical analysis (3rd ed.). 2010, New York, NY:Routledge.
[34] Almeida, A. M.; Queiroz, J. A.; Sousa, F.; Sousa, A. Optimization of supercoiled HPV-16 E6/E7 plasmid DNA purification with arginine monolith using design of experiments. J Chromatogr B Anal Technol Biomed Life Sci. 2015, 978, 145–150.
[35] Sousa, A.; Almeida, A. M.; Faria, R.; Konate, K.; Boisguerin, P.; Queiroz, J. A.; Costa, D. Optimization of peptide-plasmid DNA vectors formulation for gene delivery in cancer therapy exploring design of experiments. Colloids Surf. B. 2019, 183.
[36] Florea, B. I.; Meaney, C.; Junginger, H. E.; Borchard, G. Transfection efficiency and toxicity of polyethylenimine in differentiated Calu-3 and nondifferentiated COS-1 cell cultures. AAPS PharmSci. 2002, 4: E12.
[37] Utsuno, K.; Kono, H.; Tanaka, E.; Jouna, N.; Kojima, Y.; Uludağ, H. Low molecular weight branched PEI binding to linear DNA. Chem. Pharm. Bull. 2016, 64, 1484-1491.
[38] Ziebarth, J. D.; Kennetz, D. R.; Walker, N. J.; Wang, Y. Structural comparisons of PEI/DNA and PEI/siRNA complexes revealed with molecular dynamics simulations. J. Phys. Chem B. 2017, 121, 1941-1952.
[39] Costa, D.; Valente, A. J. M.; Queiroz, J. A.; Sousa, A. Finding the ideal polyethylenimine-plasmid DNA system for co-delivery of payloads in cancer therapy. Colloids Surf. B. 2018, 170, 627-636.
[40] Sadeghpour, H.; Khalvati, B.; Entezar-Almahdi, E.; Savadi, N.; Alhashemi, S.; Raoufi, M.; Dehshahri, A. Double domain polyethylenimine-based nanoparticles for integrin receptor mediated delivery of plasmid DNA. Sci. Rep. 2018, 8, 6842.
[41] Du, J.; Zhang, P.; Zhao, X.; Wang, Y. An easy gene assembling strategy for light-promoted transfecion by combining host-guest interaction of cucurbit[7]uril and gold nanoparticles. Sci. Rep. 2017, 7, 6064.
[42] Faria, R.; Sousa, A.; Neves, A. R.; Queiroz, J.A.; Costa, D. Methotrexate-plasmid DNA polyplexes for cancer therapy: characterization, cancer cell targeting ability and tuned *in vitro* transfection. J. MOL. LIQ. 2019, 292, 111391.
[43] Zhang, Q-F.; Luan, C-R.; Yin, D-X.; Zhang, J.; Liu, Y-H.; Peng, Q.; Xu, Y.; Yu, X-Q. Amino acid-modified polyethylenimines with enhanced gene delivery efficiency and biocompatibility. Polymers. 2015, 7, 2316-2331.
[44] Hunter, E.A.; Haaland, P.D. Experimental Design in Biotechnology, CRC Press, 2006.
[45] Johansson, E., Eriksson, L., Kettaneh-Wold, N., Wikstrom, C., Wold, S. (2008). Design of experiments: Principles and applications (third ed.). Sweden: MKS Umetrics AB.
[46] Patil, S. A.; Surwase, S. N.; Jadhav, S. B.; Jadhav, J. P. Optimization of medium using response surface methodology for l-DOPA production by Pseudomonas sp. SSA, Biochem. Eng. J. 2013, 74, 36–45.

[47] Tay, C. Y.; Menon, N.; Leong, D. T.; Tan, L. P. Molecular architecture governs cytotoxicity and gene transfection efficiency of polyethylenimine based nanoplexes in mammalian cell lines. J. Inorg. Organomet. Polym. 2015, 25, 301-311.
[48] Coelho, J.; Eusébio, D.; Gomes, D.; Frias, F.; Passarinha, L. A.; Sousa, A. Biosynthesis and isolation of gellan polysaccharide to formulate microspheres for protein capture. Carbohydr. Polym. 2019, 220, 236-246.
[49] Sekerak, N. M.; Hutchins, K. M.; Luo, B.; Kang, J. G.; Braun, P. V.; Chen, Q.; Moore, J. S. Size control of cross-linked carboxy-functionalized polystyrene particles: Four orders of magnitude of dimensional versatility. Eur. Polym. J. 2018, 101, 202-210.
[50] Eriksson, L.; Johansson, E.; Kettaneh-Wold, N.; Wikström, C.; Wold, S. Design of experiments, principles and applications. J. Chemom. 2001, 15, 495-496.
[51] Gelman, A. Analysis of variance – why it is more important than ever. Ann. Stat. 2005, 33, 1-53.

Chapter 4

Physicochemical characterization and targeting performance of triphenyl-phosphonium nano-polyplexes

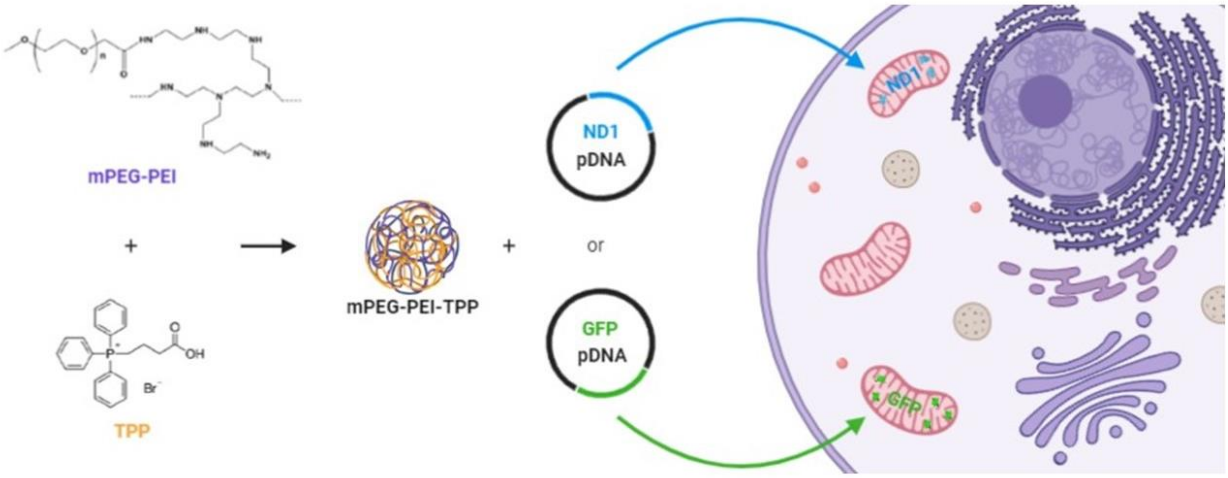

This chapter was published in:
Rúben Faria, Tânia Albuquerque, Ana R. Neves, Himanshu Bhatt, Swati Biswas, Ana M. Cardoso, Maria C. Pedroso de Lima, Amália S. Jurado, and Diana Costa. 2020. 'Physicochemical characterization and targeting performance of triphenylphosphonium nano-polyplexes', Journal of Molecular Liquids, 316.
https://doi.org/10.1016/j.molliq.2020.113873

4.1 Abstract

Mitochondrial gene therapy can be seen as a promising tool and a revolutionary approach toward mitochondrial diseases arising from mitochondrial DNA mutations. To pursue this goal, the mitochondria-targeted polycation polyethylenimine (PEI)/triphenylphosphonium (TPP) conjugate has been used to complex and condense both GFP or ND1 encoded plasmid DNA (pDNA) aiming at the formation of suitable vectors for mitochondrial gene therapy. The properties of pDNA-based TPP-polyplexes have been addressed and appear to be valuable for gene delivery applications. *In vitro* studies using fluorescent pDNA demonstrated the internalization of the developed carriers and mitochondria targeting. The evidence of gene expression into mitochondria are also reported. Following this achievement, significant levels of both mitochondrial recoded GFP and ND1 proteins were quantified. This work represents a great step towards effective mitochondria-targeting gene delivery and functional protein expression, providing a significant contribution to the mitochondrial gene therapy field.

4.2 Introduction

The mitochondrion is the cellular organelle responsible for energy production through the oxidative phosphorylation system (OXPHOS), involving four enzymatic complexes, which promote electron transport and generate a proton gradient and whose organization in supercomplexes in the mitochondrial membrane cristae has been supported by accumulated evidence [1,2]. The H+-ATP synthase constitutes the fifth complex of OXPHOS and has been revealed as a rotary motor-molecular machine that uses mitochondrial chemiosmotic gradient for ATP generation [3]. The mitochondrion is also involved in cellular signaling, ion homeostasis, the metabolism of amino acids, lipids, cholesterol, steroids, and nucleotides, as well as, in the control of both cell cycle and cell growth [4,5]. The relevant role of mitochondria in apoptosis, involving the activation of caspase proteases or a caspase-independent process, is also well documented [6–8].

As the cell nucleus, the mitochondrion has its own genome: the mitochondrial DNA (mtDNA), a double-stranded circular molecule with approximately 16 kbp and containing 37 genes that encode 13 polypeptides that take part in the oxidative phosphorylation chain, 2 rRNAs and 22 tRNAs, all exclusive to the mitochondria. Mutations in mtDNA are based on several metabolic and neuromuscular degenerative syndromes and/or pathologies especially affecting both the heart and the brain, are linked with Parkinson's and Alzheimer's diseases, diabetes, and even the propensity for cancer development [9–18]. The treatment of mtDNA-based diseases has been largely supportive rather than curative and, in general, ineffective [19]. Mitochondrial gene therapy opens up the possibility of offering a powerful and therapeutic benefit to affected individuals, as it addresses the disease at its source. For the direct transfection of mitochondria, the development of a suitable mitochondrial gene-based vector is a priority and, surely, will unveil new knowledge and relevant advances in research studies focused on this therapeutic target. To accomplish this goal, physical methods have been tested [20–22], the potential of peptide nucleic

acids has been investigated [23], other studies focused on the mitochondrial import pathway [24,25] while other researchers explore the conjugation between bacteria and mitochondria to promote DNA transfection into the mitochondrial networks of mammalian tissue culture cells [26]. A great contribution has been made by Harashima's group with the conception of a liposome-based vector that targets mitochondria [27,28]. Lyrawati *et al*. brought innovation with the expression of recoded GFP in mammalian mitochondria [29]. Taking advantage of this pDNA specifically expressed in the mitochondria, Cardoso *et al*. progressed on mitochondria targeting and gene delivery using gemini-surfactant-based DNA complexes [30]. Pursuing the same goal, our team cloned, for the first time, the mitochondrial gene ND1 (mitochondrially encoded NADH dehydrogenase 1 protein) in *E. coli*, which was maintained in a plasmid [31]. Furthermore, significant achievements were made by using delivery systems based on mitochondriotropic compounds highlighting the feasibility of mitochondrial gene therapy [31–34]. Such molecules present some degree of lipophilicity and have delocalized charges accumulating in the mitochondria by the mitochondrial membrane potential [35]. Triphenylphosphonium (TPP), a lipophilic cation, revealed a high affinity for mitochondria and a range of 1000-fold accumulation in this organelle [36]. The conjugation of TPP with therapeutic molecules has been explored to ensure mitochondria targeting [33,37–41]. Despite the efforts of many scientists worldwide, to date, few studies have demonstrated effective gene delivery and protein expression in mitochondria [42]. Unlike nuclear gene therapy which has been extensively investigated in the past decades with several ongoing clinical trials, mitochondrial gene therapy has still a large space for considerable evolution. In order to contribute to this field, we synthesized a polyethyleneimine (PEI)-based non-viral gene delivery system, by conjugating poly(ethylene glycol) (PEG) and TPP moiety to PEI of various molecular weights. The polycationic polymers efficiently condensed both mitochondrial recoded GFP [29] and ND1 [31] based plasmids, which are, by far, the most advanced non-viral bioengineered reporter vectors to explore mitochondrial transgene expression. Due to its high cationic charge density, PEI can strongly interact with negatively charged DNA, condensing it into nanoparticles [43–45]. Besides this asset, PEI also demonstrates a great endosomolytic activity [46]. In previous work, PEI has been conjugated with TPP to form a polycation with mitochondria affinity and potential application in mitochondrial gene delivery. Moreover, the design of experiments (DoE) has been conveniently explored to optimize the PEG-PEI-TPP/pDNA complexes formation to reveal the most suitable vectors [47]. The study revealed that the nitrogen-to-phosphate groups (N/P) ratio greatly influences the capacity to condense ND1-based pDNA along with PEI molecular weight, favoring the formulation of optimal carriers exhibiting high positive surface charges and low particle sizes [47]. In the current report, the capacity of such vectors for cellular uptake, intracellular trafficking, and mitochondria targeting, as well as, both gene expression and protein production were monitored/quantified. We demonstrate here that PEG-PEI-TPP/pDNA carriers can be internalized into mammalian cells and targeted to mitochondria where gene expression can occur with concomitant protein expression. This achievement can be considered great progress in the challenging issue of expressing a therapeutic gene within mammalian mitochondria, instigating advances toward effective treatments for mitochondrial DNA disorders.

4.3 Materials and methods

4.3.1 Materials

Branched polyethylenimine (PEI) was obtained from Polysciences, Inc., Warrington, PA, USA (M.W.: 1800 Da and 10,000 Da) and Sigma Aldrich, St. Louis, MO (M.W.: 25,000 Da). 3-Carboxypropyltriphenylphosphonium bromide (TPP) and fluorescein isothiocyanate (FITC) were obtained from Sigma Aldrich, diisopropyl ethylamine (DIPEA) from Avra Chemical (Mumbai, India), DAPI from Invitrogen (Carlsbad, CA) and Mito Tracker Orange CMTMRos from Molecular Probes. All chemicals were of analytical grade. All solutions were freshly prepared using ultra-pure grade water, purified with a Milli-Q system from Millipore (Billerica, MA, USA). Cancer HeLa cells were purchased from Invitrogen.

4.3.2 Plasmids

Two different plasmids have been considered in this study: the recoded plasmid DNA encoding green fluorescent protein (5.9 kbp) exclusively translated in the mitochondria which was a kind gift from Dr. Diana Lyrawati [29,30] and a pCAG-GFP-ND1 plasmid (5.4 kbp) developed, for the first time, by our research group which involved a successful cloning of the mitochondrial NADH dehydrogenase 1 protein encoded gene (mtND1) in *E. coli*, the multi-copy pCAG-GFP plasmid remaining stable. Full details from gene cloning and plasmid production are described in a previous work [31].

4.3.3 Synthesis of polymer, PEG-PEI-TPP

PEI of different molecular weights (1.8, 10, and 25 kDa) was used and subjected to the same reaction condition to obtain the TPP and PEG-conjugated PEI. The PEI was initially conjugated with mPEGs, followed by anchoring of the TPP group on PEI. Briefly, the reaction procedure is as follows:

For the synthesis of PEG-PEI, PEI and DIPEA were added into a solution of mPEG-SCM in chloroform (mol ratio of mPEG-SCM:PEI = 1:1). The reaction took place overnight, under stirring. The solvent was then evaporated to dryness under vacuum, and the crude reaction mixture was dialyzed using cellulose ester membranes (1, 3.5, and 12–14 kDa MWCO for 1.8, 10, and 25 KDa PEI, respectively) and lyophilized. For the synthesis of PEG-PEI-TPP, 3-carboxypropyltriphenylphosphonium bromide was activated by using the zero-order cross-linker, EDC/NHS in the presence of DIPEA in DMSO, and mPEG-PEI was added at the mol ratio of mPEG-PEI:TPP of 1:1. The reaction was left to occur overnight and the solvent was then evaporated, the crude material was dialyzed and the dialysate was freeze-dried. In a previous work, the products were characterized by ^{1}H, and ^{31}P nuclear magnetic resonance (NMR), Fourier-transform infrared spectroscopy (FTIR), and size exclusion chromatography [47].

4.3.4 Preparation of pDNA-based polyplexes

For the preparation of polymer-plasmid DNA systems, PEG-PEI-TPP, PEG-PEI, and pDNA stock solutions were prepared in sodium acetate buffer (0.1mM sodium acetate/0.1M acetic acid, pH 4.5) with a concentration of 0.5 mg/mL for the polymers and 100 μg/mL for pDNA solutions.
The calculation of the N/P ratio for the polyplexes is defined as the molar relation of amine groups in the PEI, which represent the positive charges, to phosphate groups in the pDNA which represent the negative charges. The polymer/pDNA polyplexes were prepared at N/P ratios of 1, 2, 5, and 10 considering the mass per charge ratio of pDNA (330 g/mol, relative to one phosphate group) and PEI (correspondent to one amine group) [48]. For pDNA, 330 g/mol corresponds to one phosphate group. 1 μg × 330 g/1 μg = 1 mol phosphate.
1 μg pDNA = 1 mol phosphate x 10^{-6}/330:
1 μg pDNA = 3.03 x 10^{-9} mol phosphate:

For the PEI, only primary amines have been considered, as both secondary and tertiary amines exhibit very low pKa values. The number of N atoms in 25 KDa of PEI = 25,000 / 43.1 = 580.0464 ≈ 580.05. If we intend, for instance, to prepare nanoparticles at N/P ratio of 1, we must consider: N = 1 x P and N = 1 x 30.3 x 10^{-9} = 30.3 x 10^{-9}.

To determine the number of moles of PEI correspondent:
30.3 × 10^{-9} / 580.05 = 0.05 × 10^{-9} mol of PEI and the respective mass can be determined by multiplying the number of moles by 25,000 g/mol.

Following this, for the preparation of polyplexes at various N/P ratios, different concentrations of PEG-PEI-TPP or PEG-PEI (100 μL) were added to a fixed volume of pDNA (400 μL), vortex mixed for 15 s, and left for equilibration for 30 min at 4 °C before use. The mixture was then centrifuged at 10,000 g for 20 min and the pellet containing the PEG-PEI-TPP-pDNA nanoparticles was recovered. The amount of non-bound pDNA was determined spectrophotometrically by measuring the absorbance of the supernatant at 260 nm using a NanoPhotometer™ (Implen, Inc.; CA, USA). The pDNA complexation capacity (CC) was obtained from the equation:

$$CC\ (\%) = [(pDNA)T - (pDNA)F/(pDNA)T] \times 100$$

where (pDNA)T stands for the total amount of pDNA and (pDNA)F is the non-bound fraction of pDNA found free in the supernatant.

4.3.5 Determination of morphology, size, and surface charges

Scanning electron microscopy was applied to obtain information regarding the morphology of PEG-PEI-TPP-pDNA complexes. The various systems were centrifuged (10,000 g, 20 min, 4 °C) and the pellet was recovered and suspended in an aqueous solution containing 20μL of tungsten (2%). The solution n was placed in a roundly shaped cover slip and dried overnight at room

temperature. The samples were sputter coated with gold by using an Emitech K550 (London, England) sputter coater. A scanning electron microscope, Hitachi S-2700 (Tokyo, Japan) with an accelerating voltage of 20 kV at various magnifications was used to determine the morphology of nanoparticles. The mean size has been determined from the observation and counting of individual particles, using a line measurement tool to determine the diameters of particles within ImageJ software. Approximately 20 SEM images were acquired for each sample and, on average, five particles were counted per image, considering 1 pixel=0.95 nm. Particle area was determined assuming that all particles are spherical, and using the following equation for the determination of diameter: $d = 2\sqrt{(A/\pi)}$

The average particle size and the zeta potential of pDNA-based vectors have been determined by Dynamic Light Scattering (DLS) and Electrophoretic Light Scattering (ELS), at 25 °C, using a Zetasizer nano ZS. The pellet containing the polyplexes was suspended in 5% glucose with 1 mM NaCl. DLS using a He-Ne laser 633 nm with non-invasive backscatter optics (NIBS) and ELS using M3-PALS laser technique (Phase Analysis Light Scattering) were applied for the determination of polyplex size and charge, respectively. The Malvern Zetasizer software v 6.34 was used.

4.3.6 FITC plasmid staining

The plasmid was labeled with FITC by mixing 8 μL of pDNA, 75 μL of labeling buffer (0.1 M sodium tetraborate, pH 8.5) and 4 μL of FITC (in sterile anhydrous dimethyl sulfoxide, 500 mg/mL). Samples were placed under constant stirring for 4 h at room temperature and protected from light. One volume of 3 M NaCl (85 μL) and 2.5 volumes of 100% ethanol (212.5 μL) were added to the samples containing the labeled pDNA, followed by overnight incubation at −20 °C. Thereafter, the samples were centrifuged at 4 °C for 30 min and the pellet was washed with 75% ethanol.

4.3.7 *In vitro* studies

Cancer HeLa cells were grown in 75 cm^3 T-flasks in Dulbecco's Modified Eagle's Medium with High Glucose (DMEM-HG) (Sigma) supplemented with 10% heat-inactivated fetal calf serum, 0.5 g L–1 sodium bicarbonate, 1.10 g HEPES L^{-1} and 100 μg/mL of streptomycin and 100 units mL^{-1} of penicillin (Sigma), at 37°C in a humidified atmosphere, until confluence was attained. Afterward, cells were sub-cultivated to maintain their exponential growth. For transfection studies, cells were seeded at a density of 2 × 105 cells/well onto the poly-L-lysine coated coverslip in 12-well plates and grown in 1.5 mL complete medium. After 24 h and before transfection, the complete medium was replaced by a medium supplemented with 10% FBS and without antibiotics, in order to promote transfection. At confluency (50–60%), the medium was removed and the cells were washed with PBS. HeLa cells were transfected with different nanosystems (150 μL of vectors were added to each well) and incubated for various periods.

4.3.8 Detection of associated/internalized pDNA

Cancer Hela cells were cultured as described above. For transfection, FITC-pDNA-based vectors (100 μL) were added to each well. Untreated cells were used as control. After different periods, during 24 h, cells were washed twice with PBS, and pDNA levels were measured in the transfected cells by fluorescence quantification using a fluorimeter plate reader (excitation and emission wavelengths at 495 nm and 525 nm, respectively). All the experiments were performed in triplicate. For each cell line, the protein content of each well was measured with a bicinchoninic acid (BCA) protein assay kit (BCA1-1KT, Sigma Aldrich Chemicals, St. Louis, MO, USA). Fluorescence/microgram protein readings were then determined by averaging the background corrected fluorescence of triplicate wells and dividing by the protein content per well. The use of this kit aids in correcting for cell density differences between different sets of experiments. The fluorescence of FITC–pND1 in each organelle sample was normalized with the amount of protein and expressed as fluorescence/μg protein.

4.3.9 Separation of cellular organelles

After transfection mediated by the developed nanosystems, mitochondria were isolated from the other cellular fractions through the use of the Mitochondria Isolation Kit for Cultured Cells (#89874, ThermoFisher Scientific Inc., Rockford, USA), following the manufacturer's instructions in order to separate essentially the mitochondria and the cytosol. This kit ensures an efficient isolation of mitochondria with optimized purity along with high and consistent yield. A full description of this assay is available elsewhere [31]. Summarizing, HeLa cells were transferred to Falcon tubes, and 800 μL of Mitochondria Isolation Reagent A was added to HeLa cells (4×10^5), followed by incubation on ice for 2 min. Then, 10 μL of Mitochondria Isolation Reagent B was added and cells were vortexed at maximum speed for 10 s, incubated on ice for 5 min, and vortexed at maximum speed every minute. Thereafter, Reagent C (800 μL) was added, the samples were centrifuged at 700 g for 10 min at 4 °C and the supernatant was centrifuged at 3000 g for 10 min at 4 °C. The supernatant contains the cytosol and the pellet consists of the intact mitochondria. Reagent C (500 μL) was added to the pellet and after centrifugation at 12,000 g for 5 min, the supernatant was discarded. The pellets containing the mitochondria were resuspended in 50 μL of ice-cold PBS, mixed with 500 μL of carbonate buffer (fresh cold 0.1 M Na_2CO_3), and used in the subsequent experiments.

4.3.10 Detection of GFP fluorescent levels

Hela cells were cultured as described before. For transfection, PEG-PEI-TPP-pGFP nanoparticles (100 μL) were added to each well and after 24 h or 48 h of transfection, cells were washed twice with PBS. Untreated cells were used as control. The cell-associated GFP fluorescence intensity has been measured in both cytosolic and mitochondrial fractions. The fluorescence intensity of GFP was assessed by the use of a microplate reader, at 480 nm and 520 nm as excitation and emission wavelengths, respectively. The levels of GFP fluorescence in each well were quantified through

the use of a standard curve. Measurements were performed in triplicate and data were expressed as Relative Fluorescence Units (RFU).

4.3.11 Reverse transcription polymerase chain reaction (RT-PCR)

RT-PCR was used to detect the mRNA expression of both ND1 and GFP gene. After transfection, the medium was removed and the cells were washed with PBS. Untreated cells were used as control. To extract total RNA, the cells were lysed through the addition of TRIzol (Thermo Scientific, Lisbon, Portugal) (250 µL) and incubated at room temperature for 5 min, followed by the addition of chloroform and vigorous stirring, according to manufacturer's instructions. The obtained samples were quantified by using a NanoPhotometer™ and were run on an agarose gel (1%) and analyzed by electrophoresis to detect possible contaminations with genomic DNA or RNA degradation. The cDNA synthesis was performed by using the "Xpert cDNA Synthesis Kit" from Grisp (GRiSP, Porto, Portugal), following the manufacturer's protocol. PCR amplification of GFP cDNA was performed by adding in each PCR reaction 3.95 µL of RNase-free water, 0.40 µL of primer reverse (5′-CGTTCTTGTACGTAGCCTTC-3′) and primer forward (5′-CTGCACCACCGGAAAACTCC-3′), 0.5 µL of MgCl2, 6.25 µL of Taq DNA polymerase and 1 µL of cDNA. The samples were homogenized and a mini-spin was performed. Samples were then placed in a T100™ Thermal Cycler (Bio-Rad Laboratories, Inc., Hercules, California, USA), using the following reaction conditions: denaturation (95 °C for 40 s), annealing (57 °C for 30 s), and extension (72 °C for 1 min) for 27 cycles. Assays were performed in triplicate.

PCR products were analyzed by electrophoresis on an agarose gel stained with GreenSafe Premium (NZYTech, Lda. Lisbon, Portugal), and were visualized in the UVItec Gel documentation system under UV light (UVItec Limited, Cambridge, United Kingdom).

4.3.12 Quantification of protein

After *in vitro* transfection with the different PEG-PEI-TPP-pGFP vectors (n = 5), GFP content was determined using a GFP ELISA kit (MitoSciences, ab 117992, Abcam, United Kingdom). This method consists of an enzyme immunoassay that allows the sensitive detection and quantification of GFP. Transfected cell lysates were prepared from detergent lysis (lysis buffer-tissue, 50:50 vol vol^{-1}) in lysis buffer (1% Triton X-100 and 0.1% SDS in PBS, pH 7.4 and proteinase inhibitor cocktail) and homogenization. This assay uses a specific GFP antibody coated onto well plate strips, through which the GFP included in the samples can bind to the wells. The wells were then washed and a primary anti-GFP detector antibody was added. After a further washing step, HRP conjugated secondary detector antibody specific to the primary detector antibody was added to the wells. 3,3′,5,5′-Tetramethylbenzidine (TMB) Substrate was also added to the wells, the presence of GFP being revealed through the observation of a blue color. The GFP concentration was determined by measuring the absorbance at 600 nm in a spectrophotometer. Similarly, after *in vitro* transfection with the different PEG-PEI-TPP/pND1 vectors (n = 5), ND1 protein has been quantified by a ND1 ELISA kit (Biomatik, EKL54820, USA), following manufacturer's guidelines. This sandwich enzyme immunoassay allows for the *in vitro* quantitative measurement of ND1 in

human serum, plasma, cell lysates, cell supernatants, or other biological fluids. Transfected HeLa cells were lysed according to standard procedures. Briefly, cells were detached with trypsin and collected by centrifugation, washed three times in cold PBS, resuspended in PBS, and ultrasonicated 4 times. Cells were then centrifuged at 1500 g for 10 min at 4 °C to remove cellular debris. Reagent solutions were prepared by following the provided instructions. Detection Reagent A was added to each well, and incubated for 1 h at 37°C, followed by the addition of Reagent B and incubation step. Thereafter, TMB substrate solution was added to each well, and the samples were incubated for 15–30 min at 37 °C, protected from light. The Stop solution was added and yellow colored solution was formed. ND1 protein was immediately quantified in a microplate reader taking measurements at 450 nm.

4.3.13 Statistical analysis

One-way or two-way analysis of variance (ANOVA), with the Bonferroni test, was used for comparing data of control and multiple experimental groups. Some specific comparisons between the two groups were analyzed by t-test. A confidence interval of 95% ($p < 0.05$) was considered statistically significant. Data analysis was performed in GraphPad Prism v.6.01 (GraphPad software Inc., CA, USA).

4.4 Results and discussion

4.4.1 Formation and characterization of TPP-based polyplexes

A significant progress in the development of non-viral vectors for nucleic acid delivery to mammalian cells, *in vitro* and *in vivo*, has been made in recent years [27,29,30,43,44,49]. PEI possesses a high ability to condense nucleic acids and to act as a possible “proton sponge”, which may facilitate nucleic acid endosomal escape, being therefore, widely employed in gene delivery strategies [43–46]. PEI contains primary, secondary, and tertiary amine groups, which contribute to its high positive charge at physiological pH. The polyplexes were formulated based on the strong electrostatic interaction between the PEI polycation and pDNA [43,44], at various N/P ratios (1, 2, 5, and 10) to explore the influence of this parameter on polyplex properties. The effect of polymer molecular weight has been also evaluated. As evidenced by SEM images, presented in **Figure 4.1**, spherical or oval particles at the nanoscale can be formed for both pGFP- and pND1-PEG-PEI-TPP systems, with size varying with both the PEI molecular weight and N/P ratio used. Polyplexes with lower size were formed when both higher PEI molecular weight and N/P ratio were considered. Particle size has been determined using ImageJ software and this tendency has been confirmed. The data is shown in the Supplementary Material (SM), **Table S4.1**. Although valuable information on size can be obtained by using this semi-automated method, a more accurate particle size measurement can be accomplished by employing automated methods based on automated software that enables the user to measure and count the constituent particles through a control interface [50]. Dynamic Light Scattering was employed to further investigate

the properties of the several PEG-PEI-TPP/pDNA vectors, namely the average size and the surface charges. The results, for polyplexes formulated with both plasmids, are summarized in **Tables 1A and B**. For comparison, the zeta potential for both pDNAs and the size displayed by the various PEI suspensions are also presented. All formed polyplexes were demonstrated to be monodisperse, with PDI values of approximately 0.4 when formulated with PEI 1.8 kDa and 10 kDa and 0.2 when formulated with PEI 25 kDa. The above-mentioned tendency observed in SEM images was confirmed by DLS. Thus, the size of the vectors decreases with increased PEI molecular weight ($p < 0.05$) and N/P ratio ($p < 0.05$). For the lowest PEI molecular weight systems, the resulting complexes exhibit large sizes, especially, for the lower N/P ratios. For the same N/P ratio, smaller and smaller particles are formed as PEI molecular weight increases. PEI with a molecular weight of 25 kDa ensures the formation of the lowest size vectors for each N/P ratio. This fact can be related to a stronger compaction polymer ability as the molecular weight increases. Despite the PEI molecular weight effect, it seems that the N/P ratio is the most determining size tailoring parameter as its increment can dramatically reduce the size of the systems ($p < 0.01$), even for low PEI molecular weight complexes (Table 1A and B) ($p < 0.05$). A comparison of particle size obtained from SEM and DLS exhibits some discrepancy in the size values. As demonstrated earlier and discussed elsewhere, this fact can be related to the principles, advantages, and limitations of each technique [51]. Regarding the surface charges of the several PEG-PEI-TPP-pDNA carriers, both the N/P ratio and polymer molecular weight affect this parameter. Negative zeta potential values were obtained for all vectors produced at the N/P ratio of 1. As the N/P ratio increases, more positive polymer charges are available to neutralize the negative pDNA charges and, therefore the zeta potential of the particles shifts to increasingly high positive values. Although to a less extent, PEI molecular weight also affects the surface charges displayed by the different complexes. The lowest molecular weight PEI-based vectors present negative zeta potential values up to an N/P ratio of 5; however, positive zeta potential values were determined for all systems for N/P ratios from 2 to 10. The higher PEI positive charge density at higher molecular weights and, most importantly, a higher N/P ratio induce the observed size and surface charge characteristics of the developed carriers. As presented in **Tables 1A and B**, this profile is common for both pGFP- and pND1-based polyplexes with small variations between them, with lower sizes and more positive zeta potential values for PEG-PEI-TPP/pND1 in each combination of PEI molecular weight and N/P ratio. As the developed polyplexes may exhibit different sizes and zeta potential values in cell culture medium due to different salt concentrations and pH conditions, some control experiments have been performed in cell culture medium. For these experiments, pDNA polyplexes were prepared as described and the pellet containing the polyplexes was suspended in DMEM-HG, without serum, and both the average particle size and the zeta potential of the several pDNA-based systems have been determined by DLS and ELS, respectively. The results are presented in **Table S4.2**, available in the SM, and show that, for all the polyplexes studied, the size and the zeta potential increased when the pellet containing the polyplexes was suspended in DMEM-HG. Concerning the pDNA complexation capacity displayed by the conceived complexes, a similar pattern was revealed. The results listed in Table 1A and B for both pDNAs, are consistent with a higher pDNA complexation for vectors with higher

molecular weight PEI and N/P ratios. Thus, polyplexes made from higher molecular weight PEI and at higher N/P ratios can efficiently load and condense pDNA to a high extent. It should be stressed that the N/P ratio parameter becomes extremely relevant in tailoring pDNA CC, as great differences were found, for each system, when varying N/P ratios. In general, these observations are in close agreement with findings from previous works on PEI/pDNA systems [47,51]. From our results, supported by the DoE study previously performed that considered N/P ratio and pDNA volume as DoE inputs revealing the formulation conditions that gave rise to adequate pDNA CC, complexes size, and surface charges [47], the most adequate PEG-PEI-TPP/pDNA formulations for cellular uptake and, consequently, efficient cell transfection were selected. According to published literature in this field, spherical particles with sizes below 300 nm are adequate to promote cellular internalization. Moreover, vectors possessing positive charges, and in particular those showing zeta potential higher than +30 mV, strongly enable the interaction with the negatively charged proteoglycans present in the cellular membrane, which facilitates their entry into the cell [52,53]. This process is then followed by vector transportation, possibly mediated by an endocytosis mechanism, into the organelle of interest. Based on these arguments, polyplexes synthesized from lower molecular weight PEIs were excluded from subsequent studies, and further experiments were performed with PEG-PEI_{25kDa}-TPP/pDNA carriers prepared at N/P ratios of 2, 5, and 10, due to their adequate sizes, surface charges and higher pDNA CCs, which seem to be promising for *in vitro* application in the mitochondrial gene therapy field.

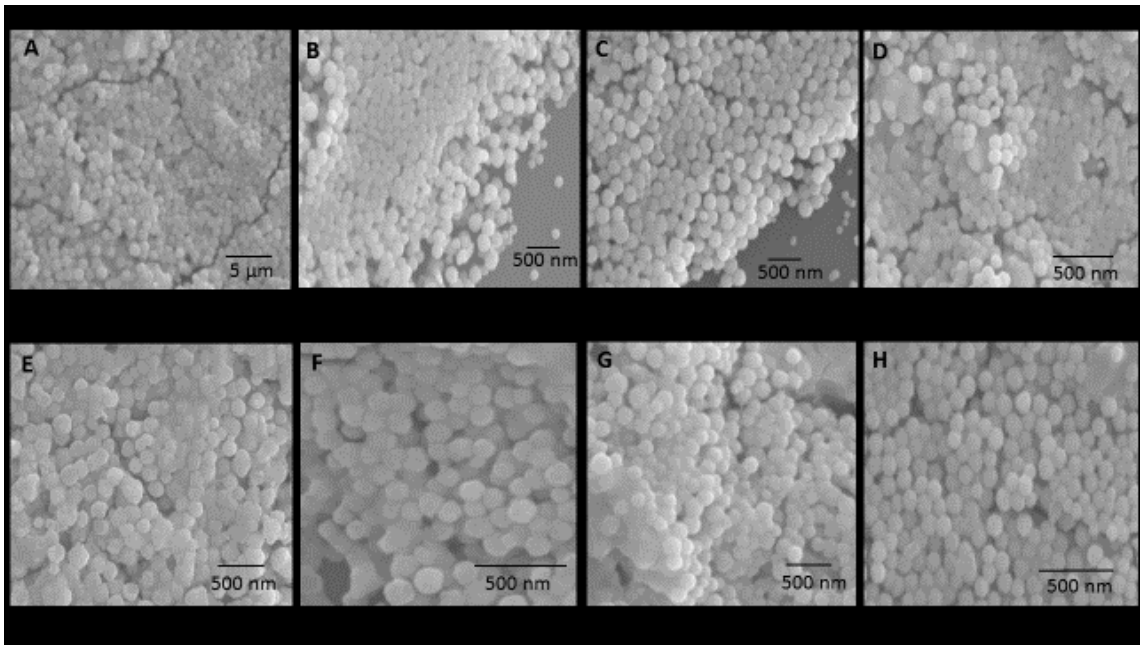

Figure 4.1 - Scanning electron micrograph of PEG-PEI-TPP-pGFP nanoparticles formulated with PEI 1.8 kDa and N/P of 1 (A), PEI 10 kDa and N/P of 5 (B), PEI 25 kDa and N/P of 2 (C) PEI 25 kDa and N/P of 10 (D) and PEG-PEI-TPP-pND1 nanoparticles with PEI 1.8 kDa and N/P of 10 (E), PEI 10 kDa and N/P of 10 (F) PEI 25 kDa and N/P of 2 (G) and PEI 25 kDa and N/P of 10 (H).

Table 4.1 - Mean size (nm), average zeta potential (mV) and pDNA complexation capacity (CC) for the different PEI-TPP-PEG/pDNA systems at N/P ratios of 1 to 10. Average zeta potential values of the pure PEIs and pDNAs were also presented. The values were calculated with the data obtained from three independent measurements (mean ± SD, n=3) and analyzed by one-way or two-way ANOVA. Statistical significance was accepted at a level of $p < 0.05$.

A. PEG-PEI-TPP-pGFP

N/P	PEI 1.8 kDa			PEI 10 kDa			PEI 25 kDa		
	Size (nm)	Zeta (mV)	CC (%)	Size (nm)	Zeta (mV)	CC (%)	Size (nm)	Zeta (mV)	CC (%)
PEI	794 ± 6.0	+38 ± 3.1		827 ± 4.7	+47 ± 5.4		892 ± 7.2	+64 ± 6.1	
1	766 ± 7.7	−37 ± 1.6	9 ± 1.1	522 ± 8.4	−16 ± 0.5	20 ± 2.2	456 ± 5.9	−8 ± 0.8	40 ± 1.9
2	602 ± 3.9	−28 ± 2.5	14 ± 0.6	408 ± 6.8	+5 ± 0.2	29 ± 4.5	268 ± 5.3	+9 ± 1.3	56 ± 3.6
5	434 ± 6.2	−2 ± 1.2	37 ± 2.4	231 ± 2.9	+13 ± 2.1	60 ± 4.7	197 ± 2.5	+21 ± 0.9	78 ± 6.1
10	361 ± 4.5	+7 ± 0.6	49 ± 0.7	189 ± 6.2	+22 ± 4.8	71 ± 2.0	126 ± 6.1	+37 ± 3.4	80 ± 4.7
pGFP, ζ = −106 ± 3.9									

B. PEG-PEI-TPP-pND1

N/P	PEI 1.8 kDa			PEI 10 kDa			PEI 25 kDa		
	Size (nm)	Zeta (mV)	CC (%)	Size (nm)	Zeta (mV)	CC (%)	Size (nm)	Zeta (mV)	CC (%)
1	655 ± 8.2	−33 ± 0.8	11 ± 3.0	511 ± 3.9	−8 ± 0.9	23 ± 1.6	421 ± 6.1	−6 ± 0.5	42 ± 3.7
2	581 ± 4.6	−21 ± 1.9	17 ± 2.1	379 ± 5.5	+9 ± 1.3	32 ± 2.3	215 ± 4.7	+11 ± 3.1	60 ± 2.9
5	401 ± 5.7	+3 ± 0.4	44 ± 0.9	280 ± 4.7	+18 ± 3.0	64 ± 4.1	153 ± 3.9	+24 ± 2.6	80 ± 5.0
10	330 ± 3.8	+10 ± 2.3	57 ± 4.2	151 ± 3.5	+29 ± 2.4	75 ± 3.8	101 ± 3.6	+42 ± 4.2	82 ± 4.9
pND1, ζ = −100 ± 2.5									

4.4.2 Cellular and mitochondrial uptake of polyplexes

To follow the cellular uptake of TPP-based carriers, which is the first step in pDNA delivery into mitochondria and subsequent gene expression, a study using FITC-labelled pDNA was performed. FITC fluorescence intensity in the cytosol and mitochondrial cellular fractions was quantified after 24 h of transfection mediated by PEG-PEI_{25kDa}-TPP/pGFP-FITC or PEG-PEI_{25kDa}-TPP/pND1-FITC nanoparticles. As shown in **Figure 4.2**, the results obtained for both plasmids are very similar and consistent with a poor accumulation of pDNA in the cytosolic fraction and an intense accumulation of labeled pDNA in the mitochondria of HeLa cells, at an extent dependent on the N/P ratio considered. As shown, a higher N/P ratio leads to an increased FITC fluorescence intensity in the mitochondria. The difference is more pronounced between the carriers prepared at the N/P ratio of 2 and N/P of 5 or 10, and it becomes smaller when comparing the highest N/P ratios, independently of the pDNA system. Moreover, between the two plasmids, small differences can be observed, with the vectors based on pND1 exhibiting slightly higher FITC fluorescence levels in the mitochondria of HeLa cells. This result and those presented in the section above, probably, contribute to the smaller particle size and the more positive zeta potential values found for the PEG-PEI_{25kDa}-TPP/pND1 delivery system, which certainly may improve cellular uptake. Moreover, for all systems studied, the fluorescence levels found in the cytosol are quite low (**Figure 4.2**). These results demonstrate that the formulated particles can be internalized and efficiently targeted to mitochondria. Furthermore, our data suggest that the N/P ratio used in the formulation of the vectors can tailor the extent of mitochondria targeting/internalization. To gain a deeper insight into the mitochondria targeting phenomenon, the FITC fluorescence intensity in the mitochondria has been monitored as a function of transfection time for both pDNA systems. The results are presented in **Figure 4.3 A** and **B**. As shown, the mitochondria internalization

profile seems to be quite similar for both pDNAs studied. Independently of the N/P ratio at which the polyplexes were prepared, lower levels of FITC were detected in the mitochondria of HeLa cells at early time points, which increased with the time of transfection. After 4 h of transfection, an intense accumulation of pDNA-FITC into mitochondria can be detected, being more pronounced for carriers generated at N/P ratios of 5 and 10. Although, particles at the N/P ratio of 2 seem to ensure mitochondria targeting and pDNA/FITC accumulation into this organelle as the time of transfection increases, the FITC fluorescence levels are always lower when compared with those found for the corresponding complexes at higher N/P ratios, especially for the N/P of 10. For vectors formulated at N/P ratios of 5 and 10, FITC levels significantly increase with time until a plateau is reached after 12 h of transfection. Our results seem to indicate that the N/P ratio can tailor the pDNA/FITC internalization into mitochondria, as the highest value for the N/P parameter leads to the highest levels of FITC fluorescence. This assumption is valid for both pDNA-based systems. To support the evidence of the targeting ability displayed by the PEG-PEI_{25kDa}-TPP/pDNA systems, FITC fluorescence intensity in the mitochondria of HeLa cells, as a function of time, after transfection mediated by PEG-PEI_{25kDa}/pGFP-FITC or PEG-PEI_{25kDa}/pND1-FITC vectors was monitored. The results, available in the Supplementary Material (Fig. S1), show the poor accumulation of pDNA-FITC into mitochondria, indicating that PEG-PEI_{25kDa}/pDNA carriers do not target mitochondria. This deeply confirms that TPP-polymer conjugation is an efficient strategy to confer mitochondrial targeting ability to PEG-PEI-pDNA delivery systems. Other authors also successfully developed mitochondria-targeted vectors for novel therapeutic strategies implementation. These systems were designed for practical applications such as drug delivery for cancer treatment, eradication of drug resistance, or mitochondrial gene therapy [54–58]. They also demonstrated that the incorporation of mitochondriotropic compounds significantly enhances the mitochondria targeting ability, promoting the delivery of therapeutic cargoes into this organelle [54–58]. In some cases, fluorometric analysis on isolated mitochondria was also performed to prove the selective and efficient mitochondria-targeting performance displayed by the nanocarriers [54].

In a previous study, a fluorescence confocal microscopy study was conducted for PEG-PEI_{25kDa}-TPP/pND1-FITC vectors and corroborated well with the above results [47]. The confocal microscopy images, at 24 h of transfection, illustrate the co-localization of pDNA with mitochondria. Microscopy results confirm the mitochondrial targeting ability of the formulated particles [47], which seems to be enhanced with the increase of the N/P ratio. Unexpectedly, no GFP fluorescence was detected in HeLa cells after 24 h transfection mediated by PEG-PEI_{25kDa}-TPP-pGFP carriers, as assessed by confocal microscopy. This result was also confirmed by the low GFP fluorescence levels found when measuring the cell-associated GFP fluorescence 24 h after transfection with the pGFP-based polyplexes, as shown in **Figure 4.4A**. However, significant GFP fluorescence can be found in the mitochondria of HeLa cells 48 h after transfection ($p < 0.0001$) (**Figure 4.4B**). This indicates that PEG-PEI_{25kDa}-TPP/pGFP carriers are being internalized into the cancer cells, which were successfully transfected, resulting in protein expression. Once more, the N/P ratio parameter seems to influence this process, in that higher N/P ratios lead to higher levels of GFP fluorescence in HeLa cells ($p < 0.0001$). In contrast, the

GFP fluorescence levels observed in the cytosol are quite low for all N/P ratios assayed (not significant). Additionally, and as discussed in the following sections, gene expression and the consequent GFP production in HeLa cells were found. Confocal microscopy and co-localization studies have also been performed by other researchers to demonstrate cellular uptake and mitochondrial targeting of the payloads [54,56]. For instance, Ahn *et al*. when searching for more effective and selective mitochondria-targeting drug nanocarriers, reported the accumulation of non-peptidic guanidinium-functionalized silica nanoparticles into mitochondria within only 5 min [54].

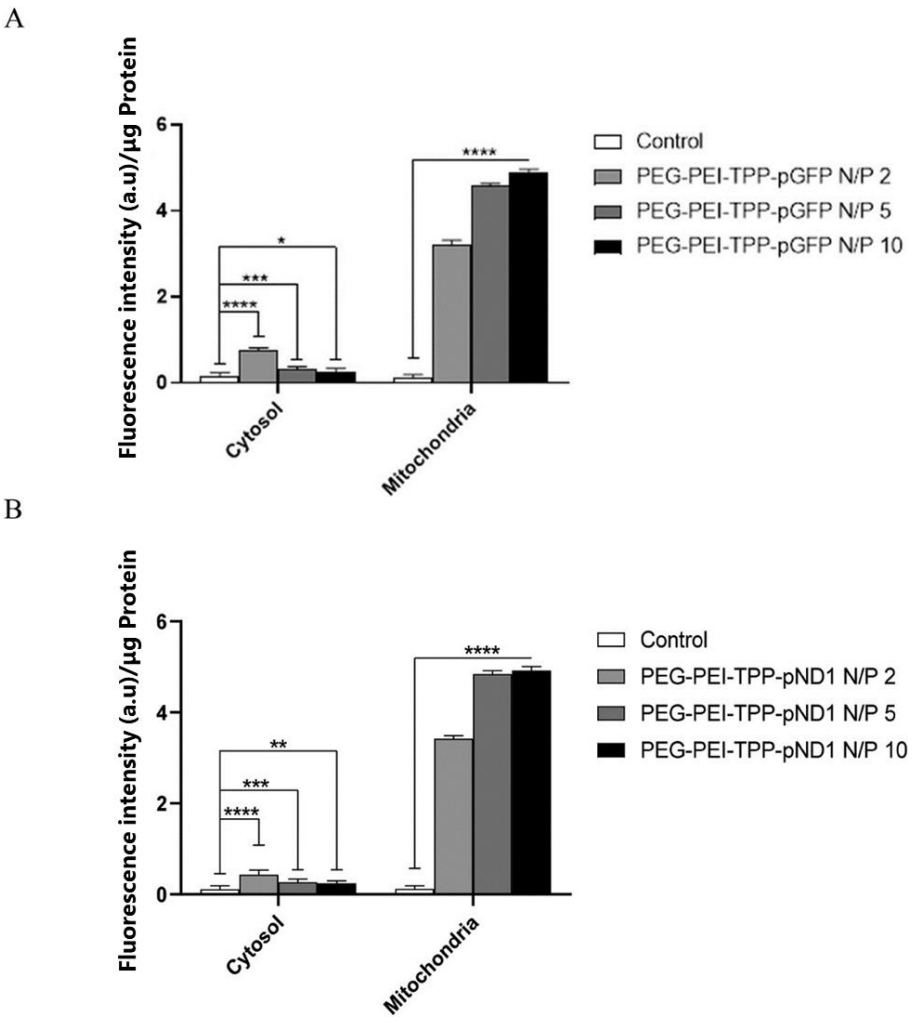

Figure 4.2 - FITC fluorescence intensity ((a.u)/µg Protein) in the cytosol and mitochondria of HeLa cells after 24 h transfection mediated by PEG-PEI-TPP-pGFP (A) or PEG-PEI-TPP-pND1 (B) systems. Untreated cells were used as control. The data, obtained by calculating the average of nine independent experiments, are presented as mean ± SD and analyzed by two-way ANOVA followed by the Bonferroni test, *p <0.033, **p <0.002, ***p <0.001 and ****p <0.0001. A comparison between cytosol and mitochondria for corresponding vectors was performed by two-way ANOVA followed by the Bonferroni test. For both pDNA-based systems: not significant, for control and ****p < 0.0001 for all vectors.

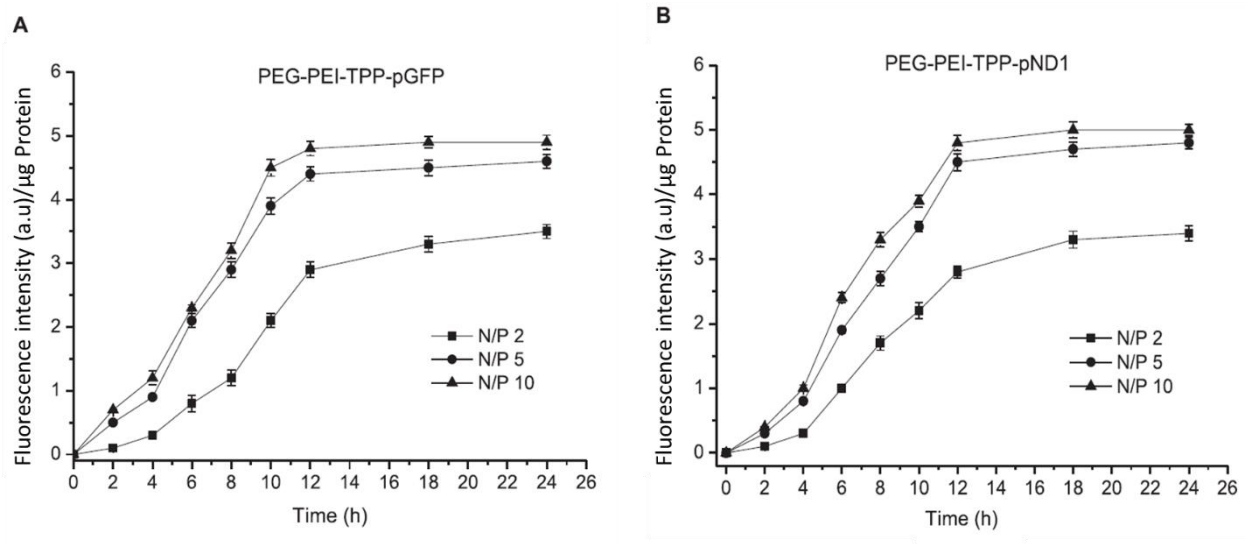

Figure 4.3 - FITC fluorescence intensity ((a.u)/µg Protein) in the mitochondria of HeLa cells as a function of time after transfection mediated by PEG-PEI-TPP/pGFP (A) or PEG-PEI-TPP/pND1 (B) systems. The data, obtained by calculating the average of three independent experiments, are presented as mean ± SD.

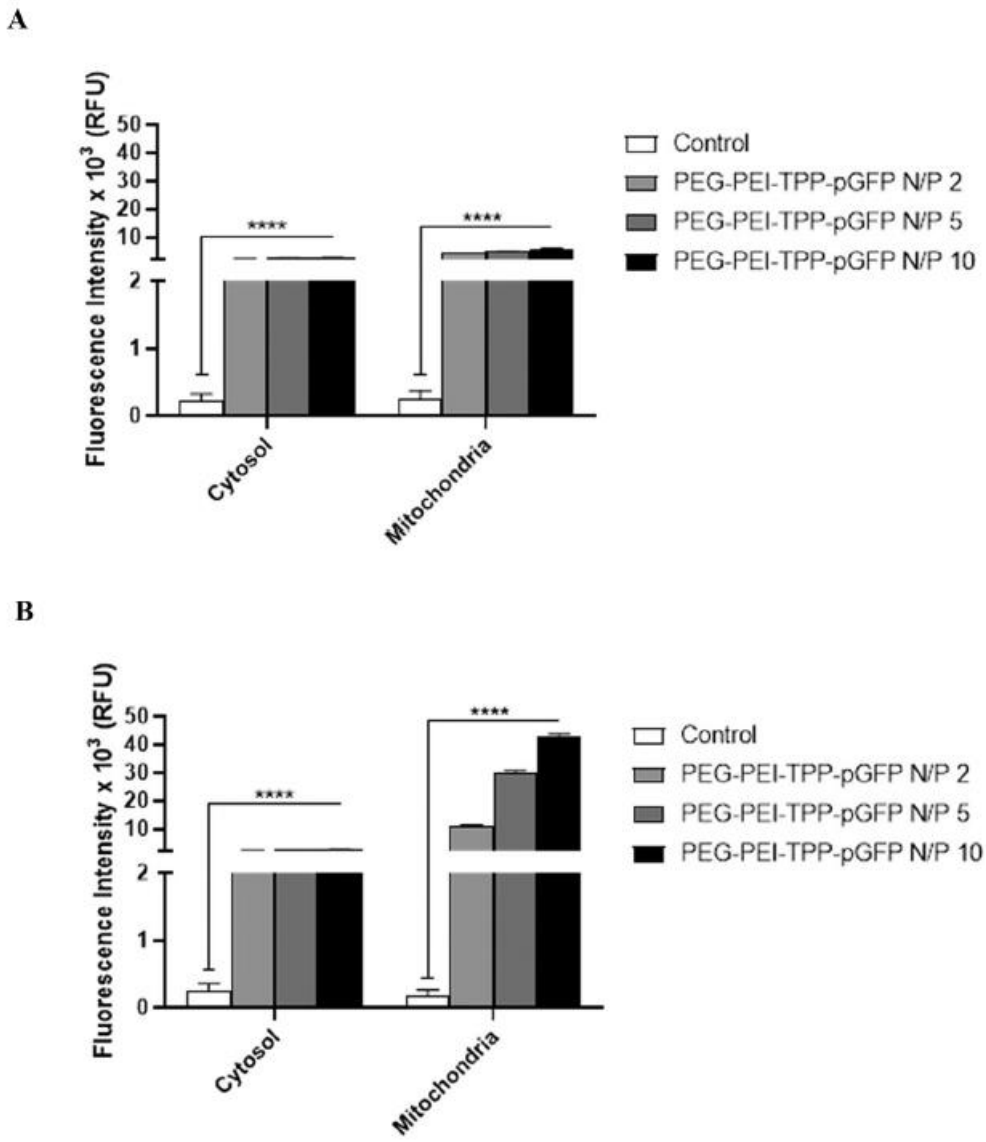

Figure 4.4 – GFP fluorescence (relative fluorescence units, RFU) in the cytosol and mitochondria of HeLa cells 24 h (A) and 48 h (B) after transfection with PEG-PEI-TPP-pGFP vectors at different N/P ratios. Untreated cells were used as control. Data are presented as mean ± SD, n = 9, and analyzed by two-way ANOVA followed by the Bonferroni test, with statistical significance as indicated. ****p <0.0001 for all vectors.

4.4.3 Mitochondrial gene and protein expression

After evidencing cellular internalization and mitochondria targeting when transfection was mediated by the developed polyplexes, GFP gene expression was evaluated. RT-PCR was performed in RNA samples extracted from mitochondria isolated from untreated cells (control) and from HeLa cells transfected with the pGFP-based formulations, using specific primers. The results are summarized in **Figure 4.5**. **Figure 4.5** presents gel electrophoresis of the amplification products of the mitochondrial GFP gene, with well-resolved bands at expected sites,

when compared with the control DNA ladder. Considerable levels of GFP mRNA were observed in cells transfected with all PEG-PEI_{25kDa}-TPP/pGFP vectors when compared to the mRNA content detected in control cells. The intensity of the bands seems to vary with the N/P ratio, with polyplexes conceived at N/P of 10 leading to a more intense band from GFP transcripts. This demonstrates their ability to promote efficient mitochondrial gene expression. A similar result has been achieved by Cardoso *et al.* when HeLa cells have been transfected by surfactant-pGFP complexes. Agarose gel electrophoresis also shows the amplification products of the mitochondrial GFP gene on isolated mitochondria, confirming the efficient mitochondrial gene expression mediated by the surfactant/pDNA vectors [30]. In a remarkable work, Kawamura *et al.* used amplification refractory mutation system (ARMS)-quantitative PCR to examine mutant levels resulting from the transfection of wild-type mitochondrial $pretRNA^{Phe}$ encapsulated in the MITO-Porter. Following this approach, they found a significant decrease in the mutant rate of $tRNA^{Phe}$ and showed that the therapeutic effect was sustained [59]. Moreover, Park *et al.* wisely reviewed the techniques for investigating mitochondrial gene expression giving a good perspective of the possibilities and challenges for future research of gene expression into mitochondria [60]. The ongoing work of our team on this topic will deeply focus on techniques described in this review article.

The expression of mitochondrial recoded GFP and ND1 proteins were evaluated after 48 h cell transfection by the different nanoparticle formulations. As a control, cells were also transfected with PEG-PEI_{25kDa}/pDNA complexes, and the expression of proteins was evaluated. Proteins were quantified by using the ELISA immunoassay, as described above, and the results are displayed in **Table 2**. Mitochondrial GFP protein (**Table 2A**) was not detected in control cells nor cells transfected by PEG-PEI_{25kDa}/pGFP complexes, demonstrating their inability to target mitochondria. The PEG-PEI_{25kDa}/pGFP complexes should be able to cellular internalization, promoting gene and protein expression in the cytosol. However, mitochondrial recoded GFP cannot be expressed in the cytosol due to the different genetic codes exhibited by mitochondrion. Mitochondrial genetic code is different from the nucleus, therefore, some codons correspond to different amino acids in mitochondria than in nuclear code [61]. Protein-coding genes are all components of the respiratory complexes in the mitochondrial matrix (MM). mtDNA-encoded proteins are synthesized inside the matrix and co-translationally inserted directly into the inner mitochondrial membrane by the mitochondrial ribosome aided by the insertase Oxa1, the inner membrane protein Mba1, and a variety of other factors [62].

On the contrary, cellular transfection mediated by the PEG-PEI_{25kDa}-TPP/pGFP vectors leads to protein expression to an extent dependent on the N/P ratio. HeLa cells transfected with particles at the N/P ratio of 2 present the lowest GFP amount, while as the N/P ratio increases, significantly higher protein levels are observed (**$p < 0.01$). The differences found, in protein expression following transfection with the TPP polyplexes prepared at higher N/P ratios are small (*$p < 0.05$). In the same way, while PEG-PEI_{25kDa}/pND1 formulations are unable to mediate the ND1 protein expression in both cytosol and mitochondria, this protein can be produced in HeLa cells after transfection with PEG-PEI_{25kDa}-TPP/pND1 carriers. As ND1 is an endogenous mitochondrial gene, control cells present significant levels of ND1 protein (**Table 4.2B**).

However, this protein content can be incremented upon cell transfection with PEG-PEI$_{25kDa}$-TPP/pND1 carriers, as considerable protein levels are produced for all N/P ratios with respect to control (**$p < 0.01$). The variation of protein expression with the N/P ratio seems to follow the same trend observed for GFP production. As the N/P ratio increases, more efficient seems to be the transfection process and a higher amount of mitochondrial proteins can be produced. The difference in protein expression obtained with polyplexes at N/P ratios of 2 and 5 (**$p < 0.01$) or N/P ratios of 2 and 10 (**$p < 0.01$) is, however, more significant than the difference observed when the polyplexes exhibit higher ratios (*$p < 0.05$), for both pDNAs. This finding on protein expression agrees well with the results presented earlier in this report, which is consistent with efficient cellular uptake and mitochondrial internalization for particles with higher N/P ratios and, therefore, a transfection leading to high levels of produced mitochondrial protein.

Table 4.2 - Quantification of GFP and ND1 protein levels (ng/mL) in the cytosol and mitochondria of HeLa cells after 48 h of transfection mediated by the formulated PEG-PEI-pGFP, PEG-PEI-TPP-pGFP, PEG-PEI-pND1 and PEG-PEI-TPP-pND1 vectors, at different N/P ratios. The values were calculated with the data obtained from three independent measurements (mean±SD, n=3). Data were analyzed by one-way or two-way ANOVA (GraphPad Software version 6.01, Inc., CA, USA). Statistical significance was accepted at a level of $p < 0.05$.

A. GFP (ng/mL)

System	Cytosol	Mitochondria
Control cells	0	0
PEG-PEI-pGFP N/P 2	0	0
PEG-PEI-pGFP N/P 5	0	0
PEG-PEI-pGFP N/P 10	0	0
PEG-PEI-TPP-pGFP N/P 2	0	210 ± 3.8
PEG-PEI-TPP-pGFP N/P 5	0	448 ± 6.6
PEG-PEI-TPP-pGFP N/P 10	0	563 ± 6.4

B. ND1 (ng/mL)

System	Cytosol	Mitochondria
Control cells	0	98 ± 4.2
PEG-PEI-pND1 N/P 2	0	98 ± 3.9
PEG-PEI-pND1 N/P 5	0	100 ± 5.1
PEG-PEI-pND1 N/P 10	0	100 ± 3.8
PEG-PEI-TPP-pND1 N/P 2	0	266 ± 4.6
PEG-PEI-TPP-pND1 N/P 5	0	420 ± 5.0
PEG-PEI-TPP-pND1 N/P 10	0	485 ± 6.9

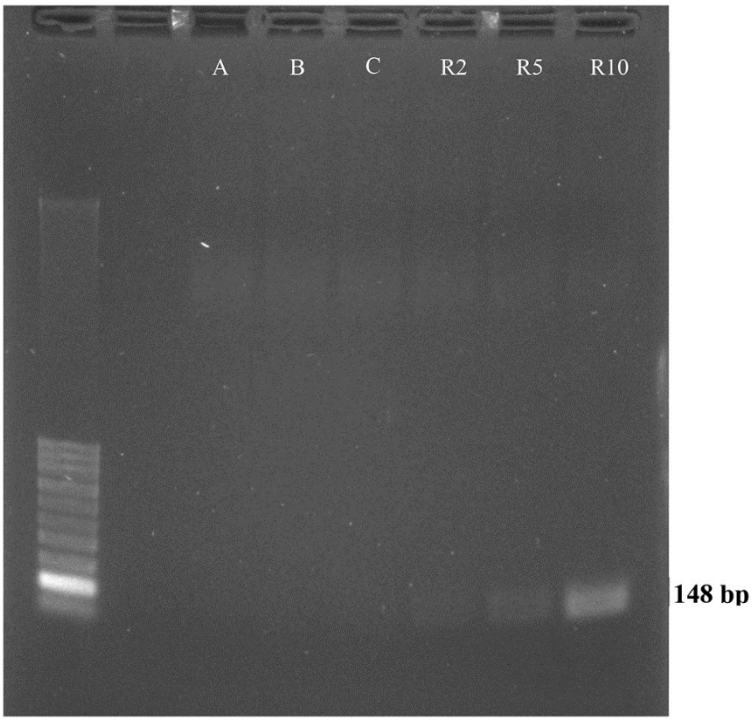

Figure 4.5 - PCR analysis of GFP mRNA extracted from mitochondria isolated from HeLa cells after 24 h of transfection mediated by PEG-PEI-TPP-pGFP based polyplexes, at the N/P ratios of 2, 5 and 10 (R2, R5 and R10, respectively). A – negative control, RT-PCR reaction containing all of the necessary components except cDNA; B – mRNA samples from mitochondria of untreated cells; C – mRNA from mitochondria of cells transfected with pGFP.

From the above findings, it becomes clear that the N/P ratio appears as a relevant tailoring parameter for desired mitochondrial targeting and protein expression when using PEG-PEI_{25kDa}-TPP/pDNA polyplexes in mitochondrial gene therapy. Moreover, research on the design/formulation of mitochondrial-targeted delivery systems, aiming for long-term expression of transgenes, will deeply benefit from the conception of disease models covering the wide range of mitochondrial genetic mutations. Altogether, these efforts will, certainly, make mitochondrial gene delivery clinically feasible in the near future. Moreover, strategies based on mtDNA editing via protein-only nucleases or CRISPR/Cas9-based editing have recently been deeply investigated and show valuable potential for treating mitochondrial disorders [62–64].

4.5 Conclusions

The mitochondrial-targeted PEI/TPP polymer successfully condenses both GFP and ND1-encoded plasmid DNA, resulting in the formation of nanometer complexes. It was found that PEI molecular weight and N/P ratio can deeply tailor the properties exhibited by PEI/TPP/pDNA carriers. *In vitro* transfection studies demonstrate that higher molecular weight PEI-based vectors are able of uptake to be internalized by mammalian cells and target mitochondria, to an extent dependent on the N/P ratio. Confocal microscopy analysis of transfected HeLa cells

strongly supports the mitochondrial targeting ability of the developed polyplex formulations. Importantly, after transfection mediated by the pDNA delivery systems, mitochondrial gene expression occurred and significant GFP and ND1 protein levels were quantified in cancer cells. This study represents a great advance in gene delivery into mitochondria and protein expression to restore mitochondrial function. Therefore, it paves the way for further research into the challenging topic of long-term mitochondrial transgenes expression, advancing therapeutic strategies for mitochondrial DNA disorders.

4.6 Supplementary Material

Supporting Information for Chapter 4

Table S4.1 – Mean particle size (nm), determined by SEM analysis and using ImageJ software, for the different PEG-PEI-TPP/pDNA systems prepared at N/P ratios ranging from 1 to 10. Approximately 20 SEM images were acquired for each sample and, on average, five particles were counted per image, considering 1 pixel = 0.95 nm. The data are presented as mean ± SD.

PEG-PEI-TPP-pGFP

	PEI 1.8 kDa	PEI 10 kDa	PEI 25 kDa
N/P		Size (nm)	
1	786 ±4.1	539 ±3.8	461 ±1.9
2	616 ±2.9	420 ±2.8	270 ±3.7
5	437 ±2.6	246 ±4.6	201 ±4.2
10	370 ±5.1	200 ±3.9	138 ±3.0

PEG-PEI-TPP-pND1

N/P		Size (nm)	
1	659 ±3.3	517 ±4.8	431 ±3.9
2	582 ±1.6	376 ±6.9	223 ±5.4
5	415 ±3.9	291 ±5.8	155 ±5.1
10	330 ±4.8	153 ±4.8	116 ±2.9

Table S4.2 – Mean particle size (nm) and average zeta potential (mV) for the different PEI-TPP-PEG/pDNA systems at N/P ratios of 1 to 10, in Dulbecco´s Modified Eagle´s Medium with High Glucose. The values were calculated with the data obtained from three independent measurements (mean ± SD, n = 3) and analyzed by one-way or two-way ANOVA (GraphPad Software version 6.01, Inc., CA, USA). Statistical significance was accepted at a level of *p <0.05.

PEG-PEI-TPP-pGFP

	PEI 1.8 kDa		PEI 10 kDa		PEI 25 kDa	
N/P	Size (nm)	Zeta (mV)	Size (nm)	Zeta (mV)	Size (nm)	Zeta (mV)
1	796 ±2.9	-28 ±0.8	545 ±6.5	-13 ±1.9	480 ±5.7	-5 ±0.6
2	623 ±4.7	-22 ±1.9	429 ±3.2	+8 ±2.2	284 ±6.8	+12 ±1.1
5	449 ±5.1	+4 ±1.5	260 ±3.6	+15 ±3.0	210 ±5.2	+25 ±2.5
10	378 ±5.9	+9 ±2.8	201 ±2.8	+24 ±2.1	142 ±3.0	+39 ±1.8

PEG-PEI-TPP-pND1

	PEI 1.8 kDa		PEI 10 kDa		PEI 25 kDa	
N/P	Size (nm)	Zeta (mV)	Size (nm)	Zeta (mV)	Size (nm)	Zeta (mV)
1	668 ±7.7	-26 ±1.2	522 ±6.6	-6 ±0.2	438 ±8.1	-4 ±0.8
2	590 ±5.1	-17 ±1.5	384 ±4.7	+13 ±1.1	231 ±4.2	+14 ±0.7
5	421 ±6.3	+6 ±1.2	296 ±5.1	+21 ±2.0	160 ±3.3	+28 ±1.0
10	339 ±4.6	+13 ±2.1	164 ±4.0	+31 ±1.9	119 ±4.4	+44 ±0.9

4.7 References

[1] Cogliati, S.; Enriquez, J. A.; Scorrano, L. Mitochondrial Cristae: where beauty meets functionality. Trends Biochem. Sci. 2016, 41, 261-273.

[2] Milenkovic, D.; Blaza, J. M.; Larsson, N-G.; Hirst, J. The enigma of the respiratory chain supercomplex. Cell Metabolism. 2017, 25, 765-776.

[3] Jonckheere, A. I.; Smeitink, J. A. M.; Rodenburg, R. J. T. Mitochondrial ATP synthase: architecture, function and pathology. J. Inherit. Metab. Dis. 2012, 35, 211-225.

[4] Ajioka, R. S.; Phillips, J. D.; Kushner, J. P. Biosynthesis of heme in mammals. Biochim. Biophys. Acta. 2006, 1763, 723-736.
[5] Hajnóczky, G.; Csordás, G.; Das, S.; Garcia-Perez, C.; Saotome, M.; Sinha Roy, S.; Yi, M. Mitochondrial calcim signalling and cell death: approaches for assessing the role of mitochondrial Ca2+ uptake in apoptosis. Cell Calcium. 2006, 40, 553-560.
[6] Tiwari, M.; Prasad, S.; Tripathi, A.; Pandey, A. N.; Ali, I.; Singh, A. K.; Shrivastav, T. G.; Chaube, S. K. Apoptosis in mammalian oocytes: a review. Apoptosis. 2015, 20, 1019-1025.
[7] Tavassoly, I.; Parmar, J.; Shajahan-Haq, A. N.; Clarke, R.; Baumann, W. T.; Tyson, J. J. Dynamic modelling of the interaction between autophagy and apoptosis in mammalian cells. CPT Pharmacometrics Syst. Pharmacol. 2015, 4, 263-272.
[8] Galluzzi, L.; Vitale, I.; Abrams, J. M.; Alnemri, E. S.; Baehrecke, E. H.; Blagosklonny, M. V.; Dawson, T. M.; Dawson, V. L.; El-Deiry, W. S.; Fulda, S.; Gottlieb, E.; Green, D. R.; Hengartner, M. O.; Kepp, O.; Knight, R. A.; Kumar, S.; Lipton, S. A.; Lu, X.; Madeo, F.; Malorni, W.; Mehlen, P.; Nuňez, G.; Peter, M. E.; Piacentini, M.; Rubinsztein, D. C.; Shi, Y.; Simon, H. U.; Vandenabeele, P.; White, E.; Yuan, J.; Zhivotovsky, B.; Melino, G.; Kroemer, G. Molecular definitions of cell death subroutines: recommendations of the Nomenclature Committee on Cell Death 2012. Cell Death and Differ. 2012, 19, 107-120.
[9] Zhao, D.; Hong, D.; Zhang, W.; Yao, S.; Qi, X.; Lv, H.; Zheng, R.; Feng, L.; Huang, Y.; Yuan, Y.; Wang, Z. Mutations in mitochondrially encoded complex I enzyme as the second common cause in a cohort of Chinese patients with mitochondrial myopathy, encephalopathy, lactic acidosis and stroke-like episodes. J. Hum. Genet. 2011, 56, 759-764.
[10] Monlleo-Neila, L.; Del Toro, M.; Bornstein, B.; Garcia-Arumi, E.; Sarrias, A.; Roig-Quilis, M.; Munell, F. Leigh syndrome and the mitochondrial m.13513G > A mutation: expanding the clinical spectrum. J. Child Neurol. 2013, 28, 1531-1534.
[11] Zsurka, G.; Kunz, W. S. Mitochondrial dysfunction and seizures: the neuronal energy crisis. Lancet Neurol. 2015, 14, 956-966.
[12] Rodenburg, R. J. Mitochondrial complex-I linked disease. Biochim. Biophys. Acta. 2016, 1857, 938-945.
[13] Zaragoza, M.V.; Fass, J.; Diegoli, M.; Lin, D.; Arbustini, E. Mitochondrial DNA variant discovery and evaluation in human cardiomyophaties through next-generation sequencing. PLoS One. 2010, 5, e12295.
[14] Hadzsiev, K.; Maasz, A.; Kisfali, P.; Kalman, E.; Gomori, E.; Pal, E.; Berenyi, E.; Komlosi, K.; Melegh, B. Mitochondrial DNA 11777C>A mutation associated Leigh syndrome: case report with a review of the previously described pedigrees. Neuromol. Med. 2010, 12, 277-284.
[15] Castellani, R.; Hirai, K.; Aliev, G.; Drew, K. L.; Nunomura, A.; Takeda, A.; Cash, A. D.; Obrenovich, M. E.; Perry, G.; Smith, M. A. Role of mitochondrial dysfunction in Alzheimer´s disease. J. Neuros. Res. 2002, 70, 357-360.
[16] Ciccone, S.; Maiani, E.; Bellusci, G.; Diederich, M.; Gonfloni, S. Parkinson´s disease: a complex interplay of mitochondrial DNA alterations and oxidative stress. Int. J. Mol. Sci. 2013, 14, 2388-2409.

[17] Spangenberg, L.; Graña, M.; Greif, G.; Suarez-Rivero, J. M.; Krysztal, K.; Tapié, A.; Boidi, M.; Fraga, V.; Lemes, A.; Gueçaimburú, R.; Cerisola, A; Sánchez-Alcázar, J. A.; Robello, C.; Raggio, V.; Naya, H. 3697G >A in MT-ND1 is a causative mutation in mitochondrial disease. Mitochondrion. 2016, 28, 54-59.
[18] Yu, M. Somatic mitochondrial DNA mutations in human cancers. Adv. Clin. Chem. 2012, 57, 99-138.
[19] Chinnery, P. F.; Majamaa, K.; Turnbull, D. M.; Thorburn, D. R. Treatment for mitochondrial disorders. Cochrane Database Syst. Rev. 2006, 1, CD004426.
[20] Remacle, C.; Cardol, P.; Coosemans, N.; Gaisne, M.; Bonnefoy, N. High-efficiency biolistic transformation of Chlamydomonas mitochondria can be used to insert mutations in complex I genes. Proc. Natl. Acad. Sci. USA. 2006, 103, 4771-4776.
[21] Bonnefoy, N.; Fox, T. D. Directed alteration of Saccharomyces cerevisiae mitochondrial DNA by biolistic transformation and homologous recombination. Methods Mol. Biol. 2007, 372, 153-166.
[22] Yasuzaki, Y.; Yamada, Y.; Ishikawa, T.; Harashima, H. Validation of mitochondrial gene delivery in live rand skeletal muscle via hydrodynamic injection using an artificial mitochondrial reporter DNA vector. Mol. Pharm. 2015, 12, 4311-4320.
[23] Muratovska, A.; Lightowlers, R. N.; Taylor, R. W.; Turnbull, D. M.; Smith, R. A.; Wilce, J. A.; Martin, S. W.; Murphy, M. P. Targeting peptide nucleic acid (PNA) oligomers to mitochondria within cells by conjugation to lipophilic acids: implications for mitochondrial DNA replication, expression and disease. Nucleic Acids Res. 2001, 29, 1852-1863.
[24] Geromel, V.; Cao, A.; Briane, D.; Vassi, J.; Rotig, A.; Rustin, P.; Coudert, R.; Rigaut, J. P.; Munnich, A.; Taillandier, E. Mitochondria transfection by oligonucleotides containing a signal peptide and vectorised by cationic liposomes. Antisense Nucleic Acid Drug Dev. 2001, 11, 175-180.
[25] Flierl, A.; Jackson, C.; Cottrell, B.; Murdock, D.; Seibel, P.; Wallace, D. C. Targeted delivery of DNA to the mitochondrial compartment via import sequence-conjugated peptide nucleic acid. Mol. Ther. 2003, 7, 550-557.
[26] Yoon, Y. G.; Koob, M. D. Transformation of isolated mammalian mitochondria by bacterial conjugation. Nucleic Acids Res. 2005, 33, e139.
[27] Yamada, Y.; Fukuda, Y.; Harashima, H. An analysis of membrane fusion between mitochondrial double membranes and MITO-Porter, mitochondrial fusogenic vesicles. Mitochondrion. 2015, 24, 50-55.
[28] Yamada, Y.; Ishikawa, T.; Harashima, H. Validation of the use of an artificial mitochondrial reporter DNA vector containing a Cytomegalovirus promoter for mitochondrial transgene expression. Biomaterials. 2017, 136, 56-66.
[29] Lyrawati, D.; Trounson, A.; Cram, D. Expression of GFP in mitochondrial compartment using DQAsome-mediated delivery of an artificial mini-mitochondrial genome. Pharm. Res. 2011, 28, 2848-2862.
[30] Cardoso, A. M.; Morais, C. M.; Cruz, A. R.; Cardoso, A. L.; Silva, S. G.; Vale, M. L.; Marques, E. F.; Lima, C. P.; Jurado, A. Gemini Surfactants Mediate Efficient Mitochondrial Gene Delivery and Expression. Mol. Pharm. 2015, 12, 716-730.

[31] Coutinho, E.; Batista, C.; Sousa, F.; Queiroz, J. A.; Costa, D. Mitochondrial Gene Therapy: Advances in mitochondrial gene cloning, plasmid production and nanosystems targeted to mitochondria. Mol. Pharm. 2017, 14, 626-638.
[32] Weissig, V.; D´Souza, G. G.; Torchilin, V. P. DQAsome/DNA complexes release DNA upon contact with isolated mouse liver mitochondria. J. Control Release. 2001, 75, 401-408.
[33] Biswas, S.; Dodwadkar, N. S.; Piroyan, A.; Torchilin, V. P. Surface conjugation of triphenylphosphonium to target poly(amidoamine) dendrimers to mitochondria. Biomaterials. 2012, 33, 4773-4782.
[34] Santos, J.; Sousa, F.; Queiroz, J.; Costa, D. Rhodamine based plasmid DNA nanoparticles for mitochondrial gene therapy. Colloids Surf. B. 2014, 121, 129-140.
[35] Boddapati, S. V.; Tongcharoensirikul, P.; Hanson, R. N.; D´Souza, G. G.; Torchilin, V. P.; Weissig, V. Mitochondriotropic liposomes. J. Liposome Res. 2005, 15, 49-58.
[36] Yousif, L. F.; Stewart, K. M.; Kelley, S. O. Targeting mitochondria with organelle-specific compounds: strategies and applications. ChemBioChem. 2009, 10, 1939-1950.
[37] Gruber, J.; Fong, S.; Chen, C. B.; Yoong, S.; Pastorin, G.; Schaffer, S.; Cheah, I.; Halliwell, B. Mitochondria-targeted antioxidants and metabolic modulators as pharmacological interventions to slow ageing. Biotechnol. Adv. 2013, 31, 563-592.
[38] Wang, B.; Wang, Y.; Wu, H.; Song, X.; Guo, X.; Zhang, D.; Ma, X.; Tan, M. A mitochondria-targeted fluorescent probe based on TPP-conjugated carbon dots for both one- and two-photon fluorescence cell imaging. RSC Advances. 2014, 4, 49960-49963.
[39] Bielski, E. R.; Zhong, Q.; Brown, M.; Rocha, S. R. P. Effect of the conjugation density of triphenylphosphonium cation on the mitochondrial targeting of poly(amidoamine) dendrimers. Mol. Pharmaceutics. 2015, 12, 3043-3053.
[40] Zhang, X-P.; Zhang, P-Y. Mitochondria targeting nano agents in cancer therapeutics. Oncol. Lett. 2016, 12, 4887-4890.
[41] Ozsvari, B.; Sotgia, F.; Lisanti, M. P. Exploiting mitochondrial targeting signal(s), TPP and bis-TPP, for eradicating cancer stem cells (CSCs). Aging. 2018, 10, No. 2.
[42] Jang, Y.; Lim, K. Recent advances in mitochondria-targeted gene delivery. Molecules. 2018, 23, E2316.
[43] Costa, D.; Briscoe, W. H.; Queiroz, J. Polyethylenimine coated plasmid DNA-surfactant complexes as potential gene delivery systems. Colloids Surf. B. 2015, 133, 156-163.
[44] Zhang, Y.; Liu, L.; Lin, L.; Chen, J.; Tian, H.; Chen, X.; Maruyama, A. In-situ dual-crosslinked nanoparticles for tumor targeting gene delivery. Acta Biomater. 2017, 65, 349-362.
[45] Penacho, N.; Simões, S.; Lima, M. C. P. Polyethylenimine of various molecular weights as adjuvante for transfection mediated by cationic liposomes. Mol. Membr. Biol. 2009, 26, 249-263.
[46] Benjaminsen, R. V.; Mattebjerg, M. A.; Henriksen, J. R.; Moghimi, S. M.; Andresen, T. L. The possible “proton sponge” effect of polyethylenimine (PEI) does not include change in lysosomal pH. Mol. Ther. 2013, 21, 149-157.
[47] Sousa, A.; Faria, R.; Albuquerque, T.; Bhatt, H.; Biswas, S.; Queiroz, J. A.; Costa, D. Design of experiments to select triphenylphosphonium-polyplexes with suitable physicochemical properties for mitochondrial gene therapy. J. Mol. Liq. 2020, 302, 112488.

[48] Al-Deen, F. N.; Selomulya, C.; Ma, C.; Coppel, R. L., in Rinaldi, M.; Fioretti, D. and Iurescia, S. (Eds), DNA Vaccines: Methods and Protocols, Methods in Molecular Biology, vol. 1143, Springer Science+Business Media, New York, 2014, Chapter 12.
[49] Durymanov, M.; Reineke, J. Non-viral delivery of nucleic acids: insight into mechanisms of overcoming intracellular barriers. Front. Pharmacol. 2018, 9: 971.
[50] Ghomrasni, N. B.; Chivas-Joly, C.; Devoille, L.; Hochepied, J-F.; Feltin, N. Challenges in sample preparation for measuring nanoparticles sizes by scanning electron microscopy from suspensions, powder form and complex media. Powder Technol. 2020, 259, 226-237.
[51] Costa, D.; Valente, A. J. M.; Queiroz, J. A.; Sousa, A. Finding the ideal polyethylenimine-plasmid DNA system for co-delivery of payloads in cancer therapy. Colloids Surf. B. 2018, 170, 627-636.
[52] Salatin, S.; Maleki Dizaj, S.; Yari, A. Effect of the surface modification, size and shape on cellular uptake of nanoparticles. Cell Bio Int. 2015, 39, 881-890.
[53] Liu, X.; Wu, F.; Tian, Y.; Wu, M.; Zhou, Q.; Jiang, S.; Niu, Z. Size dependent cellular uptake of rod-like bionanoparticles with different aspect ratios. Sci. Rep. 2016, 6, 24567.
[54] Ahn, J.; Lee, B.; Choi, Y.; Jin, H.; Lim, N. Y.; Park, J.; Kim, J. H.; Bae, J.; Jung, J. H. Non-peptidic guanidinium-functionalized silica nanoparticles as selective mitochondria-targeting drug nanocarriers. J. Mater. Chem. B. 2018, 6, 5698-5707.
[55] Wang, W.; Liu, J.; Feng, W.; Du, S.; Ge, R.; Li, J.; Liu, Y.; Sun, H.; Zhang, D.; Zhang, H.; Yang, B. Targeting mitochondria with Au-Ag@Polydopamine nanoparticles for papillary thyroid cancer therapy. Biomater. Sci. 2019, 7, 1052-1063.
[56] Cohen-Erez, I.; Harduf, N.; Rapaport, H. Oligonulceotide loaded polypeptide-peptide nanoparticles towards mitochondrial-targeted delivery. Polym. Adv. Technol. 2019, 30, 2506-2514.
[57] Zhu, X-J.; Li, R-F.; Xu, L.; Yin, H.; Chen, L.; Yuan, Y.; Zhong, W.; Lin, J. A novel self-assembled mitochondria-targeting protein nanoparticle acting as a theranostic platform for cancer. Small. 2019, 15, 1803428.
[58] Wang, H.; Zhang, F.; Wen, H.; Shi, W.; Huang, Q.; Huang, Y.; Xie, J.; Li, P.; Chen, J.; Qin, L.; Zhou, Y. Tumor- and mitochondria-targeted nanoparticles eradicate drug resistant lung cancer through mitochondrial pathway of apoptosis. J. Nanobiotechnol. 2020, 18, 8.
[59] Kawamura, E.; Maruyama, M.; Abe, J.; Sudo, A.; Takeda, A.; Takada, S.; Yokota, T.; Kinugawa, S.; Harashima, H.; Yamada, Y. Validation of gene therapy for mutant mitochondria by delivering mitochondrial RNA using a MITO-Porter. Mol. Ther. Nucleic Acids. 2020.
[60] Park, D.; Lee, S.; Min, K-T. Techniques for investigating mitochondrial gene expression. BMB Rep. 2020, 53, 3-9.
[61] Scheffler, I. E. Mitochondria make a come back. Adv. Drug Delivery Rev. 2001, 49, 3-26.
[62] Slone, J.; Huang, T. The special considerations of gene therapy for mitochondrial diseases. Genom. Med. 2020, 5, 7.
[63] Gammage, P. A.; Viscomi, C.; Simard, M-L.; Costa, A. S. H.; Gaude, E.; Powell, C. A.; Haute, L. V.; McCann , B. J.; Rebelo-Guiomar, P.; Cerutti, R.; Zhang, L.; Rebar, E. J.; Zeviani, M.; Frezza,

C.; Stewart, J. B.; Minczuk, M. Genome editing in mitochondria corrects a pathogenic mtDNA mutation *in vivo*. Nat. Med. 2018, 24, 1691-1695.
[64] Bian, W-P.; Chen, Y-L.; Luo, J-J.; Wang, C.; Xie, S-L.; Pei, D-S. Knock-In strategy for editing human and zebrafish mitochondrial DNA using Mito-CRISP/Cas9 system. ACS Synth. Biol. 2019, 8, 621-632.

Chapter 5

Development of Peptide-Based Nanoparticles for Mitochondrial Plasmid DNA Delivery

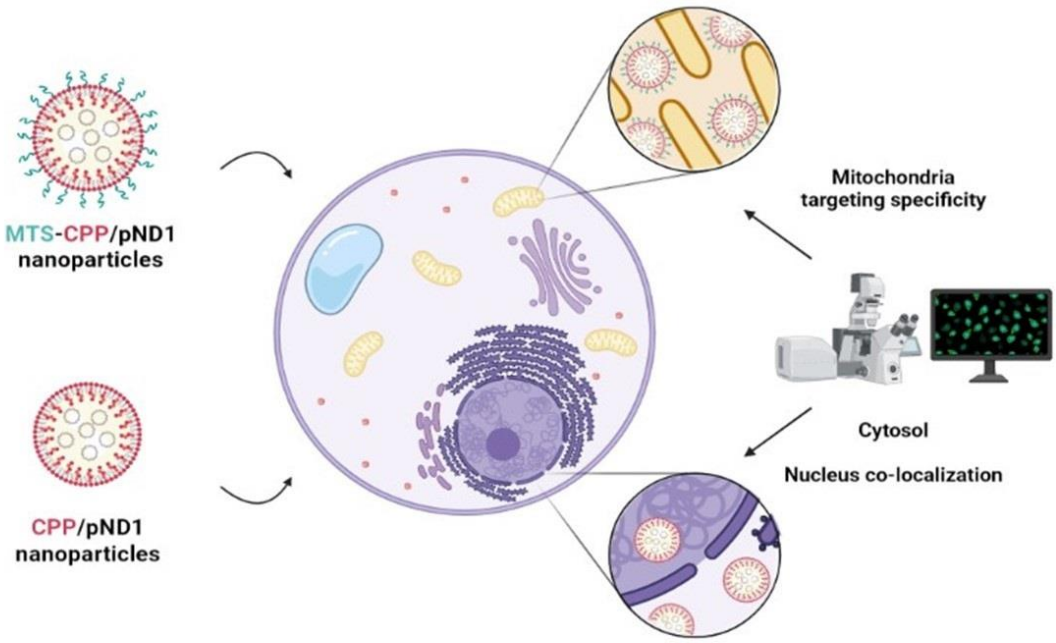

This chapter was published in:
Rúben Faria, Eric Vivès, Prisca Boisguérin, Ângela Sousa, and Diana Costa. 2021. 'Development of Peptide-Based Nanoparticles for Mitochondrial Plasmid DNA Delivery', Polymers, 13.
https://doi.org/10.3390/polym13111836

5.1 Abstract

A mitochondrion is a cellular organelle able to produce cellular energy in the form of adenosine triphosphate (ATP). As in the nucleus, mitochondria contain their own genome: the mitochondrial DNA (mtDNA). This genome is particularly susceptible to mutations that are at the basis of a multitude of disorders, especially those affecting the heart, the central nervous system and muscles. Conventional clinical practice applied to mitochondrial diseases is very limited and ineffective; a clear need for innovative therapies is demonstrated. Gene therapy seems to be a promising approach. The use of mitochondrial DNA as a therapeutic, optimized by peptide-based complexes with mitochondrial targeting, can be seen as a powerful tool in the reestablishment of normal mitochondrial function. In line with this requirement, in this work and for the first time, a mitochondrial-targeting sequence (MTS) has been incorporated into previously researched peptides, to confer on them a targeting ability. These peptides were then considered to complex a plasmid DNA (pDNA) which contains the mitochondrial gene ND1 (mitochondrially encoded NADH dehydrogenase 1 protein), aiming at the formation of peptide-based nanoparticles. Currently, the ND1 plasmid is one of the most advanced bioengineered vectors for researching mitochondrial gene expression. The formed complexes were characterized in terms of pDNA complexation capacity, morphology, size, surface charge, and cytotoxic profile. These data revealed that the developed carriers possess suitable properties for pDNA delivery. Furthermore, *in vitro* studies illustrated the mitochondrial targeting ability of the novel peptide/pDNA complexes. A comparison between the different complexes revealed the most promising ones that complex pDNA and target mitochondria. This may contribute to the optimization of peptide-based non-viral systems to target mitochondria, instigating progress in mitochondrial gene therapy.

Keywords

Cell-penetrating peptides; mitochondrial DNA diseases; mitochondria targeting; nano-delivery systems; biocompatibility; plasmid DNA

5.2 Introduction

Mitochondria are cytoplasmic organelles responsible for energy production to ensure normal cell metabolic function. This organelle synthesizes ATP via oxidative phosphorylation, in which four enzymatic systems are involved to promote electron transport and generate a proton gradient [1,2]. Mitochondria are also involved in cellular signaling, ion homeostasis, and the metabolism of amino acids, lipids, cholesterol, steroids, and nucleotides [3,4]. Beyond this, its role in the regulation of the cell cycle, cell growth, and apoptosis is also reported [5,6]. Along with chloroplasts, mitochondria emerged from bacterial ancestors, and through evolution, retained specialized structures and haploid genomes [7]. Much of their genetic content is included in the nuclear genome, but a significant part remains in mitochondria. The mitochondrial genome, mtDNA, is a double-stranded molecule, 16 kbp in size, containing 37 genes that encode 13

polypeptides that take part in the oxidative phosphorylation chain, 2 rRNAs and 22 tRNAs, all exclusive to the mitochondria [8]. Mutations in mtDNA have been associated with multiple metabolic and neuromuscular degenerative syndromes, and connected with Parkinson's and Alzheimer's diseases, diabetes, and several types of cancer [9-17]. The therapeutic approaches to treat mtDNA diseases have been largely ineffective, as they focus on alleviation of the symptoms. In this sense, mitochondrial gene therapy can be seen as a valuable and powerful tool to deal with these disorders, as it fights the disease at its source [18-20]. The direct and efficient transfection of mitochondria, with regard to replacing mutated mitochondrial genes, requires a suitable delivery system. This vehicle should protect, carry, and target the genetic content to mitochondria, promoting its efficient release, and thus, ensuring mitochondrial gene and protein expression.

In the last decades, considerable advances have been made in the conception of nucleic acid-based delivery systems to overcome the major drawbacks of payload delivery to eukaryotic cells, namely, cellular uptake/internalization, endosomal escape, targeting a specific subcellular compartment, and ultimately, the induction of therapeutic action [19-24]. In line with this aim, micelles, polymers, lipid- and peptide-based nanoparticles are among the most studied systems for gene release [25-28]. In particular, cell-penetrating peptides (CPP) offer exceptional properties to be explored as gene delivery vehicles for successful gene therapy [28-32]. CPPs are short peptides, usually of fewer than 30 amino acids, and can be separated into arginine-rich and amphipathic peptides. The amphipathic ones possess both hydrophilic and hydrophobic domains that confer on these peptides the ability to interact with the genetic material, promoting its membrane translocation, followed by cell entry [28-33]. However, the exact mechanism CPPs use to penetrate cells is still not fully understood, with endocytosis and direct penetration being the most probable hypothesis [30,33]. Despite this fact, their great potential in conjugation with therapeutic molecules and their cellular internalization has been well recognized, leading to the significant participation of CCPs in biomedical applications [31-36].

In this work, a set of CPPs have been designed/synthesized to complex the mitochondrial gene ND1-encoded pDNA (pND1) and ensure its targeting of mitochondria. To the best of our knowledge, to date, this pND1 is by far one of the most advanced bioengineered vectors in research toward mitochondrial gene expression. It enables us to get close to the concrete reality of mitochondrial protein expression. The formed nano-complexes were developed at various nitrogen-to-phosphate group (N/P) ratios and adequately characterized. Their biocompatibility has been assessed, and *in vitro* studies have been performed to evaluate the ability of the developed peptide/pND1 complexes to target mitochondria. The suitable physicochemical properties of the novel delivery systems, along with their mitochondria-targeting capacity, make them useful nano-platforms for mitochondrial gene therapy. Furthermore, a comparison between the various peptide/pND1 complexes revealed differences in their physicochemical properties and showed the ones with high potential for mitochondria targeting. This work may contribute to optimizing the conception of novel peptide-based systems for long-term mitochondrial gene expression.

5.3 Materials and Methods

5.3.1 Materials

Fmoc-amino acids, dimethylformamide (DMF), trifluoroacetic acid (TFA), diisopropylcarbodiimide (DIC), diisopropylethylamine (DIEA), dichloromethane (DCM), piperidine, oxyma, diethyl ether, acetonitrile and fluorescein isothiocyanate (FITC) were all obtained from Sigma-Aldrich (St Louis, MO, USA). Resin for peptide synthesis (AmphiSpheres 40™) was obtained from Agilent Technologies (Les Ulis, France). The Liberty Blue HT12™ Automated Microwave Peptide Synthesizer was obtained from CEM (NC, USA). The FC 204 Fraction Collector and 321 HPLC Pumps were obtained from Gilson. The Pharmacia LKB-REC 102 was obtained from Pharmacia (Stockholm, Sweden). The Waters Alliance 2695 HPLC System was obtained from Waters Corporation. DAPI was from Invitrogen (Carlsbad, CA, USA), and MitoTracker Orange CMTMRos from Molecular Probes (Leiden, The Netherlands). All solutions were freshly prepared using ultra-pure water, and purified with a Milli-Q system from Millipore (Billerica, MA, USA).

Normal Human Dermal Fibroblasts (NHDF), Ref. C-12302 (cryopreserved cells), and cancer HeLa cells were purchased from PromoCell (Heidelberg, Germany) and Invitrogen (Carlsbad, CA, USA), respectively.

The plasmid pCAG-GFP-ND1 (5.4 kbp) was developed by our research group through the cloning of the mitochondrial NADH dehydrogenase 1 protein-encoded gene (mtND1) in Escherichia coli. The full description of gene cloning and plasmid production are described elsewhere [19].

5.3.2 Methods

5.3.2.1 Synthesis of Peptides

Peptide synthesis was performed using the Liberty Blue HT12™ Automated Microwave Peptide Synthesizer. The peptides were produced by following the Fmoc approach of solid-phase peptide synthesis (SPPS) methodology. Amino acid-COOH activation was performed using a 1M solution of DIC (39.4 mL in 250 mL of DMF) and oxyma + DIEA (17.76 g + 6.25 mL in 125 mL of DMF). After the addition of amino acid, the Fmoc group was removed using a 20% solution of piperidine in DMF. The peptides were deprotected and cleaved from their respective resins by TFA treatment (TFA 92.5%, triisopropylsilane 5%, and water 2.5%). Peptides were purified by semi-preparative HPLC (Waters Corp., Wilmslow, UK), using an octadodecyl carbon chain (C18) column. The tryptophan-(W) and arginine-(R) rich amphipatic peptides (WRAP) WRAP1, WRAP5 and MTS peptides were dissolved in H_2O + 0.1% TFA, and MTS-WRAP1, MTS-WRAP5, $(KH)_9$, MTS-$(KH)_9$ and CpMTP were resuspended in H_2O + 30% acetonitrile. The purification of all peptides was carried out using the same gradient (20% to 60% of acetonitrile for 40 min at a flow rate of 5 mL/min). LC/MS analysis was performed to assess the molecular mass of each peptide, confirming a purity of ≥95%.

5.3.2.2 Formulation of Peptide/pND1 Complexes

pND1 stock solution was prepared in sodium acetate buffer (0.1 mM sodium acetate/0.1 M acetic acid, pH 4.5). Peptide/pND1 complexes were formed at different N/P ratios. The calculation of the N/P ratio is defined as the molar relation of amine groups in the peptide, which represent the positive charges, to phosphate groups in the pND1, which represent the negative charges, considering the mass per charge ratio of pND1 (330 g/mol, relative to one phosphate group) [19]. Therefore, for the preparation of peptide/pND1 complexes at various N/P ratios, different concentrations of each peptide (50 µL) were added to the pND1 solution at a fixed concentration of 1.4 nM. The mixture was vortexed for 30 s and left for equilibration for 25 min at room temperature. The complexes were then centrifuged at 13,000× g for 20 min at 4 °C and the pellet, containing the pND1-based nanoparticles, was recovered.

The presence of pND1 in the supernatant was evaluated by the horizontal electrophoresis technique for 30 min under 120 V in 1% agarose gel stained with GreenSafe Premium (NZYTech, Lda. Lisbon, Portugal). The gels were visualized using the Gel documentation system under UV light (UVItec Limited, Cambridge, UK).

5.3.2.3 Scanning Electron Microscopy (SEM)

The morphology of peptide/pND1 complexes was investigated by scanning electron microscopy (SEM). Freshly prepared complexes were washed three times with 300 µL of ultra-pure grade water and centrifuged (13,000× g, 12 min, 4 °C). Then, the pellet was recovered and resuspended in 40 µL of 2% tungsten solution. The samples were diluted 1:20 in ultra-pure water, 10 µL pipetted to the roundly shaped coverslip (10 mm), and left to dry overnight at room temperature. On the following day, the samples were mounted on aluminum supports, fixed with double-sided adhesive tape, and sputter coated with gold using an Emitech K550 (London, UK) sputter coater. A scanning electron microscope, Hitachi S-2700 (Tokyo, Japan), with an accelerating voltage of 20 kV at various magnifications, was used to determine the morphology of peptide/pND1 complexes.

5.3.2.4 Particle Size and Zeta Potential Measurements

The average particle size and the zeta potential of peptide/pND1 complexes were determined by dynamic light scattering (DLS) using a Zetasizer Nano ZS (Malvern Instruments, Worcestershire, UK). The pellet containing the complexes was suspended in 5% glucose with 1 mM NaCl. DLS using a He-Ne laser 633 nm with non-invasive backscatter optics (NIBS) and electrophoretic light scattering using M3-PALS laser technique (phase analysis light scattering) were applied for size and charge determination, respectively. The Malvern Zetasizer software v 6.34 (Worcestershire, UK) was used.

5.3.2.5 Cell Culture

Cancer HeLa cells and fibroblast cells were grown in Dulbecco´s Modified Eagle´s Medium, high glucose (DMEM-HG) (Sigma-Aldrich, St. Loius, MO, USA) supplemented with 10% heat-inactivated bovine fetal serum (FBS), 0.5 g/L sodium bicarbonate, 1.10 g/L HEPES, 100 µg/mL of streptomycin and 100 units/mL of penicillin (Sigma-Aldrich, St. Loius, MO, USA). The cells were kept at 37 °C in a 5% CO_2 humidified atmosphere until confluence was attained.

5.3.2.6 Cytotoxicity Evaluation

The biocompatibility of the systems was evaluated on HeLa cells using a MTT (3-[4,5dimethyl-thiazol-2-yl]-2,5-diphenyltetrazolium bromide) assay. MTT assay is a colorimetric method that quantifies the metabolic active cells. HeLa cells were plated in a 96-well plate, at a density of 1×10^4 cells/well, and grown at 37 °C in a 95% O2/5% CO_2 humidified atmosphere. The complexes (50 µL), in serum-free DMEM medium, were applied to the well plates. After 24 h or 48 h incubation, the redox activity was assessed through the reduction of MTT. Absorbance at 570 nm was measured using a Biorad Microplate Reader Benchmark. The spectrophotometer was calibrated to zero absorbance using the culture medium without cells. Non-transfected cells were used as negative control and ethanol-treated cells were used as positive control. The relative cell viability (%) related to control wells was calculated by [A]test/[A]control × 100, where [A] test is the absorbance of the test sample and [A] control is the absorbance of the negative control sample. All the experiments were repeated three times in triplicate.

5.3.2.7 Detection of Associated/Internalized pND1

pND1 was labeled with FITC by mixing 5 µL of pDNA, 73 µL of labeling buffer (0.1 M Sodium Tetraborate, pH 8.5) and 2 µL of FITC (in sterile anhydrous dimethyl sulfoxide, 500 mg/mL). The samples were placed under constant stirring for 4 h at room temperature and protected from light. One volume of 3 M sodium chloride (85 µL) and 2.5 volumes of 100% ethanol (212.5 µL) were added, and samples with the stained pND1 were incubated overnight at −20 °C. Thereafter, the solution was centrifuged at 12,000× g for 30 min at 4 °C, and the pellet was washed with 75% ethanol.

Cancer HeLa or fibroblast cells were cultured as described, and for transfection, 100 µL of peptides/FITC-pND1 complexes were added to each well. After 12 h, cells were washed twice with PBS, and pND1 levels were estimated by measuring FITC fluorescence levels using a fluorimeter plate reader (excitation and emission wavelengths at 495 nm and 525 nm, respectively). For each cell line, the protein content of each well was measured with a bicinchoninic acid (BCA) protein assay kit (BCA1-1KT, Sigma Aldrich Chemicals, St. Louis, MO, USA). Fluorescence/microgram protein readings were then determined by averaging the background corrected fluorescence of triplicate wells and dividing by the protein content per well. The use of this kit aids in correcting for cell density differences between different sets of experiments. The fluorescence of FITC–pND1 in each organelle sample was normalized with the amount of protein and expressed as fluorescence/µg protein.

5.3.2.8 Cellular Organelle-Associated Fluorescence

The mitochondrial targeting capacity of the developed peptide/pND1 complexes has been evaluated by monitoring the associated FITC-pND1 fluorescence. Transfection has been mediated in HeLa or fibroblast cells by the peptide/pND1 complexes, as described before, and thereafter mitochondria and cytosol have been separated using the Mitochondria Isolation Kit for Cultured Cells (#89874, Thermo Fisher Scientific Inc., Rockford, IL, USA). This method leads to the efficient isolation of mitochondria with optimized purity and high/consistent yield [18] HeLa cells (1×10^4) or fibroblasts (2×10^4) were transferred to Falcon tubes and 800 µL of mitochondria isolation reagent A was added to the cells, followed by incubation on ice for 2 min. Afterward, mitochondria isolation reagent B (10 µL) was added and HeLa or fibroblast cells were vortexed at maximum speed for 10 sec, incubated on ice for 5 min, and vortexed again at maximum speed every minute. At this point, 800 µL of Reagent C was then added, the samples were centrifuged at 800,000× g for 10 min at 4°C and the supernatant was centrifuged at 3000× g for 10 min at 4°C. Following this procedure, the obtained pellet contains the mitochondria, while the supernatant contains the cytosolic fraction. Reagent C (500 µL) was added to the pellet, new centrifugation at 12,000× g for 5 min was performed, and the supernatant was discarded. The pellets consisting of mitochondria were resuspended in 50 µL of ice-cold PBS, mixed with 500 µL of carbonate buffer (fresh cold 0.1 M Na_2CO_3), and used in the FITC-pND1 fluorescence quantification experiments.

5.3.2.9 Fluorescence Confocal Microscopy on living cells

The cellular uptake and mitochondria targeting ability of peptide/pND1 complexes were evaluated by confocal laser scanning microscopy (CLSM). FITC-labeled pDNA was complexed with the different peptides to form the nanoparticles, as described before. HeLa cells (2×10^3) were grown in µ-slide 8-well until 50–60% confluence was achieved. The nucleus was marked with DAPI and the mitochondria with MitoTracker Orange dye. The complete medium was replaced by a serum-free culture medium 12 h before transfection. Labeled FITC at 1 µg pND1 were added to each well. The images of HeLa cells transfected with the different peptide/pDNA complexes were acquired. Real live transfection was visualized using an LSM 710 confocal microscope (Carl Zeiss SMT, Inc., Oberkochen, Germany) under a 63× oil immersion objective and analyzed with the LSM software (Carl Zeiss SMT, Inc., Oberkochen, Germany). During the experiment, HeLa cells were maintained at 37°C with 5% CO_2. All images were acquired with the laser and the filters corresponding to the respective DAPI (445/450 nm), FITC (525/550 nm), and MitoTracker (555/580 nm) dyes.

5.3.2.10 Statistical Analysis

Normality tests (D´Agostino & Pearson omnibus and Kolmogorov–Smirnov) were applied to determine the normality of the distribution of the sample data. One-way or two-way analysis of variance (ANOVA), with the Bonferroni test, was used for comparing the data of control and multiple experimental groups. A confidence interval of 95% ($p < 0.05$) was considered statistically

significant. Data analysis was performed with GraphPad Prism v.8.01 (GraphPad Software, Inc., San Diego, CA, USA).

5.4 Results and Discussion

5.4.1 Synthesis of Peptides

CPPs have been demonstrated to facilitate payload delivery into the cells, especially by forming nanoparticles. In this study, we were interested in synthesizing peptides with mitochondria-targeting ability to promote the targeting of peptide/pND1 nanoparticles to this organelle. This is a crucial step for developing a suitable delivery system for mitochondrial gene therapy. To accomplish this, we took advantage of the previously developed family of short tryptophan-(W) and arginine-(R) rich amphipathic peptides (WRAP) [29-31]. WRAP peptides demonstrated the ability to easily and efficiently encapsulate nucleic acids, including siRNA [30] and pDNA [29], leading to the conception of stable nano-systems. This asset has been explored to promote the delivery of genetic material to different cell types; this also contributes to the fact that WRAP-based nanoparticles enter cells mainly via direct translocation [31]. The peptide $(KH)_9$ consists of a lysine–histidine repeats with high cationic charge density, a property that favors its penetration into cells. The amino acid lysine promotes the condensation of nucleic acids, facilitating their cellular uptake, while histidine plays a crucial role in avoiding endosomal sequestration, due to the proton sponge effect, allowing nucleic acids to reach the cytosol [37]. Despite the convenient properties, displayed by the mentioned peptides for cell uptake and gene delivery, none of the peptides exhibit mitochondrial affinity. Therefore, in this work, MTS was incorporated into each peptide. The chosen sequence consists of a 12-residue partial pre-sequence of yeast cytochrome c oxidase subunit IV, known to grant mitochondrial affinity to CPPs. The addition of MTS to WRAP1, WRAP5, and $(KH)_9$ allowed the creation of multifunctional dual-domain peptides, capable of formulating nanoparticles with a hydrophilic core where pDNA was condensed and MTS located mostly on the surface, providing targeting to mitochondria [38]. The CpMTP peptide, which was synthesized based on the signal sequence of human mitochondrial methionine-R-sulfoxide reductase B2, has a natural affinity for mitochondria [39]. This peptide can condense and deliver high molecular weight cargo molecules, and bind pDNA.

After synthesis, all peptides were purified by HPLC to obtain >95% purity and their mass and sequences were confirmed by mass spectrometry. The properties of the peptides, namely, sequence, total residues, isotopic mass, and positive charges, are presented in **Table 5.1**.

Table 5.1 - List of the synthesized peptides and MTS sequence, including information on peptide sequence, total residues, isotopic mass and positive charges.

Peptide	Peptide Sequence	Total Residues	Isotopic Mass (g/mol)	Positive Charges
MTS	NH2-MLSLRQSIRFFK-CONH2	12	1523.88	3
WRAP1	NH2-LLWRLWRLLWRLWRLL-CONH2	16	2290.42	5
WRAP5	NH2-LLRLLRWWWRLLRLL-CONH2	15	2104.34	5
(KH)9	NH2-KHKHKHKHKHKHKHKHKH-CONH2	18	2403.41	9
CpMTP	NH2-ARLLWLLRGLTLGTAPRRA-CONH2	19	2132.32	4
MTS-WRAP1	NH2-MLSLRQSIRFFK-LLWRLWRLLWRLWRLL-CONH2	28	3797.27	8
MTS-WRAP5	NH2-MLSLRQSIRFFK-LLRLLRWWWRLLRLL-CONH2	27	3611.19	8
MTS-(KH)9	NH2-MLSLRQSIRFFK-KHKHKHKHKHKHKHKHKH-CONH2	30	3910.26	12

5.4.2 pND1 Complexation Capacity

Over the past decade, there has been growing interest in the development of nano-delivery systems capable of transporting genetic material to the vicinity of mitochondria and promoting its long-term expression - a promising strategy to address diseases associated with mtDNA mutations [19,20,40-44]. In this work, peptide/pND1 complexes have been developed aiming to target mitochondria and deliver pND1 plasmid into this organelle, as the first step for efficient mitochondrial gene expression. In addition, our work also aimed to perform a comparison study to reveal the most promising peptide/pND1 complexes for subsequent studies on mitochondrial gene/protein expression. To accomplish this, MTS-peptide/pND1 and CpMTP/pND1 complexes were formed by a co-precipitation method—an approach used by other authors to encapsulate DNA and form DNA-based nanoparticles [19,40,44]. For comparison purposes and to unravel the role of the MTS sequence, WRAP1-, WRAP5-, and $(KH)_9$ peptides/pND1 complexes were also formulated. Each peptide interacted, mainly by electrostatic forces, with the negatively charged pND1 forming nano-sized particles. The extent of this interaction and, therefore, the capacity to complex pND1, may vary with the peptide and strongly depends on the N/P ratio considered at the complexes formulation step. The pND1 degree of complexation for the different peptide/pND1 systems and at various N/P ratios has been investigated by agarose gel electrophoresis. The results are shown in **Figure 5.1**. For each peptide, a screening study revealed the range of N/P ratios adequate to promote an efficient pND1 complexation. Although the study demonstrated that all peptides were able to complex pND1, differences arose concerning the N/P ratio required to ensure an efficient plasmid complexation. As can be observed in **Figure 5.1A**, the CpMTP peptide induced pND1 complexation from an N/P ratio of 0.5. From this N/P, the peptide efficiently neutralized the charges of pND1 and, thus, could not migrate through the agarose gel. As the N/P ratio further increases, it is expected that the positive charges from the amines strengthen the interaction between CpMTP and pND1, increasing the complexation degree of the latter molecule. **Figure 5.1B** demonstrated that WRAP1 started to induce pND1 complexation at

a higher N/P ratio (3). When WRAP5 was considered to complex pND1, a lower N/P ratio (0.5), the same ratio as for CpMTP, was needed to induce pND1 complexation (**Figure 5.1C**). On the other hand, $(KH)_9$ exhibited a higher ability in condensing pND1, as confirmed in **Figure 5.1D**. As observed, from a low N/P ratio of 0.1, $(KH)_9$ peptide was able to neutralize the negative charges of the plasmid, and, therefore, no band was visible in the agarose gel. This result has been confirmed by determining the complexation capacity (CC) of the $(KH)_9$/pND1 complexes. CC has been calculated from the following equation:

$$CC\ (\%) = [(pND1)T - (pND1)F/(pND1)T] \times 100 \quad (1)$$

where (pND1)T stands for the total amount of pND1 and (pND1)F is the non-bound fraction of pND1 found free in the supernatant.

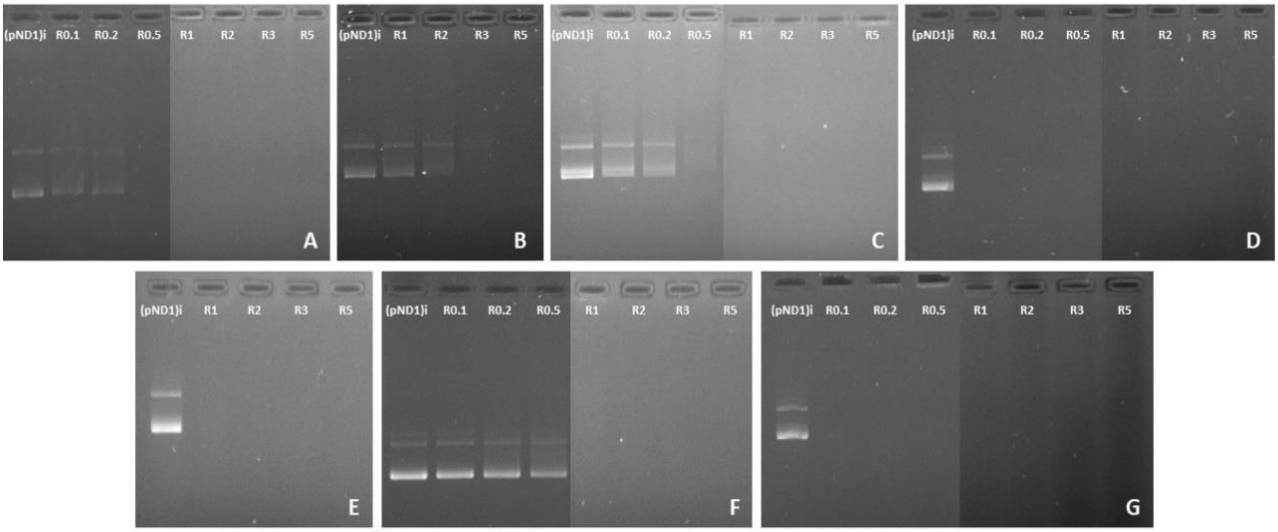

Figure 5.1 - Analysis of pND1 complexation capacity of CpMTP/pND1 (A); WRAP1/pND1 (B); WRAP5/pND1 (C); $(KH)_9$/pND1 (D); MTS-WRAP1/pND1 (E); MTS-WRAP5/pND1 (F) and MTS-$(KH)_9$/pND1 (G) complexes at various N/P ratios, investigated by agarose gel electrophoresis. The samples were loaded at the application site at the upper end of the image (anode) and migrated then to the lower end (cathode).

The CC at the N/P ratio of 0.1 was, approximately, 86%, which was in agreement with the results obtained from agarose gel electrophoresis (Figure 1D). The great capacity of $(KH)_9$ peptide to condense pND1 could be attributed to its high cationic charge density, which is higher than those of WRAP1, WRAP5, or CpMTP (**Table 5.1**).

The effect of the addition of the MTS sequence to the peptides did not seem to follow a trend concerning the pND1 complexation. As illustrated in **Figure 5.1E**, for MTS-WRAP1, the incorporation of this sequence into the WRAP1 peptide led to an efficient pND1 complexation at lower N/P ratios (3➔1). The opposite effect was, however, observed for WRAP5, where the

addition of MTS seemed to hinder the capacity of the peptide for pND1 complexation, as can be seen in **Figure 5.1F** (0.5➔1). Moreover, the MTS-$(KH)_9$ peptide greatly promoted pND1 complexation at the investigated N/P ratios (**Figure 5.1G**) and this capacity was comparable to the one exhibited by the $(KH)_9$ peptide.

5.4.3 Physicochemical Properties of Peptide/pND1 Complexes

The morphology of peptide/pND1 complexes has been investigated by SEM. **Figure 5.2** shows the obtained images for all complexes formulated at an N/P ratio of 5. All the particles exhibit a spherical or oval shape and an apparently homogeneous structure. No relevant differences in morphology can be ascribed between peptide/pND1 and MTS-peptide/pND1 systems. Further information on the properties of all the conceived carriers has been evaluated by DLS. The results can be consulted in **Table 5.2**. The average size of the formed complexes at different N/P ratios has been determined. The selection of an N/P ratio for each complex studied was based on the ratios that can promote efficient pND1 complexation (**Figure 5.1**). All the nano-systems presented sizes below 500 nm, and this parameter was shown to be dependent on the N/P ratio considered at the formulation stage. Independently of the used peptide, there was a visible tendency for particle size to decrease with the increase of the N/P ratio (**** $p < 0.0001$). The increment of peptide positive charges intensified the interaction with the plasmid, leading to pND1 condensation to a higher extent. This phenomenon creates smaller-sized complexes. Additionally, for all peptide/pND1 particles and most of the N/P ratios considered, the addition of the MTS sequence to the peptide led to higher sizes (**** $p < 0.0001$ for WRAP1 versus MTS-WRAP1; * $p < 0.05$ for WRAP5 versus MTS-WRAP5; *** $p < 0.001$ for $(KH)_9$ versus MTS-$(KH)_9$). Moreover, the sizes displayed by the developed delivery systems, and particularly, at higher N/P ratios such as an N/P of 5, seemed to be adequate for cellular uptake/internalization purposes. The cellular internalization is clearly influenced by the size, shape, surface charge, and surface chemistry of the nano-system, and it may also greatly depend on the cell type [45,46]. In general, spherical complexes displaying a low size (~100–200 nm) are preferentially captured by cells compared to higher-sized carriers (>200 nm). Optimizing the size of nanoparticles can, thus, facilitate both cell uptake and payload delivery into the cells.

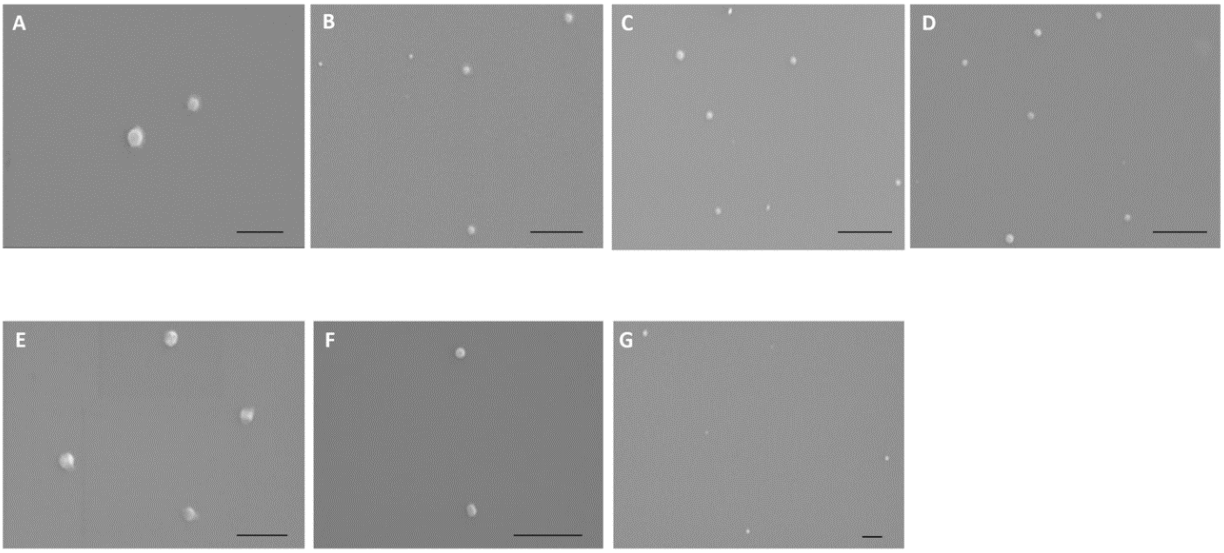

Figure 5.2 - Scanning electron micrographs of CpMTP/pND1 (A); WRAP1/pND1 (B); WRAP5/pND1 (C); $(KH)_9$/pND1 (D); MTS-WRAP1/pND1 (E); MTS-WRAP5/pND1 (F) and MTS-$(KH)_9$/pND1 (G) complexes formulated at N/P ratio of 5. Scale bar = 500 nm.

Table 5.2 - Average zeta potential, mean size and polydispersity index (PdI) for the various peptide/pND1 complexes formulated at various N/P ratios. The values were calculated with the data obtained from six independent measurements (mean ± SD, n = 6), and analyzed by one-way or two-way ANOVA (GraphPad Software version v.8.01, Inc., San Diego, CA, USA). Statistical significance was accepted at a level of * p <0.05.

System	Zeta (mV)	Size (nm)	PdI
CpMTP/pND1 N/P 0.5	−3.50 ± 0.76	492.00 ± 29.58	0.60 ± 0.1
CpMTP/pND1 N/P 1	+2.00 ± 0.58	401.50 ± 25.12	0.52 ± 0.5
CpMTP/pND1 N/P 2	+3.50 ± 0.50	384.50 ± 14.26	0.24 ± 0.04
CpMTP/pND1 N/P 3	+5.83 ± 0.69	313.17 ± 10.34	0.30 ± 0.02
CpMTP/pND1 N/P 5	+12.67 ± 0.75	235.67 ± 12.60	0.21 ± 0.02
WRAP1/pND1 N/P 3	+25.17 ± 0.69	254.17 ± 13.90	0.34 ± 0.05
WRAP1/pND1 N/P 5	+32.67 ± 0.47	161.00 ± 8.82	0.30 ± 0.02
WRAP5/pND1 N/P 0.5	+1.17 ± 0.37	401.00 ± 19.15	0.54 ± 0.1
WRAP5/pND1 N/P 1	+2.00 ± 0.58	388.33 ± 14.75	0.31 ± 0.02
WRAP5/pND1 N/P 2	+10.83 ± 1.21	298.50 ± 12.96	0.33 ± 0.01
WRAP5/pND1 N/P 3	+14.17 ± 0.90	272.33 ± 10.70	0.24 ± 0.02
WRAP5/pND1 N/P 5	+20.67 ± 0.75	186.00 ± 9.82	0.32 ± 0.03

(KH)9/pND1 N/P 0.1	−2.50 ± 0.76	488.17 ± 22.34	0.62 ± 0.05
(KH)9/pND1 N/P 0.2	+1.50 ± 0.50	412.67 ± 18.60	0.53 ± 0.1
(KH)9/pND1 N/P 0.5	+2.67 ± 0.47	403.33 ± 15.75	0.41 ± 0.04
(KH)9/pND1 N/P 1	+4.50 ± 0.50	375.67 ± 14.25	0.24 ± 0.02
(KH)9/pND1 N/P 2	+6.00 ± 0.58	299.67 ± 11.25	0.33 ± 0.02
(KH)9/pND1 N/P 3	+11.83 ± 1.34	260.50 ± 9.76	0.21 ± 0.03
(KH)9/pND1 N/P 5	+22.33 ± 0.75	186.33 ± 9.49	0.34 ± 0.02
MTS-WRAP1/pND1 N/P 1	−1.83 ± 0.90	406.00 ± 18.63	0.42 ± 0.06
MTS-WRAP1/pND1 N/P 2	+1.33 ± 0.75	366.50 ± 14.38	0.30 ± 0.02
MTS-WRAP1/pND1 N/P 3	+6.50 ± 0.76	276.50 ± 13.12	0.21 ± 0.01
MTS-WRAP1/pND1 N/P 5	+11.50 ± 0.76	197.33 ± 8.49	0.20 ± 0.02
MTS-WRAP5/pND1 N/P 1	−2.17 ± 0.90	399.00 ± 12.41	0.44 ± 0.04
MTS-WRAP5/pND1 N/P 2	+7.17 ± 0.90	316.17 ± 10.21	0.27 ± 0.03
MTS-WRAP5/pND1 N/P 3	+10.83 ± 1.07	266.50 ± 8.22	0.31 ± 0.02
MTS-WRAP5/pND1 N/P 5	+19.33 ± 1.60	175.17 ± 10.86	0.32 ± 0.03
MTS-(KH)9/pND1 N/P 0.1	−3.33 ± 0.94	478.50 ± 22.43	0.61 ± 0.05
MTS-(KH)9/pND1 N/P 0.2	−1.00 ± 1.00	463.50 ± 20.63	0.63 ± 0.03
MTS-(KH)9/pND1 N/P 0.5	+1.83 ± 0.37	431.00 ± 18.63	0.52 ± 0.04
MTS-(KH)9/pND1 N/P 1	+3.17 ± 0.69	400.33 ± 14.25	0.44 ± 0.03
MTS-(KH)9/pND1 N/P 2	+5.67 ± 0.75	366.67 ± 11.49	0.30 ± 0.03
MTS-(KH)9/pND1 N/P 3	+8.50 ± 0.50	309.17 ± 9.34	0.22 ± 0.04
MTS-(KH)9/pND1 N/P 5	+14.67 ± 0.75	220.67 ± 9.29	0.24 ± 0.01

A comparative analysis of the size displayed by the carriers, obtained from SEM and DLS, presented some discrepancies in the obtained values. As demonstrated earlier and explained in detail in another publication, this observation can be related to the principles, advantages, and limitations of each assay/technique [47].

Furthermore, the polydispersity index (PdI), an indication of size distribution, has been also determined. The PdI value may vary from 0.01 for monodisperse particles to 0.5–0.7 for polydisperse ones, and a value higher than 0.7 indicates a broad particle size distribution. The PdI values, listed in **Table 5.2**, indicate that peptide/pND1 nanoparticles displaying higher sizes (in the range of 400–500 nm) were polydisperse. Conversely, complexes with smaller sizes were quite monodisperse, exhibiting PdI values in the range of 0.2–0.3, which corresponded to the "expected" PdI values for peptide-based nanoparticles.

Another crucial property of a delivery system is the surface charge they carry. The zeta potential values of the developed particles have been determined by DLS. The obtained values are included in **Table 5.2**. As can be observed, peptide/pND1 systems formulated at lower N/P ratios presented negative surface charges. For each peptide under study, an increase in N/P ratio

resulted in more positive zeta potential values due to the increment of amine groups in the formulation (**** $p < 0.0001$ for the analysis concerning CpMTP and except for the two lower N/P ratios; **** $p < 0.0001$ for WRAP1; **** $p < 0.0001$ for WRAP5; **** $p < 0.0001$ for the analysis focused on $(KH)_9$ and except for the two lower N/P ratios; **** $p < 0.0001$ for MTS-WRAP1; **** $p < 0.0001$ for MTS-WRAP5; ** $p < 0.01$ for MTS-$(KH)_9$. We also detected a decrease in the positive surface charges of the particles when the MTS sequence was added to the peptides (**** $p < 0.0001$ for WRAP1 versus MTS-WRAP1; *** $p < 0.0001$ for WRAP5 versus MTS-WRAP5; *** $p < 0.0001$ for $(KH)_9$ versus MTS-$(KH)_9$). As shown in **Table 5.2**, the magnitude of this effect was more pronounced for MTS-WRAP1/pND1 carriers (**** $p < 0.0001$). Despite this, all high N/P ratio peptide/pND1 nanoparticles possessed positive zeta potential values (+10 mV to +35 mV) that may make them suitable for cellular internalization. Positively charged complexes may interact favorably with the highly anionic sulfated proteoglycan molecules present at the cell surface, promoting the uptake [48,49]. Once inside the cell, targeting specific intracellular organelles can occur due to targeting sequences attached to the translocating peptides.

At this point, it also became clear that the N/P ratio could be used as a tailoring tool to optimize the properties of peptide/pND1 complexes, enhancing its cellular uptake/internalization and, therefore, pND1 delivery.

Based on the above-mentioned arguments, peptide/pND1 complexes formulated at lower N/P ratios were excluded from subsequent studies. *In vitro* experiments, presented in the next sections, were performed with complexes prepared at N/P ratios of 3 and 5, or only an N/P ratio of 5, due to their adequate sizes, surface charges, and higher pDNA CCs. These properties seem to be promising for *in vitro* applications in the mitochondrial gene therapy field.

5.4.4 Cytotoxic Profile

The cytotoxicity of the developed peptide/pND1 complexes has been evaluated, on HeLa cells, using an MTT assay. This colorimetric method is useful in assessing the toxicity/safety of drug or gene delivery systems. The cellular viability of HeLa cells has been investigated, at 24 h and 48 h, after incubation with several nano-systems formulated at N/P ratios of 3 and 5. Non-transfected cells were used as a negative control, and ethanol-treated cells were used as a positive control. The results are shown in **Figures 5.3A** and **B** corresponding to 24 h and 48 h, respectively. **Figure 5.3A** shows that none of the developed carriers induce a cytotoxic effect on the cancer cells at 24 h, with obtained results being statistically not significant (n.s.) in relation to a negative control. A decrease in biocompatibility can be observed, for all peptide/pND1 nanoparticles, at 48 h. In addition, at this time, the effect of the incorporation of the MTS sequence into the peptides seemed to influence the cytotoxic profile displayed by the complexes. MTS-peptide/pND1 carriers exhibited less cellular viability in relation to control, * $p < 0.05$ for MTS-WRAP1/pND1 at both N/P ratios and MTS-$(KH)_9$ at N/P ratio of 5 and ** $p < 0.01$ for MTS-WRAP5/pND1 at N/P of 5. Furthermore, the N/P ratio parameter seemed, additionally, to play a role in the complex´s biocompatibility. Some of the carriers formed at an N/P ratio of 5 induced a decrease in the cellular viability to a higher extent when compared to the effect of complexes conceived at an N/P ratio of 3. This was the case for MTS-WRAP5/pND1 and MTS-$(KH)_9$/pND1. At 48 h, the

comparison between the two N/P ratios was statistically significant, MTS-WRAP5/pND1 (p = 0.0002) and MTS-$(KH)_9$/pND1 (**** p <0.0001). Despite these observations, all the developed peptide/pND1 complexes showed high cellular viability when tested in HeLa cells and, from the biocompatibility requirement, they could be safely used as gene delivery systems.

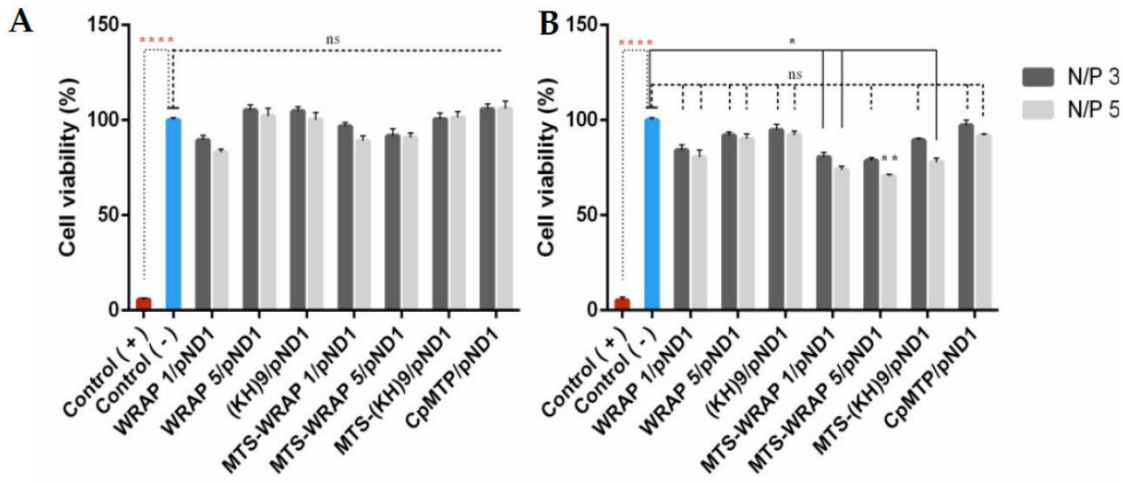

Figure 5.3 - Cellular viability of HeLa cells after 24 h (A) and 48 h (B) of incubation with WRAP1/pND1, WRAP5/pND1, $(KH)_9$/pND1, MTS-WRAP1/pND1, MTS-WRAP5/pND1, MTS-$(KH)_9$/pND1 and CpMTP/pND1 nanoparticles conceived at N/P ratios of 3 and 5. Non-transfected cells were used as the negative control and ethanol-treated cells were used as a positive control. A statistically significant difference was noticed between the positive and negative control (**** p <0.0001). The MTS-WRAP1 N/P ratios of 3 and 5, MTS-$(KH)_9$ N/P ratio of 5 (* p < 0.05), and MTS-WRAP5 N/P ratio of 5 (** p <0.01) systems demonstrated a statistical difference compared to the negative control at 48 h. The viability of cells transfected with the remaining systems did not show statistically significant differences compared to non-transfected cells (ns).

5.4.5 Mitochondria Targeting Ability

In the past few years, several research studies have demonstrated efficient mitochondria targeting [19,40,43,44,50-52] The efforts in the development of delivery systems displaying this capacity have been fruitful, with various reports on biomolecules or gene delivery into mitochondria [19,39,53-55]. Despite this achieved progress, to date, few works have demonstrated effective long-term mitochondrial transgene expression [52]. To contribute to this field, we studied the mitochondria-targeting ability of the conceived peptide/pND1 complexes. Our team also searched for relevant differences between these delivery systems to select the most promising complexes for subsequent gene/protein expression studies.

The mitochondria targeting capacity of peptide/pND1 complexes, formulated at an N/P ratio of 5, was first evaluated by monitoring the FITC-pND1 levels present in the mitochondria, after transfection of HeLa or fibroblast cells. The results of FITC fluorescence intensity, after the separation of mitochondria from the other cellular organelles, are shown in **Figure 5.4** and

Figure 5.5, for HeLa and fibroblast cells, respectively. The data correspond to 12 h transfection mediated by each of the studied peptide/pND1 systems. Untreated cells were used as control. For both cells, the results demonstrated that all the formed carriers have been internalized by the cells and can be found in a particular cellular fraction. The detailed analysis of **Figure 5.4** demonstrated that high levels of stained pND1 were found in the cytosol for the transfection of cancer cells by each MTS-free peptide/pND1 complex (**** $p < 0.0001$ versus control), with WRAP5 and $(KH)_9$ peptide systems exhibiting slightly higher fluorescence levels relative to WRAP1/pND1 particles, * $p < 0.05$. When the transfection is mediated by MTS-peptide and CpMTP/pND1 carriers, a low amount of labeled pND1 is quantified in the cytosolic fraction of HeLa cells (statistically not significant). Our finding is in agreement with other reports on the transfection efficiency of WRAP peptides. Previous studies based on WRAP1- and WRAP5-peptide/siRNA nanoparticles reported on cellular uptake and cytosol delivery, but no mitochondria targeting has been identified [30,36]. This lack of targeting displayed by MTS-free peptides was confirmed when mitochondria samples were analyzed. In this organelle, vestigial amounts of FITC-pND1 fluorescence were quantified for the transfection conducted by WRAP1-, WRAP5-, or $(KH)_9$ peptide/pND1 complexes (**Figure 5.4**). Conversely, when the MTS sequence was incorporated into these peptides, the complexes were able to target the mitochondria of HeLa cells as shown by the high fluorescence levels found in this organelle (**** $p < 0.0001$ versus control). As the results suggest, the MTS sequence incorporated into WRAP1, WRAP5 and $(KH)_9$ peptides conferred mitochondrial targeting specificity. It became clear that these peptides *per se* do not possess this targeting skill. The mitochondria targeting performance of the CpMTP peptide was also confirmed, as the transfection by CpMTP/pND1 carriers exhibits higher fluorescence levels (**** $p < 0.0001$). From **Figure 5.4**, and between MTS-peptides or CpMTP/pND1 nanoparticles, some differences arose in the obtained FITC-pND1 fluorescence intensity. The transfection mediated by MTS-WRAP5/pND1 systems showed less fluorescence in comparison with the one corresponding to transfection by the complexes based on MTS-$(KH)_9$ and CpMTP peptides, ** $p < 0.01$. This fact may indicate differences in the transfection efficiency and targeting capacity between the developed nano-systems. MTS-$(KH)_9$ and CpMTP peptide/pND1 complexes seemed to present a higher performance in mediating these processes. Similar results were obtained for the study performed on fibroblast cells, as can be observed in **Figure 5.5**. A comparison between the two cell lines showed no significant difference and proved the mitochondrial targeting capacity of the developed MTS-peptide/pND1 and CpMTP/pND1 complexes.

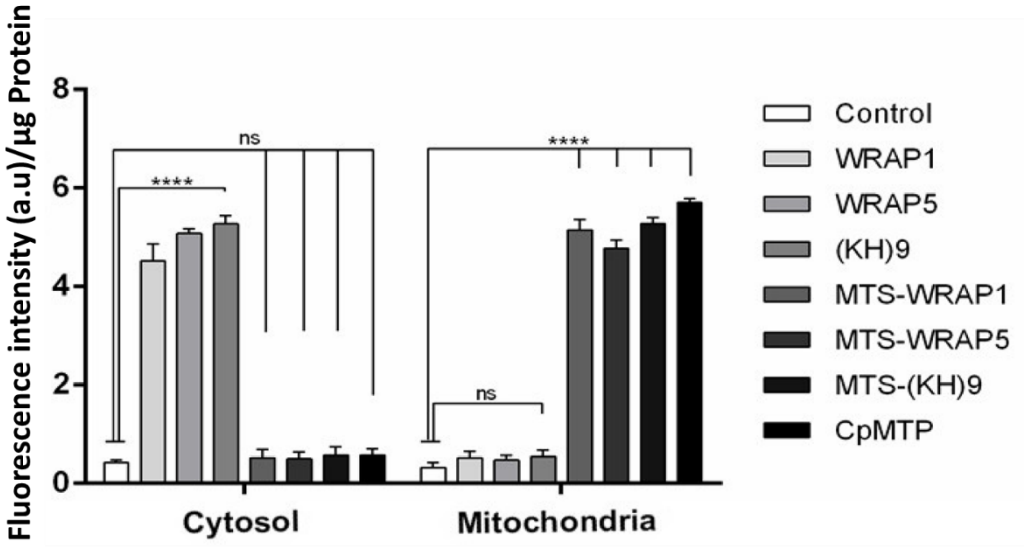

Figure 5.4 - FITC fluorescence intensity ((a.u)/µg Protein) in the cytosol and mitochondria of HeLa cells after 12 h transfection mediated by WRAP1/pND1, WRAP5/pND1, $(KH)_9$/pND1, MTS-WRAP1/pND1, MTS-WRAP5/pND1, MTS-$(KH)_9$/pND1 and CpMTP/pND1 systems conceived at N/P ratio of 5. Untreated cells were used as control. The data were obtained by calculating the average of four independent experiments and are presented as mean ± SD; not significant (n.s.) and **** p <0.0001. A comparison between cytosol and mitochondria for corresponding complexes was performed for all pND1-based systems: not significant for control and **** p <0.0001 for all systems.

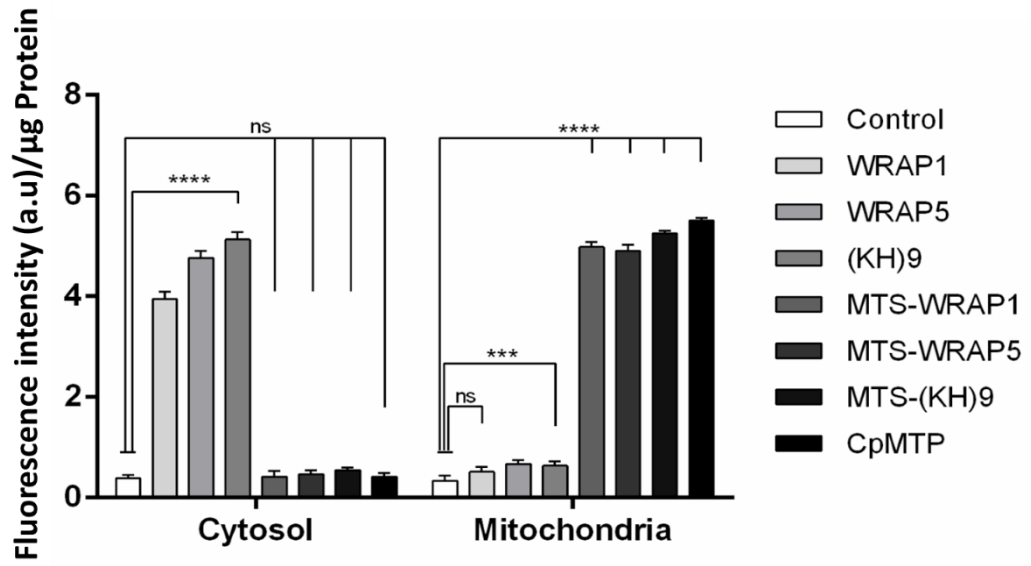

Figure 5.5 - FITC fluorescence intensity ((a.u)/µg Protein) in the cytosol and mitochondria of fibroblast cells after 12h transfection mediated by WRAP1/pND1, WRAP5/pND1, $(KH)_9$/pND1, MTS-WRAP1/pND1, MTS-WRAP5/pND1, MTS-$(KH)_9$/pND1 and CpMTP/pND1 systems conceived at N/P ratio of 5. Untreated cells were used as control. The data were obtained by

calculating the average of four independent experiments and are presented as mean ± SD; not significant (n.s.), *** p <0.001, and **** p <0.0001.

Other authors have reported on the high cell penetration ability of the CpMTP peptide on HeLa cells and on its capacity to efficiently deliver macromolecules to mitochondria. These researchers highlighted the potential application of CpMTP in the transduction and transfection of mitochondria for therapeutics [39].

The cellular uptake and mitochondrial affinity of MTS-peptide/pND1 and CpMTP/pND1 complexes, prepared at an N/P ratio of 5, have been further investigated by fluorescence confocal microscopy. Real-live transfection of cancer cells mediated by the developed carriers has been monitored. DAPI and MitoTracker dyes have been used to stain the nuclei and mitochondria, respectively; pND1 has been labeled with FITC. Images were collected from a series of consecutive Z-planes (Z-stacks, step size of 0.1 μm). **Figures 5.6**, **5.7**, **5.8,** and **5.9** summarize the obtained images, at 6 h of transfection. In all figures, A stands for mitochondria labeled with MitoTracker, B for peptide/FITC-pND1 nanoparticles, C for nuclei stained with DAPI, and D represents the merged image. As can be seen from the green fluorescence on the (B) images of all figures, effective transfection took place and all pND1-loaded carriers were internalized into cells. After cell uptake, the developed complexes were directed to the site of the mitochondrion. Image D, of all the figures, presented a significant accumulation of peptide/pND1 nano-systems into this cellular organelle, as evidenced by the orange color in the merged picture of red-stained mitochondria and green fluorescence from the pDNA in the same field. This microscopy showed that the formulated nanoparticles could be successfully targeted at mitochondria, although at this stage we cannot state if pND1 is, in fact, delivered to mitochondria. The current studies of our research team are focused on the evaluation of pND1 delivery, gene, and ND1 protein expression. Further results on this topic are expected to be reported in the near future. Here, we undoubtedly proved the mitochondria-targeting capacity of the developed complexes. This is a significant step towards mitochondrial gene therapy feasibility.

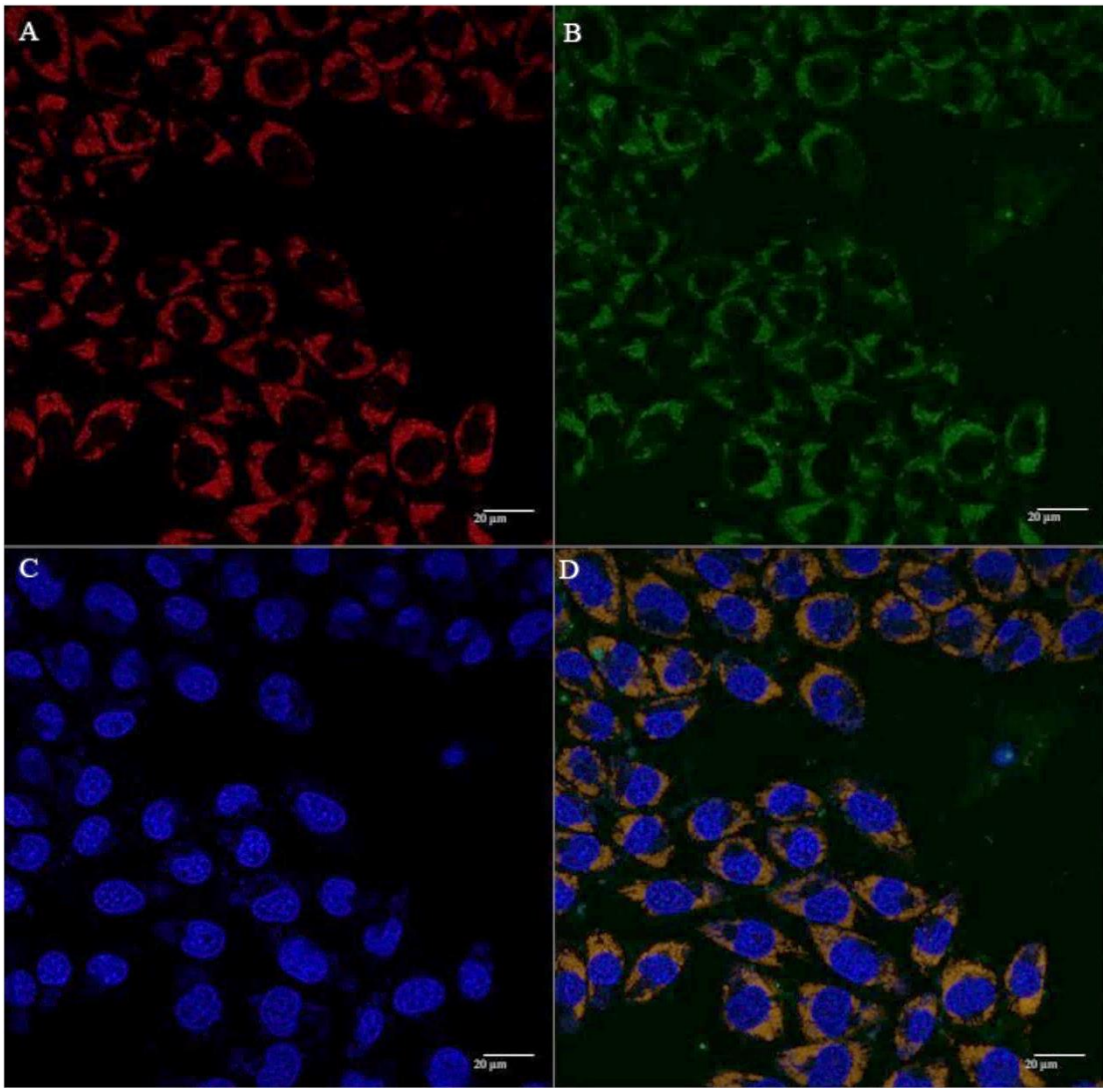

Figure 5.6 - Representative confocal fluorescence image of HeLa cells illustrating the transfection ability and intracellular co-localization of CpMTP/pND1 complexes formulated at an N/P ratio of 5. Mitochondria stained red by MitoTracker (A), pND1 green, labeled (B), nucleus marked blue by DAPI (C), and merged image (D). Scale bar = 20 µm.

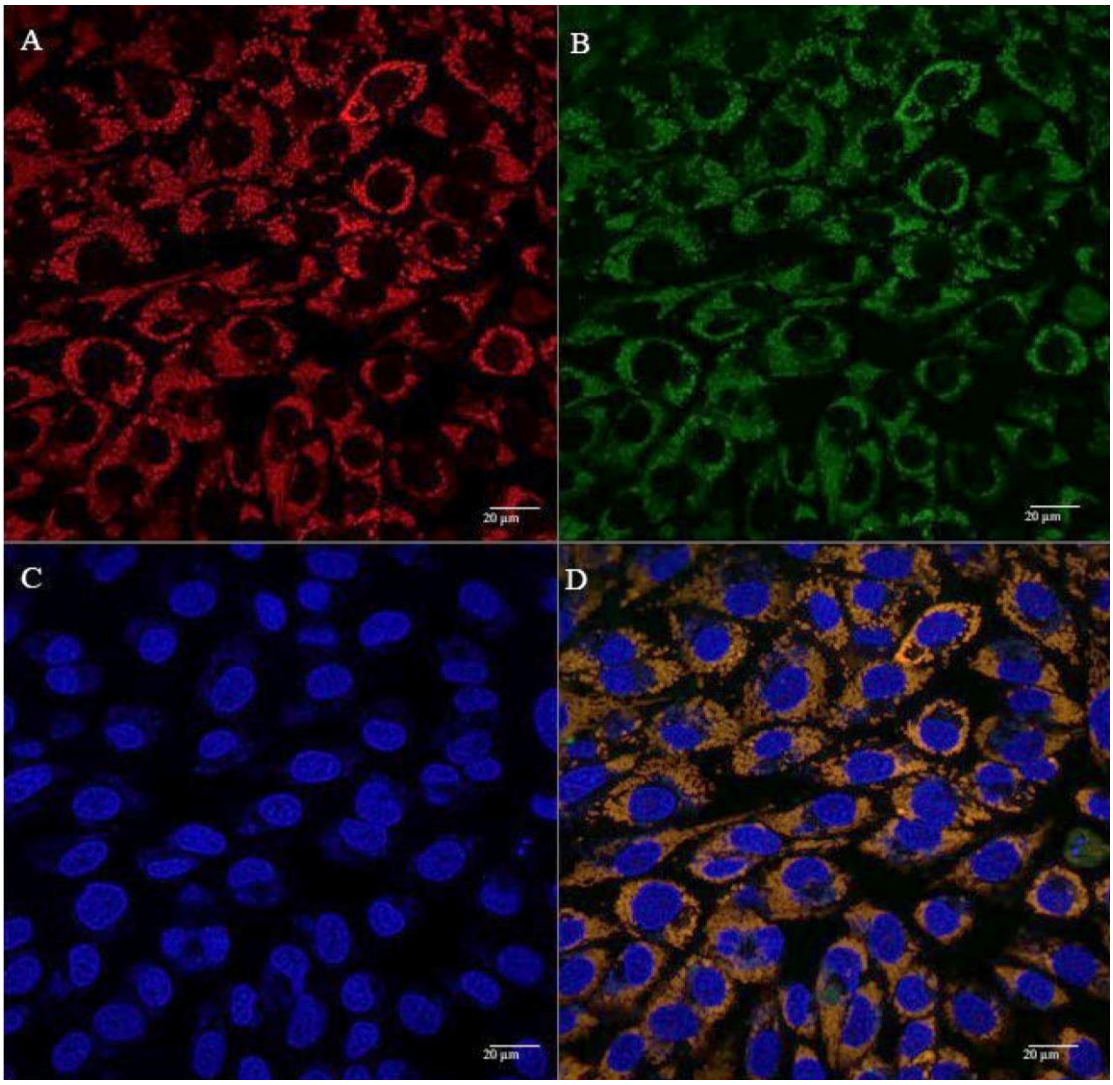

Figure 5.7 - Representative confocal fluorescence image of HeLa cells, illustrating the transfection ability and intracellular co-localization of MTS-WRAP1/pND1 complexes formulated at an N/P ratio of 5. Mitochondria stained red by MitoTracker (A), pND1 green, labeled (B), nucleus marked blue by DAPI (C), and merged image (D). Scale bar = 20 µm.

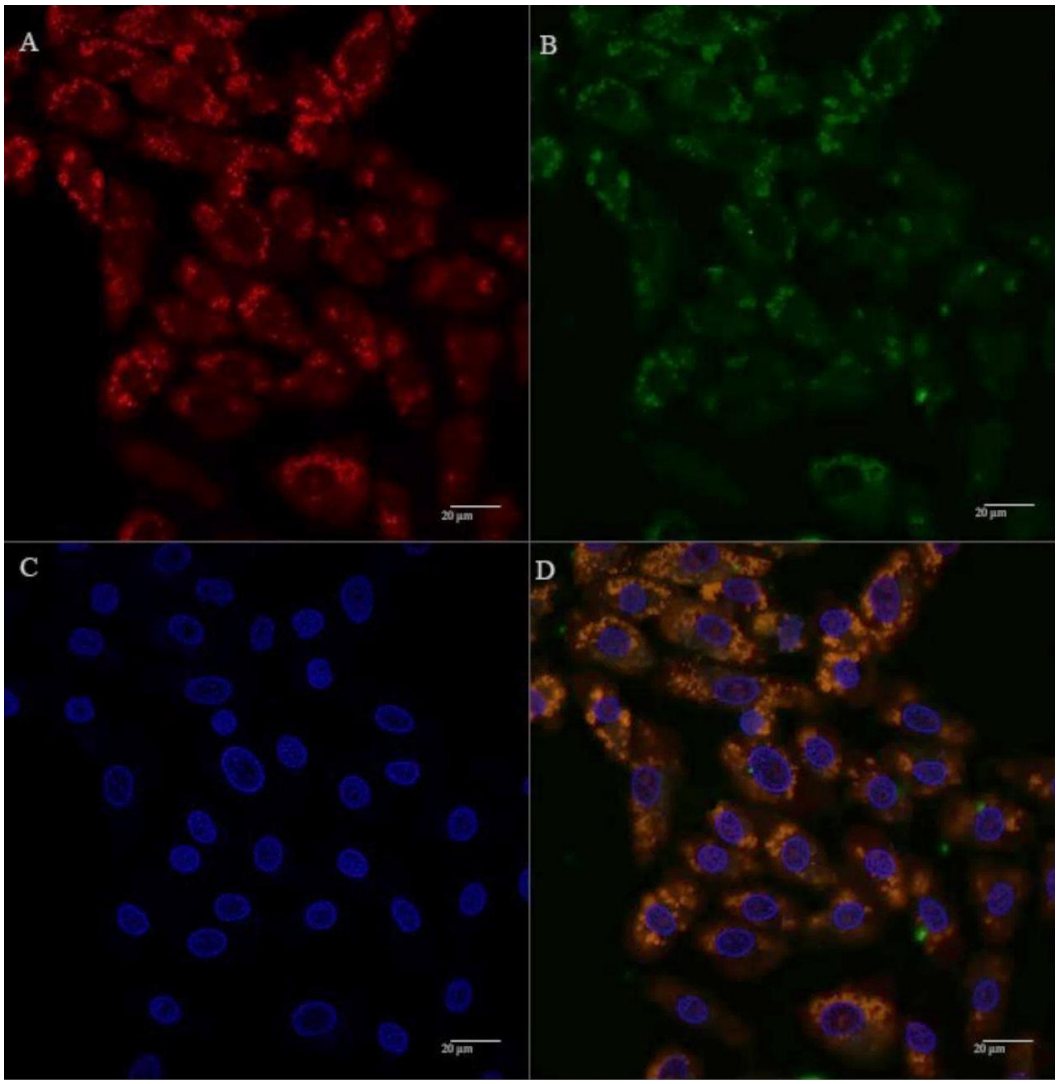

Figure 5.8 - Representative confocal fluorescence image of HeLa cells, illustrating the transfection ability and intracellular co-localization of MTS-WRAP5/pND1 complexes formulated at an N/P ratio of 5. Mitochondria stained red by MitoTracker (A), pND1 green, labeled (B), nucleus marked blue by DAPI (C), and merged image (D). Scale bar = 20 µm.

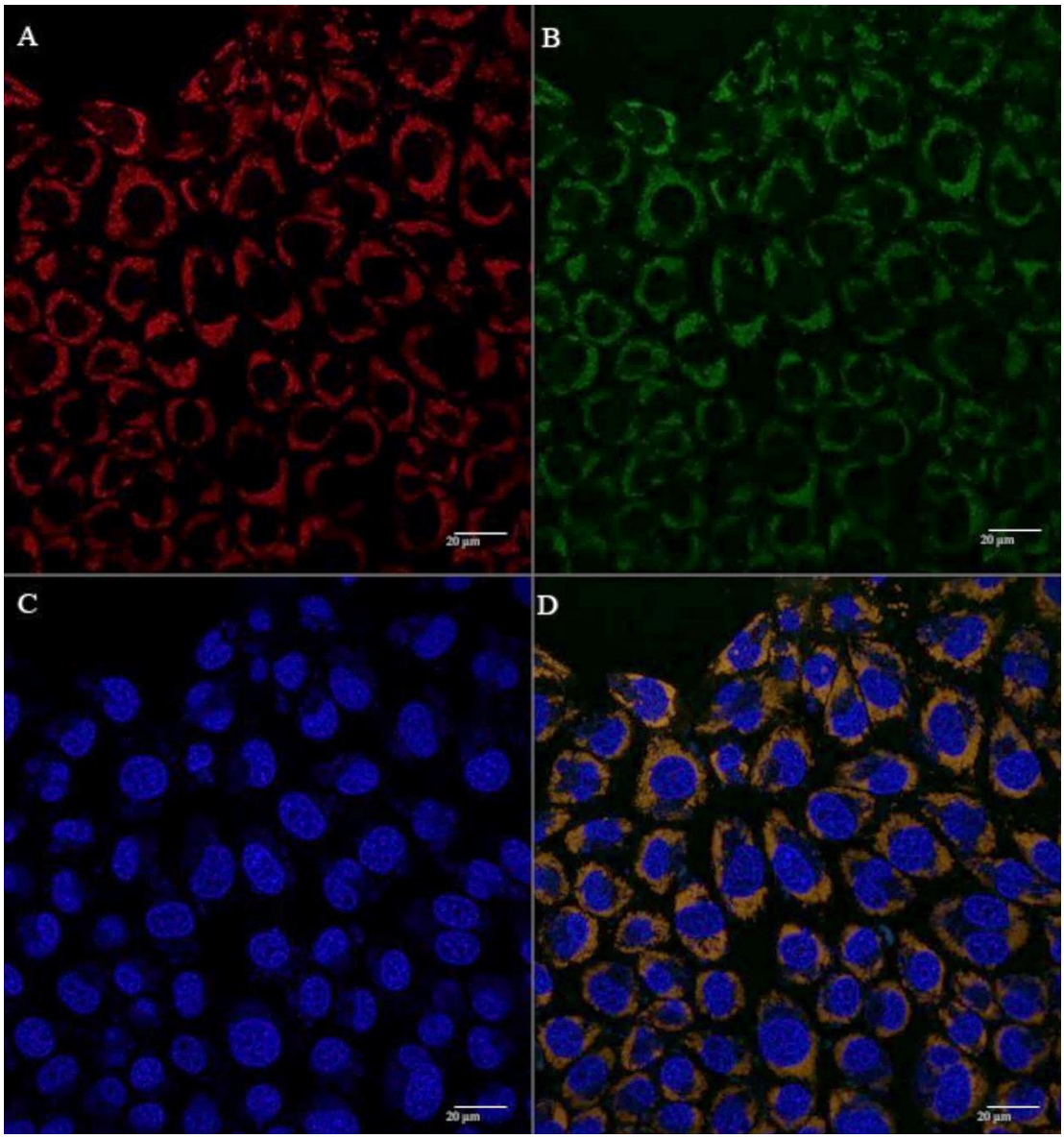

Figure 5.9 - Representative confocal fluorescence image of HeLa cells, illustrating the transfection ability and intracellular co-localization of MTS-$(KH)_9$/pND1 complexes formulated at an N/P ratio of 5. Mitochondria stained red by MitoTracker (A), pND1 green, labeled (B), nucleus marked blue by DAPI (C), and merged image (D). Scale bar = 20 µm.

5.5 Conclusions

The feasibility of mitochondrial gene therapy seeks the conception of a suitable gene delivery system capable of mitochondria targeting. Pursuing this aim, a mitochondrial-targeting sequence has been incorporated into WRAP1, WRAP5 and $(KH)_9$ peptides, and, along with the CpMTP peptide, they were used to complex pND1. Instead of studying model cargos, in this work, we approached the concrete reality by using pND1, currently one of the most advanced vectors in the mitochondrial gene therapy field. The formed peptide/pND1 complexes, at various N/P ratios, were revealed to possess adequate physicochemical properties for gene delivery applications,

namely, pND1 complexation ability, morphology, size, and surface charges. It was found that the N/P ratio could be an effective tool to optimize the characteristics of the developed complexes. Moreover, the new nano-systems did not induce a cytotoxic effect in cancer HeLa cells. An evaluation of mitochondria targeting ability showed the internalization of MTS-peptides/pND1 and CpMTP/pND1 complexes into cells and their targeting to mitochondria. A comparison study revealed differences between the various peptide/pND1 complexes, concerning both their physicochemical properties and targeting skill. Although all MTS-peptides/pND1 complexes offer remarkable properties that can be applied in mitochondrial gene therapy, the ones based on MTS-$(KH)_9$ and CpMTP peptides exhibited a greater capacity to complex pND1 and higher targeting performance. These complexes constitute a promising bet for further research studies on mitochondrial gene/protein expression. The knowledge provided by this report can significantly contribute to optimizing the development of novel peptide-based systems for mitochondrial gene expression.

5.6 References

[1] Milenkovic, D.; Blaza, J.; Larsson, N.-G.; Hirst, J. The Enigma of the Respiratory Chain Supercomplex. Cell Metab. 2017, 25, 765–776.

[2] Hertweck, K.L.; Dasgupta, S. The Landscape of mtDNA Modifications in Cancer: A Tale of Two Cities. Front. Oncol. 2017, 7, 262.

[3] Popov, L. Mitochondrial biogenesis: An update. J. Cell. Mol. Med. 2020, 24, 4892–4899.

[4] Javadov, S.; Kozlov, A.V.; Camara, A.K.S. Mitochondria in Health and Diseases. Cells 2020, 9, 1177.

[5] Tiwari, M.; Prasad, S.; Tripathi, A.; Pandey, A.N.; Ali, I.; Singh, A.K.; Shrivastav, T.G.; Chaube, S.K. Apoptosis in mammalian oocytes: A review. Apoptosis 2015, 20, 1019–1025.

[6] Tavassoly, I.; Parmar, J.; Shajahan-Haq, A.; Clarke, R.; Baumann, W.T.; Tyson, J.J. Dynamic Modeling of the Interaction Between Autophagy and Apoptosis in Mammalian Cells. CPT Pharmacomet. Syst. Pharmacol. 2015, 4, 263–272.

[7] Boguszewska, K.; Szewczuk, M.; Kaźmierczak-Barańska, J.; Karwowski, B.T. The Similarities between Human Mitochondria and Bacteria in the Context of Structure, Genome, and Base Excision Repair System. Molecules 2020, 25, 2857.

[8] Filograna, R.; Mennuni, M.; Alsina, D.; Larsson, N. Mitochondrial DNA copy number in human disease: The more the better? FEBS Lett. 2021, 595, 976–1002.

[9] Monlleo-Neila, L.; Del Toro, M.; Bornstein, B.; Garcia-Arumi, E.; Sarrias, A.; Roig-Quilis, M.; Munell, F. Leigh syndrome and the mitochondrial m.13513G > A mutation: Expanding the clinical spectrum. J. Child Neurol. 2013, 28, 1531–1534.

[10] Zsurka, G.; Kunz, W.S. Mitochondrial dysfunction and seizures: The neuronal energy crisis. Lancet Neurol. 2015, 14, 956–966.

[11] Rodenburg, R.J. Mitochondrial complex I-linked disease. Biochim. Biophys. Acta Bioenerg. 2016, 1857, 938–945.

[12] Wang, W.; Zhao, F.; Ma, X.; Perry, G.; Zhu, X. Mitochondria dysfunction in the pathogenesis of Alzheimer's disease: Recent advances. Mol. Neurodegener. 2020, 15, 1–22.
[13] Martín-Jiménez, R.; Lurette, O.; Hebert-Chatelain, E. Damage in Mitochondrial DNA Associated with Parkinson's Disease. DNA Cell Biol. 2020, 39, 1421–1430.
[14] Jiang, W.; Mingliang, G.; Zhang, Y.; Wang, P.; Wu, T.; Lin, J.; Yu, J.; Gu, M. Mitochondrial DNA Mutations Associated with Type 2 Diabetes Mellitus in Chinese Uyghur Population. Sci. Rep. 2017, 7, 1–9.
[15] Pinti, M.V.; Fink, G.K.; Hathaway, Q.; Durr, A.J.; Kunovac, A.; Hollander, J.M. Mitochondrial dysfunction in type 2 diabetes mellitus: An organ-based analysis. Am. J. Physiol. Metab. 2019, 316, E268–E285.
[16] Ju, Y.S.; Alexandrov, L.B.; Gerstung, M.; Martin, S.; Nik-Zainal, S.; Ramakrishna, M.; Davies, H.R.; Papaemmanuil, E.; Gundem, G.; Shlien, A.; et al. Origins and functional consequences of somatic mitochondrial DNA mutations in human cancer. eLife 2014, 3.
[17] Prag, H.A.; Murphy, M.P. mtDNA mutations help support cancer cells. Nat. Rev. Cancer 2020, 1, 941–942.
[18] Coutinho, E.; Batista, C.; Sousa, F.; Queiroz, J.; Costa, D. Mitochondrial Gene Therapy: Advances in Mitochondrial Gene Cloning, Plasmid Production, and Nanosystems Targeted to Mitochondria. Mol. Pharm. 2017, 14, 626–638.
[19] Faria, R.; Albuquerque, T.; Neves, A.R.; Bhatt, H.; Biswas, S.; Cardoso, A.M.; de Lima, M.C.P.; Jurado, A.S.; Costa, D. Physicochemical characterization and targeting performance of triphenylphosphonium nano-polyplexes. J. Mol. Liq. 2020, 316, 113873.
[20] Kawamura, E.; Maruyama, M.; Abe, J.; Sudo, A.; Takeda, A.; Takada, S.; Yokota, T.; Kinugawa, S.; Harashima, H.; Yamada, Y. Validation of Gene Therapy for Mutant Mitochondria by Delivering Mitochondrial RNA Using a MITO-Porter. Mol. Ther. Nucleic Acids 2020, 20, 687–698.
[21] Costa, D.; Costa, C.; Caldeira, M.; Cortes, L.; Queiroz, J.A.; Cruz, C. Targeting of celular organelles by fluorescente plasmid DNA nanoparticles. Biomacromolecules 2017, 18, 2928–2936.
[22] Li, Y.; Thambi, T.; Lee, D.S. Co-Delivery of Drugs and Genes Using Polymeric Nanoparticles for Synergistic Cancer Therapeutic Effects. Adv. Heal. Mater. 2018, 7, 1700886.
[23] Faria, R.; Sousa, Â.; Neves, A.R.; Queiroz, J.; Costa, D. Methotrexate-plasmid DNA polyplexes for cancer therapy: Characterization, cancer cell targeting ability and tuned *in vitro* transfection. J. Mol. Liq. 2019, 292, 111391.
[24] Chen, W.; Liu, J.; Wang, Y.; Jiang, C.; Yu, B.; Sun, Z.; Lu, L. AC5N2 Nanoparticle Based Direct Nucleus Delivery Platform for Synergistic Cancer Therapy. Angew. Chem. Int. Ed. 2019, 58, 6290–6294.
[25] Wang, H.; Ding, S.; Zhang, Z.; Wang, L.; You, Y. Cationic micelle: A promising nanocarrier for gene delivery with high transfection efficiency. J. Gene Med. 2019, 21, e3101.
[26] Muhammad, K.; Zhao, J.; Gao, B.; Feng, Y. Polymeric nano-carriers for on-demand delivery of genes via specific responses to stimuli. J. Mater. Chem. B 2020, 8, 9621–9641.

[27] Gómez-Aguado, I.; Rodríguez-Castejón, J.; Vicente-Pascual, M.; Rodríguez-Gascón, A.; Del Pozo-Rodríguez, A.; Aspiazu, M.; Ángeles, S. Nucleic Acid Delivery by Solid Lipid Nanoparticles Containing Switchable Lipids: Plasmid DNA vs. Messenger RNA. Molecules 2020, 25, 5995.
[28] Neves, A.; Sousa, A.; Faria, R.; Albuquerque, T.; Queiroz, J.; Costa, D. Cancer gene therapy mediated by RALA/plasmid DNA vectors: Nitrogen to phosphate groups ratio (N/P) as a tool for tunable transfection efficiency and apoptosis. Colloids Surf. B Biointerfaces 2020, 185, 110610.
[29] Sousa, Â.; Almeida, A.M.; Faria, R.; Konate, K.; Boisguerin, P.; Queiroz, J.; Costa, D. Optimization of peptide-plasmid DNA vectors formulation for gene delivery in cancer therapy exploring design of experiments. Colloids Surf. B Biointerfaces 2019, 183, 110417.
[30] Deshayes, S.; Konate, K.; Dussot, M.; Chavey, B.; Vaissiére, A.; Van, T.N.N.; Aldrian, G.; Padari, K.; Pooga, M.; Vivès, E.; et al. Deciphering the internalization mechanism of WRAP:siRNA nanoparticles. Biochim. Biophys. Acta Biomembr. 2020, 1862, 183252.
[31] Konate, K.; Dussot, M.; Aldrian, G.; Vaissière, A.; Viguier, V.; Neira, I.F.; Couillaud, F.; Vivès, E.; Boisguerin, P.; Deshayes, S. Peptide-based nanoparticles to rapidly and efficiently "Wrap'n roll" siRNA into cells. Bioconjugate Chem. 2019, 30, 592–603.
[32] Falanga, A.; Lombardi, L.; Galdiero, E.; Del Genio, V.; Galdiero, S. The world of cell penetrating: The future of medical applications. Futur. Med. Chem. 2020, 12, 1431–1446.
[33] Ruseska, I.; Zimmer, A. Internalization mechanisms of cell-penetrating peptides. Beilstein J. Nanotechnol. 2020, 11, 101–123.
[34] Derakhshankhah, H.; Jafari, S. Cell penetrating peptides: A concise review with emphasis on biomedical applications. Biomed. Pharmacother. 2018, 108, 1090–1096.
[35] Gessner, I.; Neundorf, I. Nanoparticles Modified with Cell-Penetrating Peptides: Conjugation Mechanisms, Physicochemical Properties, and Application in Cancer Diagnosis and Therapy. Int. J. Mol. Sci. 2020, 21, 2536.
[36] Khan, M.M.; Filipczak, N.; Torchilin, V.P. Cell penetrating peptides: A versatile vector for co-delivery of drug and genes in cancer. J. Control. Release 2021, 330, 1220–1228.
[37] Leng, Q.; Goldgeier, L.; Zhu, J.; Cambell, P.; Ambulos, N.; Mixson, A. Histidine-lysine peptides as carriers of nucleic acids. Drug News Perspect. 2007, 20, 77–86.
[38] Chuah, J.-A.; Matsugami, A.; Hayashi, F.; Numata, K. Self-Assembled Peptide-Based System for Mitochondrial-Targeted Gene Delivery: Functional and Structural Insights. Biomacromolecules 2016, 17, 3547–3557.
[39] Jain, A.; Chugh, A. Mitochondrial transit peptide exhibits cell penetration ability and efficiently delivers macromolecules to mitochondria. FEBS Lett. 2016, 590, 2896–2905.
[40] Cohen-Erez, I.; Harduf, N.; Rapaport, H. Oligonucleotide loaded polypeptide-peptide nanoparticles towards mitochondrial-targeted delivery. Polym. Adv. Technol. 2019, 30, 2506–2514.
[41] Slone, J.; Huang, T. The special considerations of gene therapy for mitochondrial diseases. NPJ Genom. Med. 2020, 5, 1–7.
[42] Park, D.; Lee, S.; Min, K.T. Techniques for investigating mitochondrial gene expression. BMB Rep. 2020, 53, 3–9.

[43] Cerrato, C.P.; Kivijärvi, T.; Tozzi, R.; Lehto, T.; Gestin, M.; Langel, Ü. Intracellular delivery of therapeutic antisense oligonucleotides targeting mRNA coding mitochondrial proteins by cell-penetrating peptides. J. Mater. Chem. B 2020, 8, 10825–10836.
[44] Su, S.; Cao, S.; Liu, J.; Xu, X. Mitochondria-specific delivery system for targeted regulation of mitochondrial gene expression. STAR Protoc. 2021, 2, 100275.
[45] Shang, L.; Nienhaus, K.; Nienhaus, G.U. Engineered nanoparticles interacting with cells: Size matters. J. Nanobiotechnol. 2014, 12, 5.
[46] Sabourian, P.; Yazdani, G.; Ashraf, S.; Frounchi, M.; Mashayekhan, S.; Kiani, S.; Kakkar, A. Effect of Physico-Chemical Properties of Nanoparticles on Their Intracellular Uptake. Int. J. Mol. Sci. 2020, 21, 8019.
[47] Costa, D.; Valente, A.J.; Queiroz, J.; Sousa, Â. Finding the ideal polyethylenimine-plasmid DNA system for co-delivery of payloads in cancer therapy. Colloids Surf. B Biointerfaces 2018, 170, 627–636.
[48] Clogston, J.D.; Patri, A.K. Characterization of nanoparticles intended for drug delivery. In Methods in Molecular Biology; Christine, V., Gilles, P., Eds.; Springer: Cham, Switzerland, 2011; Volume 697, 641p.
[49] Rasmussen, M.K.; Pedersen, J.N.; Marie, R. Size and surface charge characterization of nanoparticles with a salt gradient. Nat. Commun. 2020, 11, 1–8.
[50] Zhang, X.-Y.; Zhang, P.-Y. Mitochondria targeting nano agents in cancer therapeutics. Oncol. Lett. 2016, 12, 4887–4890.
[51] Ozsvari, B.; Sotgia, F.; Lisanti, M.P. Exploiting mitochondrial targeting signal(s), TPP and bis-TPP, for eradicating cancer stem cells (CSCs). Aging 2018, 10, 229–240.
[52] Jang, Y.-H.; Lim, K.-I. Recent Advances in Mitochondria-Targeted Gene Delivery. Molecules 2018, 23, 2316.
[53] Cardoso, A.M.; Morais, C.M.; Cruz, A.R.; Silva, S.G.; Vale, M.L.D.; Marques, E.; de Lima, M.P.; Jurado, A.S. Gemini Surfactants Mediate Efficient Mitochondrial Gene Delivery and Expression. Mol. Pharm. 2015, 12, 716–730.
[54] Ahn, J.; Lee, B.; Choi, Y.; Jin, H.; Lim, N.Y.; Park, J.; Kim, J.H.; Bae, J.; Jung, J.H. Non-peptidic guanidinium-functionalized silica nanoparticles as selective mitochondria-targeting drug nanocarriers. J. Mater. Chem. B 2018, 6, 5698–5707.
[55] Zhu, X.-J.; Li, R.-F.; Xu, L.; Yin, H.; Chen, L.; Yuan, Y.; Zhong, W.; Lin, J. A Novel Self-Assembled Mitochondria-Targeting Protein Nanoparticle Acting as Theranostic Platform for Cancer. Small 2018, 15, e1803428.

Chapter 6

Peptides vs. Polymers: Searching for the Most Efficient Delivery System for Mitochondrial Gene Therapy

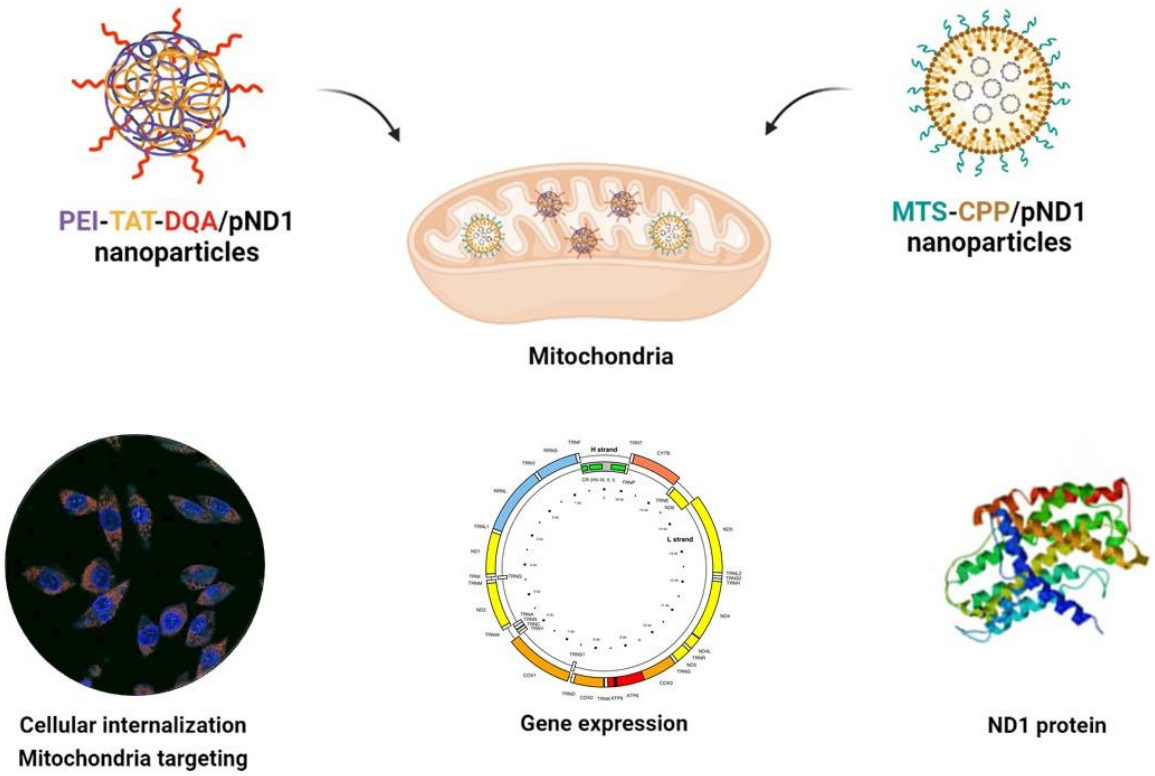

This chapter was published in:
Rúben Faria, Milan Paul, Swati Biswas, Eric Vivès, Prisca Boisguérin, Ângela Sousa, and Diana Costa. 2022. 'Peptides vs. Polymers: Searching for the Most Efficient Delivery System for Mitochondrial Gene Therapy', Pharmaceutics, 14.
https://doi.org/10.3390/pharmaceutics14040757

6.1 Abstract

Together with the nucleus, the mitochondrion has its own genome. Mutations in mitochondrial DNA are responsible for a variety of disorders, including neurodegenerative diseases and cancer. Current therapeutic approaches are not effective. In this sense, mitochondrial gene therapy emerges as a valuable and promising therapeutic tool. To accomplish this goal, the design/development of a mitochondrial-specific gene delivery system is imperative. In this work, we explored the ability of novel polymer- and peptide-based systems for mitochondrial targeting, gene delivery, and protein expression, performing a comparison between them to reveal the most adequate system for mitochondrial gene therapy. Therefore, we synthesized a novel mitochondria-targeting polymer (polyethylenimine–dequalinium) to load and complex a mitochondrial-gene-based plasmid. The polymeric complexes exhibited physicochemical properties and cytotoxic profiles dependent on the nitrogen-to-phosphate-group ratio (N/P). A fluorescence confocal microscopy study revealed the mitochondrial targeting specificity of polymeric complexes. Moreover, transfection mediated by polymer and peptide delivery systems led to gene expression in mitochondria. Additionally, the mitochondrial protein was produced. A comparative study between polymeric and peptide/plasmid DNA complexes showed the great capacity of peptides to complex pDNA at lower N/P ratios, forming smaller particles bearing a positive charge, with repercussions on their capacity for cellular transfection, mitochondria targeting, and, ultimately, gene delivery and protein expression. This report is a significant contribution to the implementation of mitochondrial gene therapy, instigating further research on the development of peptide-based delivery systems towards clinical translation.

Keywords

Cell-penetrating peptides; mitochondrial gene therapy; mitochondrial DNA diseases; mitochondria targeting; nano delivery systems; PEI-based complexes

6.2 Introduction

Mitochondria play a key role in maintaining the normal functioning of cells, especially metabolic functions. This cell organelle has its own genome, called mitochondrial DNA (mtDNA). Mitochondrial DNA is a circular, double-stranded molecule with a size of around 16 kbp and contains 37 genes [1]. These genes encode 13 polypeptides that participate in the oxidative phosphorylation chain, 2 rRNAs, and 22 tRNAs—all exclusive to the mitochondria [2,3]. In addition to being responsible for the production of ATP through oxidative phosphorylation, in recent years many other cellular processes have been discovered revealing the involvement of mitochondria [4,5]. Their participation in cellular mechanisms ranging from inflammation to regulation of stem cell generation [6,7], cell signaling, ion homeostasis, and metabolism of amino acids, lipids, cholesterol, steroids, and nucleotides has been demonstrated [8,9]. They also contribute to cell cycle control, cell growth, and apoptosis mechanisms [10]. In this way, mutations in mtDNA cause excessive cell death and promote the appearance of several

pathologies, including metabolic and neurodegenerative syndromes linked to Parkinson's, Alzheimer's, amyotrophic lateral sclerosis, Huntington's disease, and diabetes [11]. Loss of influence on cell cycle control and cell death regulation, due to mutations in mtDNA, leads to cancer and autoimmune diseases [12,13]. Currently, treatments available for diseases associated with mtDNA mutations are not effective and only serve to mitigate symptoms, without providing a cure [14,15].

In line with this, the need to develop new, effective therapies arises. Since most mitochondrial diseases are associated with mutations in mtDNA, mitochondrial gene therapy emerges as a very promising approach to treat the problem at its root [16-18]. This type of therapy is focused on the delivery of genetic material to the mitochondria to suppress, alter, or complement the effect of defective genes [16]. To deliver genes of interest directly into the mitochondria, it is necessary to develop a vector that allows the encapsulation of DNA while providing targeting specificity [19]. This vehicle must also protect, transport, and direct the genetic content to the mitochondria, promoting its efficient release and, thus, guaranteeing the expression of both mitochondrial genes and respective proteins [20]. Viral vectors, such as retroviruses, adenoviruses, and lentiviruses, have been widely used in gene delivery due to their ability to transfect cells [21]. Among these vectors, adeno-associated viruses (AAVs) are the most applied in preclinical studies [21]. Due to their high loading capacity, biocompatibility, antigenicity, and lack of immune response, non-viral delivery systems based on cell-penetrating peptides (CPPs), micelles, polymers, and lipids have been commonly used in gene release studies [22-25]. Furthermore, ternary non-viral systems, for instance, constituted by polymers and/or peptides, have proven to be a valuable strategy to enhance payload encapsulation efficiency, thereby contributing to efficient gene delivery and expression [26-28].

CPPs have gained considerable interest in the gene therapy field due to their beneficial properties. CPPs are small (between 15 and 30 amino acids) and can be divided into arginine-rich and amphipathic peptides [29-32]. Because they have hydrophilic and hydrophobic domains, amphipathic peptides make it possible to formulate delivery systems that can encapsulate DNA and enable its membrane translocation and subsequent entry into cells [22,30]. Due to these characteristics, CPP-based vectors have demonstrated their ability to internalize in cells and to deliver therapeutic molecules, in several studies [33-36].

Polymer-based systems are also widely explored as gene carriers, due to their favorable physicochemical properties, low toxicity, and tailor ability [28,37-39]. In this context, one of the most used polymers is polyethylenimine (PEI), due to its ability to transport different types of nucleic acids, regardless of their type and size [40,41]. Moreover, PEI has characteristics that allow it to go beyond the endosome/lysosome membrane [42]. PEI is a cationic polymer displaying a high positive charge density. This charge enables strong electrostatic interactions between its amine groups and DNA phosphate groups, resulting in the formation of nanoparticles in which the genetic material is mostly condensed. PEI-based systems demonstrate high endosomolytic activity, critical to the potential success of mitochondrial gene delivery [43,44].

Currently, gene therapy with mitochondria as a therapeutic target is still a challenging strategy. However, some studies have demonstrated the feasibility of this type of therapy using

mitochondrial targeting sequences (MTSs) and focused on the mitochondrial genes ATP6 (mitochondrially encoded synthase membrane subunit 6′) and ND4 (mitochondrially encoded NADH: ubiquinone oxidoreductase core subunit 4). Following this approach, their function was restored within their respective respiratory chain complexes and, consequently, the production of ATP was reestablished [45,46]. Other investigations revealed interesting therapeutic outcomes when addressing one of the most prevalent mitochondrial diseases—Leber's hereditary optic neuropathy (LHON). The introduction of functional ND1 (mitochondrially encoded NADH dehydrogenase 1 protein) and ND4 genes, usually mutated in this type of disease, provided the replacement of the normal activity of complex I in the respiratory chain [47,48].

In this study, we aimed to define the most suitable delivery system for mitochondrial gene therapy by comparing the efficacy of peptide- and polymer-based complexes. To this end, CPP- and PEI-based compounds were designed and synthesized to complex the mitochondrial gene ND1-plasmid DNA (pDNA). To ensure mitochondrial specificity, targeting moieties were covalently attached. In the case of PEI, dequalinium chloride (DQA) [49] was conjugated, resulting in the compound PEI–SA–DQA, whereas for CPPs, the MTS sequence [50] was added. DQA—a lipophilic cation—and especially its vesicular form (DQAsomes), has been demonstrated to selectively accumulate in the mitochondrial matrix [51-53]. To overcome the lack of stability exhibited by DQAsomes under conditions of low temperature and/or high salt concentration, researchers have conceived DQA-based carriers for payload release [53-55]. In this context, polymer–DQA delivery systems have been developed and optimized for mitochondrial targeting, leading to great advances in drug delivery to mitochondria [53,56-58].

Furthermore, as PEI–SA–DQA revealed a low ability to complex pND1—even at very high N/P ratios—TAT (the transcriptional activator protein in HIV-1—an 11-amino-acid peptide with 6 arginine and 2 lysine residues) was additionally included in PEI–DQA/pND1 complexes to complex pND1. These PEI-based ternary complexes were developed at various N/P ratios and adequately characterized. The biocompatibility profile was evaluated, and *in vitro* studies were carried out to assess the capacity of the developed complexes to reach the mitochondria. The physicochemical properties exhibited by the novel delivery systems, together with their ability to target the mitochondria and promote transgene expression, confer them with promising applicability as carriers for mitochondrial gene therapy. In addition, the comparison between various complexes based on CPPs and PEI revealed differences in their physicochemical properties, with repercussions on the capacity for mitochondrial targeting, gene delivery, and protein expression. This work demonstrated the efficacy of both peptide- and polymer-based delivery systems for mitochondrial targeting and mitochondrial gene expression. Furthermore, our study draws a comparison between peptides and polymers to reveal the most adequate delivery system to promote mitochondrial targeting and functional protein production, contributing to improvements/advances in the design of pDNA complexes for mitochondrial gene expression.

6.3 Materials and Methods

6.3.1 Materials

The following reagents were obtained from Sigma-Aldrich (St. Louis, MO, USA): trifluoroacetic acid (TFA), piperidine, oxyma, diisopropyl carbodiimide (DIC), Fmoc-amino acids, dimethylformamide (DMF), diisopropylethylamine (DIEA), dichloromethane (DCM), acetonitrile, and diethyl ether. AmphiSpheres 40™ resin was acquired from Agilent Technologies (Les Ulis, France). The Peptide Synthesizer Liberty Blue HT12™ was obtained from CEM (Matthews, NC, USA). The HPLC Pumps (321) and the FC 204 Fraction Collector were purchased from Gilson. The LKB-REC 102 was obtained from Pharmacia (Stockholm, Sweden). The HPLC System (Waters Alliance 2695) was obtained from Waters Corporation. The dialysis against water was carried out using 3k MCWO Dialysis Tubes (Spectrum Laboratories Inc. Rancho Dominguez, CA, USA). The lyophilization was performed with a FreeZone 1 L Laboratory Lyophilizer (LABCONCO). DAPI was purchased from Invitrogen (Carlsbad, CA, USA), and MitoTracker Orange CMTMRos from Molecular Probes (Leiden, The Netherlands). TAT (47–57) peptide (YGRKKRRQRRR), chemically synthesized, was supplied as a lyophilized powder from Biomatik (Cambridge, ON, Canada). Commercial branched polyethylenimine (PEI) with average Mw of 10 kDa and 25 kDa, fluorescein isothiocyanate (FITC), succinic anhydride (SA), and N-hydroxysulfosuccinimide (NHS) were obtained from Sigma-Aldrich. Agarose and GreenSafe Premium were obtained from NZYTech Lda (Lisbon, Portugal). HeLa cancer cells were purchased from Invitrogen (Carlsbad, CA, USA), and human dermal fibroblasts (NHDF, Ref. C-12302, cryopreserved cells) were obtained from PromoCell (Heidelberg, Germany).

All solutions for the preparation of the peptide-based systems were freshly prepared by using ultrapure-grade water, purified with a Milli-Q system from Millipore (Billerica, MA, USA).

In this study, two different plasmids were used: the recoded plasmid DNA encoding a green fluorescent protein (pGFP) (5.9 kbp)—a plasmid developed for exclusive mitochondrial translation, a kind gift from Dr. Diana Lyrawati [51]—and the plasmid pCAG-GFP-ND1 (pND1) (5.4 kbp), developed previously by our team through the cloning of the mitochondrial NADH dehydrogenase 1 protein-encoded gene (mtND1) in the pDNA vector. All details concerning gene cloning and plasmid production can be consulted elsewhere [59].

6.3.2 Methods

6.3.2.1 Synthesis of Peptides and PEI–DQA

The peptides used in this work were synthesized according to the protocol described in a previous work [18]. The synthesis of the PEI–DQA polymer was carried out in two steps: The first step was the synthesis of PEI–SA. To the solution of PEI (10 and 25 kDa) in DMSO, succinic anhydride (molar ratio of PEI: SA = 1:10, 1:25, respectively) was added. The reaction mixture was stirred at room temperature for 24 h. The solvent was evaporated from the crude reaction mixture and

dialyzed for 48 h in water using cellulose ester membranes. The dialysate was lyophilized to obtain a fluffy white powder at a yield of ~57%. In the second and final step of this synthesis, 200 mg of PEI–SA was dissolved in 5 mL of DMF, and EDC, NHS, and triethylamine solution was slowly added dropwise under vigorous stirring for 2 h. Then, 77.18 mg of dequalinium was dissolved in 2 mL of DMF, and this solution was added dropwise into the vigorously stirred solution described above. Thereafter, the reacting mixture was evaporated by rotovap, and 3 mL of distilled water was added to completely dissolve the product. The mixture was dialyzed (3 k MWCO membrane) against distilled water for 24 h. Finally, the product was lyophilized for 24 h. The average reaction yield was ca. 65%.

6.3.2.2 Nuclear Magnetic Resonance Spectroscopy (NMR)

A proton nuclear magnetic resonance spectroscope (Bruker spectrometer-300 MHz, Bruker, Billerica, MA, USA) was used to examine the conjugate's chemical structure in $CDCl_3$ solution at 25 °C. The conjugates dissolved in $CDCl_3$ (10 mg/mL) were measured with 64 scans.

6.3.2.3 Formulation of Peptide/pDNA and PEI–DQA/TAT/pDNA Complexes

Peptide-based complexes were formulated according to the procedure described in a recent publication by our team [18].

PEI–DQA, TAT, and plasmid DNA stock solutions were prepared in sodium acetate buffer (0.1 mM sodium acetate/0.1 M acetic acid, pH 4.5) at a concentration of 0.5 mg/mL for PEI–DQA and TAT solutions, and 100 µg/mL for pDNA solutions. In ternary complexes, the determination of the N/P ratio was established by considering the proportion of charges, individually, for PEI or TAT in relation to pDNA. This parameter was defined as the molar ratio of the amine groups in the polymer or peptide, which represents the positive charges to negatively charged phosphate groups in the pDNA. Different concentrations of PEI–DQA and TAT (50 µL) were added, drop by drop, to 150 µL of pDNA under vortex for 1 min. The mixture was left for equilibration for 30 min at room temperature to promote the formation of complexes. Thereafter, the formed complexes were centrifuged (12,000 rpm) for 20 min, and the pellet containing the complexes was recovered. The amount of non-complexed pDNA on the supernatants was visualized by horizontal electrophoresis for 30 min under 120 V in 1% agarose gel stained with GreenSafe Premium. Samples were analyzed under ultraviolet (UV) light using a FireReader Imaging System (UVITEC, Cambridge, UK).

The ability of the systems to complex pND1 was also evaluated by quantifying the intensity of the bands of the respective agarose gels and compared with the band intensity of the initial pND1 sample of each gel. The quantification of the band's intensity was performed by densitometry using Image Lab software version 6.1. The percentage of complexation capacity (CC) was calculated according to the following formula:

$$\text{Complexation capacity (\%)} = 100 - ((\text{Band intensity}/\text{Band intensity of initial pND1}) \times 100) \quad (1)$$

6.3.2.4 Determination of Size and Surface Charge

The average size and the surface charges exhibited by PEI–DQA/TAT/pDNA complexes were both inferred by dynamic light scattering (DLS) in a Zetasizer Nano ZS device (Malvern Instruments, Malvern, UK), at 25 °C. The pellet with the complexes was suspended in 5% glucose with 1 mM NaCl. For size determination, a He–Ne laser at 633 nm with a non-invasive backscatter (NIBS) was applied, while zeta potential values were measured by electrophoretic light scattering optics with an M3-PALS laser (phase analysis light scattering). Data were considered from 3 independent measurements, each performed with 12 runs. Malvern Zetasizer software v 6.34 was employed to analyze the set of results.

6.3.2.5 Cell Culture

HeLa cells were grown in Dulbecco's modified Eagle's medium with Ham's F12 Nutrient Mixture (DMEM-F12) and L-glutamine supplemented with 0.5 g/L sodium bicarbonate, 1.10 g/L HEPES, 10% heat-inactivated fetal bovine serum (FBS), and 1% (v/v) of a mixture of penicillin (100 µg/mL) and streptomycin (100 µg/mL). Cells were maintained in a 5% CO_2 humidified atmosphere, at 37 °C until confluence was achieved.

6.3.2.6 Cytotoxicity Evaluation

The cytotoxicity profile of PEI–DQA/TAT/pND1 complexes was monitored in HeLa cells by MTT (3-[4,5dimethyl-thiazol-2-yl]-2,5-diphenyltetrazolium bromide) assay. Cancer cells were seeded in a 96-well plate, at a density of 1×10^4 cells/well, and were grown at 37 °C in a 95% O_2/5% CO_2 humidified atmosphere. Complexes (100 µL) were first resuspended in serum-free DMEM medium and then applied to the well plates for 6 h. The medium was changed to end the transfection process. After incubation for periods of 24 h and 48 h, the redox activity was evaluated by MTT reduction. Measurements of absorbance at 570 nm were performed on a Bio-Rad Microplate Reader Benchmark. The medium without cells was settled as zero absorbance and considered for spectrophotometer calibration. Non-transfected cells were used as positive controls, while ethanol-treated cells were used as negative controls. The relative cell viability (%) compared to control wells was calculated by [A] test/[A] control × 100, where [A] test is the absorbance of the test sample and [A] control is the absorbance of the control sample. All measurements were performed in triplicate.

6.3.2.7 Fluorescence Confocal Microscopy

6.3.2.7.1 FITC Plasmid Labeling

For the preparation of FITC-labelled pDNA, 2 µg of pDNA, 2 µL of FITC (in sterile anhydrous dimethyl sulfoxide, 50 mg/100 µL), and 81 µL of labeling buffer (0.1 M sodium tetraborate, pH 8.5) were mixed. The mixture was stirred for 4 h at room temperature and in the dark. Two-and-a-half volumes of 100% ethanol (212.5 µL) and one volume of 3 M NaCl (85 µL) were added. FITC

pDNA samples were incubated at −20°C overnight. Thereafter, they were centrifuged at 4°C for 30 min, and the pellet was washed with ethanol (75%).

6.3.2.7.2 Live Cell Imaging

The cellular internalization and mitochondrial targeting capacity of PEI–DQA/TAT/FITC–pND1 complexes were monitored by confocal laser scanning microscopy (CLSM). HeLa cells (2×10^3) were grown in µ-slide 8-plate wells until 50–60% confluence was attained. Cell nuclei and mitochondria were stained with DAPI and MitoTracker Orange dye, respectively. The complete medium was replaced with serum-free culture medium 12 h before transfection; 1 µg of complexed FITC–pND1 was added to each well. Images of transfected cancer cells were acquired after 6 h. The LSM 710 confocal microscope (Carl Zeiss SMT, Inc., Oberkochen, Germany) was used to observe real live transfection, under a 63× oil immersion objective. Images were analyzed with LSM software (Carl Zeiss SMT, Inc., Oberkochen, Germany). Throughout the study, HeLa cells were kept at 37 °C with 5% CO_2. All images were acquired using the same parameters, with the laser and filters corresponding to the respective DAPI (445/450 nm), FITC (525/550 nm), and MitoTracker (555/580 nm) dyes. After the acquisition, the images were processed under the same conditions and parameters using ImageJ software.

6.3.2.8 Reverse Transcription Polymerase Chain Reaction (RT-PCR)

Reverse transcription polymerase chain reaction (RT-PCR) was used to qualitatively analyze mRNA GFP expression. HeLa cells were seeded in 12-well plates at a density of 2×10^5 cells/well. The medium was removed 24 h after transfection, and cells were washed with PBS. Untreated cells were used as controls. The cells were lysed with TRIzol (250 µL/well), incubated for 5 min at room temperature, chloroform was added and the mixture was stirred to promote RNA extraction. The samples were incubated for 10 min at room temperature and then centrifuged at 10,000 rpm, at 4°C, for 15 min. The aqueous phase was withdrawn and 125 µL of ice-cold isopropanol was added to ensure RNA precipitation. Another centrifugation cycle (10,000 rpm, 4 °C, 15 min) was performed; 125 µL of 75% ethanol in DEPC water was added to the obtained pellet to remove the organic compounds. After centrifugation, 20 µL of DEPC water was added to rehydrate the pellet, and samples were quantified using a NanoPhotometer™. In complement, electrophoresis analysis on agarose gel (1%) was carried out. The “Xpert cDNA Synthesis Kit” from GRiSP (GRiSP, Porto, Portugal) was utilized for the cDNA synthesis. All of the instructions provided by the manufacturer were followed. The amplification of cDNA was performed through the addition of 10 µL of RNase-free water, 1 µL of reverse primer (5′-CGTTCTTGTACGTAGCCTTC-3′), 1 µL of forward primer (5′-CTGCACCACCGGAAAACTCC-3′), 12 µL of Speedy Supreme NZYTaq 2× Green Master Mix (NZYTech, Lisbon, Portugal), and 1 µL of cDNA, in each PCR reaction. After homogenization of the samples, they were placed in a T100™ thermal cycler (Bio-Rad Laboratories, Inc., Hercules, CA, USA). The following reaction conditions were established: denaturation (94 °C for 2 s), annealing (57 °C for 5 s), and extension (72 °C for

5 s) for 35 cycles. Agarose gel electrophoresis was used to analyze the PCR products. The visualization was performed on a UV FireReader Imaging System (UVITEC, Cambridge, UK).

6.3.2.9 Mitochondrial Isolation

Mitochondria were isolated from other cellular organelles with the Mitochondria Isolation Kit for Cultured Cells (Thermo Fisher Scientific Inc., Rockford, IL, USA). This kit ensures the separation of mitochondria with high purity and yield. The instructions provided by the manufacturer were followed. Briefly, HeLa cells (1×10^4) were transferred to Falcon tubes, and 800 µL of Reagent A was added to the cells, followed by incubation on ice for 2 min. Then, 10 µL of Reagent B was added, and the cells were vortexed for 10 s at maximum speed, incubated on ice for 5 min, and vortexed again at maximum speed every minute for 10 min. After this, Reagent C (800 µL) was added, and samples were centrifuged (20,000× g) for 10 min at 4 °C. Then, 500 µL of Reagent C was added to the resultant pellet containing the mitochondria. Final centrifugation at 12,000× g for 5 min was performed, and the supernatant was discarded. The obtained pellets full of mitochondria were resuspended in 50 µL of ice-cold PBS and mixed with 500 µL of carbonate buffer (fresh cold 0.1 M Na_2CO_3).

6.3.2.10 Protein Quantification

The ND1 protein produced by transfection of HeLa cells with the developed systems was identified using an ND1 ELISA kit (Biomatik, EKL54820, Wilmington, DE, USA), following the procedure described by the manufacturer. ND1 protein was quantified by a sandwich enzyme immunoassay. Transfected HeLa cells with different peptide- or polymer-based complexes were lysed following standard cell lysis methods. Cells were detached with trypsin and centrifuged. They were then washed three times in cold PBS, resuspended in PBS, and ultrasonicated 4 times. After this procedure, HeLa cells were centrifuged at 15,000× g for 10 min at 4°C. The manufacturer provided reagent solutions that were used according to instructions. In summary, Reagent A was added to each well and incubated for 1 h at 37°C, followed by incubation with Reagent B. Thereafter, TMB substrate solution was added to each well, and samples were incubated for 20 min at 37°C in the dark. A sample displaying a yellow color was obtained after the addition of Stop Solution. The content of ND1 protein was inferred by measuring the absorbance in a microplate reader at 450 nm.

6.3.2.11 Statistical Analysis

The normality of the distribution of sample data was evaluated by running appropriate tests, such as the D'Agostino–Pearson omnibus. The statistical analysis performed was a one-way or two-way analysis of variance (ANOVA), followed by Bonferroni's multiple comparison test. A p-value below 0.05 was considered statistically significant. Data analysis was conducted with GraphPad Prism v.8.01 (GraphPad Software, Inc., San Diego, CA, USA).

6.4 Results and Discussion

6.4.1 Synthesis and Characterization of PEI–SA, and PEI–DQA

The synthesis of PEI conjugates was carried out following the general scheme depicted in **Figure 6.1**. The amine-terminated PEI was succinated to further react with DQA. The terminal carboxylic acid group of succinic acid provided the attachment point with DQA via the acid–amine coupling reaction. The reaction conditions produced optimal yield at each step. The analysis of synthesized PEI derivatives was carried out using spectroscopic methods. The 1H NMR spectra of PEI-SA (10 and 25 kDa) are shown in **Figure 6.2A, B**, respectively. In both spectra, broad multiplet peaks were observed at δ3.12–3.42 ppm, corresponding to the methylene groups present in the primary amine group of PEI, along with the introduced succinic substituent ((PEI)–$(CH_2)_2$–NH–CO–$(CH_2)_2$–COOH). For DQA conjugates, the characteristic signals of the aromatic ring protons were present at δ7.25–7.35 ppm (**Figure 6.3A, B**). The peak located at δ3.32 ppm was identified as benzyl–CH_2 protons. The methylene moiety had a broad multiplet at δ3.63–3.72 ppm. The successful conjugation in PEI–DQA (10 and 25 kDa) was confirmed from 1H NMR. **Figure 6.3C** shows the DQA spectrum. Fourier-transform infrared (FTIR) spectroscopy was carried out to confirm the success of the modification. **Figure S6.1**, available in the Supplementary Materials (SM), shows the FTIR spectra of PEI–DQA (10 kDa and 25 kDa) (A) and the FTIR spectra of DQA (B). The signals at 3300 cm–1 and 2822–2530 cm–1 indicated the N–H stretching and aliphatic C–H stretching vibrations, respectively, in all PEI–SA conjugates. The PEI–DQA (10 and 25 kDa) displayed a broad peak at 1720 cm–1 as the stretching vibrations of the C=O moiety. Similarly, the C-O-C (1228 cm–1) and N-H (3,210 cm–1) stretching vibrations were observed in the PEI–DQA conjugates. The chromatogram obtained via gel permeation chromatography (GPC) is represented in **Figure S6.2**, available in the SM. The peak shift on the left due to the change in retention time of the polymer and polymer conjugates indicated the increase in molecular weight. According to the molecular weights of the conjugates obtained through GPC analysis (**Table S6.1** in the SM), ~11 molecules of SA were attached to PEI (10 kDa), which conjugated ~9 molecules of DQA. Similarly, PEI (25 kDa) was attached to ~15 molecules of SA, which resulted in ~13 molecules of DQA attachment. The critical micelle concentration (CMC) was observed to be 12.5 µg/mL for PEI–DQA (10 and 25 kDa) conjugates. The reduced CMC showed that PEI–DQA conjugates can readily develop a core-shell structure in an aqueous environment (**Figure S6.3** in SM).

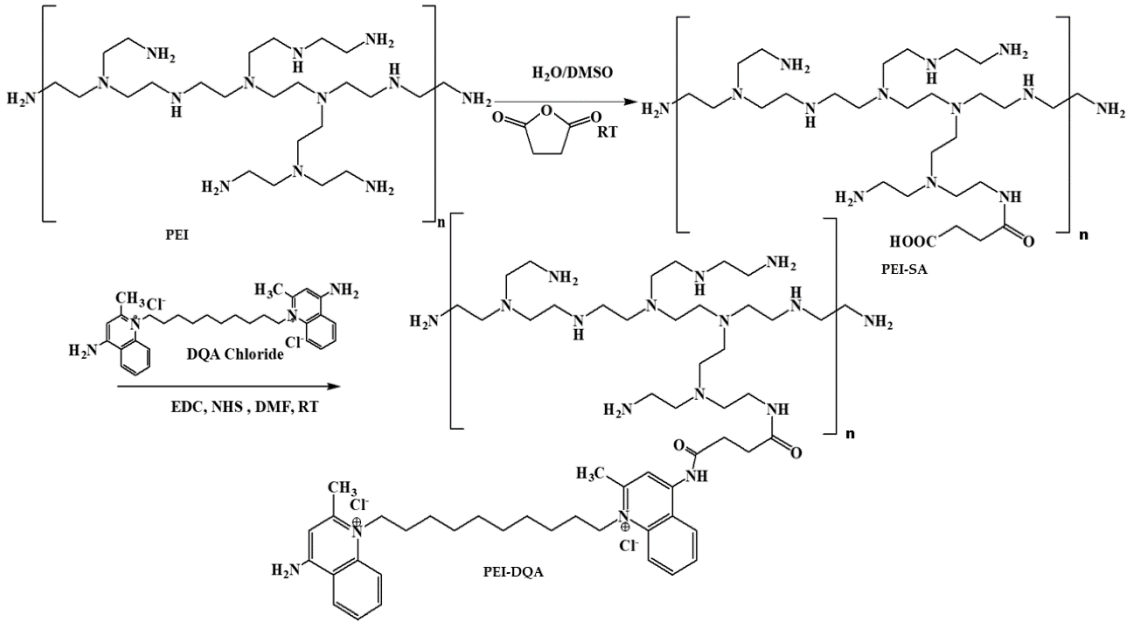

Figure 6.1 - Scheme illustrating the synthesis of the polymer PEI–DQA. RT: room temperature.

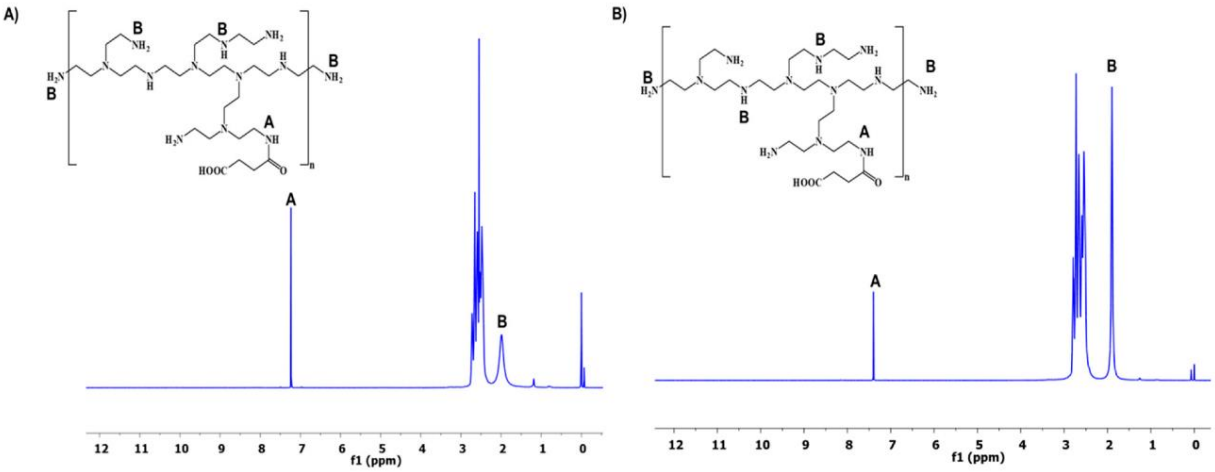

Figure 6.2 - 1H NMR spectra of the intermediate PEI–SA: PEI-10 kDa (A) and PEI-25 kDa (B).

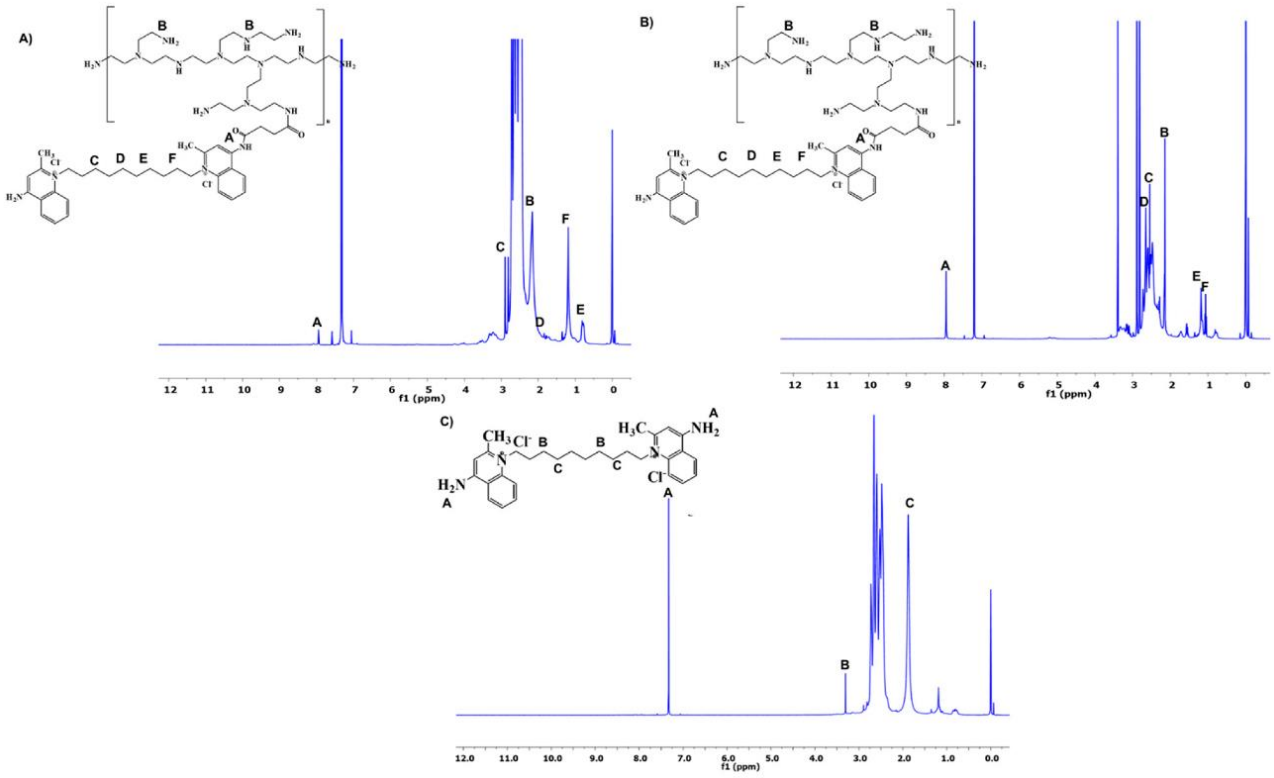

Figure 6.3 - 1H NMR spectra of PEI–DQA: PEI (10 kDa) (A) and PEI (25 kDa) (B); the spectrum of DQA (C).

6.4.2 pDNA Complexation Capacity

The formulation of PEI–DQA/TAT/pND1 systems was elaborated using a dropwise precipitation method. First, PEI–DQA solution was added to the pDNA solution for 1 min, after which TAT peptide solution was added. Electrostatic interactions are the main force that allows the encapsulation of pDNA by PEI–DQA and TAT. These interactions occur due to the negative charges on pND1 that bind to the positive charges on both PEI and TAT, forming nanoscale systems. The interaction strength is dependent on the N/P ratio considered at the formulation step, and the higher the ratio, the greater the availability of positive charges to interact with pND1. Moreover, in previous research by our team, the cytotoxicity of TAT/pDNA complexes was evaluated as a function of the N/P ratio on both fibroblasts and HeLa cells [26]. The results demonstrated that TAT/pDNA complexes formulated at N/P ratios of 1, 2, 4, 8, and 10 are all biocompatible. After incubation with TAT-based complexes, a moderate increment in cellular viability was observed as the N/P ratio increased.

Here, the complexation capacity of the systems and the influence of the N/P ratio were evaluated using agarose gel electrophoresis. The ratios of PEI–DQA to pND1 used were 10, 20, 50, 100, 200, and 500, and the ratios of TAT to pND1 were 1 and 2. Results are shown in **Figures 6.4**, **6.5,** and **6.6**. In **Figure 6.4** we can see that the 10 kDa and 25 kDa PEI–DQA systems had a low capacity to encapsulate pND1, even at the highest ratios (100:1 and 200:1). **Figure 6.5** concerns 10 kDa and 25 kDa PEI–DQA systems to which TAT was added, where N/P = 1. By analyzing the images,

we found that all formulated systems exhibited encapsulation capacity to some extent, compared to the initial pND1 sample. However, only systems prepared at a 500:1:1 ratio of both PEIs demonstrated high encapsulation capacity. As PEI is a compound known to have considerable cytotoxicity at high concentrations, the need arose to try to improve encapsulation by keeping PEI ratios as low as possible. Following this, we doubled the TAT ratio, which resulted in a great improvement in pND1 encapsulation for all formulated systems, maintaining PEI ratios (**Figure 6.6**). The prepared systems presented a high efficiency of pND1 encapsulation, being able to neutralize its negative charges; thus, there were no bands in the agarose gel. Moreover, pND1 CC (%) was calculated from the band intensities of the agarose gels, as described in the Materials and Methods section; the results are shown in **Figure 6.7**. PEI (10 or 25 kDa)–DQA/pND1 complexes displayed poor ability to complex pND1 at lower ratios, and it was found that CC varies with the N/P ratio (**Figure 6.7A**). It seemed that an increase in the N/P ratio led to higher CC values. Additionally, PEI (25 kDa)–DQA/pND1 complexes condensed pND1 to a higher extent when compared to the capacity exhibited by the corresponding PEI (10 kDa) complexes. The incorporation of TAT peptide into PEI (10 or 25 kDa)–DQA/pND1 complexes significantly increased their capacity to condense pND1 (**Figure 6.7B, C**). Considerably high CC values were obtained for all N/P ratios investigated. At an N/P ratio of TAT/pND1 of 2, practically all complexes possessed a CC of around 100%. The exception was PEI (10 kDa)–DQA/TAT/pND1 prepared at the lowest ratio (**Figure 6.7C**). From this, there was no need to consider TAT/pND1 ratios higher than 2. In this work, we also intended to compare these PEI-based systems with previously studied systems based on peptides that also have sequences to confer specificity for mitochondrial targeting [18]. Comparing the pND1 encapsulation ability of PEI–DQA/TAT/pND1 complexes with that displayed by peptide-based complexes, PEI-based complexes showed lower efficiency for pND1 encapsulation, since to encapsulate the same amount of pND1 higher N/P ratios were required (N/P ratios of 10 versus N/P ratios of 0.5 and 1). This lower capacity can be explained by the decrease in the amines available in PEI due to the addition of DQA to the polymer, reducing the charges available to interact with pND1. Nevertheless, our study proceeded to analyze the properties of PEI–DQA/TAT/pND1 systems and their potential for mitochondrial targeting/gene delivery.

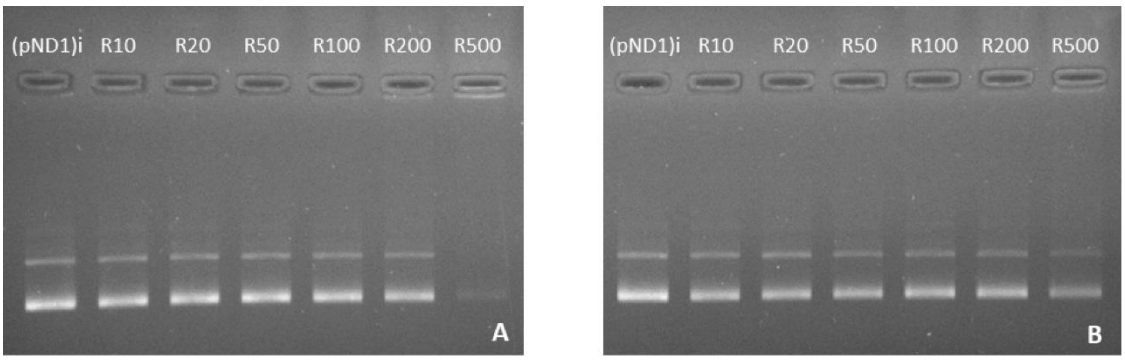

Figure 6.4 - Agarose gel electrophoresis of the initial pND1 solution ((pND1)i) and supernatants resulting from the formulation of PEI–DQA (10 kDa)/pND1 systems (PEI–DQA N/P = 10, 20, 50, 100, 200, and 500) (A) and PEI–DQA (25 kDa)/pND1 systems (PEI–DQA N/P = 10, 20, 50, 100, 200, and 500) (B).

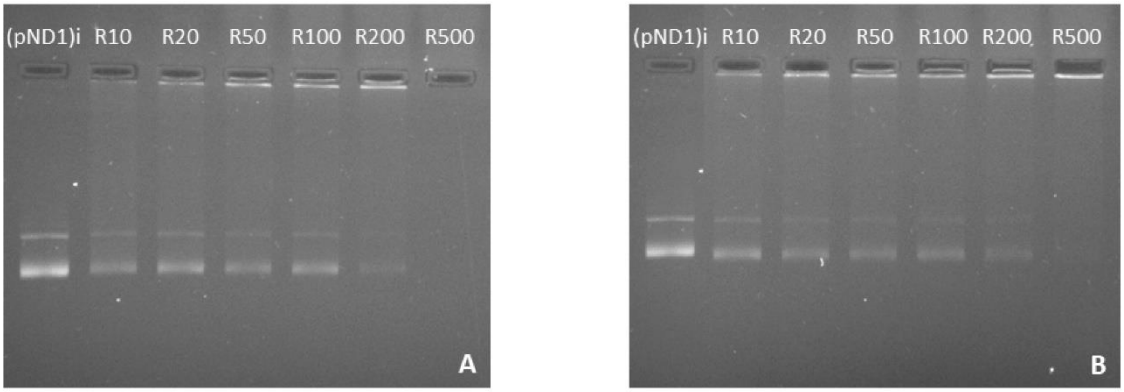

Figure 6.5 - Agarose gel electrophoresis of the initial pND1 solution ((pND1)i) and supernatants resulting from the formulation of PEI–DQA (10 kDa)/TAT/pND1 systems (PEI–DQA N/P = 10, 20, 50, 100, 200, and 500, and TAT N/P = 1) (A) and PEI–DQA (25 kDa)/TAT/pND1 systems (PEI–DQA N/P = 10, 20, 50, 100, 200, and 500, and TAT N/P = 1) (B).

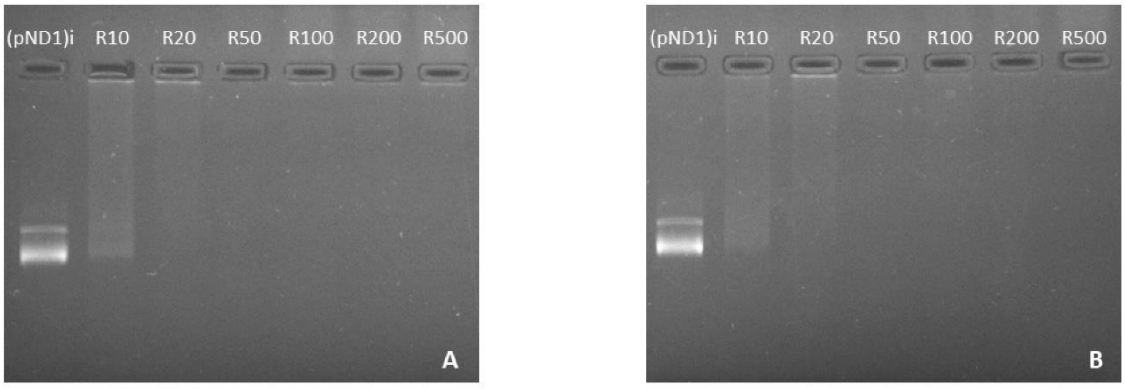

Figure 6.6 - Agarose gel electrophoresis of the initial pND1 solution ((pND1)i) and supernatants resulting from the formulation of PEI–DQA (10 kDa)/TAT/pND1 systems (PEI–DQA N/P = 10, 20, 50, 100, 200, and 500, and TAT N/P = 2) (A) and PEI–DQA (25 kDa)/TAT/pND1 systems (PEI–DQA N/P = 10, 20, 50, 100, 200, and 500, and TAT N/P = 2) (B).

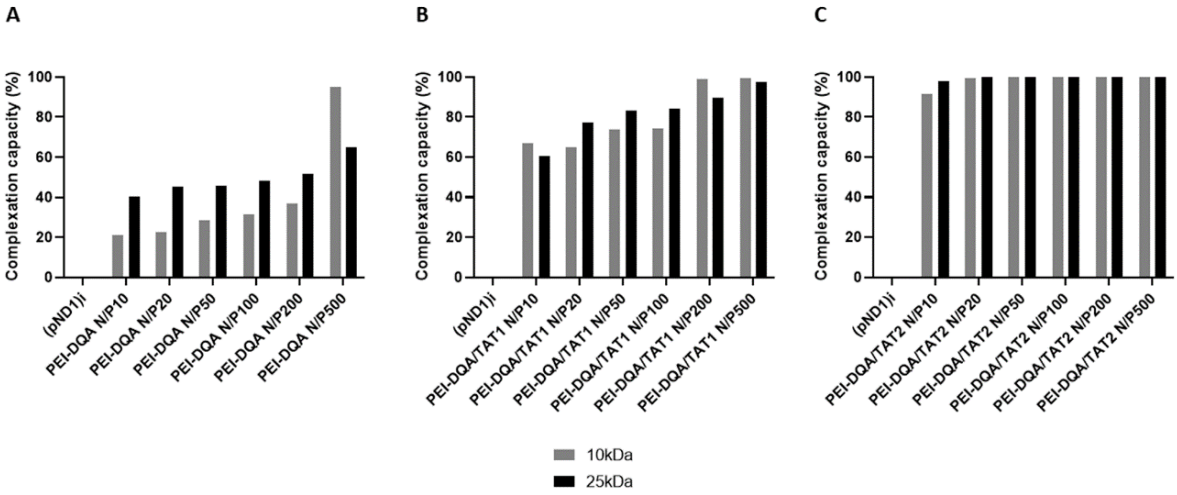

Figure 6.7 - pND1 complexation capacity (CC) of PEI–DQA (10 and 25 kDa)/pND1 (A), PEI–DQA (10 and 25 kDa)/TAT(N/P1)/pND1 (B), and PEI–DQA (10 and 25 kDa)/TAT(N/P2)/pND1 (C) complexes calculated from the band intensity of the agarose gels of Figures 6.4, 6.5, and 6.6, respectively.

6.4.3 Characterization of PEI–DQA/TAT/pND1 Complexes

After verifying the complexation capacity of the produced systems, these complexes were characterized by DLS in terms of size and surface charge. The results are shown in **Figure 6.8**, corresponding to data from PEI–DQA (10 kDa)/TAT/pND1 and PEI–DQA (25 kDa)/TAT/pND1 complexes. In addition, **Table S6.2** (in SM) presents all of the obtained values of size and zeta potential for both polymer- and peptide-based systems. The results of surface charge measured in zeta potential (mV) for systems with PEI–DQA of 10 kDa revealed a slightly negative overall charge. A decrease in this negative charge with the increase in the N/P ratio was also observed.

The complexes prepared with PEI–DQA (25 kDa), for the lowest N/P ratios under study, showed a charge very close to 0 mV, while for N/P ratios of 200:2:1 and 500:2:1 they presented positive zeta potential values (+3.2 and +5.2 mV, respectively). This low global charge can be explained by the presence of DQA, which presents a neutral charge [49], decreasing the influence of positive charges of PEI on the surface of complexes. The main contribution to zeta potential comes from the inclusion of TAT. The surface charge of TAT/pND1 complexes conceived at an N/P ratio of 2 was found to be around +2.3 mV. When compared to these later data, results regarding the physicochemical properties exhibited by the peptide/pND1 complexes [18] presented in the previous publication demonstrated that peptide-based complexes displayed a more positive surface charge, with zeta potential values of up to +20 mV for an N/P = 5, while the highest value for PEI–DQA/TAT/pND1 complexes was +5.2 mV for N/P = 500.

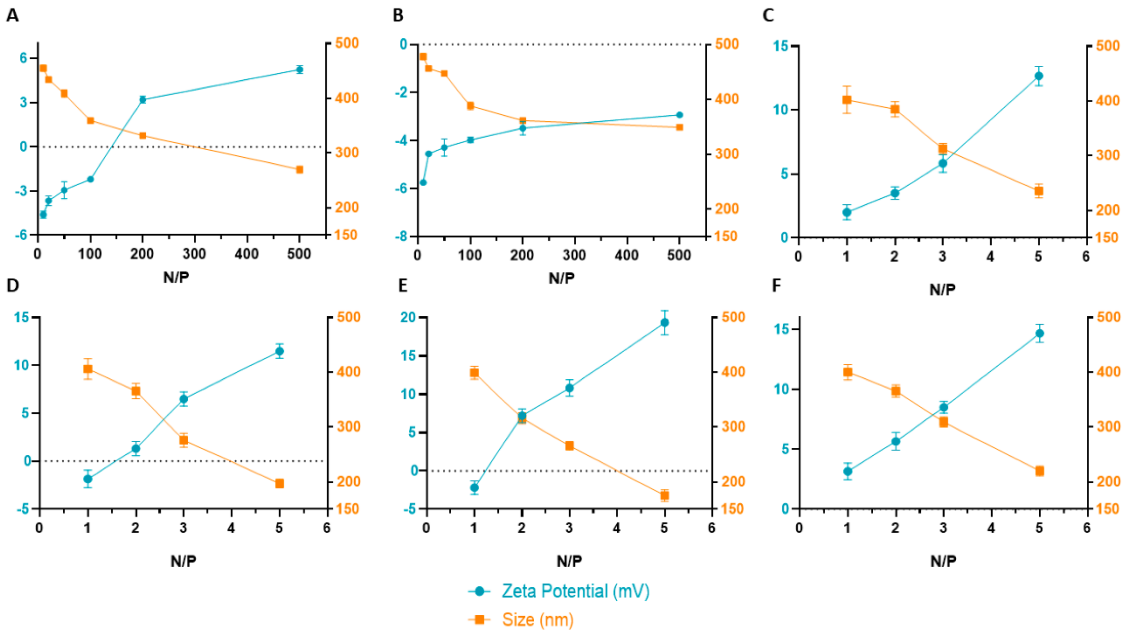

Figure 6.8 - Average zeta potential and mean size displayed by PEI–DQA (10 kDa and 25 kDa)/TAT/pND1 (A, B), CpMTP/pND1 (C), MTS-WRAP1/pND1 (D), MTS-WRAP5/pND1 (E), and MTS-$(KH)_9$/pND1 (F) complexes.

Evaluation of the size of the formulated polyplexes revealed a difference between complexes formulated with PEI of 10 kDa and 25 kDa. For the same N/P ratio, average sizes were smaller in systems prepared with 25 kDa of PEI. The effect of the N/P ratio was also evident within the same type of system—as the ratio increased, there was a decrease in the size of complexes. This evidence was due to the greater capacity of high-molecular-weight PEI to encapsulate pND1, due to high charge density that led to stronger electrostatic interactions. The sizes of all complexes were less than 500 nm, which may have facilitated cell internalization. The sizes evidenced by these systems were superior to the sizes displayed by peptide-based complexes formulated in our previous study [18]. Comparing the results, we previously found that peptide-based complexes had sizes around

150–200 nm for the highest ratios, while in this study PEI–DQA/TAT/pND1 complexes exhibited sizes around 350 nm. Thus, we can infer that peptide/pND1 complexes presented a greater capacity to condense pND1 and formulate smaller complexes. Another relevant characterization parameter is the PdI, which allows us to assess the distribution of sample sizes. PdI values close to 0.01 reveal monodisperse samples; between 0.5 and 0.7 are considered polydisperse particles and a value above 0.7 indicates a broad particle size distribution [60]. PdI data are presented in **Table S6.2**, available in the SM. Analyzing this table, we verified a PdI between 0.4 and 0.6, with an effect on the N/P ratio. Lower ratios corresponded to polydisperse samples, while higher ratio complexes were monodispersed. Compared to PdI values obtained for peptide-based complexes, the difference was minimal. PdI for peptide/pND1 systems was around 0.3, with polydisperse samples found for smaller ratios.

Complexes of MTS-CPP/pND1 and CpMTP/pND1 were previously published [18]. The values were calculated with data obtained from three independent measurements (mean ± SD, n = 3).

6.4.4 Cytotoxic Profile

The cytotoxicity of formulated polymeric complexes was evaluated using the MTT assay in HeLa cells. To verify the safety of the complexes, the viability of HeLa cells was evaluated at 24 h, 48 h, and 72 h after transfection with the various systems under study. PEI–DQA (10 kDa or 25 kDa)/TAT/pND1 was used at N/P ratios of 20, 50, 100, 200, and 500, and TAT/pND1 N/P of 2:1. The results shown in **Figure 6.9A–C** correspond to 24 h, 48 h, and 72 h transfection, respectively. Non-transfected cells were used as positive controls (100% viability), while cells treated with 70% ethanol were used as negative controls (0% viability). Statistical analysis was performed with the positive controls for comparison. Systems formulated with high ratios demonstrated cytotoxicity when compared to the positive controls (N/P ratios of 100:2:1; 200:2:1, and 500:2:1). Polymeric complexes formulated at low ratios demonstrated biocompatibility (statistically not significant (ns) *versus* positive controls). Therefore, these results showed the influence of the N/P ratio on the cytotoxicity of the developed systems. The increment in the N/P ratio led to an increased content of PEI amines, and this high cationic charge corresponded to high cytotoxicity. In this way, it can be pointed out that the N/P ratio can be viewed as a tailoring tool to adjust cellular cytotoxicity levels. At 24 h, the obtained data also demonstrated some differences between complexes formulated with PEI–DQA (10 kDa) and PEI–DQA (25 kDa). At 24 h and for the highest ratios, PEI–DQA (25 kDa) complexes were more cytotoxic than the ones based on PEI–DQA (10 kDa); there was a statistically significant difference (* $p \leq 0.05$) for the comparison between these complexes at N/P ratios of both 200:2:1 and 500:2:1. This tendency, however, was not observed at 48 h. The cytotoxicity evidenced in complexes prepared at high ratios seemed to be more pronounced in the first 24 h when compared to that obtained at 48 h and 72 h after transfection. We can hypothesize that cells suffered an initial shock during the first 24 h of incubation, with a significant loss of their viability, after which they were able to recover over time, showing higher viability. However, a clear explanation for this phenomenon cannot be anticipated at this stage. For instance, at 72 h and high N/P ratios, the difference from the positive controls was lower (* $p \leq 0.05$ or ** $p < 0.01$ for PEI–DQA (25 kDa)/TAT/pND1 at 500:2:1 versus

positive controls) than the difference found at 24 h (for high N/P ratio complexes, **** p <0.0001 *versus* positive control) or 48 h (for most N/P ratio complexes, *** p <0.001 *versus* positive control).

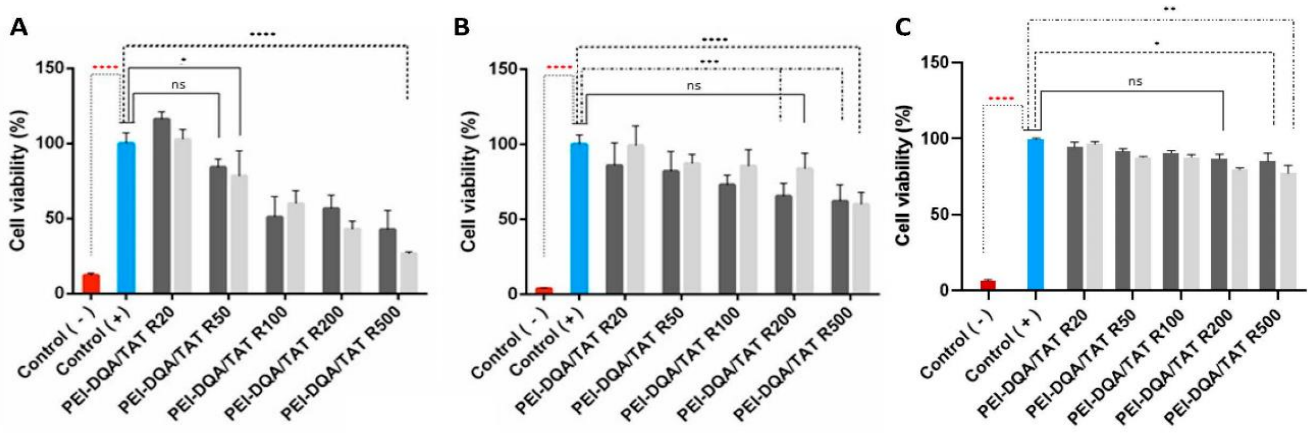

Figure 6.9 - Cellular viability of HeLa cells after 24 h (A), 48 h (B), and 72 h (C) of incubation with PEI–DQA (10 kDa or 25 kDa)/TAT/pND1 complexes conceived at N/P ratios of 20:2:1, 50:2:1, 100:2:1, 200:2:1, and 500:2:1. Non-transfected cells were used as positive controls (100 % viability) and ethanol-treated cells were considered as negative controls (0 % viability). Statistical analysis was carried out using "one-way ANOVA" with data obtained from four independent measurements (mean ± SD, n = 4).

For further *in vitro* studies, and due to their biocompatibility, lower N/P ratio PEI–DQA (10 kDa or 25 kDa)/TAT/pND1 complexes were selected.

The biocompatibility of peptide-based complexes was analyzed and discussed elsewhere [18]. All peptides/pND1 were demonstrated to be non-toxic to HeLa cells at 24 h, with the obtained results being statistically non-significant (n.s) in relation to the positive controls. At 48 h, however, a decrease in biocompatibility was observed for all peptides/pND1 nanoparticles. Furthermore, the presence of the MTS sequence in the peptides seemed to influence the cytotoxic profile displayed by the complexes. MTS-peptide/pND1 carriers exhibited less cellular viability in relation to controls [18]. Comparing cytotoxicity results between polymer and peptide/pND1 complexes, it was verified that the latter complexes presented higher safety in terms of biocompatibility, making them far superior in relation to PEI–DQA/TAT/pND1 complexes. These results can be explained by the greater efficiency of peptides in encapsulating pND1, decreasing the need to use high N/P ratios.

6.4.5 Mitochondrial Targeting Ability

Over the past few years, researchers have pursued the goal of mitochondrial targeting and mitochondrial transgene expression for the treatment of mitochondrial disorders [52]. This effort has led to the development of efficient delivery systems with the ability of cellular internalization,

followed by mitochondrial targeting [52]. Recently, our team has also contributed to this field with the conception of mitochondria-targeted peptide/pND1 complexes using a mitochondrial targeting sequence (MTS) coupled to peptides able to internalize nucleic acids such as MTS-WRAP1, MTS-WRAP5, and MTS-$(KH)_9$ [18]. In this previous work, real live transfection of HeLa cells mediated by these peptide delivery vectors, monitored by fluorescence confocal microscopy, revealed that the complexes were easily taken up by cancer cells and accumulated at the site of the mitochondria [18], unequivocally demonstrating their mitochondrial targeting specificity. Among those peptide complexes, the ones based on the CpMTP peptide seemed to display higher cell penetration ability and targeting performance [18].

In the present study, we investigated the mitochondrial targeting capacity of various synthesized PEI–DQA/TAT/pND1 complexes in HeLa cells. In this sense, the cellular internalization and mitochondrial targeting ability of these polymeric complexes were assessed by confocal microscopy, using appropriate dyes to stain the nuclei and mitochondria, while pND1 was labeled with FITC. In this way, real live transfection of HeLa cells mediated by PEI–DQA (10 kDa or 25 kDa)/TAT/pND1 vectors, conceived at different N/P ratios, was monitored. The obtained cell images, at 6 h of transfection, are visualized in **Figures 6.10** and **6.11**, corresponding to the cellular transfection mediated by PEI–DQA (10 kDa)/TAT/pND1 at an N/P ratio of 50:2:1 and PEI–DQA (25 kDa)/TAT/pND1 at an N/P ratio of 50:2:1, respectively. The images were obtained from a set of consecutive Z planes (Z-stacks; step size of 0.1 μm). In both presented figures, image A represents mitochondria labeled with MitoTracker, image B shows PEI–DQA (10 kDa or 25 kDa)/TAT/pND1 complexes, image C shows nuclei marked with DAPI, and image D corresponds to the merged image. From the green fluorescence visualized in B, we inferred that efficient transfection took place and polymeric complexes were internalized in HeLa cells.

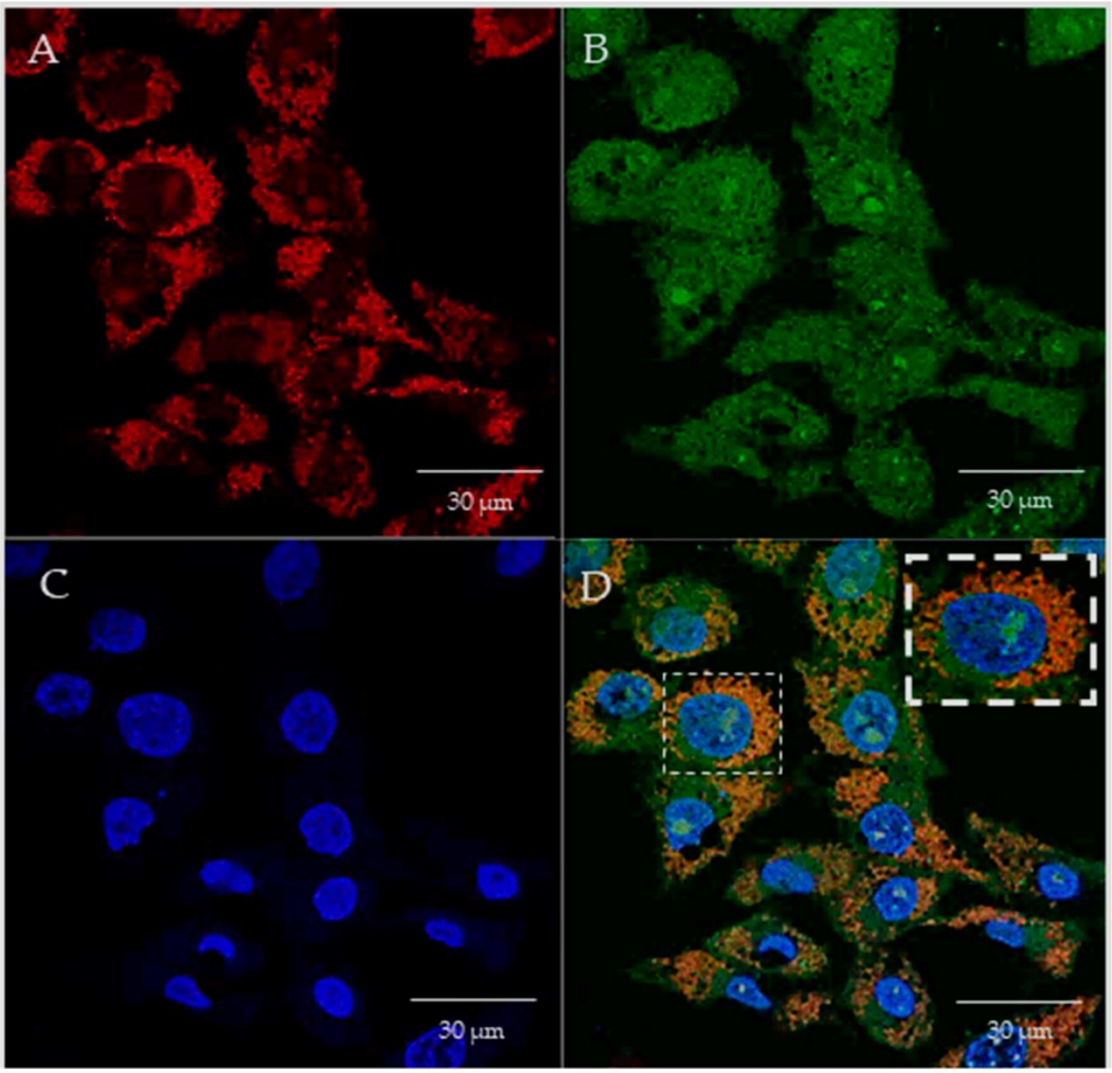

Figure 6.10 - Cellular uptake and intracellular colocalization of PEI–DQA (10 kDa)/TAT/pND1 complexes formulated at an N/P ratio of 50:2:1. Mitochondria stained red by MitoTracker (A), green-labeled pND1 (B), nuclei marked blue by DAPI (C), and merged image (D).

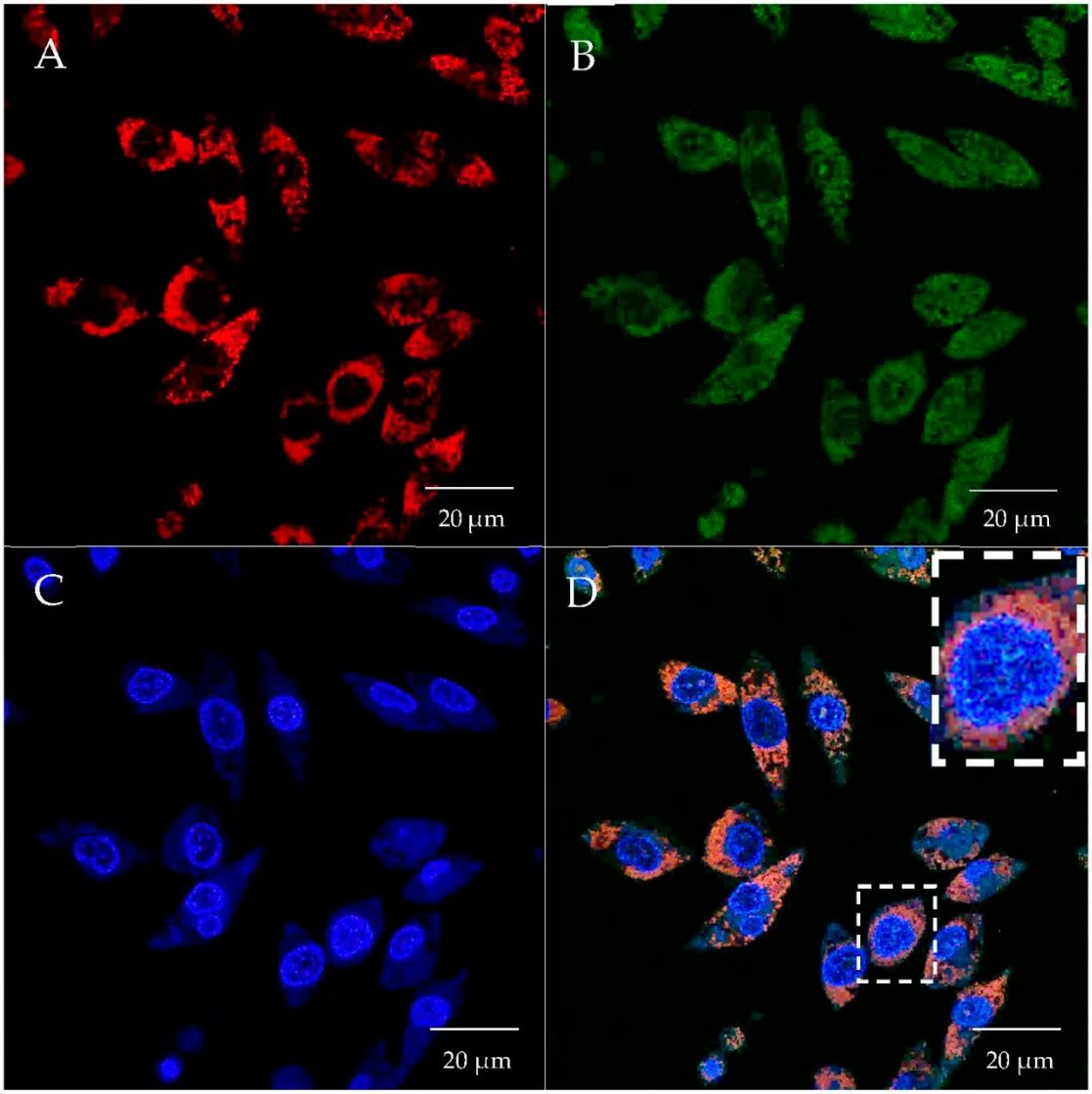

Figure 6.11 - Cellular uptake and intracellular colocalization of PEI–DQA (25 kDa)/TAT/pND1 complexes formulated at an N/P ratio of 50:2:1. Mitochondria stained red by MitoTracker (A), green-labeled pND1 (B), nuclei marked blue by DAPI (C), and merged image (D).

Moreover, after the uptake, the developed delivery complexes were targeted to the site of the mitochondria. Image D in both figures shows the specific accumulation of PEI–DQA (10 kDa or 25 kDa)/TAT/pND1 complexes in the mitochondria, demonstrating their mitochondria-specific targeting. We also evaluated the effect of the N/P ratio on the targeting capacity by performing the described microscopy study on HeLa cells using PEI–DQA (10 kDa or 25 kDa)/TAT/pND1 formed at a lower N/P ratio of 20:2:1. The collected images can be consulted in the SM (**Figures S6.4** and **S6.5**). Very similar observations were made, revealing that both studied N/P ratios were adequate to develop polymeric complexes able to target the mitochondria. This targeting skill, displayed by the novel PEI-based complexes, represents a great asset to further studies on mitochondrial gene delivery and expression. Furthermore, as evidenced in the merged panel of

Figure 6.10 and **Figure 6.11**, although the complexes were preferentially located in the mitochondria, some of the complexes were found in the nuclei (especially in the nucleoli).

6.4.6 Evaluation of Gene Expression

Gene expression was evaluated using recoded mitochondrial pGFP—a pDNA designed for specific expression in the mitochondria [51]. Polymeric and peptide/pGFP delivery systems were prepared at various N/P ratios, following the method described in the Materials and Methods section for pND1. Thereafter, HeLa cells were transfected with the formed complexes, and recoded GFP gene expression was evaluated by RT-PCR. Results obtained for PEI- and peptide-based complexes are shown in **Figure 6.12 A, B**, respectively. Non-transfected cells were used as controls. The figures show agarose gel electrophoresis of amplification products of the mitochondrial GFP gene, with bands at expected sites. The results obtained for PEI–DQA (10 kDa or 25 kDa)/TAT/pGFP complexes, at N/P ratios of 20:2:1 or 50:2:1 (**Figure 6.12A**), demonstrated the efficacy of HeLa cells' transfection and the presence of pGFP transcripts to a higher extent when compared to controls. Although the bands on the agarose gel were faint, it seemed that all considered polymeric complexes led to GFP expression in the mitochondria.

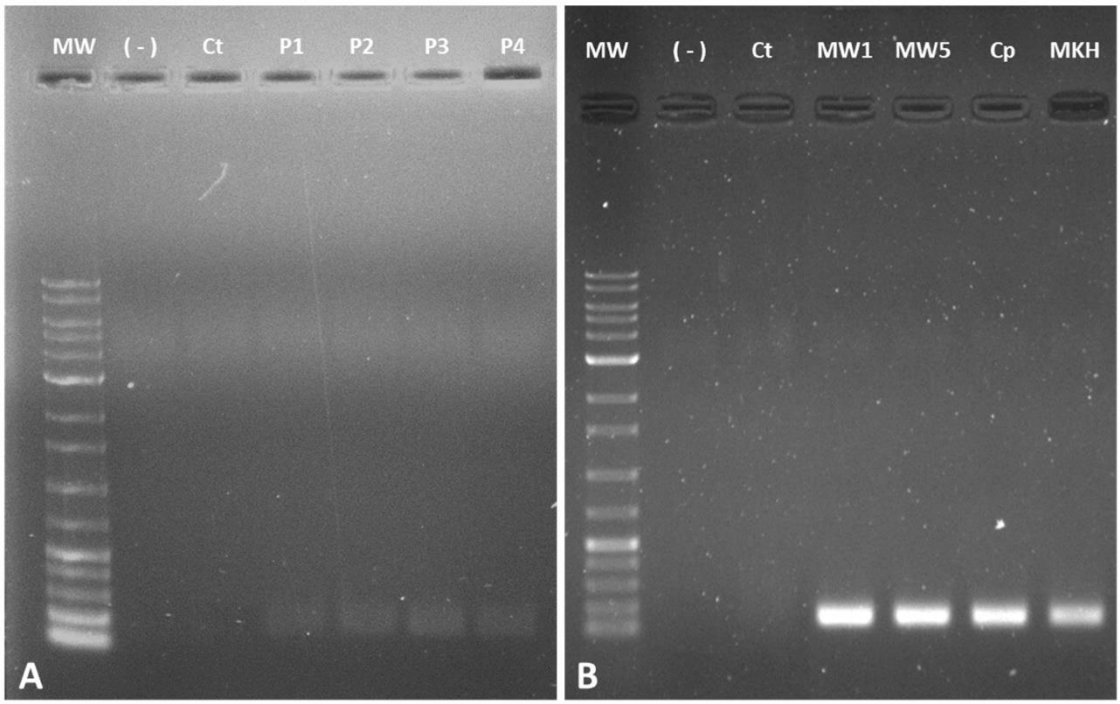

Figure 6.12 - Analysis of GFP gene expression by RT-PCR after transfection of HeLa cells with (A) P1—PEI–DQA (10kDa)/TAT/pGFP, N/P of 20:2:1; P2—PEI–DQA (10 kDa)/TAT/pGFP, N/P of 50:2:1; P3—PEI–DQA (25kDa)/TAT/pGFP, N/P of 20:2:1; P4—PEI–DQA (25 kDa)/TAT/pGFP, N/P of 50:2:1; (B) MW1—MTS-WRAP1/pGFP, N/P of 5:1; MW5—MTS-WRAP5/pGFP, N/P of 5:1; Cp—CpMTP/pGFP, N/P of 5:1 and MKH—MTS-$(KH)_9$/pGFP, N/P of 5:1. MW—molecular weight; (-)—PCR control; Ct—non-transfected cells.

The RT-PCR results for peptide/pGFP systems (**Figure 6.12B**) demonstrated a clear detection of GFP mRNA in transfected cells, when compared to mRNA levels detected in control cells. In general, wide and intense bands were obtained for all peptide-based complexes. Since the total amount of RNA transcribed to cDNA was fully comparable in both polymeric and peptide systems, (see the Materials and Methods section for details), it seemed that the extent of gene expression was higher for the latter systems. Apparently, peptide-based systems seemed to be more promising for GFP expression in the mitochondria. We are, however, aware that RT-PCR results are merely qualitative, giving first evidence of gene expression and potentiating further analysis. To deeply infer the content of both gene and protein, more accurate assays are required.

6.4.7 Quantification of Protein

The evidence of gene delivery and expression in mitochondria instigated us to quantify the produced ND1 protein, after transfection mediated by polymeric or peptide/pND1 complexes. In this way, ND1 protein expression in the mitochondria of HeLa and fibroblast cells was measured by using an ELISA kit. Non-transfected cells served as controls. The results are shown in **Figure 6.13**. Control cells presented significant levels of ND1 protein, as ND1 is an endogenous mitochondrial gene. As observed, this amount can be increased by the transfection with the developed mitochondria-targeted/delivery systems. As shown in **Figures 6.13A, B**, both fibroblast (A) and HeLa (B) cells transfected with PEI–DQA/TAT/pND1 complexes demonstrated higher levels of ND1 protein when compared to controls (*** $p < 0.001$ or **** $p < 0.0001$). Moreover, it was observed that this increase in the production of ND1 protein was influenced by both the molecular weight of PEI and the N/P ratio. The results demonstrated that PEI (25 kDa) led to a higher amount of ND1 in comparison with the protein levels when transfection was mediated by complexes based on PEI (10 kDa), even at lower N/P ratios. Moreover, high-N/P-ratio systems demonstrated higher ND1 levels compared to lower ratio systems when using PEI of the same molecular weight. The results obtained for fibroblasts and HeLa cells were very similar (**Figures 6.13A, B**, respectively), evidencing a pattern independent of the cell type.

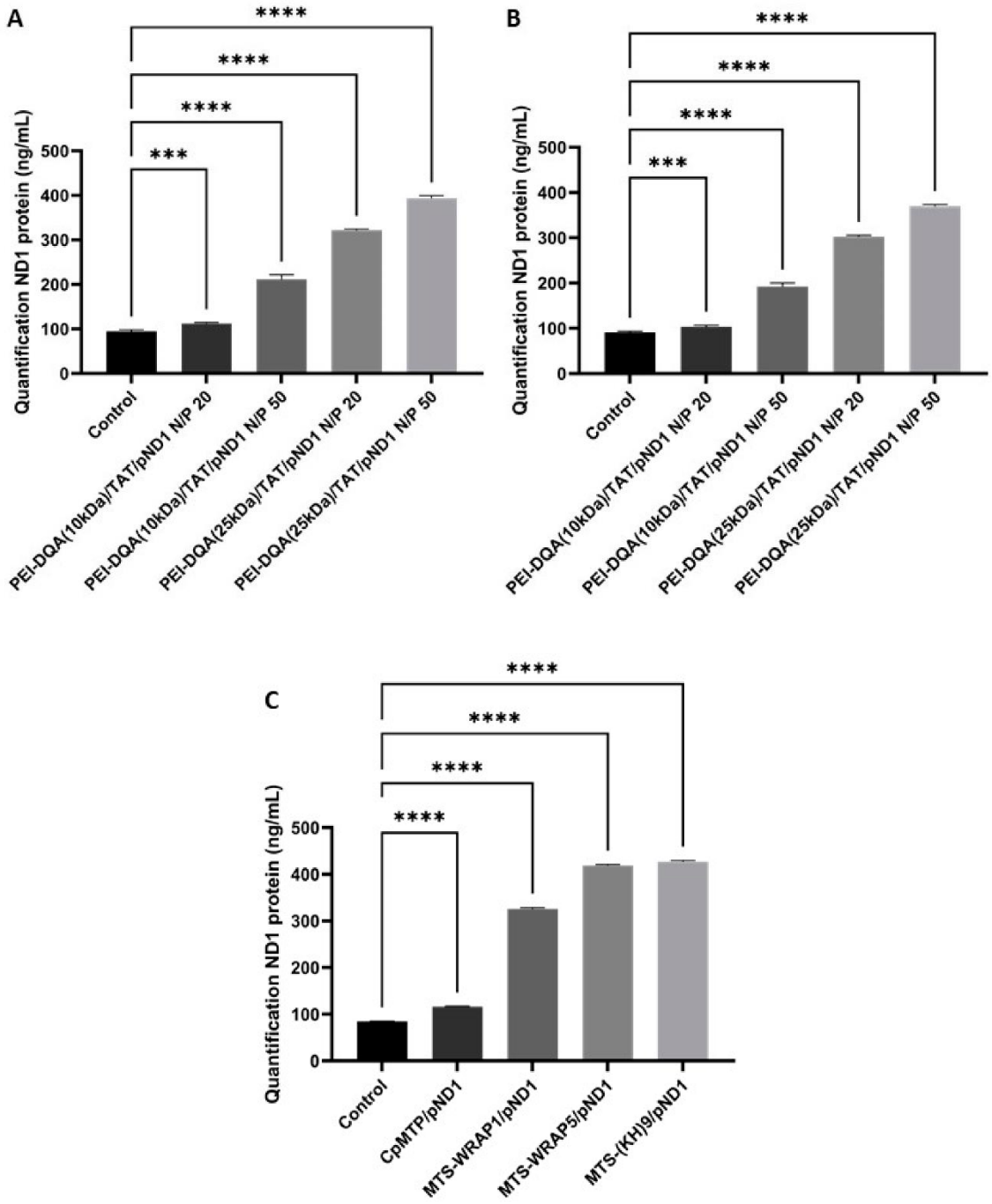

Figure 6.13 - Quantification of ND1 protein 48 h after transfection of fibroblasts (A) and HeLa cells (B) with PEI–DQA (10 kDa)/TAT/pND1, N/P = 20:2:1; PEI–DQA (10 kDa)/TAT/pND1, N/P = 50:2:1; PEI–DQA (25 kDa)/TAT/pND1, N/P = 20:2:1; and PEI–DQA (25 kDa)/TAT/pND1, N/P = 50:2:1; and 48 h after transfection of HeLa cells (C) with CpMTP/pND1, MTS-WRAP1/pND1, MTS-WRAP5/pND1, and MTS-$(KH)_9$/pND1—all complexes prepared at an N/P ratio of 5:1. Non-transfected cells were used as controls. Data were analyzed by one-way ANOVA. (*** $p < 0.001$ or **** $p < 0.0001$).

Figure 6.13C showed ND1 content produced from the transfection of HeLa cells with peptide/pND1 complexes. After 48 h of transfection, and similar to polymeric systems, peptide complexes led to high ND1 levels when compared to control cells (**** $p < 0.0001$). Among peptide complexes, the CpMTP peptide was found to induce the production of the lowest amount of ND1. Cells transfected with MTS-WRAP1, MTS-WRAP5, and MTS-$(KH)_9$ systems produced protein levels 3 to 4 times higher than non-transfected cells.

Comparing PEI complexes with peptide-based systems, we found that peptides led to ND1 concentrations above 400 ng/mL (for MTS-WRAP5/pDN1 and MTS-$(KH)_9$/pND1 complexes), while complexes based on PEI did not reach this protein concentration, even when using 10 times higher N/P ratios. Therefore, peptide/pND1 complexes seemed to be more efficient in both gene and protein expression in mitochondria than the polymeric complexes. This assumption also correlated well with previously obtained data regarding the great efficacy of peptide-based complexes for cellular uptake and mitochondrial targeting [52], as well as with the above reported results of GFP gene expression.

6.4.8 Integrity of Mitochondria

After evidence of ND1 protein production in mitochondria was obtained with the reported delivery systems, we were interested in finding out whether the transfection with complexes interfered with the normal mitochondrial function—especially concerning ATP production. To investigate this issue, measurements of ATP in isolated mitochondria of HeLa cells were performed after transfection with peptide/pND1 complexes, as these complexes offered higher performance as pND1 delivery systems to mitochondria in comparison with the complexes based on PEI–DQA. A luminescent ATP detection kit was used (experimental details are available in the SM). **Figure S6.6** (see the SM) shows the luminescence levels found in the mitochondria of cancer cells after transfection with peptide complexes. Although there was a statistically significant difference in luminescence levels in relation to control cells, peptide complexes such as the ones based on MTS-$(KH)_9$ and CpMTP allowed us to maintain the production of high ATP content. This preliminary study demonstrated that, at least, these complexes and the transfection processes they mediated did not greatly interfere with the normal performance of the mitochondria. After transfection, the mitochondria of HeLa cells were able to produce ATP. It seemed that transfection with these peptide/pND1 complexes was an innocuous process for the normal mitochondrial function and, thus, mitochondrial integrity seemed to be preserved. In contrast, the delivery system based on MTS-WRAP1 exhibited a major decrease in ATP levels, in comparison with controls (**** $p < 0.0001$) (**Figure S6.6**). The comparison between the MTS-WRAP1/pND1 systems with the other peptide complexes was also statistically significant (**** $p < 0.0001$).

At this stage, we are therefore aware that in order to deeply study the efficiency of the proposed peptide/pND1 complexes for mitochondrial gene therapy, the design/conception of ND1-mutated disease models is imperative. This would bring a realistic platform to further evaluate the capacity of peptide-based delivery vectors for long-term ND1 transgene expression in the mitochondria.

6.5 Conclusions

Mitochondrial gene therapy has emerged as a potential therapeutic strategy for mitochondrial diseases originating from mtDNA mutations. To make this therapy feasible and clinically viable, the design and conception of a mitochondria-targeted gene delivery system is crucial. To this end, we report in this work the development of novel polymeric complexes able to load/encapsulate a mitochondrial gene, target mitochondria, and promote gene delivery and protein expression in this organelle. It was found that their physicochemical properties and cytotoxic profile can be optimized by varying the N/P ratio and PEI molecular weight parameters. In addition to these PEI-based complexes, CPPs with mitochondrial targeting specificity, deeply studied in previous work for pND1 encapsulation and delivery [18], were also evaluated for mitochondrial gene delivery and protein expression. It was found that both polymeric and peptide/pND1 complexes promoted efficient transfection, with consequent gene expression and ND1 protein production in the mitochondria. Therefore, both nano-platforms can be further explored in the quest for a suitable gene delivery system to mediate mitochondrial gene therapy. Moreover, a comparison between polymeric and peptide/pND1 complexes revealed that the peptide-based ones—mainly due to their greater ability for pND1 complexation—displayed superior performance in terms of cellular uptake, gene delivery, and protein expression. Collectively, our results bring significant and relevant knowledge, instigating progress towards mitochondrial transfection mediated by pDNA complexes, as a powerful tool to fight against mitochondrial DNA diseases.

6.6 Supplementary Materials

Supporting Information for Chapter 6

6.6.1 Experimental Section

6.6.1.1 Fourier transform infrared spectroscopy

The functional groups present in the synthesized polymer were characterized by FTIR analysis using an FTIR (Jasco-4200, USA) by the KBr pellet method. The samples were prepared by triturating PEI-DQA (10, 25 KDa) and potassium bromide (KBr) at the weight ratio of 1:99, respectively, to form a pellet. The pellet was placed in the sample holder. FTIR spectra of samples were recorded by scanning pellets over a range of 4000 to 400 cm^{-1}.

6.6.1.2 Gel Permeation Chromatography (GPC)

Determination of the molecular weight of synthesized PEI-SA-DQA was carried out using gel permeation chromatography. Ultrahydrogel linear size exclusion column (7.8 mm ID × 300 mm × 6 µ) was used to elute the samples in the GPC system (Waters Alliance series). Water was used

as a mobile phase with a flow rate of 1 ml/min. The standard molecular weight compounds were run before analyzing the sample to plot the calibration curve.

6.6.1.3 Determination of Critical Micelles Concentrations (CMC)

CMC of PEI-DQA (10, 25 KDa) was assessed by pyrene incorporation method. Briefly, to glass vials containing 0.5 mg of pyrene, PEI-DQA (10, 25 KDa) solutions were added at various concentrations (3.125-150 µg/mL). The solution was shaken overnight for pyrene dissolution. The solutions were filtered using polycarbonate membranes (0.45 µm). The fluorescence was analyzed using a fluorescence plate reader (Spectramax, microplate reader, Molecular Devices, California, USA) at wavelengths λex 339 and λem 390 nm. CMC was calculated from the inflection point in the fluorescence (I339/I390) versus the log concentration graph.

6.6.1.4 Detection of ATP in mitochondria of HeLa cells

ATP produced in mitochondria of HeLa cells after transfection with peptide/pND1 complexes, at N/P ratio of 5, has been determined by using the Luminescent ATP detection kit from Abcam (ab113849; Abcam, Cambridge, UK), and following instructions provided by the manufacturer. This assay involved the lysis of the cell sample, the addition of luciferase enzyme and luciferin, followed by measurement of the emitted light. Briefly, the ATP standard was added to standard wells in the same plate containing control (untreated cells) and samples to be analyzed. After transfection with the various complexes, mitochondria of HeLa cells (1 x 10^4) were isolated from cytosol, transferred to 6-well plates (2 mL per well), and then the detergent solution was added followed by 5 min incubation, at room temperature, to lyse the cells and stabilize ATP. Then, substrate solution was added, incubated for 5 min at 25 °C, and plates were stored in the dark for 10 min. After, luminescence was quantified using a luminescence microplate reader (Molecular Devices, Sunnyvale, CA, USA).

6.6.2 Results

Table S6.1 - Gel Permeation chromatography data of the polymers.

Name	Mn	Mw	Mp	PDI	Number of molecules attached
PEI 25kDa	12759	24842	19429	1.946	-
PEI 25kDa-SA	22782	26523	29529	1.1640	17.97
PEI 25kDa-SA-DQA	25268	33092	19944	1.3096	12.45
PEI 10kDa	7832	9682	6523	1.3520	-
PEI 10kDa-SA	8875	11542	10256	1.4652	17.03
PEI 10kDa-SA-DQA	9469	17856	11452	1.0652	11.02

Table S6.2 - Average zeta potential, size and PdI for PEI-DQA (10 kDa or 25 kDa)/TAT/pND1, MTSCPP/pND1 and CpMTP/pND1 complexes.

PEI 10 kDa	Zeta Potential (mV)	Size (nm)	PdI
PEI-DQA/TAT/pND1 R10	-5.74 ± 0.11	478± 6	0.54 ± 0.03
PEI-DQA/TAT/pND1 R20	-4.56 ± 0.02	456 ± 3	0.53 ± 0.02
PEI-DQA/TAT/pND1 R50	-4.29 ± 0.36	447 ± 4	0.57 ± 0.04
PEI-DQA/TAT/pND1 R100	-3.97 ± 0.12	388 ± 7	0.61 ± 0.03
PEI-DQA/TAT/pND1 R200	-3.48 ± 0.28	361 ± 1	0.44 ± 0.02
PEI-DQA/TAT/pND1 R500	-2.94 ± 0.12	349 ± 4	0.43 ± 0.02
PEI 25 kDa			
PEI-DQA/TAT/pND1 R10	-4.60 ± 0.23	455 ± 6	0.61 ± 0.03
PEI-DQA/TAT/pND1 R20	-3.66 ±0.34	434 ± 4	0.56 ± 0.02
PEI-DQA/TAT/pND1 R50	-2.94 ±0.58	409 ± 7	0.50 ± 0.04
PEI-DQA/TAT/pND1 R100	-2.19 ±0.10	359 ± 4	0.42 ± 0.05
PEI-DQA/TAT/pND1 R200	+3.20 ±0.23	332 ± 5	0.41 ± 0.03
PEI-DQA/TAT/pND1 R500	+5.23 ±0.27	270 ± 6	0.41 ± 0.05
MTS-WRAP1 [18]			
MTS-WRAP1/pND1 N/P 1	-1.83 ± 0.90	406 ± 19	0.42 ± 0.06
MTS-WRAP1/pND1 N/P 2	+1.33 ± 0.75	366 ± 14	0.37 ± 0.02
MTS-WRAP1/pND1 N/P 3	+6.50 ± 0.76	276 ± 13	0.23 ± 0.01
MTS-WRAP1/pND1 N/P 5	+11.50 ± 0.76	197 ± 8	0.27 ± 0.02
MTS-WRAP5 [18]			
MTS-WRAP5/pND1 N/P 1	-2.17 ± 0.90	399 ± 12	0.49 ± 0.04
MTS-WRAP5/pND1 N/P 2	+7.17 ± 0.90	316 ± 10	0.22 ± 0.03
MTS-WRAP5/pND1 N/P 3	+10.83 ± 1.07	266 ± 8	0.36 ± 0.02
MTS-WRAP5/pND1 N/P 5	+19.33 ± 1.60	175 ± 11	0.30 ± 0.03
MTS-(KH)9 [18]			
MTS-(KH)9/pND1 N/P 1	+3.17 ± 0.69	400 ± 14	0.44 ± 0.03
MTS-(KH)9/pND1 N/P 2	+5.67 ± 0.75	366 ± 11	0.38 ± 0.03
MTS-(KH)9/pND1 N/P 3	+8.50 ± 0.50	309 ± 9	0.27 ± 0.04
MTS-(KH)9/pND1 N/P 5	+14.67 ± 0.75	220 ± 9	0.23 ± 0.01
CpMTP [18]			
CpMTP/pND1 N/P 1	+2.00 ± 0.58	402± 25	0.56 ± 0.05
CpMTP/pND1 N/P 2	+3.50 ± 0.50	385 ± 14	0.24 ± 0.04
CpMTP/pND1 N/P 3	+5.83 ± 0.69	313 ± 10	0.30 ± 0.02
CpMTP/pND1 N/P 5	+12.67 ± 0.75	236 ± 13	0.23 ± 0.02

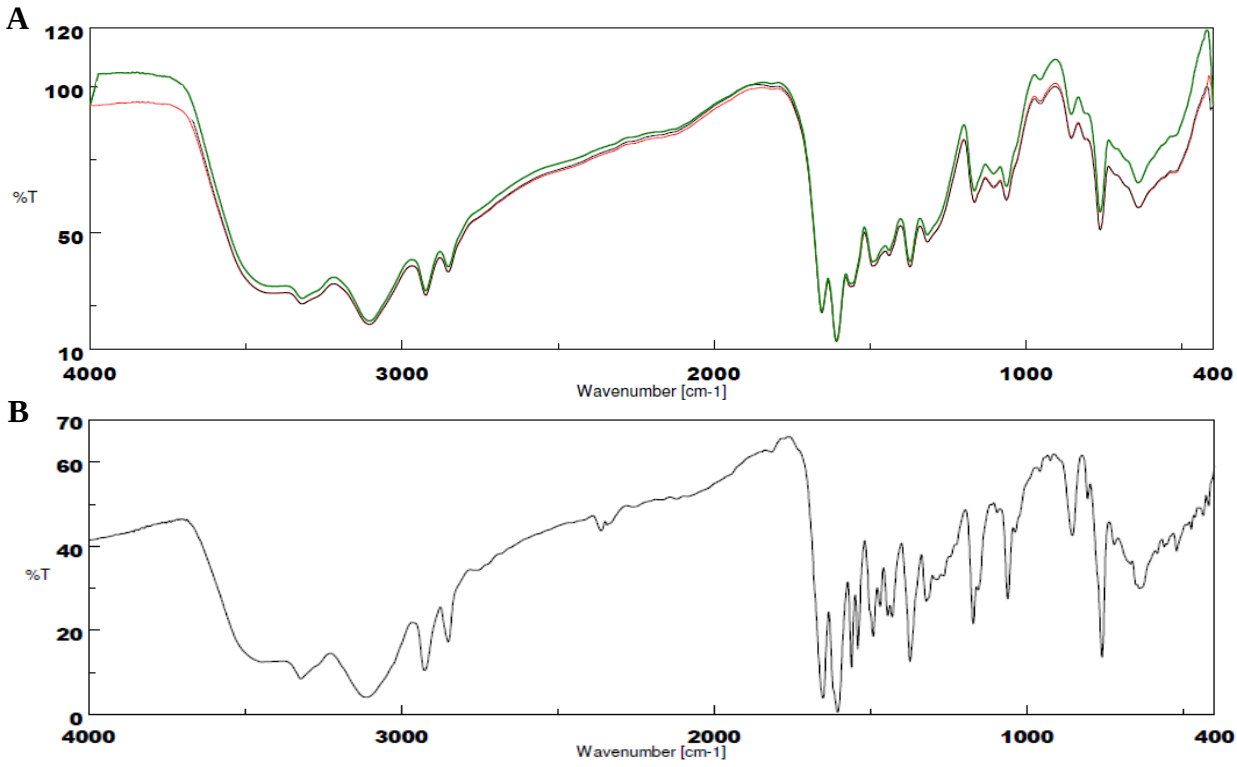

Figure S6.1 - FTIR spectra of PEI-DQA (10kDa green line and 25kDa red line) (A) and Dequalinium chloride (B).

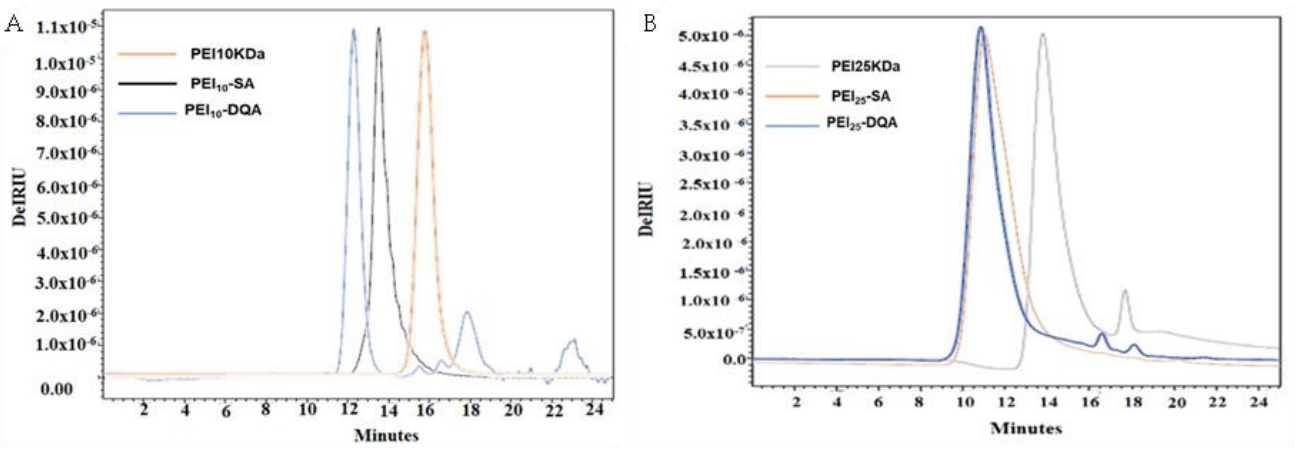

Figure S6.2 - GPC thermogram of PEI 10kDa, PEI 10kDa-SA, PEI 10kDa-DQA (A) and PEI 25kDa, PEI 25kDa-SA, PEI 25kDa-DQA (B).

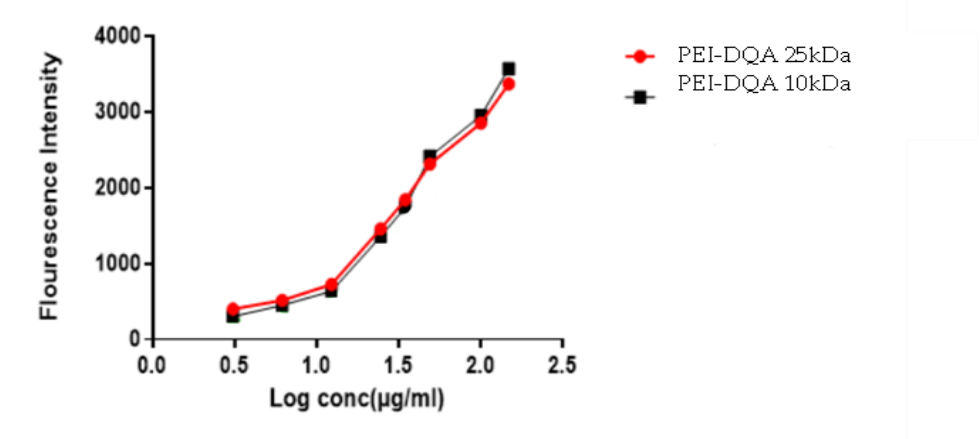

Figure S6.3 - CMC graph of PEI-DQA 25kDa and PEI-DQA 10kDa.

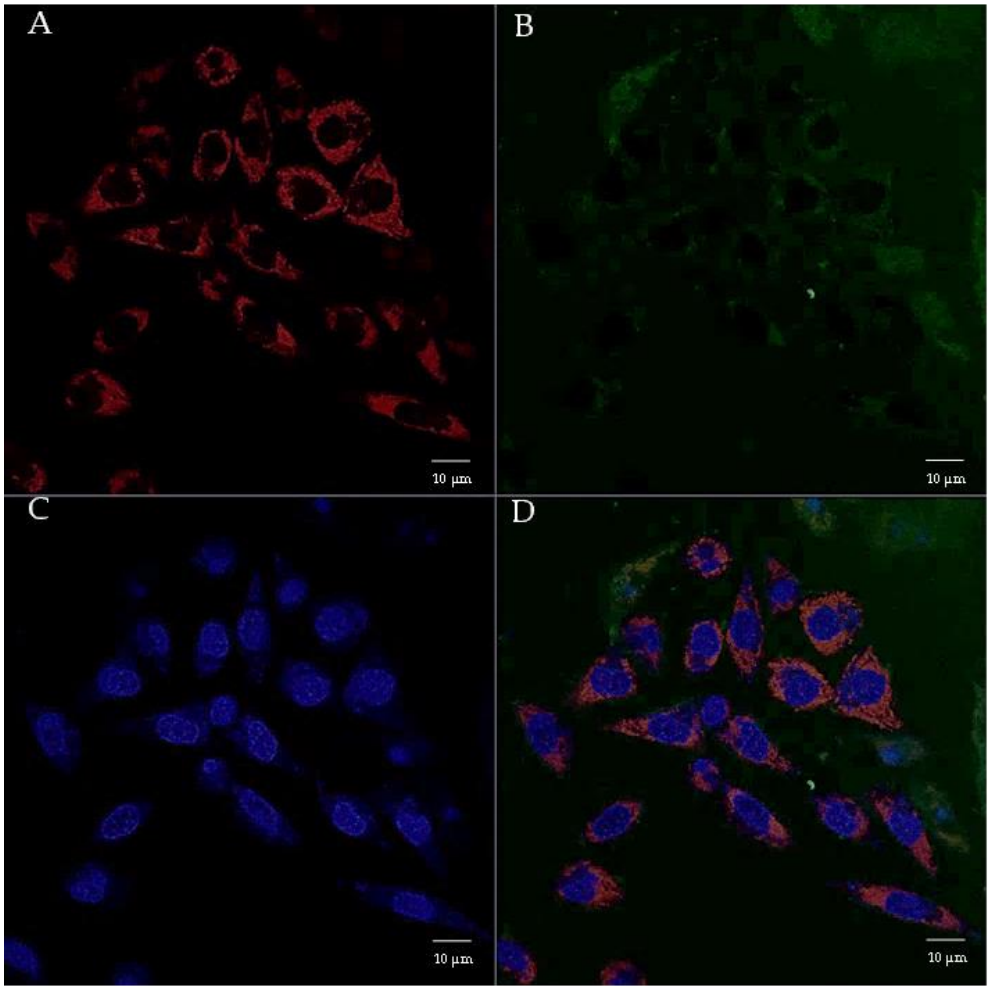

Figure S6.4 - Cellular uptake and intracellular co-localization of PEI-DQA (10kDa)/TAT/pND1 complexes formulated at N/P ratio of 20:2:1. Mitochondria stained red by MitoTracker (A) pND1 green labeled (B), Nucleus marked blue by DAPI (C) and Merged image (D).

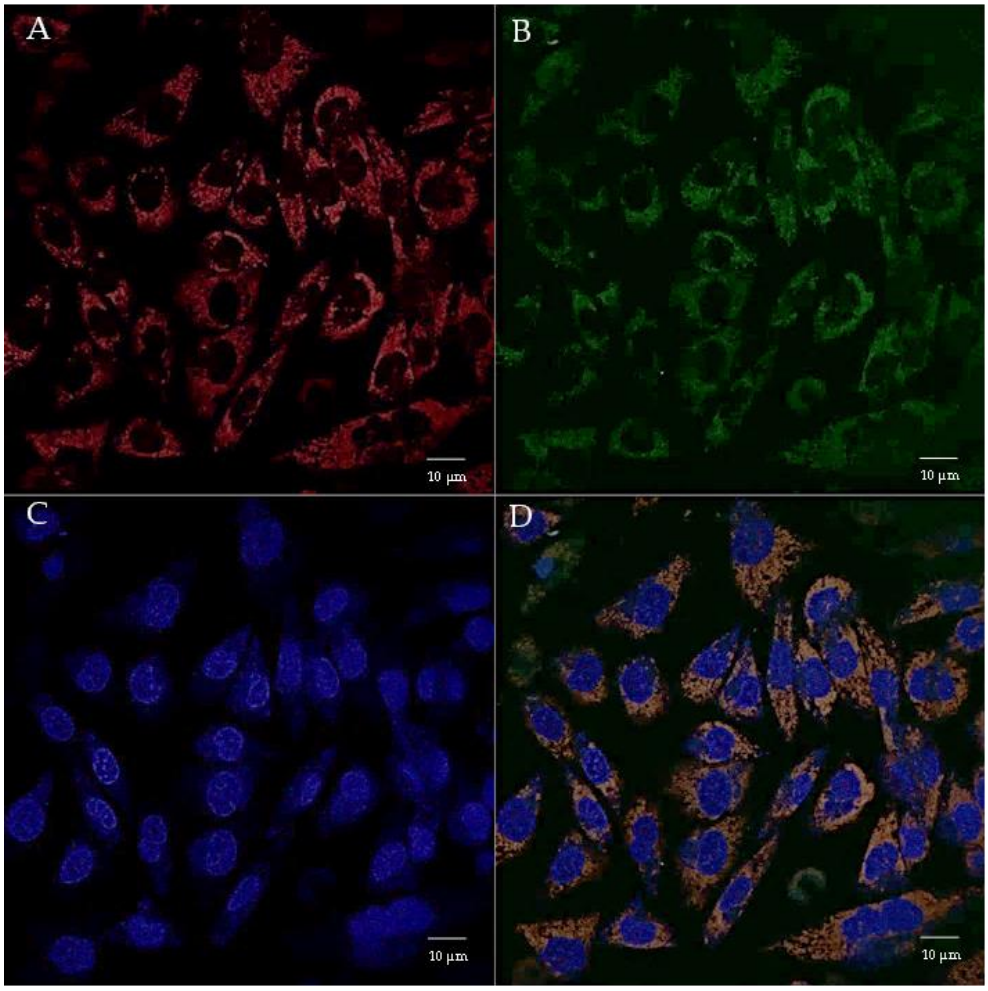

Figure S6.5 - Cellular uptake and intracellular co-localization of PEI-DQA (25kDa)/TAT/pND1 complexes formulated at N/P ratio of 20:2:1. Mitochondria stained red by MitoTracker (A) pND1 green labeled (B), Nucleus marked blue by DAPI (C) and Merged image (D).

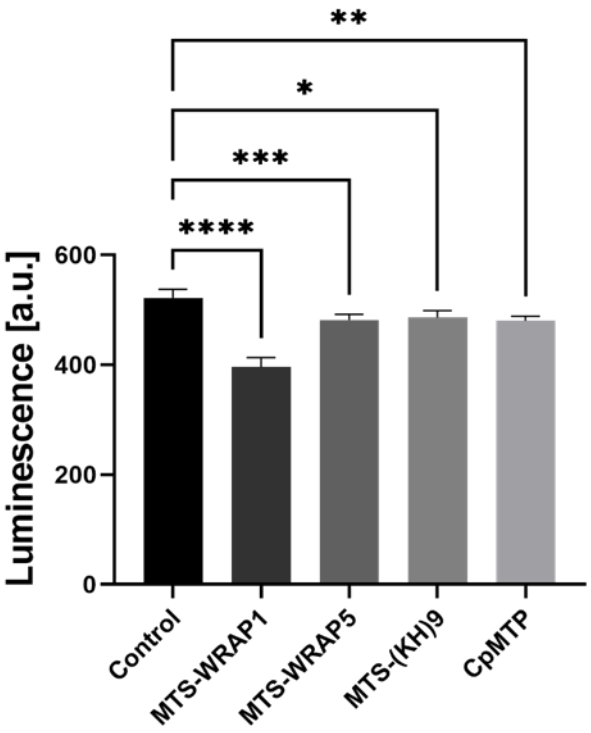

Figure S6.6 - Detection of ATP in mitochondria of HeLa cells after 48 h transfection mediated by MTSWRAP1/pND1, MTS-WRAP5/pND1, MTS-$(KH)_9$/pND1 or CpMTP/pND1 complexes, all prepared at N/P ratio of 5. Luminescence levels (arbitrary units, a. u.) were determined by using a ATP luminescence kit (ab113849). Non-transfected cells were used as control. The values were calculated with the data obtained from three independent measurements (mean ± SD, n = 3) and analyzed by oneway ANOVA followed by a Bonferroni test.

6.7 References

[1] Herst, P.M.; Rowe, M.R.; Carson, G.M.; Berridge, M.V. Functional Mitochondria in Health and Disease. Front. Endocrinol. 2017, 8, 296.

[2] Filograna, R.; Mennuni, M.; Alsina, D.; Larsson, N. Mitochondrial DNA copy number in human disease: The more the better? FEBS Lett. 2021, 595, 976–1002.

[3] Zhao, D.; Hong, D.; Zhang, W.; Yao, S.; Qi, X.; Lv, H.; Zheng, R.; Feng, L.; Huang, Y.; Yuan, Y.; et al. Mutations in mitochondrially encoded complex I enzyme as the second common cause in a cohort of Chinese patients with mitochondrial myopathy, encephalopathy, lactic acidosis and stroke-like episodes. J. Hum. Genet. 2011, 56, 759–764.

[4] Hertweck, K.; Dasgupta, S. The Landscape of mtDNA Modifications in Cancer: A Tale of Two Cities. Front. Oncol. 2017, 7, 262.

[5] Milenkovic, D.; Blaza, J.; Larsson, N.-G.; Hirst, J. The Enigma of the Respiratory Chain Supercomplex. Cell Metab. 2017, 25, 765–776.

[6] Filippi, M.-D.; Ghaffari, S. Mitochondria in the maintenance of hematopoietic stem cells: New perspectives and opportunities. Blood 2019, 133, 1943–1952.

[7] Mehta, M.; Weinberg, S.; Chandel, M.M.M.S.E.W.N.S. Mitochondrial control of immunity: Beyond ATP. Nat. Rev. Immunol. 2017, 17, 608–620.
[8] Javadov, S.; Kozlov, A.V.; Camara, A.K.S. Mitochondria in Health and Diseases. Cells 2020, 9, 1177.
[9] Popov, L. Mitochondrial biogenesis: An update. J. Cell. Mol. Med. 2020, 24, 4892–4899.
[10] Tiwari, M.; Prasad, S.; Tripathi, A.; Pandey, A.N.; Ali, I.; Singh, A.K.; Shrivastav, T.G.; Chaube, S.K. Apoptosis in mammalian oocytes: A review. Apoptosis 2015, 20, 1019–1025.
[11] Bock, F.J.; Tait, S.W.G. Mitochondria as multifaceted regulators of cell death. Nat. Rev. Mol. Cell Biol. 2020, 21, 85–100.
[12] Merino, D.; Kelly, G.L.; Lessene, G.; Wei, A.H.; Roberts, A.W.; Strasser, A. BH3-Mimetic Drugs: Blazing the Trail for New Cancer Medicines. Cancer Cell 2018, 34, 879–891.
[13] Roberts, A.W.; Davids, M.S.; Pagel, J.M.; Kahl, B.S.; Puvvada, S.D.; Gerecitano, J.F.; Kipps, T.J.; Anderson, M.A.; Brown, J.R.; Gressick, L.; et al. Targeting BCL2 with Venetoclax in Relapsed Chronic Lymphocytic Leukemia. N. Engl. J. Med. 2016, 374, 311–322.
[14] El-Hattab, A.W.; Zarante, A.M.; Almannai, M.; Scaglia, F. Therapies for mitochondrial diseases and current clinical trials. Mol. Genet. Metab. 2017, 122, 1–9.
[15] Pfeffer, G.; Majamaa, K.; Turnbull, D.M.; Thorburn, D.; Chinnery, P.F. Treatment for mitochondrial disorders. Cochrane Database Syst. Rev. 2012, 2012, CD004426.
[16] Siva, M.A.; Mahalakshmi, R.; Bhakta-Guha, D.; Guha, G. Gene therapy for the mitochondrial genome: Purging mutations, pacifying ailments. Mitochondrion 2019, 46, 195–208.
[17] Coutinho, E.; Batista, C.; Sousa, F.; Queiroz, J.; Costa, D. Mitochondrial Gene Therapy: Advances in Mitochondrial Gene Cloning, Plasmid Production, and Nanosystems Targeted to Mitochondria. Mol. Pharm. 2017, 14, 626–638.
[18] Faria, R.; Vivés, E.; Boisguerin, P.; Sousa, A.; Costa, D. Development of Peptide-Based Nanoparticles for Mitochondrial Plasmid DNA Delivery. Polymers 2021, 13, 1836.
[19] Yasuzaki, Y.; Yamada, Y.; Ishikawa, T.; Harashima, H. Validation of Mitochondrial Gene Delivery in Liver and Skeletal Muscle via Hydrodynamic Injection Using an Artificial Mitochondrial Reporter DNA Vector. Mol. Pharm. 2015, 12, 4311–4320.
[20] Vercauteren, D.; Rejman, J.; Martens, T.F.; Demeester, J.; De Smedt, S.C.; Braeckmans, K. On the cellular processing of non-viral nanomedicines for nucleic acid delivery: Mechanisms and methods. J. Control. Release 2012, 161, 566–581.
[21] Hirano, M.; Emmanuele, V.; Quinzii, C.M. Emerging therapies for mitochondrial diseases. Essays Biochem. 2018, 62, 467–481.
[22] Neves, A.R.; Sousa, A.; Faria, R.; Albuquerque, T.; Queiroz, J.; Costa, D. Cancer gene therapy mediated by RALA/plasmid DNA vectors: Nitrogen to phosphate groups ratio (N/P) as a tool for tunable transfection efficiency and apoptosis. Colloids Surf. B Biointerfaces 2020, 185, 110610.
[23] Gómez-Aguado, I.; Rodríguez-Castejón, J.; Vicente-Pascual, M.; Rodríguez-Gascón, A.; Del Pozo-Rodríguez, A.; Aspiazu, M. Ángeles, S. Nucleic Acid Delivery by Solid Lipid Nanoparticles Containing Switchable Lipids: Plasmid DNA vs. Messenger RNA. Molecules 2020, 25, 5995.
[24] Muhammad, K.; Zhao, J.; Gao, B.; Feng, Y. Polymeric nano-carriers for on-demand delivery of genes via specific responses to stimuli. J. Mater. Chem. B 2020, 8, 9621–9641.

[25] Wang, H.; Ding, S.; Zhang, Z.; Wang, L.; You, Y. Cationic micelle: A promising nanocarrier for gene delivery with high transfection efficiency. J. Gene Med. 2019, 21, e3101.
[26] Costa, D.; Albuqerque, T.; Queiroz, J.; Valente, A. A co-delivery platform based on plasmid DNA peptide-surfactant complexes: Formation, characterization and release behavior. Colloids Surf. B Biointerfaces 2019, 178, 430–438.
[27] Albuquerque, T.; Faria, R.; Sousa, Â.; Neves, A.R.; Queiroz, J.A.; Costa, D. Polymer-peptide ternary systems as a tool to improve the properties of plasmid DNA vectors in gene delivery. J. Mol. Liq. 2020, 309, 113157.
[28] Neves, A.R.; Albuquerque, T.; Faria, R.; Paul, M.; Biswas, S.; Sousa, Â.; Costa, D. Development of Tailor-Made Dendrimer Ternary Complexes for Drug/Gene Co-Delivery in Cancer. Pharmaceutics 2021, 13, 1256.
[29] Falanga, A.; Lombardi, L.; Galdiero, E.; Del Genio, V.; Galdiero, S. The world of cell penetrating: The future of medical applications. Future Med. Chem. 2020, 12, 1431–1446.
[30] Deshayes, S.; Konate, K.; Dussot, M.; Chavey, B.; Vaissière, A.; Van, T.N.N.; Aldrian, G.; Padari, K.; Pooga, M.; Vivès, E.; et al. Deciphering the internalization mechanism of WRAP:siRNA nanoparticles. Biochim. Biophys. Acta Biomembr. 2020, 1862, 183252.
[31] Sousa, Â.; Almeida, A.M.; Faria, R.; Konate, K.; Boisguerin, P.; Queiroz, J.; Costa, D. Optimization of peptide-plasmid DNA vectors formulation for gene delivery in cancer therapy exploring design of experiments. Colloids Surf. B Biointerfaces 2019, 183, 110417.
[32] Konate, K.; Dussot, M.; Aldrian, G.; Vaissière, A.; Viguier, V.; Neira, I.F.; Couillaud, F.; Vivès, E.; Boisguerin, P.; Deshayes, S. Peptide-Based Nanoparticles to Rapidly and Efficiently “Wrap ’n Roll” siRNA into Cells. Bioconjug. Chem. 2019, 30, 592–603.
[33] Khan, M.M.; Filipczak, N.; Torchilin, V.P. Cell penetrating peptides: A versatile vector for co-delivery of drug and genes in cancer. J. Control. Release 2021, 330, 1220–1228.
[34] Gessner, I.; Neundorf, I. Nanoparticles Modified with Cell-Penetrating Peptides: Conjugation Mechanisms, Physicochemical Properties, and Application in Cancer Diagnosis and Therapy. Int. J. Mol. Sci. 2020, 21, 2536.
[35] Derakhshankhah, H.; Jafari, S. Cell penetrating peptides: A concise review with emphasis on biomedical applications. Biomed. Pharmacother. 2018, 108, 1090–1096.
[36] Ruseska, I.; Zimmer, A. Internalization mechanisms of cell-penetrating peptides. Beilstein J. Nanotechnol. 2020, 11, 101–123.
[37] Bakar, L.M.; Abdullah, M.Z.; Doolaanea, A.A.; Ichwan, S.J.A. PLGA-Chitosan nanoparticle-mediated gene delivery for oral cancer treatment: A brief review. J. Phys. Conf. Ser. 2017, 884, 012117.
[38] Lellouche, E.; Locatelli, E.; Israel, L.L.; Naddaka, M.; Kurlander, E.; Michaeli, S.; Lellouche, J.-P.; Franchini, M.C. Maghemite-containing PLGA-PEG-based polymeric nanoparticles for siRNA delivery: Toxicity and silencing evaluation. RSC Adv. 2017, 7, 26912–26920.
[39] Piperno, A.; Sciortino, M.T.; Giusto, E.; Montesi, M.; Panseri, S.; Scala, A. Recent Advances and Challenges in Gene Delivery Mediated by Polyester-Based Nanoparticles. Int. J. Nanomed. 2021, 16, 5981–6002.

[40] Zhang, F.; Liao, X.; Zhang, G.; Mu, C. Dynamical Analysis of the Generalized Lorenz Systems. J. Dyn. Control Syst. 2017, 23, 349–362.
[41] Costa, D.; Briscoe, W.H.; Queiroz, J. Polyethylenimine coated plasmid DNA-surfactant complexes as potential gene delivery systems. Colloids Surf. B Biointerfaces 2015, 133, 156–163.
[42] Faria, R.; Sousa, Â.; Neves, A.R.; Queiroz, J.A.; Costa, D. Methotrexate-plasmid DNA polyplexes for cancer therapy: Characterization, cancer cell targeting ability and tuned *in vitro* transfection. J. Mol. Liq. 2019, 292, 292.
[43] Cheraghi, R.; Alipour, M.; Nazari, M.; Hosseinkhani, S. Optimization of conditions for gene delivery system based on PEI. Nanomedicine 2017, 4, 8–16.
[44] Benjaminsen, R.V.; Mattebjerg, M.A.; Henriksen, J.R.; Moghimi, S.M.; Andresen, T.L. The Possible "Proton Sponge" Effect of Polyethylenimine (PEI) Does Not Include Change in Lysosomal pH. Mol. Ther. 2013, 21, 149–157.
[45] Kaltimbacher, V.; Bonnet, C.; Lecoeuvre, G.; Forster, V.; Sahel, J.-A.; Corral-Debrinski, M. mRNA localization to the mitochondrial surface allows the efficient translocation inside the organelle of a nuclear recoded ATP6 protein. RNA 2006, 12, 1408–1417.
[46] Bonnet, C.; Kaltimbacher, V.; Ellouze, S.; Augustin, S.; Bénit, P.; Forster, V.; Rustin, P.; Sahel, J.-A.; Corral-Debrinski, M. Allotopic mRNA Localization to the Mitochondrial Surface Rescues Respiratory Chain Defects in Fibroblasts Harboring Mitochondrial DNA Mutations Affecting Complex I or V Subunits. Rejuvenation Res. 2007, 10, 127–144.
[47] Bonnet, C.; Augustin, S.; Ellouze, S.; Bénit, P.; Bouaita, A.; Rustin, P.; Sahel, J.-A.; Corral-Debrinski, M. The optimized allotopic expression of ND1 or ND4 genes restores respiratory chain complex I activity in fibroblasts harboring mutations in these genes. Biochim. Biophys. Acta 2008, 1783, 1707–1717.
[48] Ellouze, S.; Augustin, S.; Bouaita, A.; Bonnet, C.; Simonutti, M.; Forster, V.; Picaud, S.; Sahel, J.-A.; Corral-Debrinski, M. Optimized Allotopic Expression of the Human Mitochondrial ND4 Prevents Blindness in a Rat Model of Mitochondrial Dysfunction. Am. J. Hum. Genet. 2008, 83, 373–387.
[49] Korake, S.; Gajbhiye, K.R. Dequalinium-Derived Nanoconstructs: A Promising Vehicle for Mitochondrial Targeting. Curr. Drug Deliv. 2021, 18, 1056–1063.
[50] Chuah, J.-A.; Matsugami, A.; Hayashi, F.; Numata, K. Self-Assembled Peptide-Based System for Mitochondrial-Targeted Gene Delivery: Functional and Structural Insights. Biomacromolecules 2016, 17, 3547–3557.
[51] Lyrawati, D.; Trounson, A.; Cram, D. Expression of GFP in the Mitochondrial Compartment Using DQAsome-Mediated Delivery of an Artificial Mini-mitochondrial Genome. Pharm. Res. 2011, 28, 2848–2862.
[52] Weissig, V. DQAsomes as the Prototype of Mitochondria-Targeted Pharmaceutical Nanocarriers: Preparation, Characterization, and Use. Methods Mol. Biol. 2015, 1265, 1–11.
[53] Mallick, S.; Song, S.J.; Bae, Y.; Choi, J.S. Self-assembled nanoparticles composed of glycol chitosan-dequalinium for mitochondria-targeted drug delivery. Int. J. Biol. Macromol. 2019, 132, 451–460.

[54] Weissig, V.; Torchilin, V.P. Towards Mitochondrial Gene Therapy: DQAsomes as a Strategy. J. Drug Target. 2001, 9, 1–13.
[55] Zupančič, Š.; Kocbek, P.; Zariwala, M.G.; Renshaw, D.; Gul, M.O.; Elsaid, Z.; Taylor, K.M.G.; Somavarapu, S. Design and Development of Novel Mitochondrial Targeted Nanocarriers, DQAsomes for Curcumin Inhalation. Mol. Pharm. 2014, 11, 2334–2345.
[56] Wang, H.; Yin, H.; Yan, F.; Sun, M.; Du, L.; Peng, W.; Li, Q.; Feng, Y.; Zhou, Y. Folate-mediated mitochondrial targeting with doxorubicin-polyrotaxane nanoparticles overcomes multidrug resistance. Oncotarget 2014, 6, 2827–2842.
[57] Wang, Y.; Khan, A.; Liu, Y.; Feng, J.; Dai, L.; Wang, G.; Alam, N.; Tong, L.; Ni, Y. Chitosan oligosaccharide-based dual pH responsive nano-micelles for targeted delivery of hydrophobic drugs. Carbohydr. Polym. 2019, 223, 115061.
[58] Sun, Y.; Yang, Q.; Xia, X.; Li, X.; Ruan, W.; Zheng, M.; Zou, Y.; Shi, B. Polymeric Nanoparticles for Mitochondria Targeting Mediated Robust Cancer Therapy. Front. Bioeng. Biotechnol. 2021, 9, 755727.
[59] Faria, R.; Albuquerque, T.; Neves, A.R.; Bhatt, H.; Biswas, S.; Cardoso, A.M.; de Lima, M.C.P.; Jurado, A.S.; Costa, D. Physicochemical characterization and targeting performance of triphenylphosphonium nano-polyplexes. J. Mol. Liq. 2020, 316, 113873.
[60] Danaei, M.; Dehghankhold, M.; Ataei, S.; Hasanzadeh Davarani, F.; Javanmard, R.; Dokhani, A.; Khorasani, S.; Mozafari, M.R. Impact of Particle Size and Polydispersity Index on the Clinical Applications of Lipidic Nanocarrier Systems. Pharmaceutics 2018, 10, 57.

Chapter 7

Upgrading Mitochondria-Targeting Peptide-Based Nanocomplexes for Zebrafish *In Vivo* Compatibility Assays

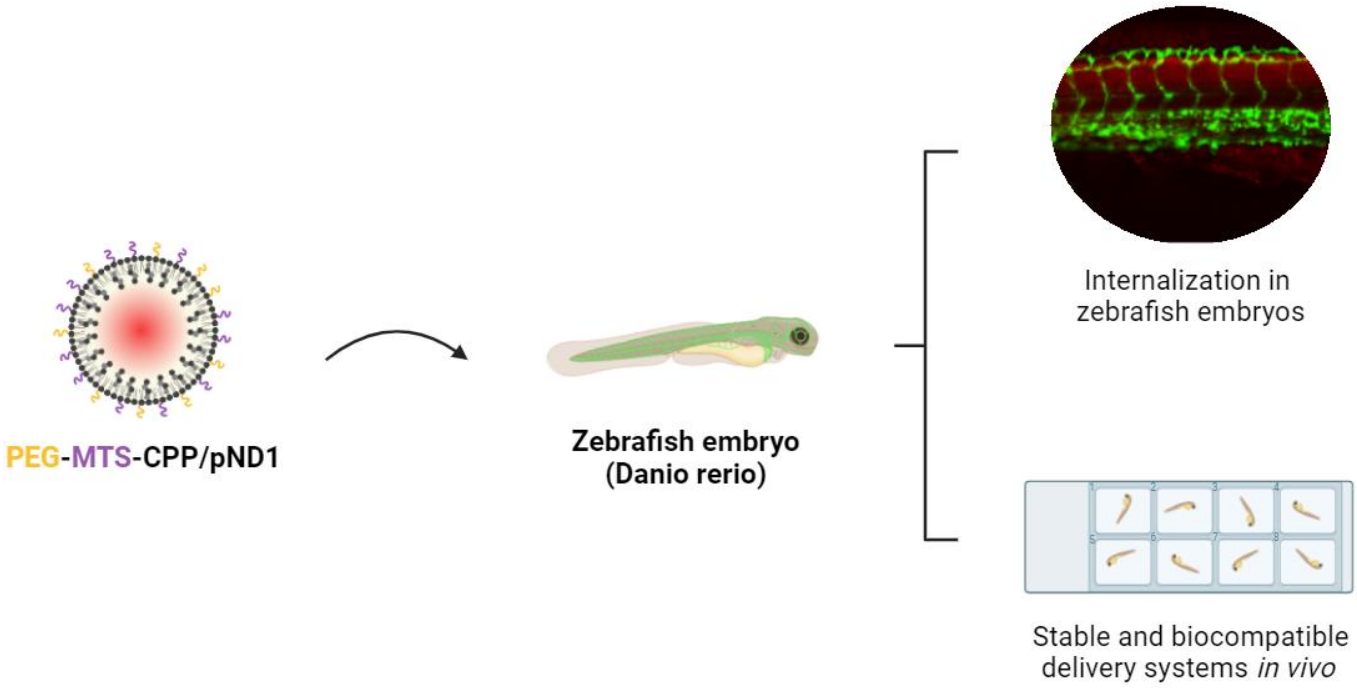

This chapter was published in:
Rúben Faria, Eric Vivès, Prisca Boisguérin, Simon Descamps, Ângela Sousa, and Diana Costa. 2024. ' Upgrading Mitochondria-Targeting Peptide-Based Nanocomplexes for Zebrafish *In Vivo* Compatibility Assays', Pharmaceutics, 16.
https://doi.org/10.3390/pharmaceutics16070961

7.1 Abstract

The lack of effective delivery systems has slowed the development of mitochondrial gene therapy. Delivery systems based on cell-penetrating peptides (CPPs) like the WRAP (tryptophan and arginine-rich peptide) family conjugated with a mitochondrial targeting sequence (MTS) have emerged as adequate carriers to mediate gene expression into the mitochondria. In this work, we performed the PEGylation of WRAP/pDNA nanocomplexes and compared them with previously analyzed nanocomplexes such as $(KH)_9$/pDNA and CpMTP/pDNA. All nanocomplexes exhibited nearly homogeneous sizes between 100 and 350 nm in different environments. The developed complexes were biocompatible and hemocompatible to both human astrocytes and lung smooth muscle cells, ensuring *in vivo* safety. The nanocomplexes displayed mitochondria targeting ability, as through transfection they preferentially accumulate into the mitochondria of astrocytes and muscle cells to the detriment of cytosol and lysosomes. Moreover, the transfection of these cells with MTS–CPP/pDNA complexes produced significant levels of mitochondrial protein ND1, highlighting their efficient role as gene delivery carriers toward mitochondria. The positive obtained data pave the way for *in vivo* research. Using confocal microscopy, the cellular internalization capacity of these nanocomplexes in the zebrafish embryo model was assessed. The peptide-based nanocomplexes were easily internalized into zebrafish embryos, do not cause harmful or toxic effects, and do not affect zebrafish's normal development and growth. These promising results indicate that MTS–CPP complexes are stable nanosystems capable of internalizing *in vivo* models and do not present associated toxicity. This work, even at an early stage, offers good prospects for continued *in vivo* zebrafish research to evaluate the performance of nanocomplexes for mitochondrial gene therapy.

Keywords

Cell-penetrating peptides; hemocompatibility; *in vivo* toxicity; mitochondria-targeting; peptide-based nanoparticles; Zebrafish embryo model

7.2 Introduction

Mitochondria are essential for the normal functioning of eukaryotic cells. These small organelles are involved in diverse cellular processes such as signaling, growth, and regulation of cell division and ion homeostasis or apoptosis mechanisms, among others [1,2]. However, the highlight is the role they play in energy production through the process of mitochondrial oxidative phosphorylation (OXPHOS). Inside mitochondria, energy is produced in the form of adenosine triphosphate (ATP) molecules [3–5]. This organelle is responsible for producing more than 90% of all energy produced within cells and it is considered the cell's engine [6]. In addition to their crucial importance in normal cellular functioning, mitochondria have a particular characteristic that they share with the nucleus: they have their own genome [7]. The mitochondrial genome (mtDNA) is composed of circular DNA molecules, which contain 37 genes encoding 13 proteins

that act as subunits of the OXPHOS enzymatic complexes, 22 transport RNA (tRNA) molecules, and 2 ribosomal RNA (rRNA) molecules [8,9].

Mutations in mtDNA are widespread compared to mutations in the nuclear genome. This is due to the much higher number of mtDNA molecules per cell than nuclear DNA and the absence of an effective repair mechanism and protective histones [10,11]. Mutations in mtDNA can induce a wide range of pathologies: neurodegenerative diseases (Alzheimer's, Parkinson's, and Amyotrophic Lateral Sclerosis (ALS)), metabolic dysfunctions (diabetes), hereditary diseases (Leber hereditary optic neuropathy (LHON), Huntington's disease), and various types of cancer [12–15]. Therapeutics currently available on the market only slow the progression of these diseases and do not provide an effective treatment [16,17]. Thus, there is a need to develop new therapeutic approaches. Since these diseases arise from gene alterations, mitochondrial gene therapy appears as a very promising and effective strategy [18].

Mitochondrial gene therapy has as its principle the replacement of mitochondrial genes to restore the normal function of the target gene [19,20]. To achieve this, it is necessary to use a delivery system that is capable of transporting and protecting the therapeutic genetic material and that delivers the mitochondrial gene directly to the mitochondria, enabling its expression [21,22]. One of the most explored genetic material delivery systems in recent years has been cell-penetrating peptides (CPPs). CPPs are peptides with fewer than 30 amino acids that have hydrophobic and hydrophilic domains, which confers the ability to conjugate with genetic material, forming nanoparticles capable of transfecting and internalizing into cells [23–26]. To confer specificity for mitochondria—a key step in mitochondrial gene therapy—some strategies have been explored, including the utilization of the 12-residue partial pre-sequence of yeast cytochrome c oxidase subunit IV (MLSLRQSIRFFK) [27–29].

Zebrafish (*Danio rerio*) is a vertebrate animal model increasingly applied in scientific research. Due to its characteristics, its application has been explored in the most diverse areas, from biomedicine and biotechnology to environmental science [30–33]. The main advantages of zebrafish (ZF) compared to other vertebrate models are the fact that it is an animal of small size, thus easy to maintain at low costs; its reproduction rate is high (each female releases an average of between 50 and 300 fertilized eggs); one-cell-stage fertilized eggs are easily genetically manipulated; its embryos and larvae are transparent; embryonic development occurs within 24 h and formation of the heart, intestine, and blood vessels within 48 h of fertilization. Furthermore, the ZF genome is approximately 70% similar to the human genome and its physiological processes including the development of the cardiovascular, nervous, and digestive systems are similar to those in humans [32,34]. Consequently, the ZF model has been widely considered in pre-clinical trials and the most varied toxicological studies [35–37].

In this work, our goal was to add PEG (polyethylene glycol) to the MTS–WRAP (tryptophan and arginine-rich peptide) delivery systems, determine their properties, evaluate their mitochondria targeting ability, and, ultimately, evaluate them in an *in vivo* model, namely their internalization capacity and toxicity in ZF embryos. The PEG-free MTS–WRAP–based complexes were tested *in vitro* in previous publications by our team, where we demonstrated excellent results from our

physicochemical and morphological characterization to the production of the target mitochondrial protein [29,38].

The PEG–WRAP conjugate was added to the formulation of MTS–WRAP nanocomplexes, using three different percentages (5%, 10%, and 20%), and compared to previously analyzed non-PEGylated nanocomplexes such as $(KH)_9$/pDNA and CpMTP/pDNA. PEG is a biocompatible polymer that can be linear or branched, whose main characteristics are that it increases the half-life of a therapeutic agent, increases the circulation time of the biomolecule to which it is conjugated, increases its hydrophilicity, and decreases the probability of agglomeration [39,40]. PEGylation of nanoparticles has been shown to increase their stability and consequently reduce the toxicity of delivery systems. PEGylation also reduces immunogenicity, increases the biological half-life of these therapeutic agents, and enables greater efficiency with smaller doses [41–43]. The developed PEG–MTS–WRAP nanocomplexes were demonstrated to be stable over time (up to 7 days after formulation), with sizes suitable for cellular transfection. Moreover, the complexes were biocompatible and hemocompatible and displayed the ability to transfect and internalize into ZF embryos, without causing toxicity. The results evidenced in this report indicate that the conceived peptide-based delivery systems possess a set of favorable assets being a valid option for mitochondrial gene therapy implementation, and should be considered for future *in vivo* studies with a view to potential clinical translation.

7.3 Materials and Methods

7.3.1 Materials

Milli-Q water, 1-phenyl 2-thiourea (PTU), and Tricaine powder were obtained from Sigma-Aldrich (Waltham, MA USA). ULYSIS Nucleic Acid Labeling Kit was obtained from Thermo Fisher Scientific Inc. (Waltham, MA USA). All peptides were synthesized using a LibertyBlue™ Microwave Peptide Synthesizer (CEM Corporation, Stallings, NC, USA) with an additional Discover™ module (CEM Corporation, Stallings, NC, USA) combining microwave energy at 2450 MHz to the Fmoc/tert-butyl (tBu) strategy. Peptide identity and purity were checked by LC-MS (Waters, Saint-Quentin-en-Yvelines, France). 3-(4,5-Dimethylthiazol-2-yl)-2,5-diphenyltetrazolium bromide (MTT), Triton X-100, and fluorescein isothiocyanate (FITC), isomer 1, were obtained from Sigma-Aldrich Chemicals (St. Louis, MO, USA). The plasmid pCAG-GFP-ND1 (5.4 kbp) (pND1) was developed by our research group through the cloning of the mitochondrial NADH dehydrogenase 1 protein-encoded gene (mtND1) in Escherichia coli. The details concerning ND1 gene cloning and plasmid production can be consulted elsewhere [44]. Human astrocyte cell line (HA1800), lung smooth muscle cells, normal, human (PCS-130-010), and human embryonic kidney (HEK293T) cells were obtained from the American Type Culture Collection (ATCC, Manassas, VA, USA).

7.3.2 Methods

7.3.2.1 Nanoparticle Formulation

The formulation of WRAP/pND1, MTS–WRAP/pND1, $(KH)_9$/pND1, MTS–$(KH)_9$/pND1, and CpMTP/pND1 nanoparticles was carried out as previously described [29,38]. The PEG nanoparticles were formulated using the same protocol mentioned above, however, the PEG-WRAP peptide was added in 3 different percentages (5%, 10%, and 20% of the total peptide amount) to formulate the respective vectors. All nanoparticles were formulated considering a nitrogen-to-phosphate groups ratio (N/P) of 5.

7.3.2.2. Particle Size Measurements

The average size of the nanoparticles was determined by Dynamic Light Scattering (DLS) using a Zetasizer Nano ZS (Malvern Instruments, Malvern, UK) equipped with Malvern Zetasizer software v6.34. DLS using a He–Ne laser 633 nm with non-invasive backscatter optics (NIBS) was applied for size determination. All results were obtained from three independent measurements (three runs for each measurement at 25 ◦C).

7.3.2.3. Cell Culture

HA1800 and HEK293T cells were cultured in Dulbecco's modified Eagle's medium (DMEM) containing 10% FBS. Primary lung smooth muscle cells were maintained in vascular cell basal medium (ATCC, PCS-100-030) supplemented with 5% heat-inactivated FBS, 5% L-glutamine, 0.5 mL penicillin-streptomycin-amphotericin B solution (penicillin 10 units/mL, streptomycin 10 µg/mL and amphotericin B 25 ng/mL), 5 ng/mL of basic fibroblasts growth factor (b-FGF), 5 ng/mL epidermal growth factor (EGF), 50 µg/mL of ascorbic acid, and 10 ng/mL of insulin. All cell lines were incubated at 37◦C and 5% CO_2 until ~80% of confluence was attained. Cells were sub-cultivated every 3 days to maintain their exponential growth and normal metabolism.

7.3.2.4. Cytotoxicity Evaluation

The cytotoxicity of the developed MTS–CPP/pND1 systems was evaluated in human astrocyte cells and lung smooth muscle cells using the MTT (3-[4,5-dimethyl-thiazol-2-yl]-2,5-diphenyltetrazolium bromide) assay. The assay was performed in 96-well plates at a density of 1 × 104 cells/well, where the cells were serum starved 12 h before the incubation with the nanoparticles. The cells were incubated with the nanoparticles (0.1 µg of pND1 per well), and the transfection was stopped 6 h later by changing the cell medium to complete medium (with serum). After 24 and 48 h of incubation with the systems, cell viability was assessed by reducing the MTT. For this, 20 µL of MTT solution with a concentration of 2 mg/mL was added to each well for 2 h. After that, the medium was removed and 200 µL of DMSO was added to each well for 30 min with shaking to dissolve the formazan crystals. Absorbance was measured using a Benchmark Microplate Reader (BioRad, Vienna, Austria) at 570 nm. The medium without cells was set as zero

absorbance and used for spectrophotometer calibration. Non-transfected and ethanol-treated cells were considered the positive and negative controls, respectively. The relative cell viability (%) related to control wells was calculated by [A]test/[A]control × 100, where [A]test is the absorbance of the test sample and [A]control is the absorbance of the positive control sample.

7.3.2.5. Hemolysis Test

In the hemolysis test, fresh rat blood was used, which was previously collected and stored in heparinized tubes containing EDTA disodium salt. Subsequently, red blood cells (RBCs) were isolated through centrifugation (3,000 rpm for 15 min at 4 ◦C). The RBCs were washed with 0.85% w/v NaCl solution until the solution became translucent. For the assay, the nanocomplexes (PEG–MTS–WRAP/pND1 and MTS–$(KH)_9$/pND1) and RBCs were resuspended in PBS (pH 7.4). A PBS-based solution containing 3–5% RBCs was prepared. 900 µL of this solution was used for each condition, where 100 µL of each of the delivery systems under study was subsequently incubated. The negative control was performed by adding 100 µL of PBS (pH 7.4) to 900 µL of the RBC solution while the addition of 100 µL of Triton X-100 (1%) was considered for the positive control. Incubation took place for 1 h at 37◦C. After incubation, the samples were centrifuged at 8000 rpm for 20 min at 4◦C. The supernatant obtained was analyzed by measuring its absorbance at 576 nm in a UV-vis spectrophotometer. The percentage of hemolysis was calculated using the following formula:

$$\text{Hemolysis (\%)} = \frac{\text{Abs. Sample} - \text{Abs. Negative control}}{\text{Abs. Positive control} - \text{Abs. Negative control}} \times 100 \qquad (1)$$

7.3.2.6. FITC Plasmid Staining

Plasmid DNA was stained with FITC by mixing 2 µg of pDNA, 2 µL of FITC (in sterile anhydrous dimethyl sulfoxide, 50 mg/100 µL), and 81 µL of labeling buffer (0.1 M Sodium Tetraborate, pH 8.5). Samples were left in the dark, under stirring for 4 h at 25°C. To stop the reaction, 2.5 volumes of 100% ethanol (212.5 µL) and one volume of 3 M NaCl (85 µL) were added. Samples with stained pDNA were precipitated at −20°C overnight. On the following day, samples were centrifuged (10,000× g, at 4°C) for 30 min. The pellet was recovered and washed with ethanol (75%) and used for the formation of PEG/MTS–peptide/pND1 complexes.

7.3.2.7. Cellular Organelle-Associated FITC Fluorescence

Human astrocytes and lung smooth muscle cells were cultured as described above. For cellular transfection, PEG/MTS–peptide/pND1-FITC (100 µL, pND1 = 1 µg) was added to each well. Untreated cells incubated with FITC and naked pND1 stained with FITC were used as controls. After 24 h, both cells were washed twice with PBS, and FITC-pND1 levels were measured in the transfected cells by fluorescence quantification. A fluorimeter plate reader was used to determine

FITC fluorescence considering the excitation and emission wavelengths of 495 nm and 525 nm, respectively. For each cell line, the protein content of each well was measured with a bicinchoninic acid (BCA) protein assay kit (BCA1-1KT, Sigma Aldrich Chemicals, St. Louis, MO, USA). Fluorescence/microgram protein readings were then determined by averaging the background corrected fluorescence of triplicate wells and dividing by the protein content per well. After transfection of human astrocytes and lung smooth muscle cells with the developed MTS–CPP/pND1–FITC complexes, the Mitochondria Isolation Kit for Cultured Cells (#89874, Thermo Fisher Scientific Inc., Rockford, IL, USA) was applied to promote the separation of mitochondria from the cytosol. The experimental protocol provided by the manufacturer has been followed, as described elsewhere [44]. In another set of transfected astrocytes and muscle cells, with the developed MTS–peptide/pND1–FITC complexes, lysosomes were isolated by using the Lysosome Isolation kit (LYSOSO 1) according to a protocol available from the supplier and as previously presented in the literature [45]. The protein levels of each cellular organelle were determined using the BCA protein assay kit. The use of this kit aids in correcting for cell density differences between different sets of experiments. The fluorescence of FITC–pND1 in each organelle sample was normalized with the amount of protein and expressed as fluorescence/μg protein.

7.3.2.8. ND1 Protein Quantification

Mitochondrial ND1 protein levels were quantified in human astrocyte, lung smooth muscle cells using an ND1 ELISA kit (Biomatik, EKL54820, Wilmington, DE, USA), as fully described in a previous publication by our research team [38]. After 48 h of transfection with the systems under study, the cells were collected and lysed. The determination of ND1 protein content was performed according to the protocol provided by the manufacturer, which includes the incubation of Reagent A for 1 h at 37 °C, followed by the addition of Reagent B. Then, an incubation was carried out with the TMB solution for 20 min at 37 °C, in the dark. Finally, the Stop solution was added to end the reaction. The ND1 levels were determined by absorbance at 450 nm in a Bio-Rad Microplate Reader Benchmark.

7.3.2.9. Zebrafish Breeding

Zebrafishes (*Danio rerio*) were raised and used according to standard laboratory protocols. Zebrafish care and use were performed following European Union guidelines for the handling of laboratory animals. All experiments were approved by the Comité d'Ethique pour l'Expérimentation Animale and the Direction Sanitaire et Vétérinaire de l'Hérault (Aquatic model facility, ZEFIX from CRBM C-34-172-39). Tg[fli1a:EGFP]y1 transgenic line was used with GFP-labelling of all endothelial cells [46]. ZF embryos were kept for 24 h in a dish (100 mm) in E3 medium (5 mM NaCl, 0.17 mM KCl, 0.33 mM $CaCl_2$, 0.33 mM MgSO4, 0.01 mg/L Methylene Blue) in an incubator at 28°C. Thereafter, the ZF embryos were dechorionated using sharp forceps and pre-selected for GFP protein expression using an M165 FC fully apochromatic correct-ed stereo microscope (Leica, Wetzlar, Germany). Dechorionated ZF embryos were maintained in an

E3 solution with 1-phenyl 2-thiourea (PTU, final concentration of 75 μM), to avoid pigmentation formation.

7.3.2.10. pDNA Fluorescence Labeling for *In Vivo* Assays

pND1 labeling was performed using Ulysis™ Alexa Fluor™ 594 Nucleic Acid Labeling Kit (Molecular Probes, Eugene, OR, USA). 1/10 volume of 3 M sodium acetate (pH 5.2) and 2 volumes of absolute ethanol were added to 1 μg of pDN1, placed at −80°C for 30 min, and then centrifuged for 15 min at 12,000 rpm to precipitate the plasmid. The pellet was washed with 70% ethanol and allowed to air dry. The pellet was resuspended with 20 μL of labeling buffer (provided in the kit) and then 1 μL of Alexa594 dye solution was added. Labeling buffer was used until 25 μL of final volume was reached. The reaction was incubated at 80°C for 15 min and at the end of this time, the reaction was stopped by placing the tubes on ice. The tubes were centrifuged with a MiniSpin to redeposit all contents at the bottom of the tube and the labeled pND1 was stored at 4°C.

7.3.2.11. Confocal Microscopy

To evaluate the transfection efficiency and internalization capacity of the MTS–CPP/pND1 systems in ZF embryos, the confocal microscopy technique was used. For this study, ZF embryos that expressed the fluorescent protein GFP were previously selected. For each condition, 6 zebrafish embryos were transferred in a glass chamber slide (LabTek, 4-chamber slide, Sigma-Aldrich) in a volume of 200 μL E3 + PTU. Each type of nanoparticle was formulated in 50 μL as described above using Alexa594-labelled pND1 (1 μg, final concentration) and added to the ZF embryos. After 24 h of transfection, ZF embryos were washed 3 times with PBS and fixed with 4% PFA in PBS for 20 min at room temperature with stirring. ZF embryos were washed 5 times with PBS and imaged by confocal microscopy on an inverted Zeiss LSM800 microscope using a 10×/0.30 lens. All confocal acquisitions were performed using a 488 nm diode laser with the specific GFP filter (486 nm–561 nm) and a 561 nm diode laser with a specific Alexa594 filter (592 nm–614 nm). A total of 15 images per sample were acquired using z-stack mode with a z-stack interval of 3 μm. Acquired images were analyzed using ImageJ software. Z-projection for each sample was performed by summing fluorescence intensities to one image.

7.3.2.12. Toxicity Test on Zebrafish Embryos

The test to evaluate toxicity was carried out 48 h after incubation of zebrafish embryos with the different nanoparticles under study. For each condition, 6 zebrafish embryos were transferred in a glass chamber slide (LabTek, 4-chamber slide, Sig-ma-Aldrich) in a volume of 200 μL E3 + PTU. Each type of nanoparticle was formulated in 50 μL as described above using 3 different pDNA amounts (1 μg, 2 μg, and 5 μg, final concentration) and added to the ZF embryos. After 48 h incubation at 28°C, ZF embryos were anesthetized with 0.02% Tricaine solution and imaged using an M165 FC fully apochromatic corrected stereo microscope (Leica, Wetzlar, Germany). All ZF

embryos were analyzed in terms of their development and morphology. The size of each ZF embryo was subsequently determined using ImageJ software.

7.3.2.13. Statistical Analysis

Data are presented as mean ± standard error of the mean. Statistically significant differences were evaluated by one-way analysis of variance (ANOVA), with Bonferroni's multiple comparison test. Data were analyzed using GraphPad Prism software, V9.0.0 (GraphPad Software Inc., New York, NY, USA). A p-value of <0.05 was considered statistically significant.

7.4 Results and Discussion

7.4.1 Effect of PEGylation on Nanocomplexes Formulation

CPPs have been widely explored for the delivery of therapeutic genetic material. Due to their physicochemical properties, it is possible to formulate stable nanocomplexes with some of the CPPs that protect nucleic acids until their delivery to target cells [47–49]. In previous articles, it was demonstrated that the addition of the MTS sequence into certain CPPs, namely WRAP1 (W1) and WRAP5 (W5) peptides, conferred specific targeting to the mitochondria, enabling the delivery of a mitochondrial gene into the target organelle [29,38]. In this work, we evaluated the effect of incorporating a polyethylene-glycol 2000 (PEG) moiety into these nanocarriers, to form more stable delivery systems compatible with an *in vivo* delivery such as in zebrafish (ZF) embryos (described here) or, later, in other animal models. Although PEG has recently been shown to be an immunogenic molecule in certain circumstances, its incorporation into delivery systems has been widely explored. PEG has been used successfully, improving the therapeutic efficacy of various delivery systems, namely liposome-based nanoparticles and PEGylated lipid nanoparticles (LNPs) in the field of mRNA-based vaccines [40,50].

The peptide nanocomplexes were formulated using the most suitable N/P ratio described in previous works (N/P ratio = 5 in water) [29,38] in which various percentages of PEG–CPPs were tested in the complex formulation (5%, 10%, and 20%). The results for the size and polydispersity index (PdI) of PEG–nanocomplexes are presented in **Table 7.1**. WRAP1-based complexes with 5% PEG display sizes around 200 nm, while with 20% PEG, the sizes are around 160 nm, with no significant changes when compared to the results obtained for WRAP1 systems without PEG ($p = 0.9933$). In the case of WRAP5 nanocomplexes with 5 to 20% PEG, the sizes vary from 114 nm to 99 nm on average, and there is a statistically significant change in relation to the sizes of the WRAP5/pND1 systems without PEG (*** $p < 0.001$), which have an average size of 186 nm.

Table 7.1 - Average size and PdI of peptide-based nanocomplexes at N/P = 5 after formulation in water.

WRAP1 Systems		
Systems	**Average Size (nm)**	**PdI**
WRAP1/pND1 [29]	161 ± 9	0.300 ± 0.023
5% PEG–WRAP1/pND1	197 ± 26	0.446 ± 0.089
10% PEG–WRAP1/pND1	124 ± 7	0.083 ± 0.129
20% PEG–WRAP1/pND1	160 ± 11	0.346 ± 0.061
WRAP5 Systems		
Systems	**Average Size (nm)**	**PdI**
WRAP5/pND1 [29]	186 ± 10	0.320 ± 0.030
5% PEG–WRAP5/pND1	114 ± 9	0.245 ± 0.064
10% PEG–WRAP5/pND1	101 ± 15	0.263 ± 0.036
20% PEG–WRAP5/pND1	99 ± 5	0.222 ± 0.061
MTS–WRAP1 Systems		
Systems	**Average Size (nm)**	**PdI**
MTS–WRAP1/pND1 [29]	197 ± 8	0.200 ± 0.020
5% PEG–MTS–WRAP1/pND1	58 ± 7	0.190 ± 0.016
10% PEG–MTS–WRAP1/pND1	57 ± 3	0.144 ± 0.013
20% PEG–MTS–WRAP1/pND1	65 ± 8	0.158 ± 0.020
MTS–WRAP5 Systems		
Systems	**Average Size (nm)**	**PdI**
MTS–WRAP5/pND1 [29]	175 ± 11	0.320 ± 0.030
5% PEG–MTS–WRAP5/pND1	173 ± 14	0.377 ± 0.049
10% PEG–MTS–WRAP5/pND1	167 ± 19	0.321 ± 0.034
20% PEG–MTS–WRAP5/pND1	93 ± 15	0.167 ± 0.086

Notes: Explanation of the formulations: 5% PEG–WRAP = 5% PEG–WRAP + 95% WRAP; 10% PEG–WRAP = 10% PEG–WRAP + 90% WRAP; 20% PEG–WRAP = 20% PEG–WRAP + 80% WRAP; 5% PEG–MTS–WRAP = 5% PEG–WRAP + 47.5% MTS–WRAP + 47.5% WRAP; 10% PEG–MTS–WRAP = 10% PEG–WRAP + 45% MTS–WRAP + 45% WRAP; 20% PEG–MTS–WRAP = 20% PEG–WRAP + 40% MTS–WRAP + 40% WRAP. All nanocomplexes were formulated at an N/P of 5, in water with 1 μg pND1. The values were determined with the data calculated from the acquisition of three independent experiments. Data were analyzed by one-way ANOVA followed by the Bonferroni test, $p < 0.05$ was considered statistically significant.

The PEG–MTS–WRAP1/pND1 vectors exhibit sizes around 60 nm for the three analyzed PEG percentages in the formulation, with no significant changes in terms of size when comparing the three different formulations to each other ($p \geq 0.05$). However, there is a significant size reduction (**** $p < 0.0001$) compared to the MTS–WRAP1/pND1 systems without PEG. The MTS–WRAP5/pND1 systems previously presented sizes of around 175 nm. The addition of PEG only significantly influenced the size of the nanoparticles when 20% PEG was added (*** $p < 0.001$), reducing the average size to values below 100 nm. The addition of 5% and 10% PEG did not cause significant changes in the average size of these systems ($p = 0.9955$ and $p = 0.7934$, respectively). Although there are some changes in complex sizes with the addition of PEG, all nanocomplexes have sizes below 200 nm and PdI remains below 0.4, demonstrating that the systems are

monodisperse and that they exhibit ideal physicochemical properties to be further evaluated by *in vitro* and *in vivo* studies.

7.4.2 Effect of PEGylation on Nanocomplexes Stability

The stability of PEG–peptide nanocomplexes was evaluated 24 h and 7 days after formulation. The results are summarized in **Table 7.2**. In detail, the complexes remained stable during the first 24 h, with no major fluctuations in terms of size. The PEG–WRAP1 nanocomplexes with 5% PEG maintained their size after 24 h of formulation ($p = 0.9912$), while those with 10% and 20% had a significant increase in size (**** $p < 0.0001$), which may indicate some thickness of the complexes over time resulting in particle growth. For the PEG–WRAP5 nanocomplexes, there was an increase in the sizes of those formulated with 5% PEG (*** $p < 0.001$) and for those with 10% and 20%, the sizes remained identical ($p = 0.9581$ and $p = 0.1533$, respectively). In contrast, the MTS-containing complexes (PEG–MTS–WRAP1 and PEG–MTS–WRAP5) showed average sizes after 24 h very similar to the sizes obtained after formulation. The PdI values indicated no loss of homogeneity during the first 24 h, with values remaining between 0.1 and 0.4.

Table 7.2 - Average size and PdI of peptide-based nanocomplexes formulated at N/P ratio = 5 measured at 24 h and at 7 days after formulation.

WRAP1 Systems				
Systems	**After 24 h**		**After 7 Days**	
	Mean Size (nm)	**PdI**	**Mean Size (nm)**	**PdI**
5% PEG–WRAP1/pND1	203 ± 9	0.402 ± 0.029	695 ± 53	0.592 ± 0.194
10% PEG–WRAP1/pND1	260 ± 15	0.346 ± 0.040	3161 ± 197	1.000 ± 0.000
20% PEG–WRAP1/pND1	448 ± 27	0.457 ± 0.115	978 ± 30	0.956 ± 0.028
WRAP5 Systems				
Systems	**After 24 h**		**After 7 Days**	
	Mean Size (nm)	**PdI**	**Mean Size (nm)**	**PdI**
5% PEG–WRAP5/pND1	233 ± 14	0.336 ± 0.093	320 ± 18	0.233 ± 0.055
10% PEG–WRAP5/pND1	96 ± 4	0.288 ± 0.045	1640 ± 143	1.000 ± 0.092
20% PEG–WRAP5/pND1	114 ± 10	0.252 ± 0.082	309 ± 22	0.409 ± 0.058
MTS-WRAP1 Systems				
Systems	**After 24 h**		**After 7 Days**	
	Mean SIZE (nm)	**PdI**	**Mean Size (nm)**	**PdI**
5% PEG–MTS–WRAP1/pND1	67 ± 5	0.211 ± 0.063	62 ± 17	0.215 ± 0.039
10% PEG–MTS–WRAP1/pND1	60 ± 9	0.161 ± 0.028	60 ± 11	0.174 ± 0.085
20% PEG–MTS–WRAP1/pND1	65 ± 11	0.136 ± 0.041	64 ± 14	0.134 ± 0.044
MTS-WRAP5 Systems				
Systems	**After 24 h**		**AFTER 7 Days**	
	Mean Size (nm)	**PdI**	**Mean Size (nm)**	**PdI**
5% PEG–MTS–WRAP5/pND1	82 ± 6	0.473 ± 0.158	85 ± 27	0.515 ± 0.100
10% PEG–MTS–WRAP5/pND1	253 ± 21	0.338 ± 0.099	291 ± 21	0.722 ± 0.167
20% PEG–MTS–WRAP5/pND1	73 ± 2	0.155 ± 0.071	197 ± 18	0.329 ± 0.072

Notes: Explanation of the formulations: 5% PEG–WRAP = 5% PEG–WRAP + 95% WRAP; 10% PEG–WRAP = 10% PEG–WRAP + 90% WRAP; 20% PEG–WRAP = 20% PEG–WRAP + 80% WRAP; 5% PEG–MTS–WRAP = 5% PEG–WRAP + 47.5% MTS–WRAP + 47.5% WRAP; 10%

PEG–MTS–WRAP = 10% PEG–WRAP + 45% MTS–WRAP + 45% WRAP; 20% PEG–MTS–WRAP = 20% PEG–WRAP + 40% MTS–WRAP + 40% WRAP. All nanocomplexes were formulated at an N/P of 5, in water with 1 μg pND1. The values were determined with the data calculated from three independent assays. Data were analyzed by one-way ANOVA followed by the Bonferroni test, $p < 0.05$ was considered statistically significant.

After 7 days, the PEG–WRAP1 and PEG–WRAP5 did not prove to be stable, dis-playing a dramatic increase in their average sizes to values above 300 nm (**** $p < 0.0001$). The loss of stability of these nanocomplexes was also reflected in the PdI parameter, with values higher than 0.4, even reaching 1. These PdI values indicate that the complexes are polydisperse and lose their stability over time. It is reasonable to assume that the complexes experienced aggregation into larger particles over time, and after 7 days, they may cluster and form macroscopic aggregates. In contrast, the nanocomplexes containing the MTS sequence presented stability in terms of sizes, with no major changes compared to the values at the time of formulation. The sizes for the MTS–PEG–WRAP1 complexes remained around 60 nm for the three considered percentages of PEG (all p-values ≥ 0.05) after 7 days. The MTS–PEG–WRAP5 complexes increased their average size slightly after 7 days, namely from 167 nm to 291 nm (** $p < 0.01$) for complexes with 10% PEG and from 93 nm to 197 nm for those with 20% PEG (*** $p < 0.001$). However, this size increases at 7 days post-formulation of the nano-complexes and does not preclude their use since the sizes remain below 300 nm.

7.4.3 Peptide-Based Nanocomplexes Are Stable in Saline Solution

According to the results presented in **Tables 7.1** and **7.2**, we found adequate evidence to focus our investigation on the WRAP complexes bearing 20% PEG, using these to perform the subsequent tests. As the purpose of the current study was, mainly, to test the developed peptide nanocomplexes on the zebrafish (ZF) model, we then evaluated the maintenance of the sizes and PdI of the complexes after resuspending in the saline E3 solution (zebrafish medium). These measurements aimed to verify the stability of the nanocomplexes in the ZF medium since the presence of salts can interfere with the electrostatic interaction between the peptides and pND1. The results for PEG-WRAP/pND1 or PEG-MTS-WRAP/pND1 were compared to previously analyzed non-PEGylated nanocomplexes such as $(KH)_9$/pDNA and CpMTP/pDNA.

The results presented in the Supplementary Material (SM), **Table S7.2**, demonstrate that all the analyzed CPP/pND1 complexes exhibited sizes of around 100 nm–250 nm, except for CpMTP/pND1, which presented sizes of around 350 nm. The same trend is reflected through the PdI values, showing that all nanocomplexes are homogeneous when resuspended in an E3 solution (PdI values between 0.2 and 0.4). Compared to the values in Table 1, the sizes of the PEGylated nanocomplexes are significantly larger (*** $p < 0.001$) when they are in contact with the E3 medium; however, this increase does not compromise the physicochemical properties of the complexes as the sizes remained below 275 nm. In the case of the non-PEGylated complexes, there was a slight increase in sizes for the CpMTP/pND1 systems (*** $p < 0.001$) when they were in E3 medium and a decrease in sizes in the $(KH)_9$ peptide-based systems (**** $p < 0.0001$) in E3

medium, compared to the sizes previously obtained in water [29]. Therefore, we can conclude that except for CpMTP/pND1 (size over 250 nm), all analyzed peptide-based complexes under study are stable when resuspended with an E3 solution, maintaining their size and homogeneity.

7.4.4 *In Vitro* Biocompatibility of Peptide-Based Nanocomplexes

The cytotoxicity of the PEG/MTS–CPP/pND1 nanocomplexes was evaluated using the colorimetric method of the MTT assay. Toxicity was assessed in two distinct cell lines, namely human astrocyte cell line and lung smooth muscle cells. Cell viability (%) was determined after 24 h and 48 h of cell incubation with the PEG/MTS–CPP/pND1 complexes (0.1 μg of pND1 per well), formulated at an N/P ratio of 5. Non-transfected cells were used as a positive control and cells treated with ethanol were considered the negative control. The cytotoxicity results for these two types of cells are presented in the graphs of **Figure 7.1**. The results of cellular viability of human astrocyte cells for 24 h and 48 h are shown in the graphs in **Figures 7.1A** and **7.1B**, respectively. Cell viability of human astrocytes transfected with the three different nanocomplexes is greater than 80% after 24 and 48 h. The viability of these cells was around 90% after 24 h when incubated with the PEG–MTS–WRAP1/pND1 nanocomplexes and 88.8% after 48 h. For the PEG–MTS–WRAP5/pND1 complexes, the viability of human astrocytes was 89% after 24 h and 88.4% after 48 h.

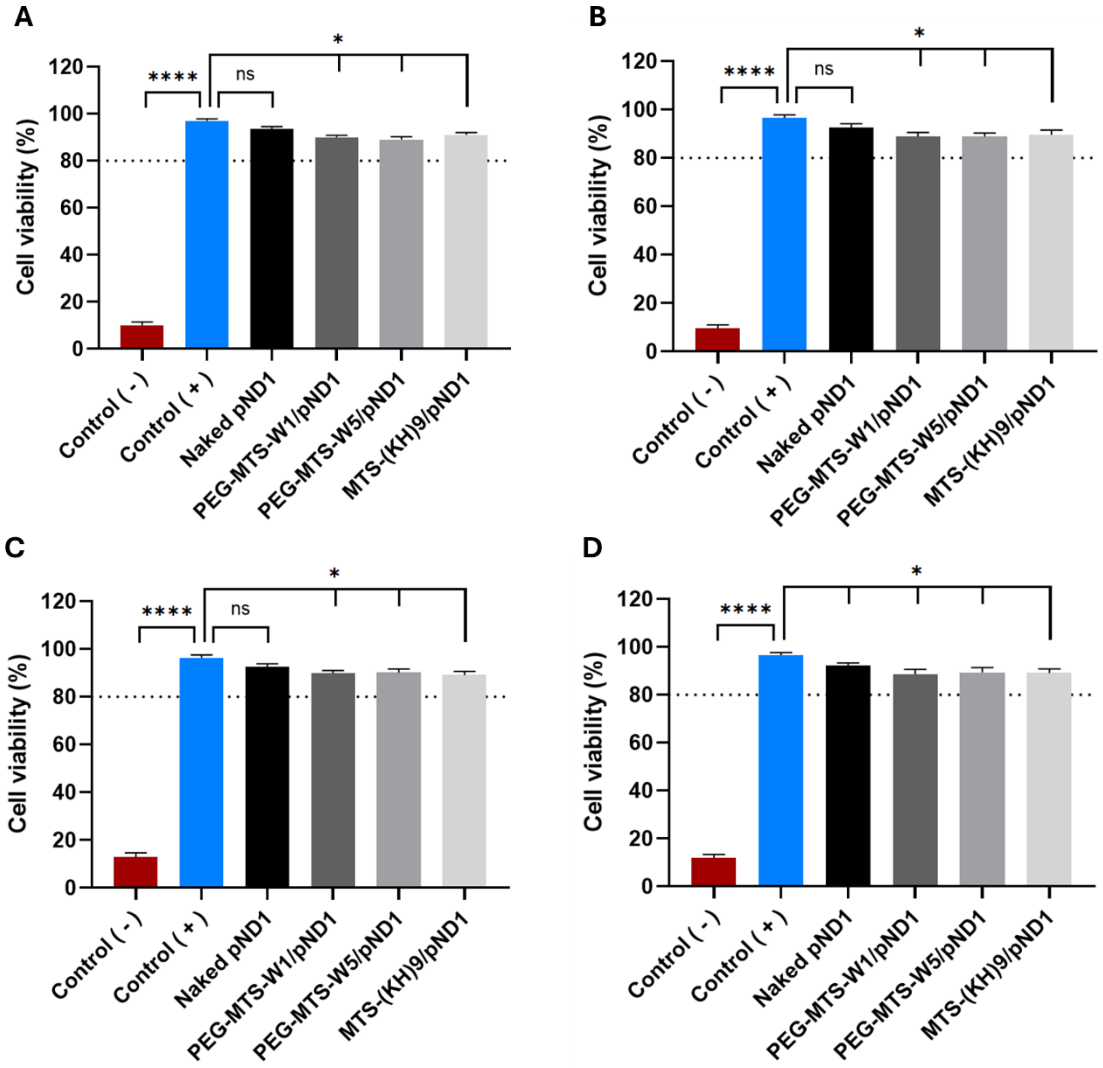

Figure 7.1 - Cellular viability of human astrocyte cells ((A) 24 h, (B) 48 h) and lung smooth muscle cells ((C) 24 h, (D) 48 h) after incubation with naked pND1 and the 20% PEG–MTS–WRAP1/pND1 (PEG–MTS–W1/pND1), 20% PEG–MTS–WRAP5/pND1 (PEG–MTS–W5/pND1) and MTS–$(KH)_9$/pND1 nanocomplexes formulated at N/P ratio of 5 (pND1 = 1 μg). Non-transfected cells were used as a positive control (Control (+)) and cells treated with ethanol were used as a negative control (Control (–)). Data were analyzed by one-way ANOVA with Bonferroni's multiple comparison test (ns—non-significant ($p > 0.05$); * $p < 0,05$; **** $p < 0.0001$).

In comparison, cells incubated with the MTS–$(KH)_9$/pND1 complexes showed a cell viability of 91% after 24 h and 89.7% after 48 h, similar to the WRAP complexes. The viability data in human astrocyte cells demonstrated that the three PEG/MTS–CPP/pND1 systems are not cytotoxic in this cell line, since cell viabilities are equal to or greater than 80%—an indication of the non-cytotoxic profile of compounds according to ISO 10993-5 [51,52].

The cellular viability results in lung smooth muscle cells are also presented in **Figure 7.1** (**Figure 7.1C** for 24 h and **Figure 7.1D** for 48 h). The results are very similar to those obtained in astrocytes. In lung smooth muscle cells transfected with the PEG–MTS–WRAP1/pND1

nanocomplexes, cell viability was 89.8% at 24 h and 88.6% at 48 h. In the case of cells incubated with PEG–MTS–WRAP5/pND1 complexes, viability at 24 h was 90.2% and at 48 h it was 89.3%. The viability for cells incubated with the MTS–$(KH)_9$/pND1 systems was 89.1% after 24 h and 88.9% after 48 h.

The results in **Figure 7.1** demonstrate that the developed peptide-based nanocomplexes are biocompatible and do not present significant cytotoxicity in the two cell lines studied. Therefore, these nanocomplexes can be considered secure and convenient delivery nanosystems to be further researched toward mitochondrial gene delivery approaches.

7.4.5. PEG/MTS-CPP/pND1 Nanocomplexes Do Not Cause Hemolysis

A hemolysis assay was carried out to consolidate the biocompatibility of these systems before moving on to toxicity tests in *in vivo* models. For this purpose, rat blood was used, wherein, RBCs were collected and subsequently incubated with the delivery systems. Two control groups were considered, a negative control in which PBS pH 7.4 was added and a positive control in which Triton X-100 was added. Triton X-100 detergent was chosen as a positive control as it was revealed in a previous study to be the best compound to cause hemolysis with more stable and reproducible results [53]. The hemolysis rate results are shown in **Figure 7.2**. For nanosystems to be considered non-hemolytic and to be used in medical applications, according to the ISO/TR 7406 standard, their hemolysis rate must be less than 5% [54]. The two PEG–MTS–CPP/pND1 nanocomplexes presented very low hemolysis rates (2.30% for PEG–MTS–WRAP1/pND1 and 3.75% for PEG–MTS–WRAP5/pND1). In comparison, the MTS–$(KH)_9$/pND1 nanocomplex has a hemolysis rate of 1.25%. Using the one-way ANOVA test, we verified that there is no statistically significant difference between the hemolysis percentages of RBCs incubated with the three types of system when compared to the negative control (RBCs incubated with PBS). The hemolysis percentages indicated that the PEG/MTS peptide-based nanocomplexes under study have good blood biocompatibility, a very promising result concerning the biosafety of these complexes for *in vivo* applications.

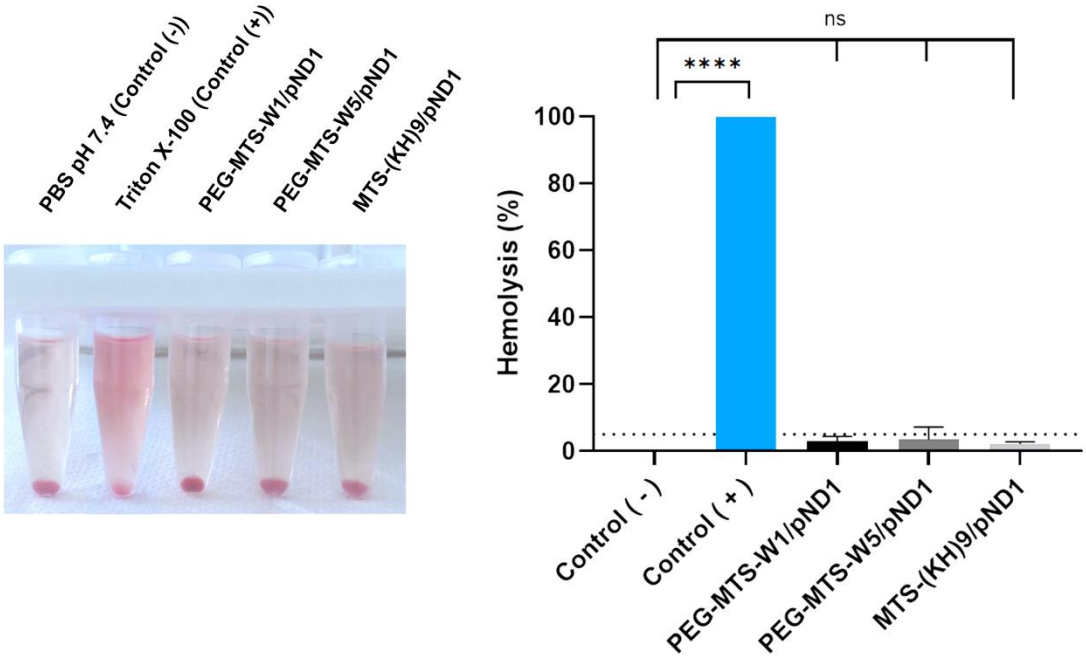

Figure 7.2 - *In vitro* hemolysis assay using rat red blood cells (RBCs), which were incubated with 20% PEG–MTS–WRAP1/pND1, 20% PEG–MTS–WRAP5/pND1, and MTS–$(KH)_9$/pND1 (1 μg of pND1, N/P ratio = 5). The negative control was incubated with PBS pH 7.4, while in the positive control, RBCs were incubated with Triton X-100 (1%) to provoke hemolysis. The hemolysis percentages were calculated according to Formula (1). Data are presented as mean (%) ± SD (n = 3). Data were analyzed by one-way ANOVA with Bonferroni's multiple comparison test (ns—non-significant ($p > 0.05$); **** $p < 0.0001$).

7.4.6 Mitochondria Targeting Capacity of PEG/MTS–CPP/pND1 Complexes

The cellular uptake of the developed PEG–MTS–WRAP/pND1–FITC complexes and their accumulation into different cellular organelles have been evaluated by monitoring the organelle-associated FITC fluorescence, 24 h after transfection mediated by these carriers. Non-transfected cells were used as control. **Figure 7.3** summarizes the obtained data for human astrocytes (**Figure 7.3A**) and lung smooth muscle cells (**Figure 7.3B**). The results demonstrated the cellular uptake of the conceived peptide nanocomplexes into both cells; however, with FITC fluorescence levels being detected to a very different extent depending on the organelle. For both cells, a strong accumulation of all the PEG–MTS–WRAP/pND1–FITC complexes into the mitochondria was observed compared with the correspondent accumulation of the complexes into the lysosomes or the cytosol (for all cases: **** $p < 0.0001$). For astrocytes, the FITC fluorescence intensity in the lysosomes was, however, statistically significant in comparison with the control cells for the transfection mediated by both PEG–MTS–WRAP1/pND1–FITC, *** $p < 0.001$, and PEG–MTS–WRAP5/pND1–FITC, ** $p < 0.01$ (**Figure 7.3A**). This indicates that a minor amount of WRAP1- and WRAP5-based complex accumulation into the lysosomes of

astrocytes cannot be excluded. On the contrary, for these cells, the FITC fluorescence detected in the cytosol showed no statistically significant differences (ns) in comparison with the control cells.

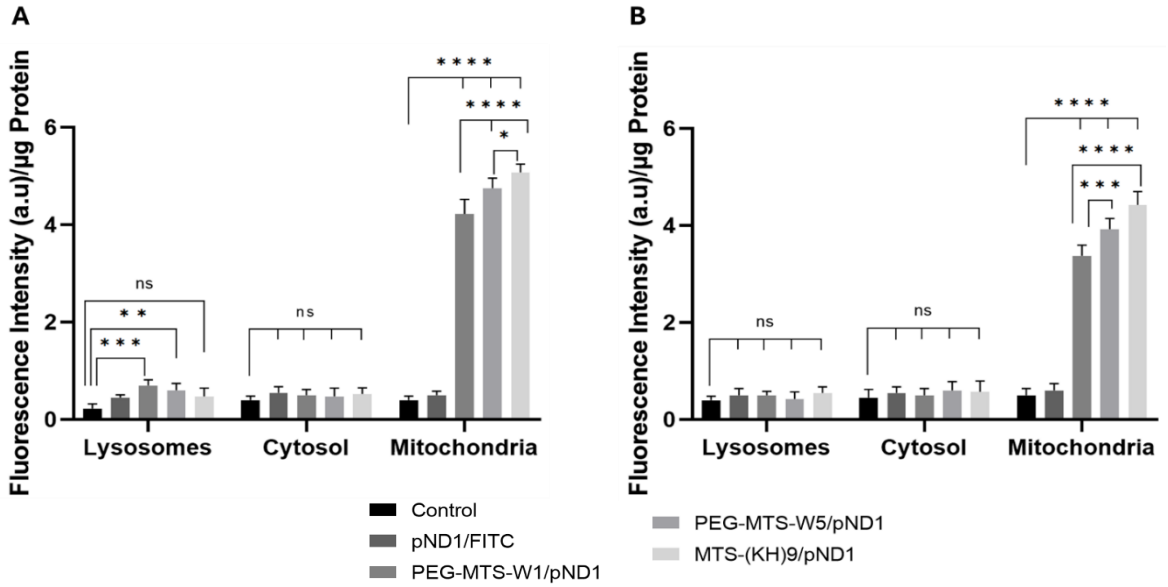

Figure 7.3 - Quantification of FITC fluorescence intensity ((a.u)/µg Protein) in the lysosomes, cytosol, and mitochondria of human astrocyte cells (A) and lung smooth muscle cells (B), after 24 h of transfection with 20% PEG–MTS–WRAP1/pND1 (PEG–MTS–W1/pND1), 20% PEG–MTS–WRAP5/pND1 (PEG–MTS–W5/pND1) and MTS–$(KH)_9$/pND1 systems. All complexes were formulated with an N/P ratio = 5 (pND1 = 1 µg). Untreated cells and naked pND1 stained with FITC were used as controls. Data were analyzed by two-way ANOVA with a Bonferroni's multiple comparison test (ns—non-significant ($p > 0.05$); * $p < 0.05$; ** $p < 0.01$; *** $p < 0.001$; **** $p < 0.0001$).

Concerning the MTS–$(KH)_9$/pND1 complex, no FITC fluorescence accumulation is observed in the lysosomes or the cytosol, but a significantly higher accumulation is observed in the mitochondria compared to that observed with PEG–MTS–WRAP/pND1.

For lung muscle cells, the FITC fluorescence intensity in both lysosomes and cytosol was comparable to the FITC levels found in the control cells and no statistically significant differences (ns) were found (**Figure 7.3B**). For both cells, it becomes clear that peptide-based nanocomplexes are internalized by the cells and efficiently target mitochondria, with variations in the FITC fluorescence intensity between the three studied carriers. The mitochondria accumulation increased in the order MTS–$(KH)_9$/pND1 > PEG–MTS–WRAP5/pND1 > PEG–MTS–WRAP1/pND1 complexes. However, in some cases the differences were low (please consult the statistical analysis available in **Figure 7.3**), which may reflect the different transfection efficiency displayed by the nanocomplexes, which may consequently influence the subsequent process of protein expression into mitochondria.

7.4.7 Peptide-Based Complexes Increase ND1 Levels *In Vitro*

The demonstrated mitochondria-targeting ability of the developed PEG/MTS–CPP/pND1 complexes enriches their value as carriers for gene delivery into this organelle. To confirm the potential for mitochondrial protein expression, the ND1 protein levels after 48 h of transfection of astrocytes and lung muscle cells mediated by these complexes were determined. As explained in the experimental section, in this assay, an Elisa Kit was employed, and non-transfected cells were considered as control. The results are presented in **Figure 7.4**. ND1 is an endogenous gene, and, therefore, this fact can explain the ND1 protein levels found in the control cells. The content of this mitochondrial protein can be considerably increased when both cells are transfected with the studied PEG/MTS–peptide/pND1 nanocomplexes. As observed in **Figure 7.4A, B**, there are statistically significant differences between each of the complexes and the control astrocytes and muscle cells: for both cells, **** $p < 0.0001$. This revealed the capacity of the conceived nanocomplexes to target mitochondria, release into this organelle the genetic carried content and, ultimately, produce the correspondent mitochondrial ND1 protein. The ND1 protein is a subunit of NADH dehydrogenase, which is located in the mitochondrial inner membrane and is the largest of the five complexes of the electron transport chain.

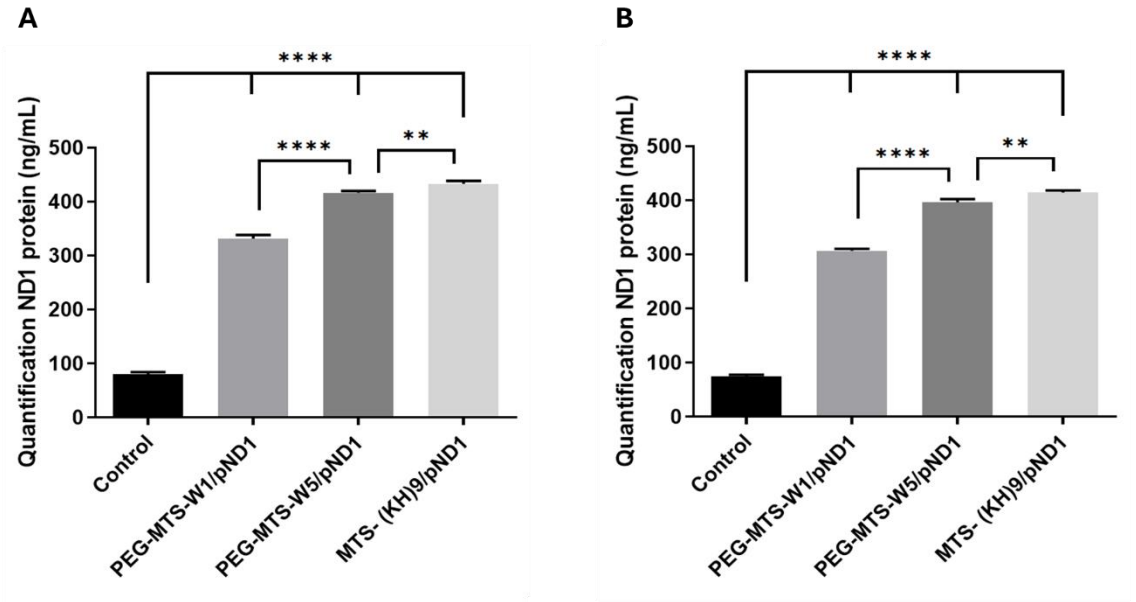

Figure 7.4 - Quantification of ND1 protein levels (ng/mL) in human astrocyte cells (A) and lung smooth muscle cells (B), after 48 h of transfection with 20% PEG–MTS–WRAP1/pND1 (PEG–MTS–W1/pND1), 20% PEG–MTS–WRAP5/pND1 (PEG–MTS–W5/pND1), and MTS–$(KH)_9$/pND1 systems (pND1 = 1 μg for all). All complexes were formulated with an N/P ratio = 5. Data were analyzed by one-way ANOVA with Bonferroni's multiple comparison tests (** $p = 0.0041$ (A) and 0.0015 (B); **** $p < 0.0001$).

In detail, among the formulated complexes, and for both cells, PEG–MTS–WRAP1/pND1 was the system leading to the lowest produced ND1 content (**** $p<0.0001$ for PEG–MTS–WRAP1/pND1 versus PEG–MTS–WRAP5/pND1, **Figure 7.4**). However, for astrocytes and muscle cells, the MTS–$(KH)_9$/pND1 complexes were the complexes leading to the superior ND1 protein levels compared to both PEG–MTS–WRAP/pND1 complexes. These observations can be correlated with the different transfection efficiency (**Figure 7.3**) displayed by the complexes, with implications in the extent of ND1 protein expression. The results presented in this work agree well with previous research focused on the transfection behavior of PEG-free CPP-based complexes, where ND1 protein levels were monitored in both HeLa and fibroblast cells [38].

7.4.8 Peptide Nanocomplexes Efficiently Internalize in Zebrafish Embryos

After confirming that peptide-based nanocomplexes possess physicochemical properties suitable for cellular transfection, are biocompatible to cells, stable in both water and E3 saline solution, target mitochondria, and are able of ND1 protein expression, the next step was to evaluate their transfection efficiency and internalization capacity in a dechorionated zebrafish embryo *in vivo* model. The choice of ZF to carry out these tests is, mainly, because this *in vivo* model is easy to reproduce, with a small size, and a large number of descendants [37,55]. Furthermore, the fact that it is possible to obtain optically transparent embryos is essential to be able to visualize and analyze the internalization of the delivery systems that are intended to be tested [56]. The use of embryos has advantages compared to the use of adult ZF since it is considered that the embryos do not feel pain or other types of discomfort [57].

To evaluate the internalization of the developed peptide nanocomplexes, a confocal microscopy study was conducted. To adequately use this technique, pND1 was labeled with an Alexa-594 dye (pND1–Alexa594) before complex formulation. To evaluate the labeling of pND1 and monitor the transfection capacity of the MTS–CPP/pND1–Alexa594 complexes, a small test was carried out on HEK293T-GFP cells before moving to studies with ZF. HEK293T-GFP cells were incubated with pND1–Alexa594 and with the MTS–WRAP1/pND1–Alexa594 complexes. The results of incubation in HEK293T-GFP cells are presented in Supplementary Materials, **Figure S7.1**. From the analysis of **Figure S7.1**, we can observe that the incubation of pND1 labeled with Alexa594 in cells (**Figure S7.1B**) only resulted in a few points of plasmid accumulation (red signal). However, these points of pND1 accumulation are located outside the cells, with no overlapping of the pND1 fluorescence with the fluorescence of the GFP protein (green signal) present in the cytoplasm nor with the fluorescence of the cell nucleus labeling with DAPI (blue signal). In the case of HEK293T-GFP cells incubated with the MTS–WRAP1/pND1–Alexa594 complexes (Figure S1C), there were also points of accumulation of pND1 (red signal), however, the fluorescent signal is mainly located within the cytoplasm of the cells. The accumulation of pND1 inside the cells reveals that the MTS–WRAP1/pND1–Alexa594 complexes were able to transfect and internalize in these cells and that the labeling of pND1 with the Alexa594 probe allows, through confocal microscopy, effective visualization of the location and distribution of these

nanocomplexes. Moreover, to confirm that PEG–MTS–CPP/pND1 complexes target the mitochondria of HEK293T cells and mediate gene/protein expression, ND1 protein levels were quantified after transfection of these cells with the developed carriers. The results for ND1 content can be consulted in Supplementary Materials, **Figure S7.2**. For the transfection mediated by the developed complexes, high ND1 levels were obtained in comparison with the control cells (**** $p < 0.0001$). This proves not only the mitochondria targeting skill exhibited by the MTS–CPP/pND1 complexes but also their successful role in promoting ND1 protein expression.

After verifying that the labeling of pND1 with the Alexa594 probe makes it possible to monitor and confirm the internalization and mitochondria targeting ability of the nanocomplexes, studies to evaluate the transfection and internalization capacity of the peptide-based complexes in ZF embryos were performed. For a better visualization, GFP-expressing ZF embryos were selected. Using the confocal microscopy technique, images of the embryos were obtained 24 h after transfection with the nanocomplexes under study. The results of transfection and internalization of the PEG–MTS–WRAP1/pND1 and PEG–MTS–WRAP5/pND1 compared to MTS–$(KH)_9$/pND1 nano-complexes are shown in **Figure 7.5**. The images in **Figure 7.5A-C** demonstrated that the 20% PEG–MTS–WRAP1/pND1 complexes were able to internalize in zebrafish embryos in a dose-dependent manner. At 2 μg of pND1–Alexa594, we observed a dotted ac-cumulation of red dots, especially on the dorsal fin of the ZF embryo. In contrast, at 1 μg, a more homogeneous and diffuse distribution throughout the embryo body was observed, whereas at 0.5 μg, no more red fluorescence was shown. For the 20% PEG–MTS–WRAP5/pND1 complexes, at 2 μg, we observed a combination of dots and homogeneous distribution through the ZF embryos (**Figure 7.5D**). The internalization of MTS-$(KH)_9$/pND1 nanocomplexes (**Figure 7.5E**) revealed a homogeneous and diffuse distribution at 2 μg comparable to that observed for 20% MTS–PEG–WRAP1/pND1 at 1 μg.

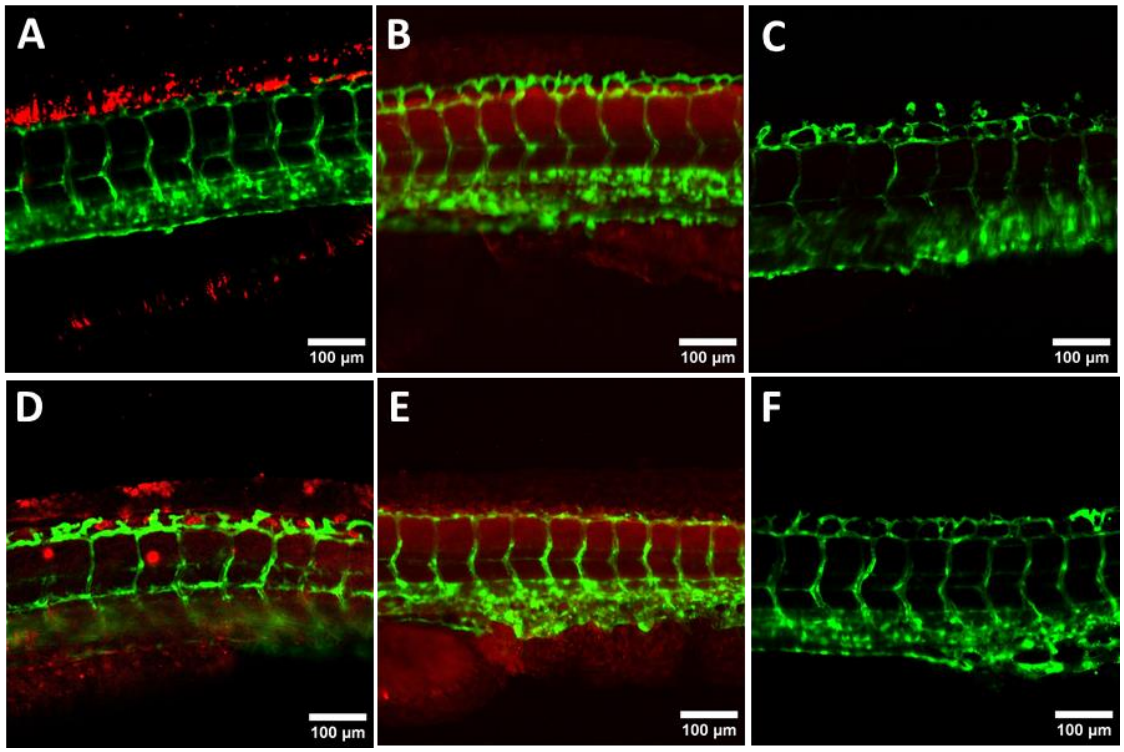

Figure 7.5 - Evaluation of the ability of CPP-based nanocomplexes for ZF embryo transfection. Representative confocal images of ZF embryos expressing the GFP protein (green signal) transfected with different CPP-based complexes encapsulating Alexa594-labelled pND1. (A) 20% PEG–MTS–WRAP1/pND1 with 2 µg, (B) 20% PEG–MTS–WRAP1/pND1 with 1 µg, (C) 20% PEG–MTS–WRAP1/pND1 with 0.5 µg, (D) 20% PEG–WRAP5/pND1 with 2 µg, and (E) MTS–$(KH)_9$/pND1 with 2 µg imaged after 24 h incubation. Peptide nanocomplexes were formulated at an N/P ratio of 5 using the indicated final plasmid concentrations. Untransfected ZF embryos were used as control (F). Bars represent 100 µm.

All tested MTS–CPP complexes demonstrated the ability to internalize in zebrafish embryos using 2–1 µg of pND1, resulting in a nearly homogeneous distribution throughout the body of the embryo compared to non-treated ZF embryos (**Figure 7.5F**). These results demonstrated the ability of these nanocomplexes to transfect into ZF embryos, highlighting their value for effective *in vivo* gene delivery. This will potentially contribute to advance *in vivo* research in the mitochondrial gene therapy field.

7.4.9 Toxicity Evaluation *In Vivo* Zebrafish Embryo Model

After verifying that the PEG–MTS–WRAP/pND1 and MTS–$(KH)_9$/pND1 complexes can successfully transfect and internalize into ZF embryos, we wanted to evaluate whether these delivery systems cause any toxicity in these *in vivo* models, particularly in terms of embryo development/growth and mortality. For this purpose, three quantities of nanocomplexes were tested for each type of system under study, namely 1 µg, 2 µg, and 5 µg, which corresponds to the amount of pND1 used to formulate the nano-complexes. The toxicity of the peptide complexes

was analyzed 48 h after incubation in ZF embryos. The results of development/growth and mortality of ZF embryos are shown in **Figure 7.6**.

The toxicity results of the 20% PEG–WRAP1/pND1 complexes (without MTS sequence) are presented in **Figure S7.3A** (available in Supplementary Materials). Embryos transfected with the 20% PEG–WRAP1/pDN1 nanocomplexes did not show changes in development/growth in relation to the non-transfected control group. No deaths occurred for the two lowest amounts of the complexes (1 and 2 μg). However, in the group of embryos transfected with 5 μg of 20% PEG–WRAP1/pDN1 complexes, 10 out of 12 embryos survived.

The toxicity of the WRAP1-based complexes was tested in the ZF embryo *in vivo* model. **Figure 7.6A** presents the obtained results for the 20% PEG–MTS–WRAP1/pND1 nanocomplexes (for 1 μg, 2 μg, and 5 μg pDNA). Embryos transfected with the 20% PEG–MTS–WRAP1/pND1 complexes exhibited a survival rate of 100% and their development/growth was identical to the control group (non-transfected embryos). For the three quantities of considered complexes, there were no changes in the morphology of the embryos or their development, with sizes around 3550 μm, similar to embryos that were not transfected. The data in **Figure 7.6A** suggested that the 20% PEG–MTS–WRAP1/pND1 nanocomplexes are stable and do not present associated toxicity in ZF embryos.

The toxicity of the WRAP5-based nanocomplexes was also analyzed. The results for the 20% PEG–WRAP5/pND1 nanocomplexes (without MTS sequence) are shown in **Figure S7.3B**, in the Supplementary Materials. The results show that the 20% PEG–WRAP5/pDN1 nanocomplexes do not present any toxicity to ZF embryos in the three pDNA quantities under study. In the three groups of ZF embryos, no associated deaths were recorded, and the development/growth of the embryos was similar to the control group. We can, therefore, conclude that the 20% PEG–WRAP5/pND1 nanocomplexes are stable and do not cause toxicity in ZF embryos.

Figure 7.6B presents the toxicity results of the 20% PEG–MTS–WRAP5/pND1 nano-complexes in ZF embryos. The 20% PEG–MTS–WRAP5/pND1 complexes were demonstrated to be stable and non-toxic to this *in vivo* model since all embryos survived in the three pDNA quantities used and there were no changes in their development/growth.

The toxicity data of the MTS-$(KH)_9$/pND1 nanocomplexes are represented in **Figure 7.6C**. As with the PEG-MTS-WRAP/pND1 complexes, the MTS–$(KH)_9$/pND1 systems do not present associated toxicity when transfected and internalized in ZF embryos. Embryos incubated with these nanocomplexes presented a development and growth profile identical to embryos in the control group for the three pDNA quantities tested. The survival rate for 1 μg and 2 μg of MTS–$(KH)_9$/pND1 nanocomplexes is 100%, with only 1 embryo in 12 dying for the amount of 5 μg of MTS–$(KH)_9$/pND1 complexes.

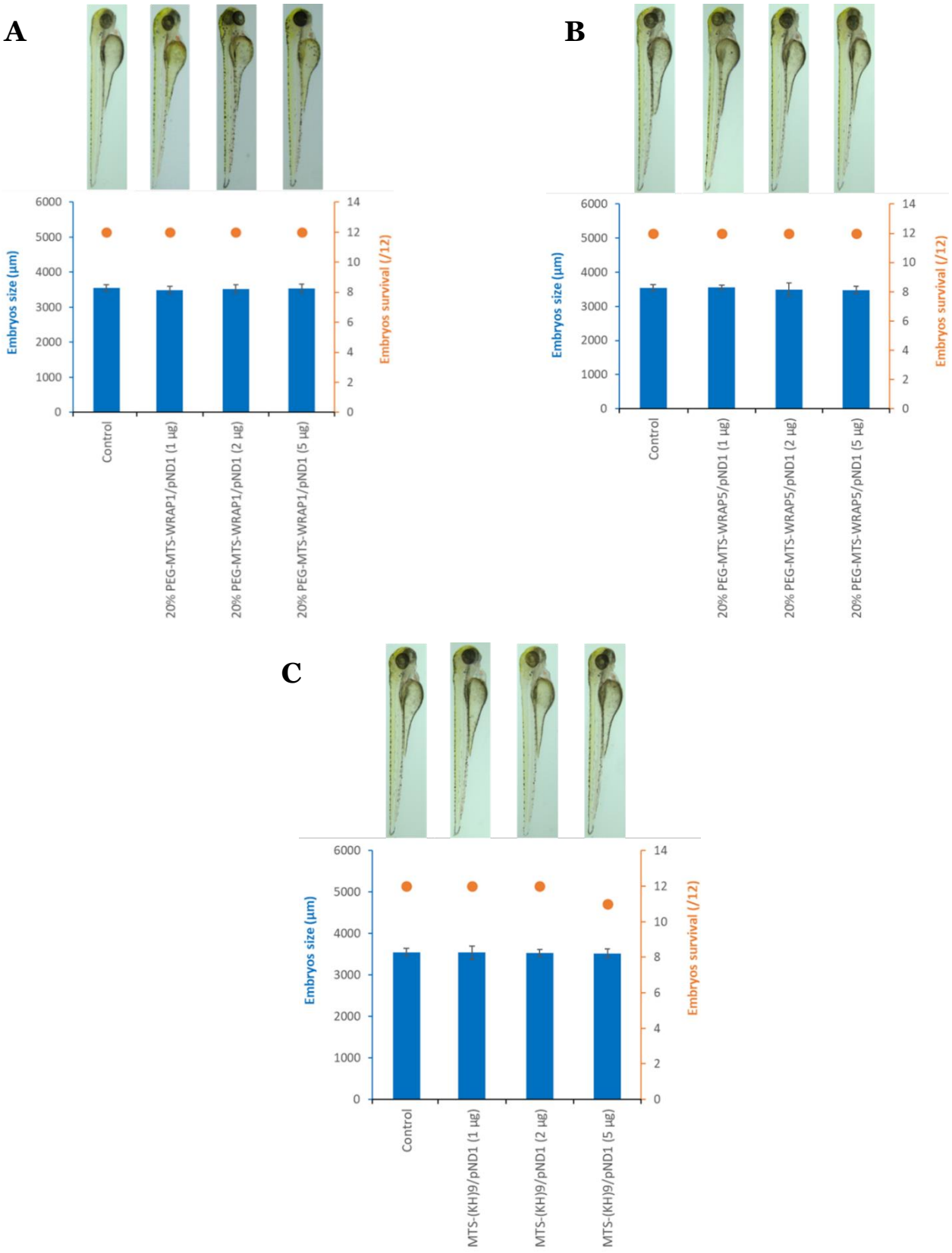

Figure 7.6 - Assessment of the toxicity of the 20% PEG–MTS–WRAP1/pND1 (A), 20% PEG–MTS–WRAP5/pND1 (B), and MTS–$(KH)_9$/pND1 (C) nanocomplexes (N/P ratio = 5) in ZF embryos. Toxicity was assessed through the average size of the embryos (µm) and their survival (/12) after 48 h of incubation. Non-transfected embryos were used as a control group. All nanocomplexes were tested at three different amounts (1, 2, and 5 µg).

The toxicity of the CpMTP/pND1 nanocomplexes was also tested in ZF embryos, as shown in Figure S4. The CpMTP/pND1 complexes did not reveal any toxic effects for ZF embryos in the three different pDNA amounts used to transfect these *in vivo* models. The embryos from these three groups demonstrated growth and development similar to the control group, with no associated deaths.

The tested peptide-based nanocomplexes were demonstrated to not elicit toxicity in zebrafish embryos, not causing changes in their morphology or growth/development, nor causing deaths associated with their use in this *in vivo* model. Therefore, the developed peptide delivery systems were revealed to be safe, stable, and biocompatible, holding great promise as carriers for *in vivo* mitochondrial gene transfection.

7.5 Conclusions

Diseases originating from mitochondrial dysfunction caused by mutations in mtDNA continue to lack therapies that enable treatment. Mitochondrial gene therapy is a very promising approach, but it is deeply dependent on a safe, biocompatible, and efficient vector to deliver therapeutic genetic material. Although MTS–CPP nanocomplexes had already demonstrated auspicious results *in vitro*, their *in vivo* evaluation was missing, retarding potential clinical translation. In this work, MTS–WRAP/pND1 complexes were PEGylated, and the formed PEG–nanocomplexes displayed adequate sizes, were stable up to 7 days after formulation, biocompatible to astrocytes and lung smooth muscle cells, and hemocompatible. The PEG–MTS–WRAP/pND1 complexes exhibited mitochondria targeting ability and promoted mitochondrial protein production. Following this, *in vivo* research was conducted in ZF embryos to determine the toxic profile of MTS–CPP-based systems—mandatory for biomedical applications—and their capacity for *in vivo* transfection. The ZF *in vivo* model was revealed to be a very useful testing platform to assess nanocomplexes toxicity, filling the distance between *in vitro* and rodent models.

Compared to the unPEGylated CpMTP/pND1 nanocomplex, we observed the formation of bigger nanoparticles (~350 nm) in the E3 solution used as an aqueous solution to care for ZF embryos. This could impact their application to ZF assays. In contrast, the other analyzed unPEGylated MTS–$(KH)_9$/pND1 complex was revealed to have slightly smaller nanocomplexes (~60 nm) and to have a more pronounced mitochondrial accumulation and ND1 protein expression compared to both PEG–MTS–WRAP/pND1 nanocomplexes. This phenomenon could be explained either by the smaller particle size (=better internalization of MTS–$(KH)_9$/pND1) or by the fact that PEGylation could mask the nanocomplexes (=lower internalization of PEG–MTS–WARP/pND1). PEGylation of lipid-based nanoparticles has proved particularly efficient in conferring longer systemic circulation, improving their pharmacokinetics and efficiency [58]. Also for peptide-based nanocomplexes, PEGylation was applied for the same reasons as shown for PEG–RICK:siRNA [59], for PEG–PepFect14:pDNA [60], and for PEG–NicFect55:pDNA [61]. In all cases, PEGylation improved the *in vivo* activity of the delivered nucleic acids (siRNA or pDNA). We observed the same improvement of nanocomplex stability in saline solution (E3 solution of

the ZF embryos) by adding a PEG moiety to the WRAP nanocomplexes (see Tables 2 and S2). Unexpectedly, MTS–$(KH)_9$ nanocomplexes showed good stability even in saline solutions without adding any PEG entity. The results presented here do not reveal the exact reason for this stability. The only visible difference is the absence of tryptophan in the CPP $(KH)_9$ sequence. We can only speculate that a possible Π-cation (tryptophan/NaCl) interaction could modify the hydration properties of tryptophan-containing CPPs, making them more sensitive to saline solutions. Further experiments are required to determine whether tryptophan can be sensitive to saline conditions.

The results obtained in ZF embryos demonstrated that the developed MTS–peptide nanocomplexes are stable, that they can internalize and distribute themselves throughout zebrafish, and that they do not present toxicity, nor do they cause malformations or changes in the normal growth and development of ZF. These very promising results demonstrate the biocompatibility and high performance of the developed MTS–$(KH)_9$/pND1 nanocomplexes and with slightly less activity also for the PEG/MTS–WRAP/pND1 nanocomplexes in a living system, opening the path for advances in mitochondrial gene therapy *in vivo* research.

7.6 Supplementary Materials

Supporting Information for Chapter 7

Table S7.1 - List of the synthesized peptides and MTS sequence, including information on peptide sequence, total residues, isotopic mass, and positive charges.

Peptide	Peptide sequence	Total residues	Isotopic mass [g/mol]	Positive charges
MTS	NH2-MLSLRQSIRFFK-CONH2	12	1523.88	3
WRAP1	NH2-LLWRLWRLLWRLWRLL-CONH2	16	2290.42	5
WRAP5	NH2-LLRLLRWWWRLLRLL-CONH2	15	2104.34	5
$(KH)_9$	NH2-KHKHKHKHKHKHKHKHKH-CONH2	18	2403.41	9
CpMTP	NH2-ARLLWLLRGLTLGTAPRRA-CONH2	19	2132.32	4
MTS-WRAP1	NH2-MLSLRQSIRFFK-LLWRLWRLLWRLWRLL-CONH2	28	3797.27	8
MTS-WRAP5	NH2-MLSLRQSIRFFK-LLRLLRWWWRLLRLL-CONH2	27	3611.19	8
MTS-$(KH)_9$	NH2-MLSLRQSIRFFK-KHKHKHKHKHKHKHKHKH-CONH2	30	3910.26	12

Results

Table S7.2 – Average size and PdI of peptide-based nanocomplexes formulated at N/P ratio of 5 resuspended in E3 solution.

Systems	Mean size (nm)	PdI
20% PEG-WRAP1/pND1	101 ± 10	0.268 ± 0.033
20% PEG-WRAP5/pND1	187 ± 6	0.474 ± 0.091
20% PEG-MTS-WRAP1/pND1	240 ± 14	0.354 ± 0.069
20% PEG-MTS-WRAP5/pND1	275 ± 29	0.217 ± 0.025
$(KH)_9$/pND1	127 ± 4	0.215 ± 0.064
MTS-$(KH)_9$/pND1	57 ± 9	0.206 ± 0.015
CpMTP/pND1	347 ± 13	0.342 0.072

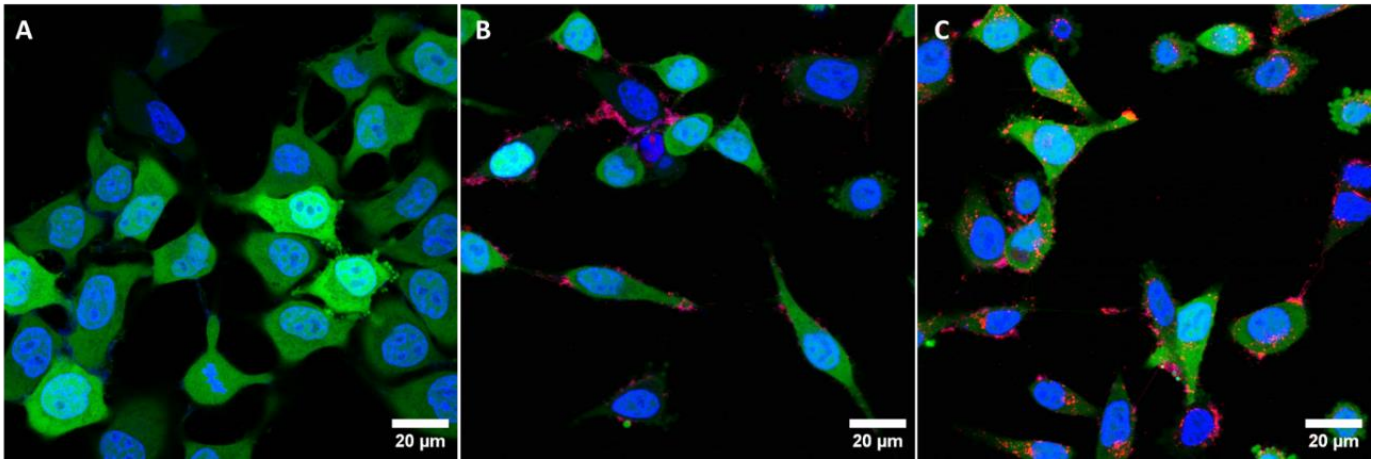

Figure S7.1 - Confocal images of non-treated HEK293T-GFP cells (**A**), HEK293T-GFP cells incubated with pND1 labeled with Alexa594 (pND1-Alexa594) (**B**) and HEK293T-GFP cells transfected with MTS-WRAP1/pND1-Alexa594 nanoparticles (**C**). The blue signal corresponds to cell nuclei labeled with Hoechst 33342, the green signal to the GFP protein produced intrinsically in HEK cells, and the red signal corresponds to the Alexa594 fluorescence of pND1. Images were obtained 2 h after cell transfection, using a 40x objective, lasers: 488 - 1.5%/700V; 405 - 1.0%/700V; 561 – 1.0%/650V.

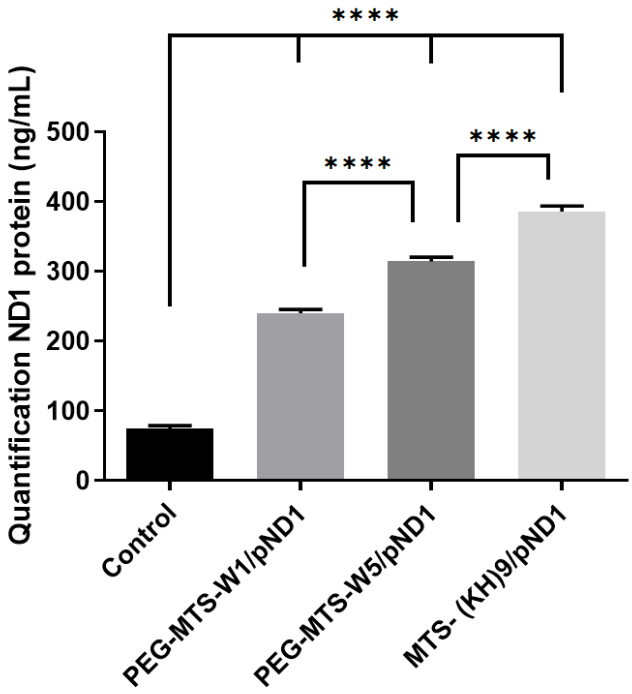

Figure S7.2 - Quantification of ND1 protein levels (ng/mL) in HEK293T cells, after 48 h of transfection with 20% PEG-MTS-WRAP1/pND1 (PEG-MTS-W1/pND1), 20% PEG-MTS-WRAP5/pND1 (PEG-MTS-W5/pND1) and MTS-$(KH)_9$/pND1 systems. All complexes were formulated with the N/P ratio = 5. Data were analyzed by one-way ANOVA with Bonferroni's multiple comparison test.

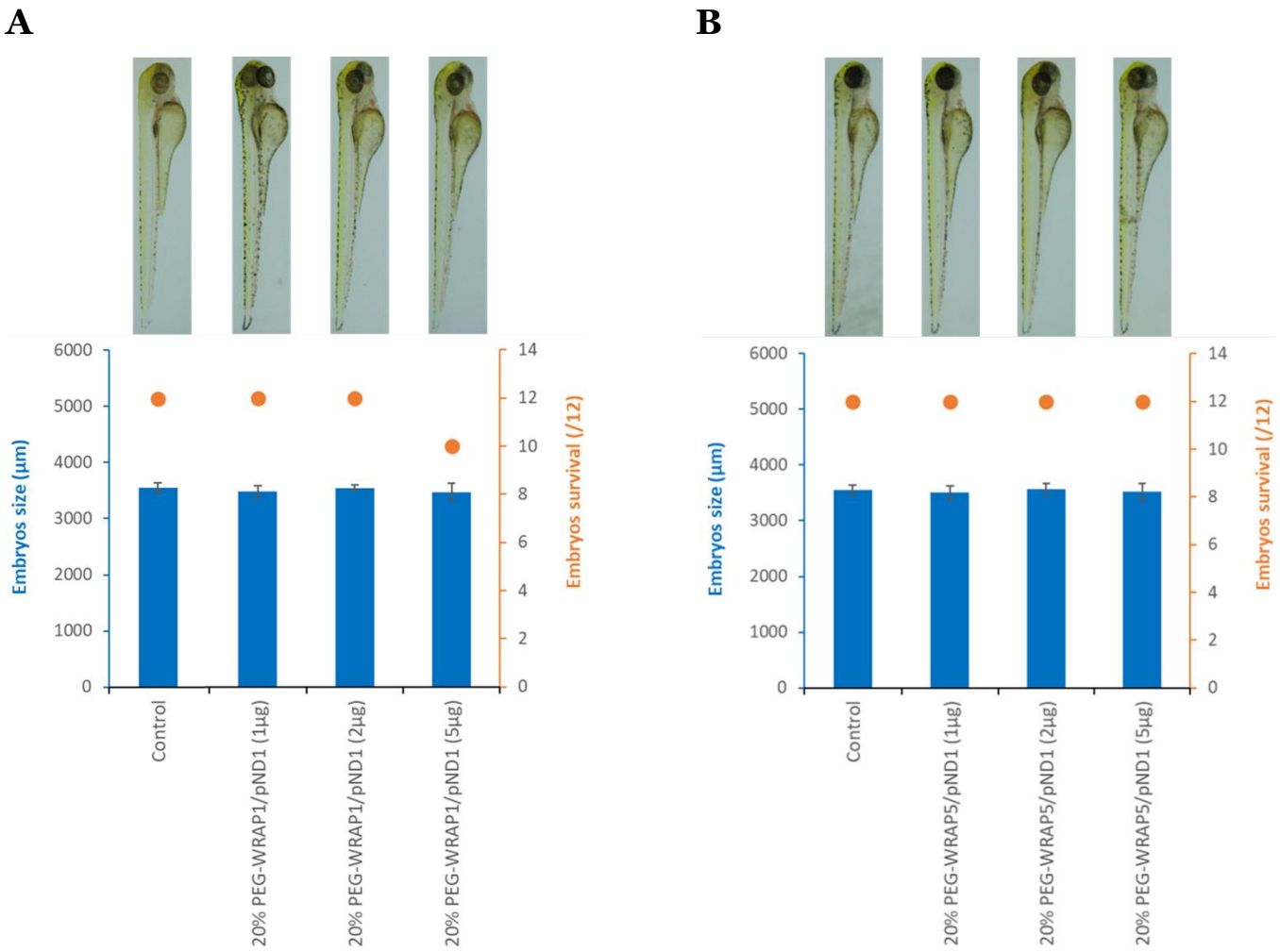

Figure S7.3 - Assessment of the toxicity of the 20% PEG-WRAP1/pND1 (**A**) and 20% PEG-WRAP5/pND1 (**B**) systems (N/P ratio of 5) in ZF embryos. Toxicity was assessed through the average size of the embryos (µm) and their survival (/12) after 48 h of incubation. Non-transfected embryos were used as a control group. Both systems were tested at 3 different amounts of pDNA (1 µg, 2 µg, and 5 µg).

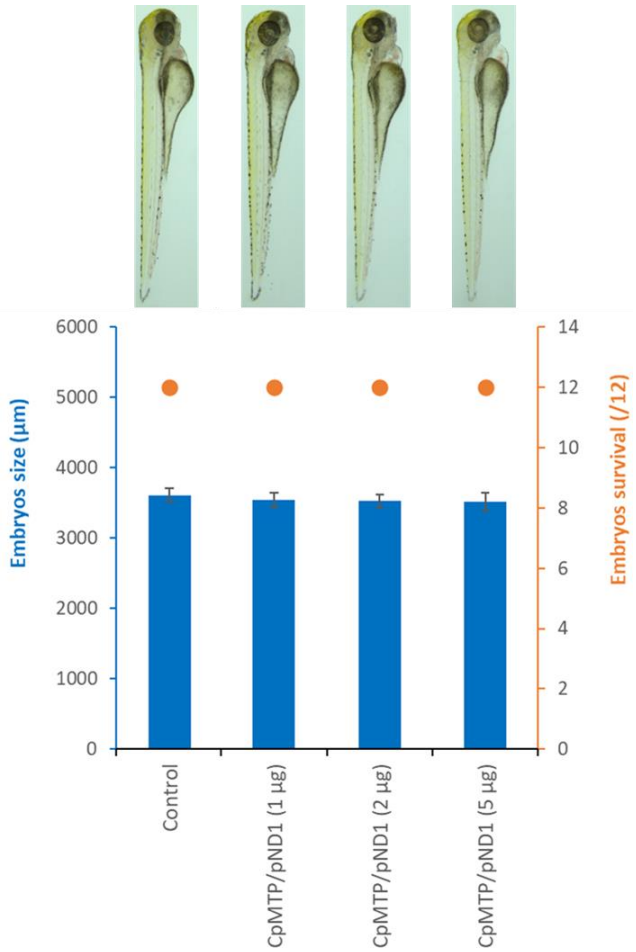

Figure S7.4 - Assessment of the toxicity of CpMTP/pND1 systems (N/P ratio of 5) in ZF embryos. Toxicity was assessed through the average size of the embryos (µm) and their survival (/12) after 48 h of incubation. Non-transfected embryos were used as a control group. The CpMTP/pND1 systems were tested at 3 different amounts of pDNA (1 µg, 2 µg, and 5 µg).

7.7 References

[1] Marchi, S.; Guilbaud, E.; Tait, S.W.G.; Yamazaki, T.; Galluzzi, L. Mitochondrial control of inflammation. Nat. Rev. Immunol. 2022, 23, 159–173.

[2] Popov, L.D. Mitochondrial biogenesis: An update. J. Cell. Mol. Med. 2020, 24, 4892–4899.

[3] Kadenbach, B. Complex IV—The regulatory center of mitochondrial oxidative phosphorylation. Mitochondrion 2021, 58, 296–302.

[4] Singh, A.P.; Salvatori, R.; Aftab, W.; Kohler, A.; Carlstrom, A.; Forne, I.; Imhof, A.; Ott, M. Molecular Connectivity of Mitochondrial Gene Expression and OXPHOS Biogenesis. Mol. Cell 2020, 79, 1051–1065.

[5] Fontecilla-Camps, J.C. Primordial bioenergy sources: The two facets of adenosine triphosphate. J. Inorg. Biochem. 2021, 216, 111347.

[6] Schlieben, L.D.; Prokisch, H. The Dimensions of Primary Mitochondrial Disorders. Front. Cell Dev. Biol. 2020, 8, 600079.
[7] Kaniak-Golik, A.; Skoneczna, A. Mitochondria-nucleus network for genome stability. Free Radic. Biol. Med. 2015, 82, 73–104.
[8] Zardoya, R. Recent advances in understanding mitochondrial genome diversity. F1000Research 2020, 9, 270–289.
[9] Stoccoro, A.; Coppedè, F. Mitochondrial DNA Methylation and Human Diseases. Int. J. Mol. Sci. 2021, 22, 4594–4621.
[10] Nissanka, N.; Moraes, C.T. Mitochondrial DNA heteroplasmy in disease and targeted nuclease-based therapeutic approaches. EMBO Rep. 2020, 21, 49612–49624.
[11] Lawless, C.; Greaves, L.; Reeve, A.K.; Turnbull, D.M.; Vincent, A.E. The rise and rise of mitochondrial DNA mutations. Open Biol. 2020, 10, 200061.
[12] La Morgia, C.; Maresca, A.; Caporali, L.; Valentino, M.L.; Carelli, V. Mitochondrial diseases in adults. J. Intern. Med. 2020, 287, 592–608.
[13] Gusic, M.; Prokisch, H. Genetic basis of mitochondrial diseases. FEBS Lett. 2021, 595, 1132–1158.
[14] Kopinski, P.K.; Singh, L.N.; Zhang, S.; Lott, M.T.; Wallace, D.C. Mitochondrial DNA variation and cancer. Nat. Rev. Cancer 2021, 21, 431–445.
[15] Kumar, R.; Harilal, S.; Parambi, D.G.T.; Kanthlal, S.K.; Rahman, M.A.; Alexiou, A.; Batiha, G.E.-S.; Mathew, B. The Role of Mitochondrial Genes in Neurodegenerative Disorders. Curr. Neuropharmacol. 2022, 20, 824–835.
[16] Zhang, L.; Zhang, Z.; Khan, A.; Zheng, H.; Yuan, C.; Jiang, H. Advances in drug therapy for mitochondrial diseases. Ann. Transl. Med. 2020, 8, 17–27.
[17] Tinker, R.J.; Lim, A.Z.; Stefanetti, R.J.; McFarland, R. Current and Emerging Clinical Treatment in Mitochondrial Disease. Mol. Diagn. Ther. 2021, 25, 181–206.
[18] Aravintha Siva, M.; Mahalakshmi, R.; Bhakta-Guha, D.; Guha, G. Gene therapy for the mitochondrial genome: Purging mutations, pacifying ailments. Mitochondrion 2019, 46, 195–208.
[19] Faria, R.; Boisguérin, P.; Sousa, Â.; Costa, D. Delivery Systems for Mitochondrial Gene Therapy: A Review. Pharmaceutics 2023, 15, 572–597.
[20] Falabella, M.; Minczuk, M.; Hanna, M.G.; Viscomi, C.; Pitceathly, R.D.S. Gene therapy for primary mitochondrial diseases: Experimental advances and clinical challenges. Nat. Rev. Neurol. 2022, 18, 689–698.
[21] Yoshinaga, N.; Numata, K. Rational Designs at the Forefront of Mitochondria-Targeted Gene Delivery: Recent Progress and Future Perspectives. ACS Biomater. Sci. Eng. 2022, 8, 348–359.
[22] Buchke, S.; Sharma, M.; Bora, A.; Relekar, M.; Bhanu, P.; Kumar, J. Mitochondria-Targeted, Nanoparticle-Based Drug-Delivery Systems: Therapeutics for Mitochondrial Disorders. Life 2022, 12, 657.
[23] Nam, S.H.; Park, J.; Koo, H. Recent advances in selective and targeted drug/gene delivery systems using cell-penetrating peptides. Arch. Pharmacal Res. 2023, 46, 18–34.

[24] Sun, Y.; Zhang, H.; Lu, G.; Wang, H.; Lu, Y.; Fan, L. Mitochondria-targeted cancer therapy based on functional peptides. Chin. Chem. Lett. 2023, 34, 107817–107824.
[25] Taylor, R.E.; Zahid, M. Cell Penetrating Peptides, Novel Vectors for Gene Therapy. Pharmaceutics 2020, 12, 225–246.
[26] Konate, K.; Dussot, M.; Aldrian, G.; Vaissiere, A.; Viguier, V.; Neira, I.F.; Couillaud, F.; Vives, E.; Boisguerin, P.; Deshayes, S. Peptide-Based Nanoparticles to Rapidly and Efficiently "Wrap 'n Roll" siRNA into Cells. Bioconjug. Chem. 2019, 30, 592–603.
[27] Abe, N.; Fujita, S.; Miyamoto, T.; Tsuchiya, K.; Numata, K. Plant Mitochondrial-Targeted Gene Delivery by Peptide/DNA Micelles Quantitatively Surface-Modified with Mitochondrial Targeting and Membrane-Penetrating Peptides. Biomacromolecules 2023, 24, 3657–3665.
[28] Yilmaz, N.; Kodama, Y.; Numata, K. Lipid Membrane Interaction of Peptide/DNA Complexes Designed for Gene Delivery. Langmuir 2021, 37, 1882–1893.
[29] Faria, R.; Vives, E.; Boisguerin, P.; Sousa, A.; Costa, D. Development of Peptide-Based Nanoparticles for Mitochondrial Plasmid DNA Delivery. Polymers 2021, 13, 1836–1855.
[30] McGrath, P.; Li, C.-Q. Zebrafish: A predictive model for assessing drug-induced toxicity. Drug Discov. Today 2008, 13, 394–401.
[31] Saleem, S.; Kannan, R.R. Zebrafish: An emerging real-time model system to study Alzheimer's disease and neurospecific drug discovery. Cell Death Discov. 2018, 4, 45–58.
[32] Teame, T.; Zhang, Z.; Ran, C.; Zhang, H.; Yang, Y.; Ding, Q.; Xie, M.; Gao, C.; Ye, Y.; Duan, M.; et al. The use of zebrafish (*Danio rerio*) as biomedical models. Anim. Front. 2019, 9, 68–77.
[33] Zhang, K.; Liang, J.; Brun, N.R.; Zhao, Y.; Werdich, A.A. Rapid Zebrafish Behavioral Profiling Assay Accelerates the Identification of Environmental Neurodevelopmental Toxicants. Environ. Sci. Technol. 2021, 55, 1919–1929.
[34] Haque, E.; Ward, A. Zebrafish as a Model to Evaluate Nanoparticle Toxicity. Nanomaterials 2018, 8, 561–579.
[35] Patton, E.E.; Zon, L.I.; Langenau, D.M. Zebrafish disease models in drug discovery: From preclinical modelling to clinical trials. Nat. Rev. Drug Discov. 2021, 20, 611–628.
[36] Bhattarai, P.; Turgutalp, B.; Kizil, C. Zebrafish as an Experimental and Preclinical Model for Alzheimer's Disease. ACS Chem. Neurosci. 2022, 13, 2939–2941.
[37] Shen, C.; Zuo, Z. Zebrafish (*Danio rerio*) as an excellent vertebrate model for the development, reproductive, cardiovascular, and neural and ocular development toxicity study of hazardous chemicals. Environ. Sci. Pollut. Res. 2020, 27, 43599–43614.
[38] Faria, R.; Paul, M.; Biswas, S.; Vives, E.; Boisguerin, P.; Sousa, A.; Costa, D. Peptides vs. Polymers: Searching for the Most Efficient Delivery System for Mitochondrial Gene Therapy. Pharmaceutics 2022, 14, 757–780.
[39] Shi, D.; Beasock, D.; Fessler, A.; Szebeni, J.; Ljubimova, J.Y.; Afonin, K.A.; Dobrovolskaia, M.A. To PEGylate or not to PEGylate: Immunological properties of nanomedicine's most popular component, polyethylene glycol and its alternatives. Adv. Drug Deliv. Rev. 2022, 180, 114079–114101.
[40] Ibrahim, M.; Ramadan, E.; Elsadek, N.E.; Emam, S.E.; Shimizu, T.; Ando, H.; Ishima, Y.; Elgarhy, O.H.; Sarhan, H.A.; Hussein, A.K.; et al. Polyethylene glycol (PEG): The nature,

immunogenicity, and role in the hypersensitivity of PEGylated products. J. Control Release 2022, 351, 215–230.
[41] Yadav, D.; Dewangan, H.K. PEGYLATION: An important approach for novel drug delivery system. J. Biomater. Sci. Polym. Ed. 2021, 32, 266–280.
[42] Harris, J.M.; Chess, R.B. Effect of pegylation on pharmaceuticals. Nat. Rev. Drug Discov. 2003, 2, 214–221.
[43] Elsadek, N.E.; Abu Lila, A.S.; Ishida, T. Immunological responses to PEGylated proteins. In Polymer-Protein Conjugates; Elsevier: Amsterdam, The Netherlands, 2020; pp. 103–123.
[44] Faria, R.; Albuquerque, T.; Neves, A.R.; Bhatt, H.; Biswas, S.; Cardoso, A.M.; Pedroso de Lima, M.C.; Jurado, A.S.; Costa, D. Physicochemical characterization and targeting performance of triphenylphosphonium nano-polyplexes. J. Mol. Liq. 2020, 316, 113873–113884.
[45] Costa, D.; Costa, C.; Caldeira, M.; Cortes, L.; Queiroz, J.A.; Cruz, C. Targeting of Cellular Organelles by Fluorescent Plasmid DNA Nanoparticles. Biomacromolecules 2017, 18, 2928–2936.
[46] Lawson, N.D.; Weinstein, B.M. *In vivo* imaging of embryonic vascular development using transgenic zebrafish. Dev. Biol. 2002, 248, 307–318.
[47] Xie, J.; Bi, Y.; Zhang, H.; Dong, S.; Teng, L.; Lee, R.J.; Yang, Z. Cell-Penetrating Peptides in Diagnosis and Treatment of Human Diseases: From Preclinical Research to Clinical Application. Front. Pharmacol. 2020, 11, 697–720.
[48] Subia, B.; Reinisalo, M.; Dey, N.; Tavakoli, S.; Subrizi, A.; Ganguli, M.; Ruponen, M. Nucleic acid delivery to differentiated retinal pigment epithelial cells using cell-penetrating peptide as a carrier. Eur. J. Pharm. Biopharm. 2019, 140, 91–99.
[49] Boisguerin, P.; Deshayes, S.; Gait, M.J.; O'Donovan, L.; Godfrey, C.; Betts, C.A.; Wood, M.J.; Lebleu, B. Delivery of therapeutic oligonucleotides with cell penetrating peptides. Adv. Drug Deliv. Rev. 2015, 87, 52–67.
[50] d'Avanzo, N.; Celia, C.; Barone, A.; Carafa, M.; Di Marzio, L.; Santos, H.A.; Fresta, M. Immunogenicity of Polyethylene Glycol Based Nanomedicines: Mechanisms, Clinical Implications and Systematic Approach. Adv. Ther. 2020, 3, 1900170–1900188.
[51] Lopez-Garcia, J.; Lehocky, M.; Humpolicek, P.; Saha, P. HaCaT Keratinocytes Response on Antimicrobial Atelocollagen Substrates: Extent of Cytotoxicity, Cell Viability and Proliferation. J. Funct. Biomater. 2014, 5, 43–57.
[52] Hao, M.; Liu, R. Molecular mechanism of CAT and SOD activity change under MPA-CdTe quantum dots induced oxidative stress in the mouse primary hepatocytes. Spectrochim. Acta A Mol. Biomol. Spectrosc. 2019, 220, 117104–117115.
[53] Saebo, I.P.; Bjoras, M.; Franzyk, H.; Helgesen, E.; Booth, J.A. Optimization of the Hemolysis Assay for the Assessment of Cytotoxicity. Int. J. Mol. Sci. 2023, 24, 2914–2934.
[54] Niza, E.; Nieto-Jimenez, C.; Noblejas-Lopez, M.D.M.; Bravo, I.; Castro-Osma, J.A.; Cruz-Martinez, F.; Buchaca, M.M.S.; Posadas, I.; Canales-Vazquez, J.; Lara-Sanchez, A.; et al. Poly(Cyclohexene Phthalate) Nanoparticles for Controlled Dasatinib Delivery in Breast Cancer Therapy. Nanomaterials 2019, 9, 1208–1222.

[55] Dubey, A.; Ghosh, N.S.; Singh, R. Zebrafish as An Emerging Model: An Important Testing Platform for Biomedical Science. J. Pharm. Negat. Results 2022, 13, 1–7.
[56] Parkkila, S.; Parikka, M.; Hammaren, M.M.; Aspatwar, A. Rapid Evaluation of Toxicity of Chemical Compounds Using Zebrafish Embryos. J. Vis. Exp. 2019, 150, e59315.
[57] Wiley, D.S.; Redfield, S.E.; Zon, L.I. Chemical screening in zebrafish for novel biological and therapeutic discovery. In The Zebrafish: Disease Models and Chemical Screens; Methods in Cell Biology Book Series; Academic Press: Cambridge, MA, USA, 2017; pp. 651–679.
[58] Tenchov, R.; Sasso, J.M.; Zhou, Q.A. PEGylated Lipid Nanoparticle Formulations: Immunological Safety and Efficiency Perspective. Bioconjug. Chem. 2023, 34, 941–960.
[59] Aldrian, G.; Vaissiere, A.; Konate, K.; Seisel, Q.; Vives, E.; Fernandez, F.; Viguier, V.; Genevois, C.; Couillaud, F.; Demene, H.; et al. PEGylation rate influences peptide-based nanoparticles mediated siRNA delivery *in vitro* and *in vivo*. J. Control Release 2017, 256, 79–91.
[60] Veiman, K.L.; Kunnapuu, K.; Lehto, T.; Kiisholts, K.; Parn, K.; Langel, U.; Kurrikoff, K. PEG shielded MMP sensitive CPPs for efficient and tumor specific gene delivery *in vivo*. J. Control Release 2015, 209, 238–247.
[61] Freimann, K.; Arukuusk, P.; Kurrikoff, K.; Vasconcelos, L.D.F.; Veiman, K.L.; Uusna, J.; Margus, H.; Garcia-Sosa, A.T.; Pooga, M.; Langel, U. Optimization of *in vivo* DNA delivery with NickFect peptide vectors. J. Control Release 2016, 241, 135–143.

Chapter 8

Conclusions and Future Challenges

Mutations in the mitochondrial genome (mtDNA) induce changes in the normal functioning of mitochondria and consequently of cells, which can affect several organs. Mitochondrial dysfunctions associated with mtDNA mutations are linked to the onset of neurodegenerative and metabolic diseases such as Alzheimer's, Parkinson's, diabetes, among others. Changes in mtDNA have also been identified in cancer patients that are associated with the onset of the disease. The solutions currently available on the market for this type of mitochondrial disease serve only to mitigate the symptoms and attempt to slow the progression of the disease. Therefore, there is a need to develop effective treatments to fight this type of pathology. Gene therapy appears to be a promising strategy, since it allows the problem to be solved at its source, replacing the mutated genes. However, the difficulty in applying this therapy lies in the fact that there are no efficient nanotransporters that can deliver the genetic material, especially to organelles inside cells such as mitochondria. Unlike nuclear gene therapy, which has been widely explored in recent years and has already demonstrated several delivery systems to be effective, mitochondrial gene therapy is very recent and there are no delivery systems that have demonstrated efective results in targeting and delivering genetic material to mitochondria. Therefore, the objective of this doctoral thesis was to design and develop polymer and peptide-based delivery systems for the delivery of a plasmid DNA encoding the mitochondrial gene ND1, using ligands that have previously demonstrated affinity for mitochondria. The aim is to contribute to the advancement of mitochondrial gene therapy so that it can be considered a viable therapy for the treatment of mitochondrial diseases.

With this aim in mind, the first step we performed was a DoE to determine the best formulation conditions for the PEG-PEI-TPP/pND1 nanoparticles to obtain delivery systems with the smallest size and that condensed the largest possible amount of pND1. The obtained vectors presented suitable physicochemical properties for both cellular uptake and payload delivery (sizes between 100 and 150 nm and surface charge of +35 mV) and pND1 complexation capacity (encapsulation rates higher than 85%). DoE allowed, with a reduced number of tests, to determine the best formulation conditions and the most suitable delivery systems for further studies aimed at the effective delivery of mitochondrial genes (**Chapter 3**). Having verified the capacity of PEI-based systems with the TPP ligand to condense genetic material within them, we continued studies with these vectors to determine their capacity for cellular internalization and delivery of genetic material to the mitochondria. It was demonstrated that the developed PEG-PEI-TPP/pDNA systems were able to not only internalize in mammalian cells but also target mitochondria and deliver both the GFP gene and the mitochondrial ND1 gene. Through confocal microscopy, their co-localization within mitochondria was verified after transfection of HeLa cells. After

transfection, an increase in gene expression and the production of their respective proteins were also observed (**Chapter 4**). In addition to polymeric systems, we developed peptide-based systems to which a mitochondrial targeting sequence (MTS) was added. The peptides used (WRAP family and $(KH)_9$), together with the CpMTP peptide, demonstrated the ability to encapsulate pND1 with high encapsulation rates (around 100% for N/P ratios ≥1). Furthermore, the peptide systems demonstrated physicochemical properties suitable for transfection and gene therapy application (sizes below 200 nm and zeta potential above +10 mV). All the developed peptide systems demonstrated *in vitro* biocompatibility. It was also demonstrated that the use of MTS in the systems allows specific targeting of mitochondria; confocal microscopy studies revealed that systems without MTS accumulate preferentially in the cytosol of cells, and systems with the sequence internalize almost entirely in the mitochondria (**Chapter 5**). Since it was found that both polymeric and peptide systems performed well, the comparison was made to determine the most efficient delivery systems for mitochondrial gene therapy. To the PEI-based polymeric systems, was added a new ligand that has an affinity for mitochondria (DQA). The comparison between the systems was made considering the ability to deliver the mitochondrial gene ND1 into mitochondria and to evaluate gene transcription and translation of the ND1 protein. It was demonstrated that both polymeric and peptide/pND1 complexes can efficiently internalize into mitochondria. The obtained results demonstrate higher gene expression into mitochondria of HeLa and Fibroblast cells and consequently higher levels of ND1 protein in cells transfected with these systems. However, was found that the CPP-based peptide systems show superior performance in terms of cellular uptake, gene delivery, and protein expression (**Chapter 6**). As the MTS-CPP/pND1 systems demonstrated better results, the next step was to test these systems in *in vivo* models, namely in ZF embryos. The CPP-based systems were modified with the addition of PEG, which made the systems more stable in saline environments, without compromising their mitochondrial targeting and ND1 gene delivery. The tests in the ZF allowed us to verify that the developed systems can internalize and distribute themselves throughout the body of the embryos, and that they do not present toxicity nor cause malformations or changes in the growth of this animal model (**Chapter 7**).

The delivery systems developed in this PhD thesis are a major contribution to mitochondrial gene therapy implementation in view of the treatment of mitochondrial diseases. However, there is the possibility of using the knowledge acquired to improve and make viable the application of these or other similar nanosystems for the treatment of mitochondrial dysfunctions through gene therapy. Thus, some of the possibilities that can be investigated for the advancement of mitochondrial gene therapy are:

1. To evaluate the capacity and functioning in *in vivo* models of the PEI-based systems developed in this thesis to assess whether they obtain similar results to those obtained *in vitro*;
2. To test the systems developed in this doctoral thesis in cells with mutations in the mitochondrial ND1 gene to evaluate the ability to restore normal levels of this gene in transfected cells;

3. To apply the peptide-based systems developed in this thesis to other *in vivo* models to assess their distribution and functioning within the organism and determine their ability to deliver the target gene to the mitochondria;
4. The results presented in this doctoral thesis could boost the creation of gene-mutated disease animal models to test the therapeutic effect of mitochondrial gene delivery systems;
5. To use the knowledge acquired as a basis and develop new delivery systems for the long-term expression of other mitochondrial genes that are responsible for the onset of mitochondrial diseases.

The work developed throughout this doctoral thesis allowed us to understand the difficulty of designing and developing delivery systems for mitochondrial gene therapy. In addition to the challenges that all delivery systems have to face, vectors targeting mitochondria face additional challenges, with more barriers to overcome. However, the results presented here are a major contribution to this field of science that is still little explored. The knowledge generated in this doctoral thesis can and should be considered, by scientific community, to promote progress in the feaseability of mitochondrial gene therapy implementation, and this for sure, will greatly contribute to make this therapy clinically viable for the treatment of mitochondrial diseases originating from mutations in the mitochondrial genome.